

2007

Characterization and in vitro biocompatibility of engineered nanomaterials

Amanda Michelle Schrand
University of Dayton

Follow this and additional works at: https://ecommons.udayton.edu/graduate_theses

Recommended Citation

Schrand, Amanda Michelle, "Characterization and in vitro biocompatibility of engineered nanomaterials" (2007). *Graduate Theses and Dissertations*. 5439.
https://ecommons.udayton.edu/graduate_theses/5439

This Dissertation is brought to you for free and open access by the Theses and Dissertations at eCommons. It has been accepted for inclusion in Graduate Theses and Dissertations by an authorized administrator of eCommons. For more information, please contact mschlange1@udayton.edu, ecommons@udayton.edu.

CHARACTERIZATION AND IN VITRO BIOCOMPATIBILITY
OF ENGINEERED NANOMATERIALS

Dissertation

Submitted to

The School of Engineering

UNIVERSITY OF DAYTON

In Partial Fulfillment of the Requirements for

The Degree

Doctor of Philosophy in Materials Engineering

by

Amanda Michelle Schrand

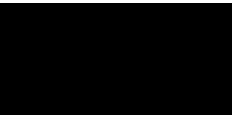
UNIVERSITY OF DAYTON

Dayton, Ohio

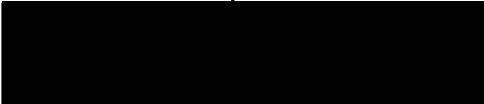
December 2007

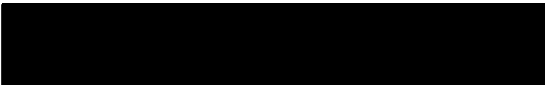
CHARACTERIZATION AND IN VITRO BIOCOMPATIBILITY
OF ENGINEERED NANOMATERIALS

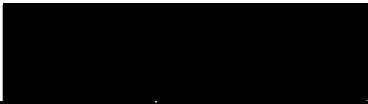
APPROVED BY:


Liming Dai, Ph.D.
Advisor, Committee Chairman
Endowed Chair of Nanomaterials
Professor, Materials Engineering


P. Terrence Murray, Ph.D.
Committee Member
Professor, Materials Engineering


Mr. Gerald Shaughnessy, M.S.
Committee Member
Associate Professor, Mathematics


Malcolm W. Daniels, Ph.D.
Associate Dean
School of Engineering


Saber M. Hussain, Ph.D.
Committee Member, Co-Advisor
Scientist, Air Force Research
Laboratory/RHPB


Donald Klosterman, Ph.D.
Committee Member
Professor, Materials Engineering


Joseph E. Saliba, Ph.D., P.E.
Dean, School of Engineering

ABSTRACT

CHARACTERIZATION AND IN VITRO BIOCOMPATIBILITY OF ENGINEERED NANOMATERIALS

Schrand, Amanda M.

University of Dayton, 2007

Advisor: Dr. Liming Dai

Co-Advisor: Dr. Saber Hussain

The purpose of this dissertation research was to investigate the biocompatibility or toxicity of carbon and metal-based nanomaterials to neuronal, lung, and skin cell lines. It was found that the cytotoxicity of carbon nanomaterials depended strongly on the residual metal catalyst remaining from nanomaterial synthesis, nanomaterial concentration, nanoparticle size, and surface chemistry. The general trend of biocompatibility was found for carbon-based nanomaterials to be: nanodiamonds (NDs) > fine carbon black nanoparticles (CB) > multi-walled carbon nanotubes (MWNTs) > single-walled carbon nanotubes (SWNTs) to both macrophages and neuroblastoma cells. A cell-specific response to different carbon nanomaterials was also

demonstrated with the internalization and reactivity response being greater in the macrophages compared to the neuroblastoma cells.

The biocompatibility of Ag nanoparticles was found to be size and surface-chemistry dependent in neuroblastoma cells. The cytotoxicity of Ag nanoparticles increased with decreasing the particle size. Ag nanoparticles synthesized by reduction of silver ions in solution with an organic polysaccharide (acacia gum) showed a better biocompatibility than their hydrocarbon-synthesized counterparts. However, both forms of Ag nanoparticles were found to attach to plasma membranes and become internalized after 24h incubation.

This research has culminated in the development of an advanced set of characterization techniques and cell-based protocols for a variety of nanomaterials. Despite the great challenge in monitoring the internalization of nanoparticles into cells due to the very low quantities of nanoparticles internalized by some cell types, this research has led to the discovery of the differential biocompatibility and cell-specific effects of carbon and metal-based nanomaterials.

ACKNOWLEDGEMENTS

First and foremost, I want to acknowledge God for directing my steps in this endeavor as I have strived to lean not on my own understanding, but on His Holy wisdom. May the completion of this dissertation be for His glory.

Standing, sitting, and waiting beside me has been my devoted husband, Brian, without whom I could not have juggled the responsibilities of life while pursuing this degree. I will not forget the sacrifices we have made together to accomplish this goal.

I appreciate our families for understanding my desire for learning and higher education. Your continued support, encouragement, and questions throughout all of my studies have been a great contribution. Now, I may answer you, that yet another degree has been completed!

To Dr. Daniel Eylon, thank you for accepting me into the Materials Engineering Program and challenging me to pursue a Ph.D. You have always been very caring, straight-forward, and willing to set me in the spot-light.

Special thanks to my advisor, Dr. Liming Dai for his strong commitment to excellence and dedication to our group. Without his openness to branch out into the new and exciting field of bionanotechnology, these studies would not have been possible. Working in such a diverse group of individuals has brought me great joy and I thank each of you.

A great gratitude and deep appreciation to Dr. Saber Hussain, who supervised the majority of this dissertation research, which was performed at AFRL/HEPB. Thank you for providing me with the opportunity to develop an outstanding set of research skills within the Biological Interactions of Nanomaterials (BIN) group through serving others. None of this work could have been done without you and the interest and assistance of our group members.

Thanks to my other committee advisors, Dr. Don Klosterman, Dr. Terry Murray, and Gerry Shaughnessy for continuing to support my studies as they changed from a more traditional materials focus while I was at AFRL/ML to the new and exciting area of bioengineering.

I also appreciate the many other individuals at WPAFB and UD that contributed their valuable expertise and time, but mentioning each of these people individually would be too long to list here. I would specifically like to

acknowledge Mr. Mike Jubara, Mr. Tom Kerschner, and Mr. John Workman from ChemSys and Mr. Tom Wittberg from UDRI.

Last, but not least, I wish to acknowledge the late Sean Crossman, whose memories have inspired me to give my all. His Spirit of faithfulness to family and pursuit of higher education is still alive.

This research was sponsored by the Dayton Area Graduate Studies Institute (DAGSI) and the Oak Ridge Institute of Science and Education (ORISE). I am tremendously thankful that I could pursue these studies with such loyal financial support.

TABLE OF CONTENTS

ABSTRACT	iii
ACKNOWLEDGEMENTS.....	v
LIST OF FIGURES	x
LIST OF TABLES	xv
LIST OF ABBREVIATIONS AND SYMBOLS	xvi
CHAPTER	
I. INTRODUCTION TO NANOTECHNOLOGY AND NANOMATERIALS.....	1
1.1 Engineered Nanomaterials.....	2
1.2 Nanomaterial Biocompatibility	6
1.3 Statement of Work and Specific Aims	16
1.4 Research Description	17
II. EXPERIMENTAL METHODS.....	21
2.1 Nanomaterials and Chemicals.....	21
2.2. Preparation of Nanomaterial Solutions.....	26
2.3 Nanomaterial Characterization	27
2.4 <i>In Vitro</i> Biocompatibility Studies	42
2.5 Statistical Evaluation	51
III. CARBON NANOTUBES.....	52
3.1 Literature Review	52
3.2 Results for Characterization	60
3.3 Results for Biocompatibility	66
3.4 Discussion.....	88

IV. NANODIAMONDS	93
4.1 Literature Review.....	93
4.2 Results for Characterization	98
4.3 Results for Biocompatibility	106
4.4 Discussion	123
 V. SILVER NANOPARTICLES	 128
5.1 Literature Review.....	128
5.2 Results for Characterization	134
5.3 Results for Biocompatibility	150
5.4 Discussion	161
 VI. SUMMARY AND CONCLUSIONS	 166
6.1 Summary	166
6.2 Conclusions	170
 VII. CHALLENGES AND SUGGESTED FUTURE RESEARCH.....	 174
7.1 Preservation of the Most Natural State for High Resolution Imaging..	176
7.2 Nanomaterial Properties Responsible for Cell Attraction, Binding, Internalization, Localization, and Accumulation.....	182
7.3 Elaboration on Mechanism of Nanomaterial Entry into Cells and Subsequent Physico-Chemical Changes	185
7.4 Quantifying Nanomaterial Internalization with Spectroscopic Techniques	189
7.5 Discussion	195
 REFERENCES	 198
 APPENDIX A Statistics for MTT and LDH Assays for PC-12 Cells with MWNTs and Controls	 219
 APPENDIX B Statistics for MTT and ROS Assays for N2A Cells with CNMs, NDs, Ag NPs, and Controls	 223
 APPENDIX C Statistics for MTT and ROS Assays for Macrophages and CNMs	 264
 VITA	 276

LIST OF FIGURES

Figure 1.1.1. Comparison of common entities on the metric scale	2
Figure 1.1.2. Common nanomaterial innovations in the marketplace	4
Figure 1.2.1. Schematic of the target cell types used in these studies	8
Figure 1.2.2. Periodic table of the elements	12
Figure 1.4.1. Solution interactions of nanomaterials.....	19
Figure 1.4.2. Schematic of the possible interactions of nanomaterials with a cell in culture	20
Figure 2.1.1. Conventional thermal chemical vapor deposition (CVD) apparatus for the synthesis of carbon nanotubes	22
Figure 2.1.2. Synthesis of carbon black.....	22
Figure 2.1.3. Synthesis of detonation nanodiamonds.....	23
Figure 2.2.1. Probe sonicator and vortexer used in these studies	26
Figure 2.3.1. Schematic representation of sample-electron beam interactions	28
Figure 2.3.2. Hitachi H-7600 transmission electron microscope (TEM)	29
Figure 2.3.3. Hitachi S-4800 high resolution field emission scanning electron microscope (HRSEM)	30
Figure 2.3.4. Schematic representation of atomic absorption spectrometer set-up.....	32
Figure 2.3.5. Schematic diagram of a typical ICP-OES instrument	33
Figure 2.3.6. Detection limits for elements of the periodic table	34
Figure 2.3.7. Renishaw invia Raman microscope.....	36

Figure 2.3.8. Perkin Elmer Spectrum One FTIR Instrument	38
Figure 2.3.9. Surface Science Labs SSX-100 system XPS	39
Figure 2.3.10. Malvern Zetasizer machine	39
Figure 2.4.0. Demonstration of appropriate lab attire and aseptic technique inside a biological hood	43
Figure 2.4.1. Illustration of the general nanoparticle dosing set-up	45
Figure 2.4.2. Olympus IX71 inverted light microscope and Cytoviva attachment	46
Figure 2.4.3. Leica Ultracut ultramicrotome	47
Figure 2.4.4. Dose-dependent toxicity of CdO in N2A cells assessed with the MTT assay.....	48
Figure 2.4.5. Production of reactive oxygen species (ROS) in cells incubated with H ₂ O ₂	50
Figure 3.1.1. One-, two-, and three-dimensional carbon nanomaterials	53
Figure 3.2.1. Size and morphology of carbon nanomaterials with TEM.....	62
Figure 3.2.2. Dynamic light scattering (DLS) and zeta potential (ZP) data for carbon nanomaterials	64
Figure 3.2.3. Change in dispersion of MWNTs	65
Figure 3.3.1. Light microscopy of PC-12 cell morphology after incubation with MWNTs	67
Figure 3.3.2. Ultrahigh resolution light microscopy of PC-12 cells incubated with MWNTs	68
Figure 3.3.3. PC-12 cell viability and membrane leakage after incubation with 0-100 µg/ml of MWNT for 24h	70
Figure 3.3.4. PC-12 cells and MWNTs	70
Figure 3.3.5. Phase contrast images of cells incubated with carbon nanomaterials	72

Figure 3.3.6. Examination of interactions between cells and carbon nanomaterials	73
Figure 3.3.7. Transmission electron microscopy of the internalization of carbon nanomaterials into N2A cells.....	74
Figure 3.3.8. Biocompatibility evaluation of various carbon nanomaterials	76
Figure 3.3.9. Mitochondrial membrane permeability of cells incubated with carbon nanomaterials	77
Figure 3.3.10. Generation of reactive oxygen species (ROS) after exposure to carbon nanomaterials.....	78
Figure 3.3.11. Morphological observation of N2A cells with carbon nanomaterials.....	79
Figure 3.3.12. Viability assay in N2A cells incubated with various functionalized carbon nanomaterials	81
Figure 3.3.13. Effect of serum concentration on cell viability.....	82
Figure 3.3.14. Effect of carbon nanomaterials on microplate reader absorbance.....	84
Figure 3.3.15. Acellular ROS response to carbon nanomaterials.....	86
Figure 3.3.16. Cell growth on SWNT paper.....	87
Figure 4.2.1. FTIR and Raman spectroscopy of NDs.....	100
Figure 4.2.2. Size and morphology of NDs with transmission electron microscopy (TEM)	101
Figure 4.2.3. Dynamic light scattering (DLS) of nanodiamonds.....	103
Figure 4.2.4. Zeta potential of nanodiamonds in water.....	105
Figure 4.3.1. Morphological observation of N2A cells with nanodiamonds	107
Figure 4.3.2. Cytoskeletal changes in N2A cells after exposure to NDs	108

Figure 4.3.3.	Representative confocal microscope images of control N2A cells or cells incubated with 10 µg/ml T-ND from 1-24h	110
Figure 4.3.4.	Confocal microscopy of N2A cells for co-localization of ND-TAMRA and lysosomes after various time points	111
Figure 4.3.5.	Confocal microscopy of N2A cells incubated with 10 µg/ml or 50 µg/ml of T-ND for 24h	113
Figure 4.3.6.	Internalization and localization of NDs into N2A cells with TEM	114
Figure 4.3.8.	Viability assessment of NDs in cells	117
Figure 4.3.9.	Mitochondrial membrane permeability of N2A cells incubated with NDs	118
Figure 4.3.10.	Reactive oxygen species (ROS) generation after Exposure to NDs	120
Figure 4.3.11.	Morphology and proliferation changes in N2A cells Exposed to NDs	121
Figure 4.3.12.	Cell growth on ND substrates	122
Figure 5.2.1.	Size and morphology of Ag nanoparticles with TEM	138
Figure 5.2.2.	Size distributions of Ag nanoparticles from TEM	139
Figure 5.2.3.	Electron microscopy characterization of Ag nanoparticles	142
Figure 5.2.4.	FTIR spectra of Ag nanoparticles	144
Figure 5.2.5.	FTIR of polysaccharide-synthesized Ag nanoparticles	144
Figure 5.2.6.	Raman spectra of Ag nanoparticles	145
Figure 5.3.1.	Binding of Ag nanoparticles to cells	152
Figure 5.3.2.	TEM of Ag nanoparticles inside N2A cells	154
Figure 5.3.3.	N2A cell interactions with Ag nanoparticles	155
Figure 5.3.4.	MTT viability assay	159

Figure 5.3.5.	Reactive oxygen species (ROS) generation after exposure to Ag nanoparticles	160
Figure 7.1.1.	TEM of macrophages incubated with 25 µg/ml Ag28 for 24h.....	178
Figure 7.1.2.	Scanning transmission electron microscopy (STEM) of N2A cells	179
Figure 7.1.3.	Wet imaging of cells under high vacuum	181
Figure 7.4.1.	Summary of UV-Vis spectroscopy of Ag26Disp in PBS..	191
Figure 7.4.2.	The effect of gravitational settling on cell-NM contact	194

LIST OF TABLES

Table 1.1.1. Applications of Nanomaterials and Estimated Global Production	5
Table 1.2.1. Summary of Applications and Recent Biocompatibility Studies of Metal Nanomaterials.....	14
Table 1.4.1. Techniques for Nanomaterial Characterization.....	18
Table 3.1.1. Summary of Carbon Nanomaterial Biocompatibility or Cytotoxicity.....	57
Table 3.2.1 Summary of Carbon Nanomaterial Characteristics.....	65
Table 4.1.1. Biocompatibility Studies of Diamond Particles.....	95
Table 4.2.1. Summary of Nanodiamond Characterization	105
Table 5.2.0. Overview of Ag Nanoparticles and Controls	135
Table 5.2.1. Ag Nanoparticle Concentration Analysis with atomic absorption spectroscopy (AAS) and inductively-coupled plasma optical emission spectroscopy (ICP-OES)	137
Table 5.2.2. Summary of Ag Primary Nanoparticle Size Data	140
Table 5.2.3. Atom % Surface Compositions of Ag Nanoparticles Determined by X-ray Photoelectron Spectroscopy	147
Table 5.2.4. Summary of Ag Size and Charge Characteristics	149
Table 6.1.1 Summary of Carbon Nanomaterial Biocompatibility	167
Table 6.1.2. Summary of Ag Nanoparticle Biocompatibility	168
Table 6.2.1. Summary of effective concentrations that reduced cell viability by 50% after 24h (EC50 values)	173

LIST OF ABBREVIATIONS AND SYMBOLS

μg	Microgram, 10^{-6} g
μl	Microliter, 10^{-6} l
μm	Micrometer, 10^{-6} m
AAS	Atomic absorption spectroscopy
AFM	Atomic force microscope
Ag	Silver
AgNO_3	Silver nitrate
Al	Aluminum
Au	Gold
ATCC	American type culture collection
ATP	Adenosine triphosphate
BET	Brunauer, Emmett, and Teller technique
BSA	Bovine serum albumin
CB	Carbon black
CdO	Cadmium oxide
CdSe	Cadmium selenide
CNM	Carbon nanomaterial
CNT	Carbon nanotube
COOH	Carboxylic acid group

CVD	Chemical vapor deposition
°C	Degrees Celsius
DCFH-DA	Dichlorofluorescein diacetate
dI H ₂ O	Deionized water
DLS	Dynamic light scattering
DMSO	Dimethylsulfoxide
DOE	Department of Energy
EDS	Energy dispersive x-ray spectroscopy
EPA	Environmental Protection Agency
eV	Electron volt
FBS	Fetal bovine serum
FTIR	Fourier-transform infrared spectroscopy
g	Gram
h	Hour
HNO ₃	Nitric acid
H ₂ O ₂	Hydrogen peroxide
H ₂ SO ₄	Sulfuric acid
HEL-30	Keratinocyte cell line
ICP-OES	Inductively-coupled plasma-optical emission spectroscopy
IGC	Inverse gas chromatography
IPA	Isopropyl alcohol
Iron	Fe
Iron Oxide	Fe ₂ O ₃

K	Thousand, Kilo-prefix
kV	Kilo-electron volts
LM	Light microscopy
m	Meter
mg	Milligram
ml	Milliliter
MMP	Mitochondrial membrane permeability
MnO	Manganese oxide
MTT	(3-(4,5-Dimethylthiazol-2-yl)-2,5-diphenyltetrazolium bromide)
MWNT	Multi-walled carbon nanotube
N2A	Neuroblastoma cell line
NaOH	Sodium hydroxide
NASA	National Aeronautics and Space Administration
N/A	Not Applicable
nm	Nanometer, 10 ⁻⁹ m
ND	Nanodiamond
NEST	Nanoscale Engineering Science and Technology Laboratory
NIST	National Institute of Standards and Technology
NM	Nanomaterial
nm	Nanometer
NP	Nanoparticle
NSF	National Science Foundation

NT	Not Tested
OD	Optical density
Ω	Ohm
p	Statistical significance level that demonstrates the probability that the differences observed in the data are due to chance.
PBS	Phosphate buffered saline
PL	Photoluminescence
ppb	Parts per billion
ppm	Parts per million
QD	Quantum dot
QSAR	Quantitative structure-activity relationship
Raman	Raman spectroscopy
ROS	Reactive oxygen species
s	Second
SADP	Selected area electron diffraction pattern
SEM	Scanning electron microscope
SiO ₂	Silica
SOP	Standard operating procedure
SWNT	Single-walled carbon nanotubes
TEM	Transmission electron microscope
TiO ₂	Titanium dioxide
$\mu\text{g/ml}$	Micrograms per milliliter
UV-Vis	UV-visible spectroscopy

V	Volt
W/O	Water-oil microemulsion
wt%	Weight percent
XPS	X-ray photoelectron spectroscopy
XRD	X-ray diffraction
ZnO	Zinc oxide
ZnS	Zinc sulfide
ZP	Zeta potential

CHAPTER 1

INTRODUCTION TO NANOTECHNOLOGY AND NANOMATERIALS

Nanotechnology is revolutionizing the world through scientific advancements in electronic, engineering, medicine, and automotive sectors. In support of the goal of nanotechnology to improve the quality of life and to contribute to economic growth, many government agencies are actively funding nanotechnology research. One such program in the United States, The National Nanotechnology Initiative (NNI), defines nanotechnology as: research and technology development at the atomic, molecular, or macromolecular levels, in the length scale of approximately 1 - 100 nanometer range, to provide a fundamental understanding of phenomena and materials at the nanoscale and to create and use structures, devices and systems that have novel properties and functions because of their small and/or intermediate size (<http://www.nano.gov/html/facts/whatIsNano.html>). Nanotechnology relies on a multidisciplinary approach utilizing the principles of physics, biology, chemistry, materials science, and engineering. Therefore, many of the envisioned benefits of nanotechnology such as computer technology (e.g. molecular switches, memory), precision manufacturing, medical advances (e.g. tools), clean drinking water, and pollution control are long-term goals that rely on skilled teams of scientists and engineers.

1.1 Engineered Nanomaterials

Nanomaterials are defined as having features in the range of 1-100 nm (10^{-7} to 10^{-9} m) in length or diameter. However, engineered nanomaterials are distinguished from naturally occurring nanomaterials due to their deliberate production in the laboratory. The size of nanomaterials can be put into perspective by comparing some common entities: a water molecule is ~ 0.3 nm across, DNA is ~ 2 nm wide, and viruses are ~ 100 nm compared to the diameter of a red blood cell, which is $\sim 7,000$ nm or the width of a single human hair, which is $\sim 80,000$ nm (Fig 1.1.1).

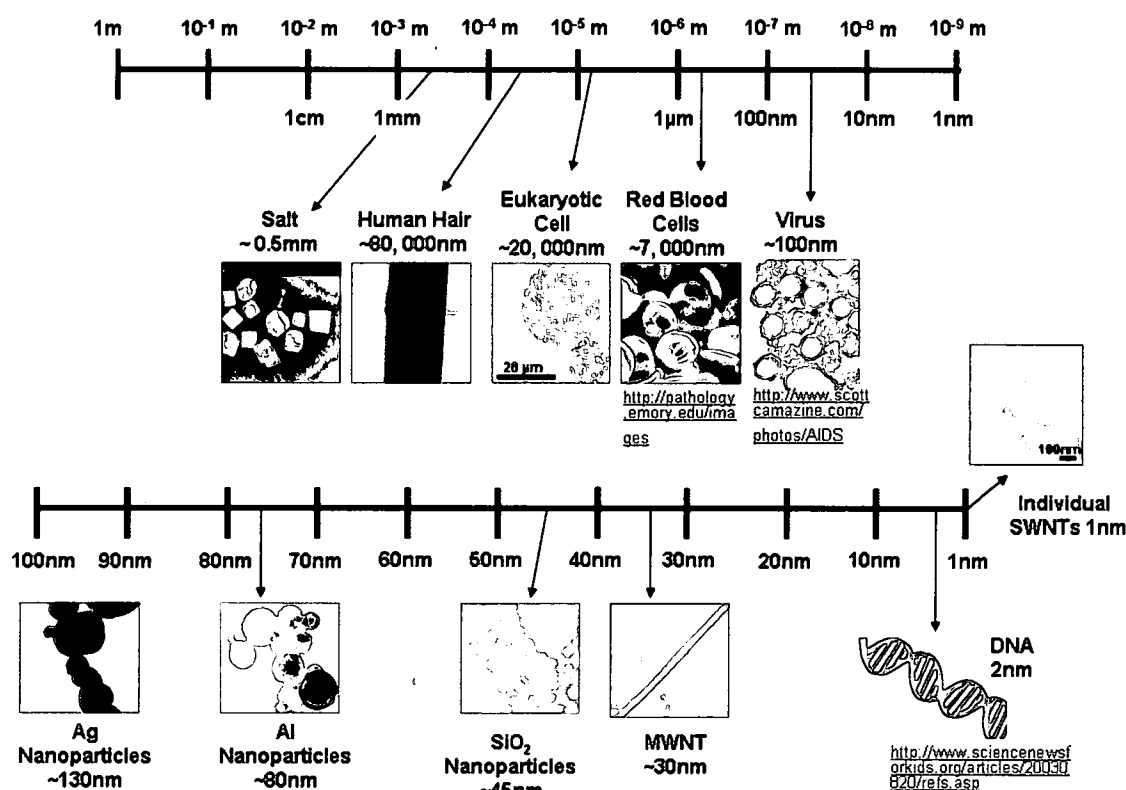


Figure 1.1.1. Comparison of common entities on the metric scale.

Nanomaterials differ from macroscale materials due to their small size, relatively larger surface area to mass ratio, and increased surface chemical reactivity. These differences are manifested in their physical behavior, which changes from classical to quantum physics with decreasing particle size producing novel optical (e.g. transparency, color, absorption/emission wavelength), chemical (e.g. solubility, catalysis), thermal (e.g. melting point), electrical (e.g. conductivity), magnetic, mechanical (e.g. strength, toughness), and biological behavior (e.g. biocompatibility or toxicity, membrane permeability) (Bergamaschi et al., 2006). Therefore, the driving force for understanding and controlling the structure and resultant properties of nanomaterials is the great potential to engineer a range of materials with novel characteristics and enhanced functions (<http://www.nanotek.org.uk>).

The research, production, and use of nanomaterials has not been limited to purely academic or industrial settings, but rather has permeated the marketplace, medical, and military arenas (Fig 1.1.2). Two dominant forms of engineered nanomaterials that are finding widespread use are metal/metal oxide nanoparticles and carbon-based nanomaterials. In the case of metal/metal oxide nanoparticles, they possess unique photocatalytic ability, electrical conductivity, UV absorption, and photo-oxidizing capabilities towards chemical and biological species with applications as additives for polymer nanocomposites, UV blockers, solar cells, anti-viral agents, and scratch-resistant coatings. Consumer products developed from metal and

metal oxide nanoparticles include band-aids and cosmetics containing silver (Ag) nanoparticles for antibacterial activity and transparent sunscreens containing nano-sized titanium dioxide (TiO_2) and zinc oxide (ZnO) (Fig 1.1.2).

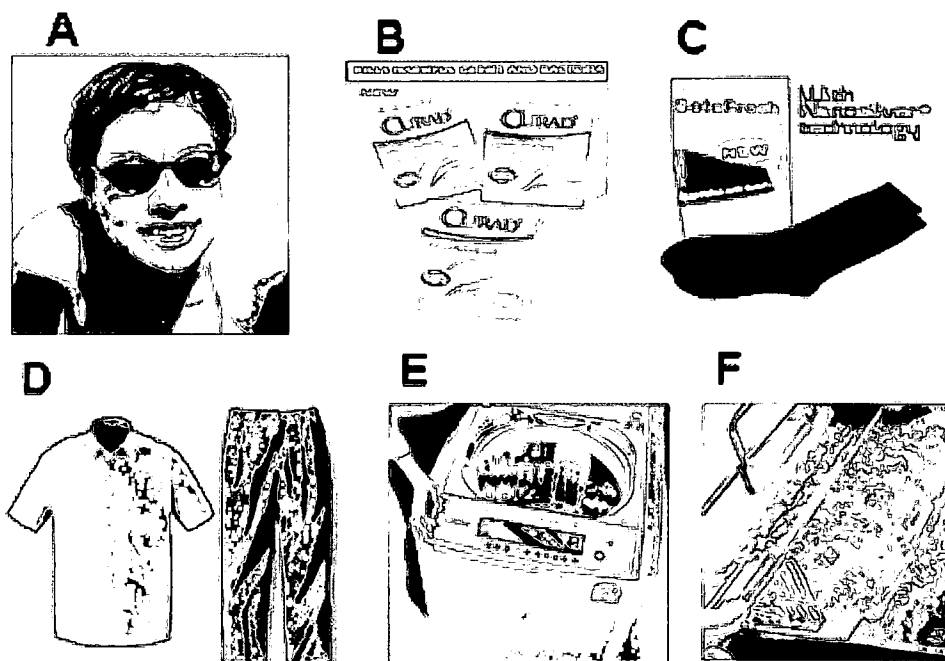


Figure 1.1.2. Common nanomaterial innovations in the marketplace. (A) Transparent Sunscreen/Cosmetics with metal oxides, (B,C) Silver in Band-aids and socks, (D) Stain-free Clothing, (E) Washing Machines that release Ag nanoparticles, and (F) Cooking oil that lasts longer (<http://www.nano.gov/html/facts/appsprod.html>, <http://www.smalltimes.com>).

For carbon nanomaterials, they demonstrate enhanced conductivity, strength, toughness, energy storage, and sensing abilities for applications in nanocomposites, electron field emitters, batteries, fuel cells, electromagnetic shields, drug, gene, or protein carriers, and in novel tissue scaffolds (Bianco et al., 2005; Dai 2006). Many other additional types of nanomaterials (e.g. ceramics, polymers) are being synthesized in the tons per year for use in

structural, cosmetic, information, biotechnology, and environmental applications (Table 1.1.1, Borm et al., 2006; Fig 1.1.1).

Table 1.1.1. Applications of Nanomaterials and Estimated Global Production
(adapted from Borm et al., 2006)

Application	Nanomaterial	Estimated Global Production (Tons/year)	
		2010	2020
Structural	Ceramics, catalysts, coatings, metals, films, composites	10^3	$10^4 - 10^5$
Cosmetic	Metal oxides (ZnO, TiO ₂)	10^3	10^3
Information	SWNT, organic light emitters, nanophosphors	10^2	$>10^3$
Biotechnology	Nanocomposites, encapsulants, delivery, diagnostics, biosensors	1	10
Environmental	Nanofiltration, membranes	10^2	$10^3 - 10^4$

1.2 Nanomaterial Biocompatibility

Although the benefits of nanomaterials are being realized every day, through the development of new and innovative products, the long-term impact on human health and the environment still warrant additional investigation (Thomas and Sayre, 2005; Hoet et al., 2004). In an effort to inform the scientific community, two recent book chapters highlight recent studies on the cytotoxicity and genotoxicity of carbon nanomaterials and the need for advancing the methods used in the toxicity testing of nanomaterials (Schrand et al., 2008a, Schrand et al., 2008b). Some of those concepts will be presented in this section. However, it must be realized that the same properties that allow nanomaterials to efficiently penetrate certain protective membranes in the body and react in a therapeutic manner are also potentially threatening to human health.

Recently, low concentrations of carbon nanotubes (CNT) and other nanomaterial particulates were found in the air during industrial processes (Maynard et al., 2004), but a full assessment of exposure levels has yet to occur. Aerosol release during the handling of unrefined SWNT suggests that concentrations released in laboratories are lower than 53 g/m^3 and glove deposit concentrations are between 0.2-6 mg/hand (Maynard et al., 2004). Current Occupational Safety and Health Administration (OSHA) and National Institute for Occupational Safety and Health (NIOSH) standards limit the exposure of Ag compounds (including solubles, metal dusts, and fumes) to

0.01mg/m³. This limit is intended to reduce the occurrence of argyria, a permanent discoloration of the skin, in the occupational setting (Drake and Hazelwood 2005). Another common health effect of workers exposed to silver dust and particulates is upper and lower respiratory infections. Overall, the toxicity of silver heavily depends upon its form. For example, liquid silver nitrates and chlorides are found to be extremely toxic, but oxides are not. Drake et al. 2005 also report that exposure to large amounts of silver iodide does not lead to argyria. Other studies involving humans have shown that elevated levels of Mn may increase the risk of developing Parkinson's disease (Olanow 2004) suggesting that metal nanoparticles can reach the central nervous system. In environments where large amounts of Mn powder is being produced, such as steel, non-steel alloy, battery, welding, and fuel additive factories, the exposure risk is greatly increased (Hussain et al., 2005).

Both *in vitro* cell culture and animal studies are being used to evaluate nanomaterials for their biocompatibility, or alternatively, their toxicity or potential to induce cell death (Eisenbrand et al., 2002; Barile 1994). The target organs and cells of particular interest are those of the respiratory, integument, and nervous systems due to the likelihood of nanomaterials exposure occurring through inhalation, dermal contact, or ingestion (Fig 1.2.1).

In vitro studies are much more widely used for assessing nanomaterials biocompatibility because of their ability to rapidly and inexpensively produce results and uncover the underlying mechanisms of selected chemicals without the use of animals. For example, data reported on the toxicity testing of series of high energy chemicals in an *in vitro* model (Hussain et al., 2005; Hussain et al., 2002) were used to derive a baseline for extrapolation to a human health risk assessment (Trohalaki et al., 2002). The data obtained from such *in vitro* systems has been used to screen, rank, and predict the acute hazards and mechanisms of compound interactions with animals or humans. The data obtained from basal toxicity studies has been found to be in good correlation with acute toxicity in animals and humans after studying a diverse array of chemicals (Clemedson et al., 2000). However, kinetic factors and target organ specificity were parameters that weakened the correlation. Although, *in vitro* data is not a substitute for whole animal studies, *in vitro* end points that reveal a general mechanism of toxicity can be a basis for further assessing the potential risk of nanomaterial exposure. *In vitro* assays consist of subcellular systems (e.g. macromolecules, organelles), cellular systems (e.g. individual cells, co-culture, barrier systems), and whole tissues (e.g. organs, slices, explants).

Several animal studies have suggested that if nanomaterials are inhaled, the increased number of sites that can interact with cell membranes could lead to nanomaterial lodging, unproductive clearance, and overloading similar to the

situation of inhaled asbestos leading to disease conditions (Kim et al., 2006; Bene et al., 2005; Beck-Speier et al. 2005). Furthermore, if nanomaterials reach the deep alveolar regions of the lung, they may enter the blood stream through the thin walls (<500nm) between the alveolar wall and capillaries (Hoet et al., 2004; Oberdorster, 2000; Zhang et al., 2005a). Other studies have shown the translocation of nanomaterials across cell membranes into critical organelles such as mitochondria (Foley et al., 2002) or translocation from the nasal and tracheobronchial regions of the respiratory tract to various nerves and even cross the blood brain barrier (Oberdorster et al. 2005, Wang et al., 2004).

Further changes in the dispersion or agglomeration of nanomaterials once inside the body or in contact with physiological solutions become a major issue unless the particles have surface chemical modifications or surfactants are added to create effective separations between the easily attracted nanoparticles. These characteristics are critical before any conclusions can be made regarding biocompatibility or size-dependent toxicity. Physical methods to disperse the nanoparticles include vortexing and sonication. Although vortexing increases dispersion, it is transient and temporary and the added effects of processing on nanomaterial properties must be taken into account.

Therefore, it is critical for engineers to work with toxicologists to provide thorough characterization of nanomaterial properties before testing or use in biological systems. Through these collaborations, many studies are beginning to find that the same material properties that influenced the biocompatibility of micro-sized materials apply to nanomaterials as well. These factors include increased surface area, chemical reactivity, and ability of the material to generate free radicals (e.g. quartz or particulates in air pollution) or the physical dimensions and solubility of the particles (e.g. fibers such as asbestos) (<http://www.nano.org.uk>). However, these properties may be more prominently impact the biocompatibility of nanomaterials compared to their bulk counterparts due to the extremely small size, large surface area, and increased reactivity of nanomaterials compared to bulk materials. In support of this notion, studies have found differential biocompatibility between micro- and nano-sized materials such as TiO₂ (Oberdorster, 2000), polystyrene (Brown et al., 2001), mineral fibers (Donaldson and Tran, 2002), and Ag nanoparticles (Hussain et al., 2005, Braydich-Stolle et al., 2005). Other physico-chemical properties such as shape (e.g. carbon nanotubes vs. nano-onions; TiO₂ rods vs. dots, Au spheres vs. rods), crystal structure (e.g. TiO₂ anatase vs. rutile), porosity, surface chemistry (e.g. hydrophilic vs. hydrophobic), charge, and release of soluble impurities are suggested to play a role in the biocompatibility of nanomaterials (Ding et al., 2005; Brown et al., 2001; Muller et al., 2004; Warheit et al., 2006, Soto et al. 2005, Pal et al., 2007, Chithrani et al., 2006, Hoshino et al., 2004, Oberdorster et al., 2005,

Hohr et al., 2002, Rehn et al., 2003, Xu et al., 2006, Chien et al., 2006; Brown et al., 2000). The periodic table below demonstrates the wide variety of elements that have recently been examined in *in vitro* nanomaterial biocompatibility studies while many more compounds are being pursued in nanotechnology applications (Fig 1.2.2).

Periodic Table of the Elements															
1	2													10	11
3	4													18	19
11	12													36	37
19	20	21	22	23	24	25	26	27	28	29	30	31	32	34	35
37	38	39	40	41	42	43	44	45	46	47	48	49	50	52	53
55	56	57	58	59	60	61	62	63	64	65	66	67	68	70	71
87	88	89	90	91	92	93	94	95	96	97	98	99	100	102	103
107	108	109	110	111	112	113									

* Lanthanide Series	Ce	Pr	Nd	Pm	Sm	Eu	Gd	Tb	Dy	Ho	Er	Tm	Yb	Lu
+ Actinide Series	Th	Pa	U	Np	Pu	Am	Cm	Bk	Cf	Es	Fm	Md	No	Lr

Figure 1.2.2. Periodic table of the elements. Circled elements have recently been examined in *in vitro* nanomaterials biocompatibility studies (<http://serc.carleton.edu/images/usingdata/nasaimages/periodic-table.gif>).

In vitro studies from our laboratory with metal/metal oxide nanoparticles (e.g. Ag, Al, Au, Fe₂O₃, MnO, TiO₂) and inorganic nanoparticles (e.g. SiO₂) have demonstrated two primary factors responsible for nanomaterial biocompatibility: elemental composition and size (Table 1.2.1). As shown in the table, several nanomaterials remain biocompatible with cells in culture at concentrations >250 µg/ml (e.g. Al, Fe₂O₃, TiO₂), while many other

nanomaterials were not tested at such high concentrations, but rather limited to 100 µg/ml. The least biocompatible nanomaterials were Cu and Ag with increasingly smaller nanoparticles become more toxic at similar mass concentrations to larger sized nanoparticles of the same composition. Another nanomaterial that demonstrated size-dependent decreases in viability was SiO₂, but two different studies produced different threshold values for biocompatibility, which were likely due to the different cell-types or properties of the materials used in the studies. This was also seen in studies with Al, Ag, and Fe₂O₃. Additional factors that were found to influence the results were changes in phagocytotic ability, dopamine depletion, generation of reactive oxygen species, and cell signaling pathways.

Table 1.2.1. Summary of Applications and Recent Biocompatibility Studies of Metal Nanomaterials

NM	Applications	Non-toxic Dose	NM Size	Cell Type	Reference
Al	Fuel additive, Coatings, Thin films	$\geq 250 \mu\text{g/ml}$, $> 50 \mu\text{g/ml}$	50, 80, 103, 120nm	Mac, BRL-3A, HEL-30	Wagner et al., 2007, Hussain et al., 2005, Murdock et al., 2007
Ag	Anti-microbial, anti-bacterial, anti-viral, anti-biotic and anti-fungal	25-50 $\mu\text{g/ml}$ (PC-12, 15nm), 24 $\mu\text{g/ml}$ (BRL-3A, 15nm), 8.75 $\mu\text{g/ml}$ (C18-4, 15nm), 19 $\mu\text{g/ml}$ (BRL-3A, 100nm)	15, 30, 55nm (100nm)	PC-12, BRL-3A, C18-4	Hussain et al., 2006, Hussain et al., 2005, Braydich-Stolle et al., 2005
Au	Catalysts, Photonics, Coatings, Cancer Therapy	$> 50 \mu\text{g/ml}$ (72h)	4-18nm	K562	Connor et al., 2005
Cu	Coating, Lubricant, Anti-microbial, Catalyst	$\sim 1-5 \mu\text{g/ml}$	40, 60, 80nm	Mac	Unpublished Results
Fe ₂ O ₃	Imaging, Detoxification, Drug Delivery	$> 250 \mu\text{g/ml}$, $> 500 \mu\text{g/ml}$	30, 47nm	BRL-3A, h-TERT BJ1	Hussain et al., 2005, Gupta et al., 2004
MnO	Catalyst, Batteries	$> 100 \mu\text{g/ml}$	40nm	PC-12	Hussain et al., 2006
MoO ₃	Catalyst, Pigment, Corrosion inhibitor, Lubricant	$> 100 \mu\text{g/ml}$, 75 $\mu\text{g/ml}$ C18-4, 30nm)	30, 150nm	BRL-3A, C18-4	Hussain et al., 2005, Braydich-Stolle et al., 2005
SiO ₂	Cell Delivery	1000 $\mu\text{g/ml}$	10, 26, 145nm	COS-1	Kneuer et al., 2000
TiO ₂	Paint, Cosmetics	$> 250 \mu\text{g/ml}$, $> 50 \mu\text{g/ml}$	40nm	C18-4, HEL-30	Hussain et al., 2005, Murdock et al., 2007

Therefore, as we learn more about the characteristics of nanomaterials that make them useful in technological advances, we must also take responsibility to protect the people synthesizing them through proper protective equipment and exposure limits, understand the undesirable properties that accompany any new nanomaterials-based products, and properly dispose of waste products, which are released into the environment. Currently, several government regulatory agencies, such as the Food and Drug Administration (FDA), NIOSH, and OSHA are putting in place guidelines while working closing with industry and academia to monitor nanomaterial exposure risk. At the same time, the benefits of novel nanomaterial products (e.g. bio-probes, delivery vehicles, tissue scaffolds, diagnostics, and anti-microbials) are being weighed against their risks by highly skilled, multidisciplinary teams providing links between nanomaterials characteristics and biocompatibility.

1.3 Statement of Work and Specific Aims

The purpose of these studies is to elucidate the material properties and conditions that contribute to nanomaterial biocompatibility or toxicity in relevant cell types such as lung, neuronal, and skin cell lines.

1.3.1 Specific Aims

- (1) Characterize nanomaterials for size, morphology, composition, concentration, purity, agglomeration state, charge, and reactivity.

- (2) Assess cell-nanomaterial interactions such as contact, changes in cellular morphology, internalization, and localization over 24h with an emphasis on an engineering interpretation for nanomaterial changes related to the cell culture environment.

- (3) Determine the biocompatibility of cells to carbon and metal nanomaterials of different size/morphology and chemical surface compositions over 24 h.

1.4 Research Description

Due to their increased production and proposed uses in consumer products, various carbon (e.g. nanotubes, nano-sized carbon black, and nanodiamonds) and silver nanomaterials (e.g. spherical nanoparticles synthesized via hydrocarbon or polysaccharide synthesis) were chosen for examining the relationship between nanomaterial characteristics and *in vitro* biocompatibility

Nanomaterial characteristics of interest included: morphology, size distribution, composition, purity, surface functionalization, agglomeration in various solutions, and charge, which were investigated with a variety of techniques (Table 1.4.1, See Materials and Methods for descriptions of techniques).

Table 1.4.1. Techniques for Nanomaterial Characterization

Material Property	Characterization Technique
Size Distribution (primary particles)	SEM/TEM/AFM
Agglomeration State	DLS/LM
Shape	SEM/TEM/AFM
Composition	EDS/ICP/AAS
Internal Structure	TEM
Surface Area	BET
Chemistry	FTIR/Raman/XPS
Surface Charge	ZP
Crystal Structure	XRD/SADP
Plasmon Resonance	UV-Vis
Concentration	AAS/ICP

In vitro cell cultures were incubated with carbon and metal-based nanomaterials for 24h, then examined for changes in cellular morphology and nanomaterial internalization with light microscopy, an ultrahigh resolution imaging system (Skebo et al., 2007), or transmission electron microscopy (Schrand et al., 2007a).

The dose response of cells to carbon and metal nanomaterials of different size/morphology and chemical surface compositions over 24 h was assessed with biochemical endpoints based on mitochondrial function (e.g. MTT assay for reduction of tetrazolium salt), mitochondrial membrane permeability (MMP), breakdown of the cellular permeability barrier (e.g. lactase dehydrogenase (LDH) assay), and the generation of reactive oxygen species (ROS).

Throughout these studies, an engineering interpretation was applied to define the interactions specific to nanomaterials in the cell culture environment. First, the interactions of NM with media components leading to changes in agglomeration were considered based on primary size/shape, surface chemistry (e.g. coating, formation of oxide, or reactivity), surface charge, concentration, time, temperature, and gravitational settling (Fig 1.4.1).

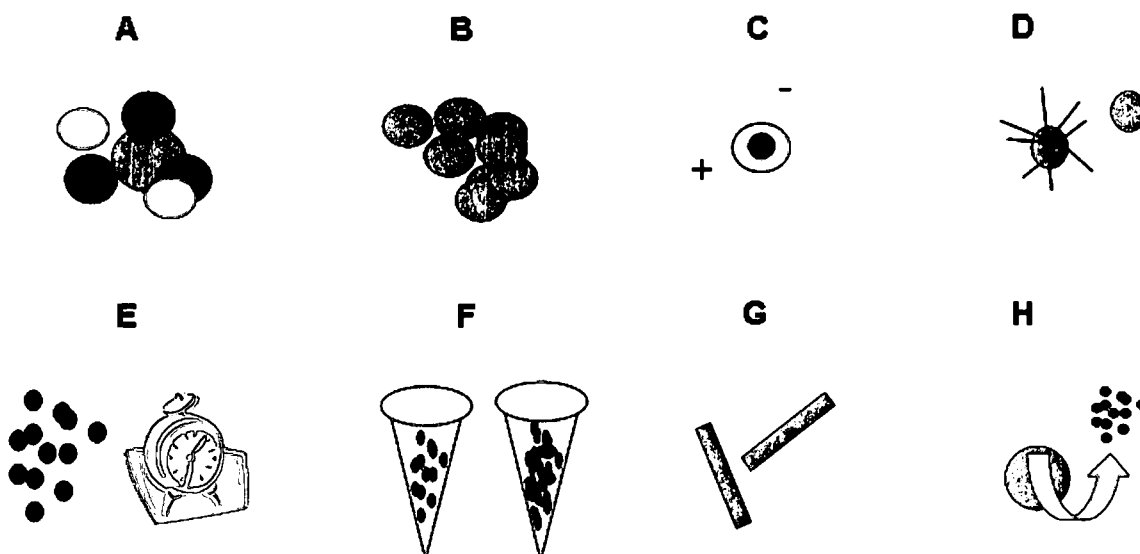


Figure 1.4.1. Solution interactions of nanomaterials. (A) Interaction with media components, (B) Formation of hard aggregates, (C) Electrostatic interactions, (D) Influence of surface chemistry, (E) Effect of concentration, time, sedimentation rate, and processing effects, (F) Effect of Temperature, (G) Steric repulsion and hydrophobic/H-bonding effects, and (H) Composition/dissolution of impurities.

Once cells were exposed to NM, interactions based on electrostatic attraction or repulsion to the cell membrane followed by internalization and localization to specific locations within the cell were assessed (Figure 1.4.2). Nanomaterial properties such as primary size/shape, agglomeration state, presence of impurities, surface chemistry, charge, concentration, and cell-specific effects were taken into account. Through these studies, a paradigm

for the relationship between nanomaterial characteristics and *in vitro* biocompatibility was developed based on results in carbon and metal-based nanomaterials.

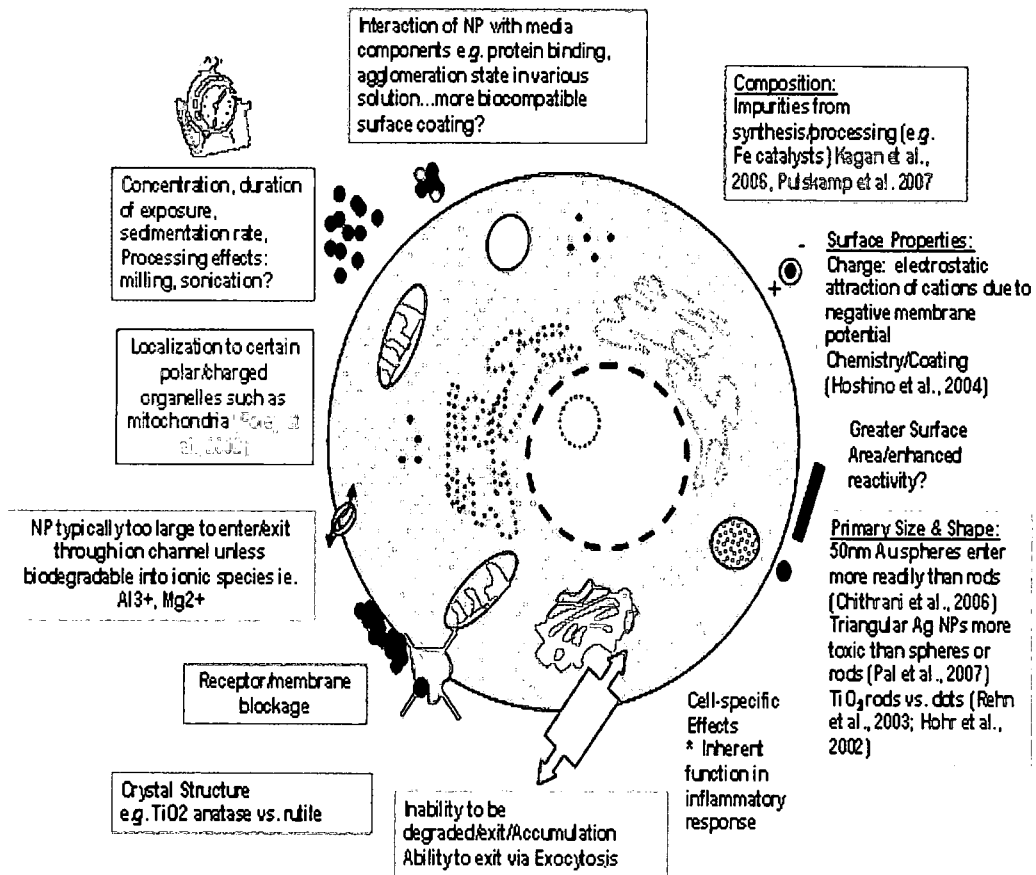


Figure 1.4.2. Schematic of the possible interactions of nanomaterials with a cell in culture (Schrand et al., 2008b).

CHAPTER 2

EXPERIMENTAL METHODS

2.1 Nanomaterials and Chemicals

2.1.1 Carbon Nanomaterials

Carbon Nanotubes. Multi-walled carbon nanotubes were purchased from Tsinghua University (Beijing, China) and single-walled nanotubes (SWNTs) were received from Rice University (Houston, TX). Both were synthesized by chemical vapor deposition (CVD), which is widely used because of its low cost and high yield. The chemical bonds of a hydrocarbon gas source (e.g. methane, carbon monoxide, or acetylene) are broken with energy from a hot filament, microwave, radio frequency, or electron cyclotron resonance microwave. Carbon molecules then diffuse toward the substrate containing catalysts such as cobalt, iron, or nickel to form carbon nanotubes. Figure 2.1.1 shows a conventional thermal CVD apparatus setup (<http://students.chem.tue.nl/ifp03/synthesis.html>).

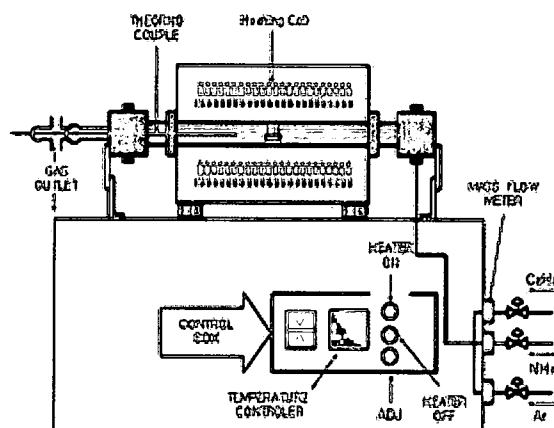


Figure 2.1.1. Conventional thermal chemical vapor deposition (CVD) apparatus for the synthesis of carbon nanotubes (<http://students.chem.tue.nl/ifp03/synthesis.html>).

Carbon Black. Carbon black was received from Shell/Cabot (Boston, MA) and was synthesized using an oil furnace process. The oil feedstock is injected into a high temperature reactor where the hydrocarbon is cracked and dehydrogenated to form carbon with a quasi-graphitic microstructure (<http://www.cabot-corp.com>). Since furnace-type carbon blacks are made from petroleum feedstocks, carbon black can contain varying amounts of other elements, such as sulfur, which can be present at levels above 1 wt%.

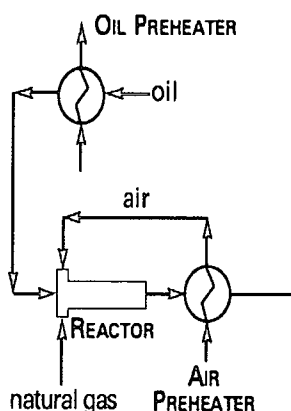


Figure 2.1.2. Synthesis of carbon black (Carbon Black User's Guide from the International Carbon Black Association, 2004).

Nanodiamonds. Nanodiamonds (NDs) were generously supplied by NanoCarbon Research Institute Ltd in Japan and were synthesized according to previously-reported detonation techniques (Krüger et al., 2005, Greiner et al., 1988). Although the industrial chemical processing of detonation nanodiamond results in surface functional groups such as -COOH , -OH , $\text{-SO}_3\text{H}$, and NH_2 (Dolmatov, 2001), the as-received nanodiamonds (ND-raw) were further subjected to purification with acid (70% HNO_3 and 98% H_2SO_4 at a ratio of 1:3) or strong base (NaOH , $\text{pH} \sim 14$). Other detonation nanodiamonds (T-ND) conjugated to a fluorescent dye derivative of rhodamine (TAMRA) were purchased from ITC, Inc.

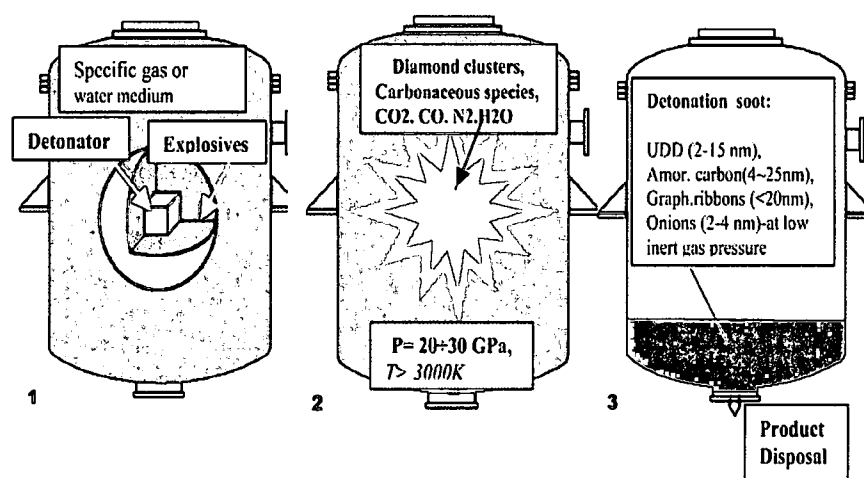


Figure 2.1.3. Synthesis of detonation nanodiamonds (Shenderova et al., 2002).

2.1.2 Silver Nanoparticles

Hydrocarbon synthesized silver nanoparticles (Ag13, Ag28, Ag43) were generously received from Dr. Karl Martin, Novacentrix Co. (Austin, TX). According to the manufacturer, hydrocarbon synthesized Ag nanoparticles were synthesized out of a plasma gas, which includes silver and a mixture of other gases in a proprietary form including hydrocarbons. As the plasma cools, graphitic carbon and silver are both concurrently formed, with the resulting hydrocarbons reducing the ability of the silver nanoparticles to sinter together. The approximately 2% amorphous carbon (confirmed with XRD and EDS) in the final product is not chemically bound to the silver, but rather surrounds it as a matrix to prevent agglomeration.

Polysaccharide synthesized silver nanoparticles (Ag10Disp, Ag26Disp, Ag52Disp) were received from Dr. Dan Goia of Clarkson University (Potsdam, NY). In contrast to the hydrocarbon synthesized Ag nanoparticles, the polysaccharide synthesized Ag nanoparticles were produced through a reduction of silver ions in an aqueous solution by a naturally occurring polysaccharide polymer (MW ~250,000). In this case, the Ag is reduced by the functional groups inserted on the extended polysaccharide chains. The nanoparticles formed are wrapped into the polymer and separated from the surrounding environment.

2.1.3 Cell Culture Chemicals

Dulbeco's modified essential media (DMEM), Ham's Nutrient Mixture F-12K (Kaughn's Modification), and normal fetal bovine serum (FBS) were purchased from American type culture collection (ATCC, Manassas, VA). Pencillin-streptomycin, and 3-(4,5-dimethylthiazol-2-yl)-2,5-diphenyltetrazolium bromide (MTT) were purchased from Sigma Chemical Company (St. Louis, MO). 10x Phosphate buffered saline (pH 7.4) and 2.5% trypsin were purchased from Gibco Invitrogen™ Corporation (Carlsbad, CA). Dichlorofluorescein diacetate (DCFH-DA) was purchased from Molecular Probes™ (Carlsbad, CA). Cadmium oxide (CdO-1000nm) was purchased from Fluka Chemicals. Silver nitrate (AgNO₃, Sigma) and Cadmium oxide (CdO, Fluka Chemical Company) were used as positive controls in viability and mitochondrial membrane permeability assays due to their ability to cause significant ($p < 0.05$) decreases in cell viability and mitochondrial function at doses as low as 0.5 µg/ml. Serial dilutions of hydrogen peroxide in PBS were derived from 30% H₂O₂ (Sigma) to create a standard curve for reactive oxygen species (ROS) assays.

2.2. Preparation of Nanomaterial Solutions

Nanomaterials were diluted to 1 mg/ml stock concentrations in deionized, sterile water. A brief sonication for 5-10 s at 30 Watts (Cole Palmer probe sonicator) was performed to increase dispersion in solution. Immediately prior to each experiment, the stock solutions were diluted to final dosing concentrations ranging from 0-100 $\mu\text{g/ml}$ in cell culture media and vigorously mixed by vortexing (Fig 2.2.1).

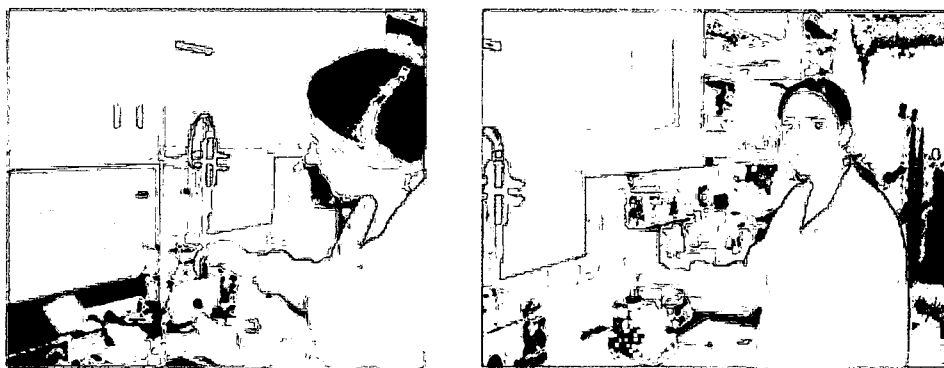


Figure 2.2.1. Probe sonicator and vortexer used in these studies.

2.3 Nanomaterial Characterization

Nanomaterial characteristics were assessed in the as-synthesized form prior to use in cell systems or after dispersion in the appropriate aqueous media for cell dosing. Nanomaterial size and dimension were determined with ultrahigh resolution light microscopy, scanning electron microscopy (SEM), or transmission electron microscopy (TEM). Several techniques were used to determine nanomaterials composition such as energy dispersive x-ray analysis (EDS) and inductively-coupled plasma optical-emission spectroscopy (ICP-OES). Concentrations of the nanomaterials were verified with atomic absorption spectroscopy (AAS). Chemistry was examined with Fourier-transform infrared spectroscopy (FTIR), Raman spectroscopy, and x-ray photoelectron spectroscopy (XPS). Solution characteristics were measured with dynamic light scattering (DLS), zeta potential, and UV-visible spectroscopy for size, charge, and composition, respectively.

2.3.1 Electron Microscopy

Electron microscopes were developed in the early 1930's due to a scientific desire to see the fine details of the interior structures of cells, which required magnifications of 10,000 times or greater. The transmission electron microscope (TEM) is arranged identically to the light transmission microscope except that instead of obtaining an image with visible light, it uses a high voltage, focused beam of electrons. The electrons are emitted from a cathode, which can be considered similar to a very strong light bulb filament.

Electromagnetic lenses are used to form and focus the electron beam down the column where it directly interacts with the sample to generate a signal, which is detected and converted into an image. The interactions of the electron beam with a sample and the resultant signals generated are shown in Figure 2.3.1. Although the maximum resolution of the (TEM) is limited by spherical and chromatic aberration, it currently reaches below 1nm when imaging atomic lattice planes. Therefore, nanomaterials, cell organelles, membranes, protein filaments, and nucleic acids can be clearly imaged in TEM once they have been correctly prepared.

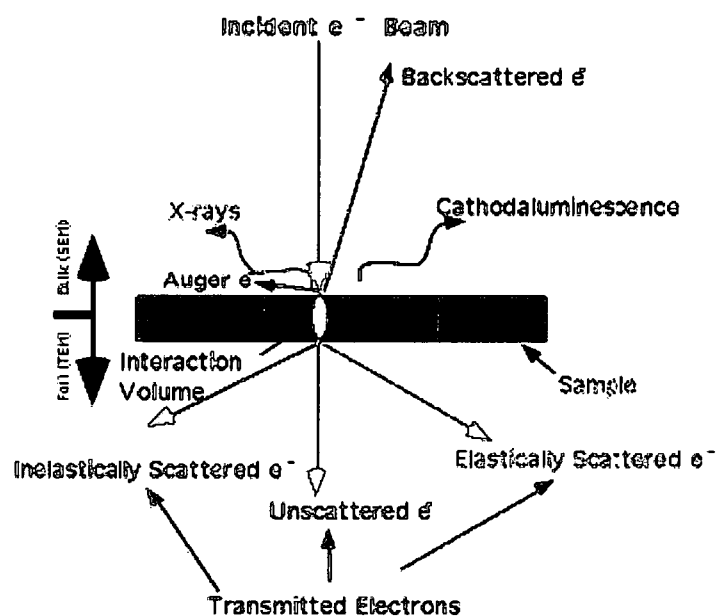


Figure 2.3.1. Schematic representation of sample-electron beam interactions. These various interaction are used to generate signals in SEM and TEM (<http://www.unl.edu/CMRacem/interact.htm>).

Nanomaterials were examined for size and morphology with a Hitachi H-7600 W-tip TEM at accelerating voltages from 100-120 kV and associated Advanced Microscopy Techniques (AMT) imaging software (Fig 2.3.2). Briefly, nanomaterials were drop cast onto formvar-carbon coated TEM grids

at concentrations of typically 1 mg/ml or less and dried before imaging in TEM. Information on mean size was calculated from a random field of view in addition to images that show general morphology of the nanomaterials. Over 100 particles were counted and measured to determine average sizes, standard deviations, and size distributions.

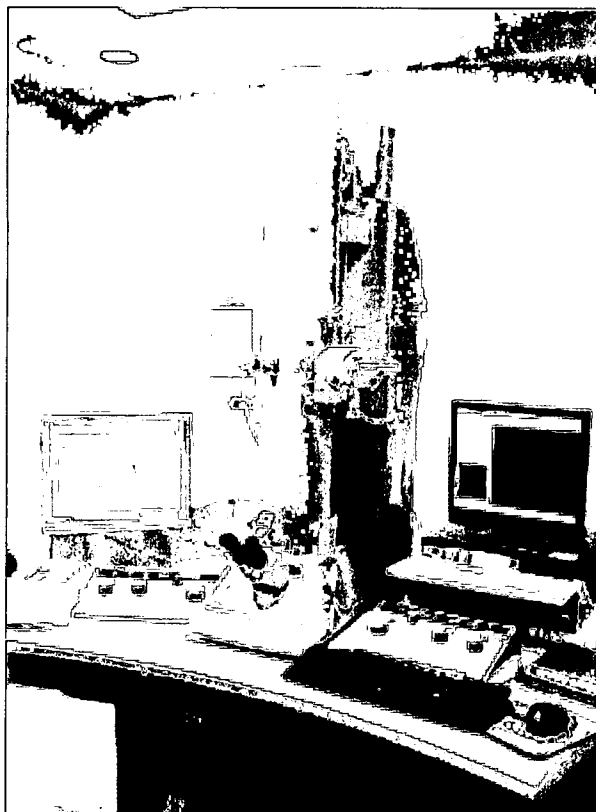


Figure 2.3.2. Hitachi H-7600 transmission electron microscope (TEM).

In contrast to TEM, where electrons are transmitted through the sample, scanning electron microscopy (SEM) produces images by rastering a primary electron beam across the sample surface while detecting secondary or backscattered electrons, which are emitted from the surface. Therefore, the images obtained in an SEM provide a 3-D quality and greater resolution than light microscopy, but about an order of magnitude lower resolution than TEM.

Most SEM spatial resolutions are greater than 4nm and magnifications can reach above 500, 000 times. While secondary electrons contribute to surface topography images, backscattered electrons and characteristic x-rays can provide compositional information. The main disadvantage of SEM is for samples which are not electrically conductive such as many biologicals. Therefore, sample charging is a problem and the use of environmental scanning electron microscopy (ESEM) or simply dehydrating and coating the surface with a thin (1-2nm) carbon or metal film may aid in reducing these problems. In these studies, a Hitachi S-4800 field emission tip SEM was used at accelerating voltages between 5-30kV after depositing the nanomaterials onto aluminum stubs with double-sided carbon adhesive tape (Fig 2.3.3). If coating the sample was required due to charging, a thin sputtered layer of gold was applied.



Figure 2.3.3. Hitachi S-4800 high resolution field emission scanning electron microscope (HRSEM).

2.3.2. Atomic Absorption Spectroscopy (AAS)

Flame spectroscopy techniques are used to quantitatively determine the amount of an element in a sample. A homogenous liquid is introduced into a flame where the thermal and chemical reactions create free atoms capable of absorbing, emitting, or fluorescing at characteristic wavelengths (Fig 2.3.4). Atomic absorption spectroscopy (AAS) was developed by Sir Alan Walsh in the mid 1950's by emitting a narrow spectral line of the characteristic energy used to excite the free atoms formed in the flame. The decrease in energy (absorption) is then measured. The absorption is proportional to the concentration of free atoms in the flame, given by the Beer-Lambert Law. The Beer-Lambert Law states that the absorbance (A) of a solute is determined by its absorptivity (a), concentration (c), and optical path length (l) through the formula:

$$A = ac l$$

In these studies, the samples were first screened with x-ray fluorescence (XRF) to determine the elements present by drop casting the solutions onto evaporated mylar film (EDAX Eagle II micro-fluorescence instrument). For AAS, nanomaterials were digested in strong acids before analysis (Varian AA240 Atomic Absorption Spectrometer). Sample concentrations were interpolated from calibrated standards. This method is considered comparative because, for a given solute under defined solution conditions, absorptivity (extinction coefficient) is a constant.

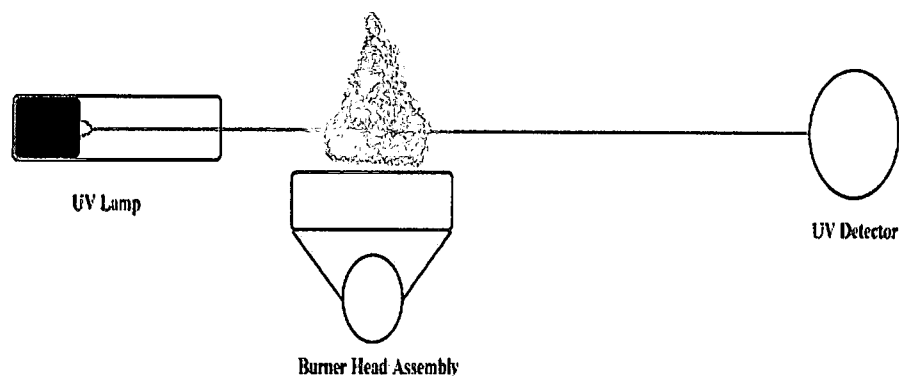


Figure 2.3.4. Schematic representation of atomic absorption spectrometer set-up. (<http://www.gmu.edu/departments/SRIF/tutorial/aas/aas3.htm>).

2.3.3. Inductively Coupled Plasma-Optical Emission Spectroscopy (ICP-OES)

Inductively coupled plasma optical emission spectroscopy (ICP-OES) is a major technique for elemental analysis consisting of vaporization, atomization, and excitation of the elements present in a sample. The solid sample is dissolved in strong acids, then mixed with water before being introduced as an aerosol vapor into the plasma. Atomization occurs within the plasma where atoms get excited to both atomic and ionic states resulting in the emission of light (photons) with characteristic wavelengths for each element. Because of their different excitation energies, different emission lines will have maximum intensities at different vertical positions in the plasma. The light is recorded by one or more optical spectrometers and calibrated against standards providing quantitative analysis of the original sample. The parts of a typical ICP machine include a sample delivery system, IC plasma to generate the signal, one or more optical spectrometers to measure the signal, and a computer for controlling the analysis (Fig 2.3.5).

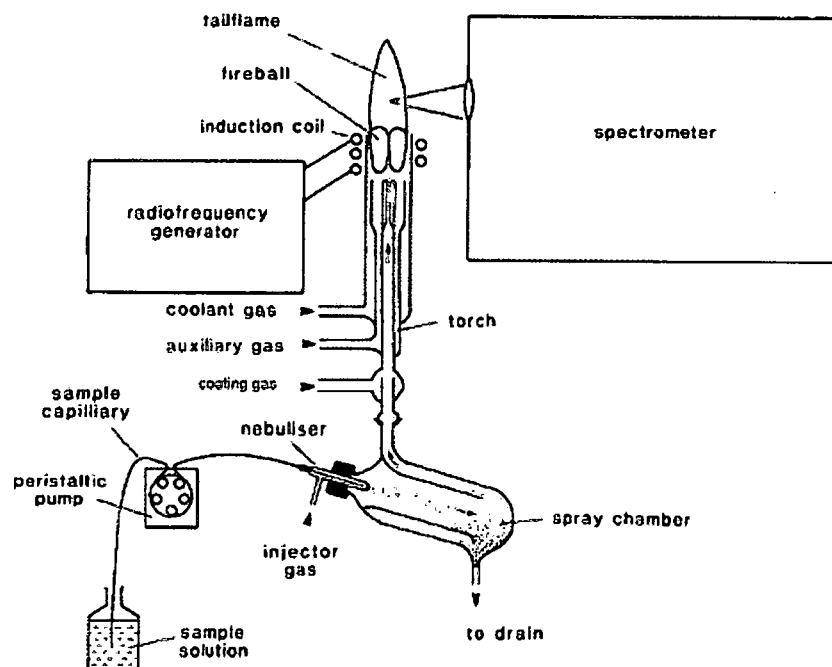


Figure 2.3.5. Schematic diagram of a typical ICP-OES instrument (<http://www.icp-oes.net/Instruments.html>).

In these studies, the samples were first screened with x-ray fluorescence (XRF) to determine the elements present by drop casting the solutions onto evaporated mylar film (EDAX Eagle II micro-fluorescence instrument). ICP-OES was performed to quantitatively analyze elemental composition expressed in wt% (Thermo-Elemental IRIS Advantage DUO machine). Prior to analysis, the instrument optics were calibrated using an internal mercury lamp emission source. The detection limit in ICP-OES for the 328.068nm line of silver is 3ppb. However, a more reasonable estimation of sensitivity is 30ppb and the instrument should be able to accurately measure concentrations above this level. Other detection limits for elements of the periodic table are color-coded in the figure below (Figure 2.3.6).

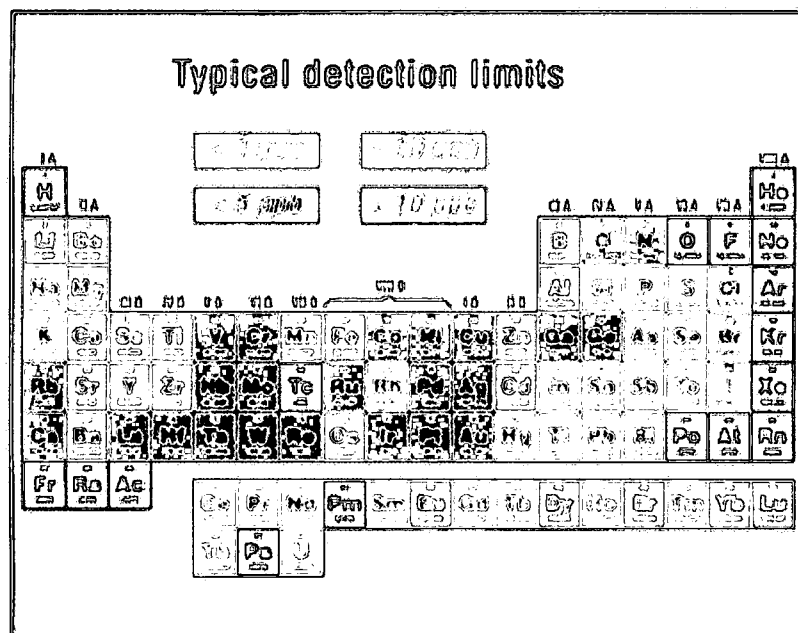


Figure 2.3.6. Detection limits for elements of the periodic table. Color coding is for concentrations in parts per billion (ppb) with ICP-OES (http://www.icp-oes.net/detection_limits.htm).

2.3.4 Raman Spectroscopy

Raman spectroscopy measures inelastically scattered light following excitation with a monochromatic laser source, which usually lies in the visible or near-UV region. When light is scattered from a molecule most photons are elastically scattered. However, a small fraction of light (approximately 1 in 10^7 photons) is scattered at optical frequencies different from, and usually lower than, the frequency of the incident photons. This process leading to inelastic scattering is termed the Raman effect and was first observed by C.V. Raman in 1928. Scattering occurs after changes in vibrational, rotational, or electronic energy of a molecule. The difference in energy between the incident photon and the Raman scattered photon is equal to the energy of a

vibration of the scattering molecule. A plot of intensity of scattered light versus energy difference is a Raman spectrum.

The advantages of Raman spectroscopy include suitability for aqueous samples, avoidance of the intense infrared (IR) absorption of water, and sharper, narrower, more distinguishable spectral bands. Materials with strong Raman scattering contain moieties with distributed electron clouds, such as carbon-carbon double bonds. The pi-electron cloud of the double bond is easily distorted in an external electric field. Bending or stretching the bond changes the distribution of electron density substantially, and causes a large change in induced dipole moment.

In these studies, a Renishaw inVia Raman microscope was used at 514nm with a He-Ne laser (Fig 2.3.7). The excitation power was 50 mW, 60% laser power, 5 scans to improve the signal-to-noise ratio, and 20s of exposure time with a 4 cm^{-1} slit width. The spectra were obtained in the range of 100-200 wavenumber (cm^{-1}).

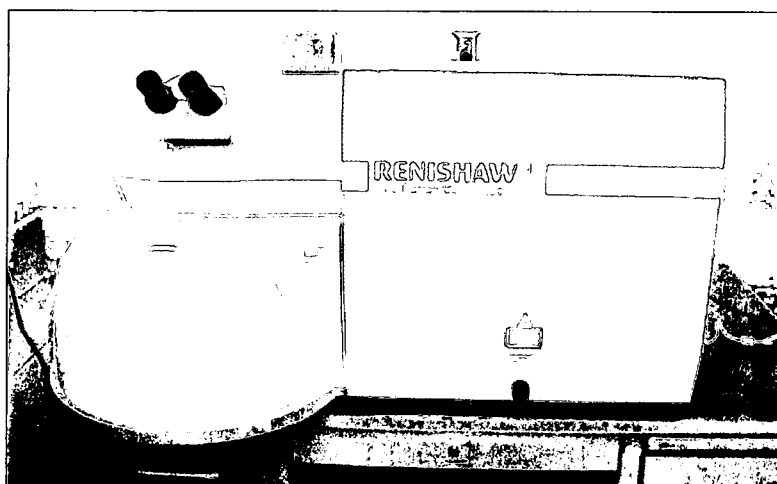


Figure 2.3.7. Renishaw invia Raman microscope.

2.3.5 FTIR Spectroscopy

Fourier Transform infrared (FT-IR) spectroscopy is based on molecular vibrations and monitors the transition between vibrational energy levels. The IR spectra of most materials consist of a large number of absorption or energy exchanges between discrete light quanta and mechanical motions such as vibrational and rotational modes of the molecules, which are excited by the absorption of IR radiation. The IR region of the spectrum extends from the visible region until it overlaps the microwave or very short radar range. The spectra is further subdivided into near infrared (NIR), mid infrared (MIR), and far infrared (FIR) and is characterized by the number of waves per centimeter or wavenumber (cm^{-1}). An IR spectrum is obtained by scanning the intensity of IR radiation before and after passage of the IR beam through the sample and is represented by the equation:

$$T = I_S/I_R$$

Where T is the transmittance, I_s the intensity of the IR beam after transmittance and I_R , the intensity of the beam before transmittance. In most cases, absorbance (A) is related to transmittance (T) through the equation:

$$A = -\log T$$

The absorbance of a sample at a given wavelength is directly proportional to the concentration of the sample according to Beer's Law. The advantages of FTIR include small sample size, rapid, sensitive, ability to perform many computer-generated scans to improve signal-to-noise ratio, no light scattering or fluorescent effects, relatively inexpensive, and simple to use.

In these studies, infrared spectra were obtained on a Perkin Elmer Spectrum One Fourier transform spectrometer (Fig 2.3.8). Spectra were collected with Spectrum software by Perkin Elmer over a range of $4000\text{--}450\text{ cm}^{-1}$, scan speed of 0.2 cm/s , and at a spectral resolution of 4 cm^{-1} . Samples were prepared by mixing the nanomaterials with potassium bromide (KBr), then pressing into pellet. A background spectrum was obtained before each measurement using a clean stainless steel plate and a KBr pellet alone at the same instrumental conditions used for sample acquisition. Purely ionic minerals such as NaCl or KBr display no pronounced absorption peaks over the mid-infrared band and every subsequent FTIR spectra obtained had the KBr background removed.

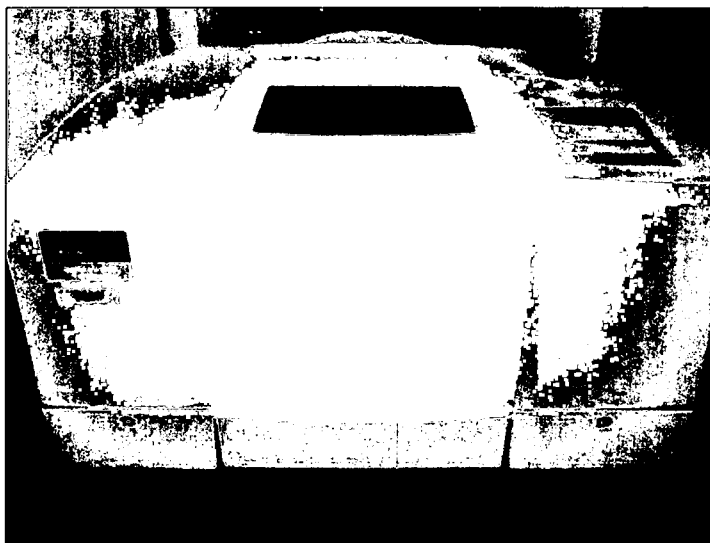


Figure 2.3.8. Perkin Elmer Spectrum One FTIR Instrument.

2.3.6. X-ray photoelectron spectroscopy (XPS)

X-ray photoelectron spectroscopy (XPS) is a primary measurement of the kinetic energy of electrons that are ejected from a sample bombarded with x-rays, which allows the calculation of electron binding energies that are element specific (Murray, 2004 Class Notes). XPS is used to detect elements (except hydrogen) present at levels > 0.5 atom % within approximately 3 nm of a sample surface. In this study, x-ray photoelectron spectroscopy (XPS) was performed on a Surface Science Labs SSX-100 system (Fig 2.3.9). This instrument has a monochromatic aluminum x-ray source with a nominal x-ray beam diameter of 600 μm . The Al K(alpha) x-ray energy is 1486.6 eV. To generate these x-rays, an aluminum anode is bombarded by an electron gun which is operating at 10 kV with a 10mA emission current (100 Watts). Sample preparation consisted of placing a drop of the nanomaterials solutions in water on a piece of clean Al foil, then allowing the water to evaporate at room temperature before measurements.



Figure 2.3.9. Surface Science Labs SSX-100 system XPS (image courtesy of Tom Wittberg, UDRI).

2.3.7 Dynamic Light Scattering (DLS)

Particle size measurements in solution were determined with dynamic light scattering (DLS) as described in Malvern Instruments, 2005 and Murdock et al., 2007 on a Malvern Instruments Zetasizer (Fig 2.3.10). This instrument can measure particle sizes ranging from 0.6 nm to 6 μm by combining laser Doppler velocimetry and phase analysis light scattering (PALS) to output size information in three forms: intensity, volume, and number distributions. In these studies, 1.5 mls of 25-50 $\mu\text{g/ml}$ solutions of nanoparticles were measured in cuvettes to obtain intensity distribution graphs.

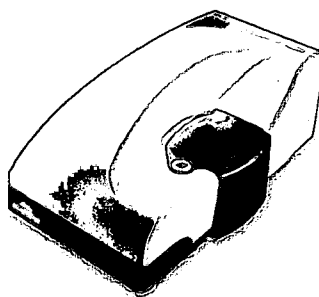


Figure 2.3.10. Malvern Zetasizer machine. Measurements can be acquired for DLS and ZP.

2.3.8 Zeta Potential

The Malvern Zetasizer can also provide zeta potential measurements on particles ranging in size from 3 μm to 10 μm (Malvern Instruments, 2005; Murdock et al., 2007). Zeta potential is defined as the charge accumulation around the surface a particle in solution and gives an indication of the stability of the colloidal system. In general, the larger the zeta potential value, whether positive or negative, the more the particles will repel each other and therefore lead to less agglomeration. Usually, when the zeta potential is more positive than +30mV or more negative than -30mV, the system is considered stable. The greatest impact on zeta potential is the pH of the solution. However, due to the unsuccessful measurement of zeta potential in cell culture media, due to the corrosion of the gold electrodes inside the zeta potential capillary tube once voltage was applied across the solution, deionized water (pH 7.0) was used in all experiments to determine charge. Because the pH of nanomaterials in cell culture media with or without serum (pH 7.4) was very similar to the pH of the deionized water, the effective charge of the nanomaterials in cell culture media should be similar to water alone. Zeta potential is determined through first acquiring the electrophoretic mobility of the particles, then applying the Henry Equation, which determines electrophoretic mobility based on zeta potential, dielectric constant of the media, viscosity of the media, and an approximation of the size of the electric double layer.

$$U_E = \frac{2 \epsilon z f(ka)}{3 \eta}$$

Henry Equation. U_E : electrophoretic mobility, ϵ : dielectric constant, z : zeta potential, $f(ka)$: Henry's Function approximation, and η : solvent viscosity.

2.4 In Vitro Biocompatibility Studies

The common routes of occupational exposure to nanomaterials are inhalation and skin contact, but studies have found translocation of both ultrafine and nano-sized particles from the nasal and tracheobronchial regions of the respiratory tract to olfactory and trigeminal nerves as well as to the brain in both animals and fish (Oberdorster et al. 2005, Oberdorster et al. 2004a, Oberdorster 2004b). Therefore, from the perspective of both deliberate targeting of nanoparticles to the nervous system or accidental exposure and subsequent translocation, we chose alveolar macrophages, keratinocytes, and two different cells representative of the nervous system, neuroblastoma (N2A) (Cool et al., 1995, Cool et al., 1997), and neuroendocrine cells (PC-12) cells for these studies. Although, *in vitro* data cannot be directly applied to human situations, such as the effect of nanoparticles on the nervous system, the use of simple *in vitro* models can provide end points that reveal cellular alterations and general biocompatibility. The use of a consistent 24h time-point provides sufficient time for nanoparticle interaction and internalization as well as the ability to detect biochemical changes in cellular function such as reduced mitochondrial function and reactive oxygen species production.

Cells were grown in a humidified incubator at 37°C and 5% CO₂ atmosphere and procedures for dosing and general cell maintenance were performed under a biological hood with aseptic technique (Fig 2.4.0).



Figure 2.4.0. Demonstration of appropriate lab attire and aseptic technique inside a biological hood.

2.4.1 Cell Culture and Dosing Protocol

Murine skin cells (HEL-30) were obtained from the Naval Health Research Center Detachment Environmental Health Effects Lab at Wright Patterson AFB, Dayton, OH. HEL-30 cells were maintained in DMEM:F12 Ham's media supplemented with 10% FBS and a 1% mixture of penicillin and streptomycin. Human skin cells (HaCat) were obtained from the German Cancer Research Center and maintained in RPMI-1640 media supplemented with 10% FBS and a 1% mixture of penicillin and streptomycin.

Rat alveolar macrophages (NR8383 line, CRL-2192) were obtained from ATCC. Macrophages were maintained in F12K medium supplemented with 20% FBS and a 1% mixture of penicillin and streptomycin.

Murine neuroblastoma cells (N2A), a neuronal phenotype, were generously received from Dr. David Cool's laboratory at Wright State University, Dayton, OH (Cool et al., 1995, Cool et al., 1997). N2A cells maintained in DMEM:F12

Ham's media supplemented with 10% FBS and a 1% mixture of penicillin and streptomycin.

Rat pheochromocytoma (PC-12, CRL-1721) cells, which are adrenal gland tumor cells, were purchased from ATCC. PC-12 cells were plated in collagen-coated flasks and maintained with RPMI-1640 cell culture media supplemented with 10% FBS, 10% heat inactivated horse serum, and a 1% mixture of penicillin and streptomycin.

All cells were counted in suspension after either trypsinization or scraping from flasks. The number of cells per ml was determined by counting on a hemocytometer slide. For all experiments, cells were plated at a specific density ($250 - 500 \times 10^3$ cells/ml) in 6-96 well culture plates or chambered slides and grown for 24-48 hours (Fig 2.4.1). Upon reaching ~80% confluency, the media was removed and dosing solutions containing nanomaterials in the range of 5-100 $\mu\text{g/ml}$ were added directly to each well. At the end of the exposure period (typically 24h), imaging or biocompatibility end-points were evaluated in control and nanomaterial-exposed cells. In our biocompatibility studies, positive, negative, and no-treatment controls were used. The well-known water soluble neurotoxin, cadmium oxide (CdO), was chosen as the positive control. The choice of negative control was a fine carbon black nanoparticle (CB, 30nm), which has historically been used in inhalation studies as a fine particle control (Shvedova et al., 2005).

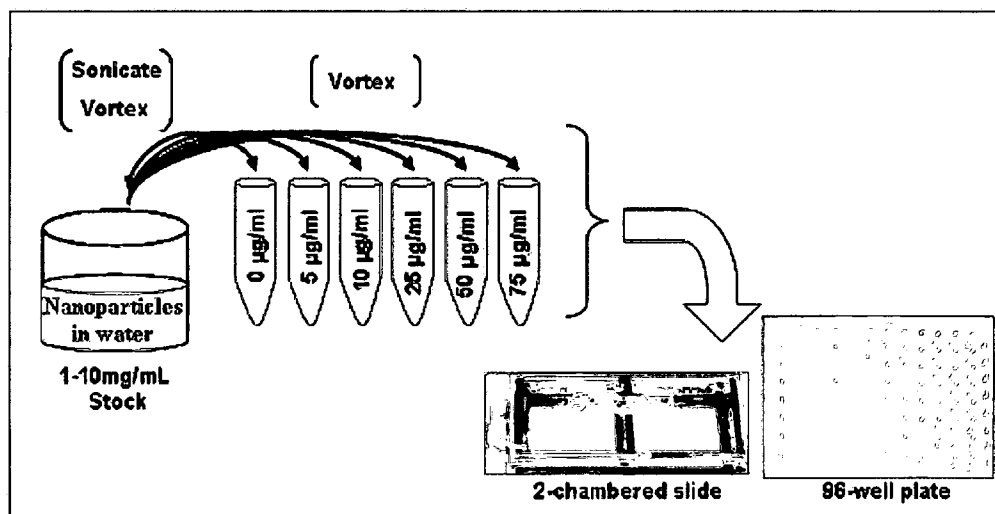


Figure 2.4.1. Illustration of the general nanoparticle dosing set-up.

2.4.2 Morphological Observation

Cells were dosed with various concentrations of nanomaterials for 24 h. After the exposure period, the nanomaterials were removed and cells were washed 1-2x with PBS before preparing slides. Cells were observed with an Olympus IX71 inverted phase contrast microscope at magnifications from 4-96x and images were captured via QCapture Pro Imaging Software. Alternatively, morphological changes to the cells were examined with high illumination light microscopy (CytoViva™150 Ultra Resolution Imaging system attachment, Aetos Technologies, Inc., Auburn, AL, Figure 2.4.2) as previously described (Skebo et al., 2007), scanning electron microscopy, or fluorescent microscopy.

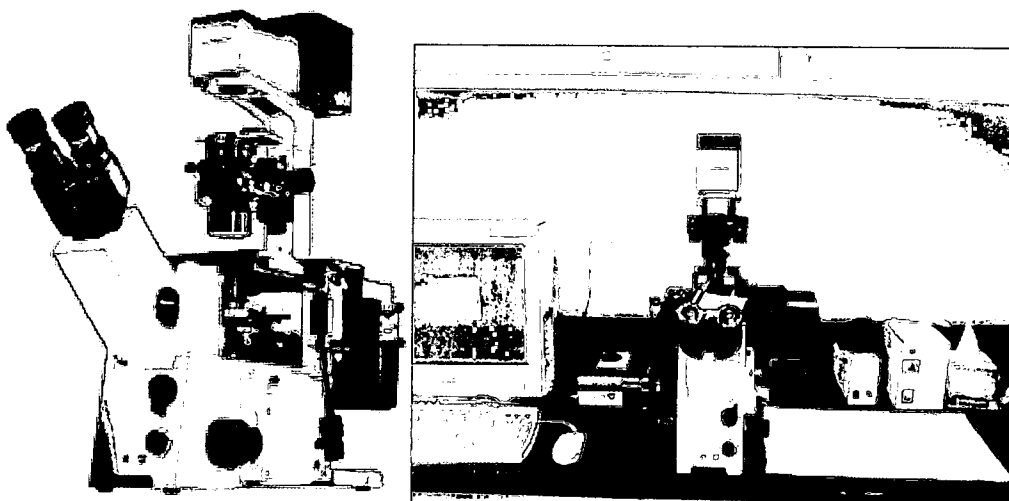


Figure 2.4.2. Olympus IX71 inverted light microscope and Cytoviva attachment.

For SEM preparation, cells were rinsed twice with PBS then fixed for 2 hours at 4 °C in 4% paraformaldehyde in PBS. Afterwards, the cells were dehydrated through a series of ethanol concentrations of 50, 70, 90, and 100% for 10 minutes each, air dried, gold sputtered, and mounted onto SEM stubs with conductive carbon tape. SEM images were taken on a Hitachi S-4800 instrument at 15kV.

Dual fluorescent staining of the actin cytoskeleton and nuclei were examined with Alexa-Fluor 555 Phalloidin (Molecular Probes) and Prolong Gold Reagent with DAPI nuclear counterstain (Molecular Probes). Fluorescence was visualized with TRITC and FITC filters on an Olympus IX71 epifluorescent microscope and images were captured with QCapture Pro software.

2.4.3 Evaluation of Nanomaterial Internalization by Cells

For TEM preparation of cells after nanomaterials treatment, they were fixed with glutaraldehyde/paraformaldehyde, post-fixed with osmium tetroxide, dehydrated through a graded series of ethanol, embedded in resin, cured, and thin sectioned on an ultramicrotome (Fig 2.4.3). TEM images were taken on a Hitachi H-7600 instrument at 100kV.



Figure 2.4.3. Leica Ultracut ultramicrotome. This instrument is used for making thin sections of embedded cells for TEM.

2.4.4 Biochemical Endpoints

Mitochondria are vulnerable targets for toxic injury by a variety of compounds because of their crucial role in maintaining cellular structure and function via aerobic adenosine triphosphate (ATP) production (Hussain and Frazier, 2002). The MTT assay is a colorimetric assay based on the ability of mitochondrial dehydrogenases (e.g. succinic dehydrogenase) in viable cells

to reduce the yellow-colored water soluble tetrazolium salt 3-(4,5-dimethylthiazol-2-yl)-2,5-diphenyltetrazolium bromide (MTT) dye to water-insoluble purple-colored formazan crystals as previously described (Carmichael et al., 1987; Hussain and Frazier, 2002). An additional centrifugation step to remove nanomaterials from the solution before microplate reading was performed in order to avoid direct interference of the absorption values as found in previous studies (Schrand et al., 2007a). The validity of the MTT assay was assessed with the positive control cadmium oxide (CdO, 1000nm), which shows dose-dependent decreases in viability at very low concentrations (<1 $\mu\text{g/ml}$) after 24h (Fig 2.4.4).

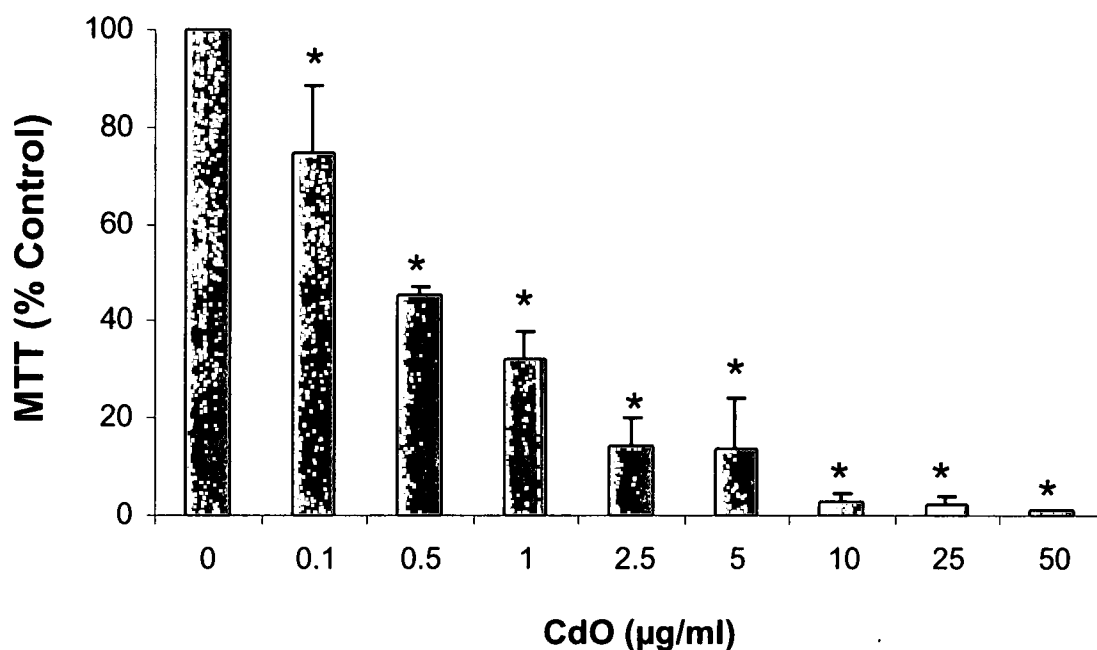


Figure 2.4.4. Dose-dependent toxicity of CdO in N2A cells assessed with the MTT assay. Values that were significantly different from the control ($p<0.05$) are denoted with asterisks (*).

An additional ATP luminescent assay (Cell Titer Glo) was used to compare the results of the MTT assay. This assay provides a homogenous method for determining the number of viable cells in culture based on the quantitation of ATP, which indicates the presence of metabolically active cells.

Plasma membrane integrity was evaluated by measuring LDH leakage with the CytoTox 96® non-radioactive cytotoxicity assay kit from Promega (Madison, WI). This colorimetric assay quantitatively measures lactate dehydrogenase (LDH), a stable cytosolic enzyme that is released upon cell lysis. Released LDH in culture supernatants is measured with a 30-minute coupled enzymatic assay, which results in the conversion of a tetrazolium salt into a red formazan product, which is proportional to the number of lysed cells.

Mitochondrial membrane permeability was determined using the Mit-E-ΨTM mitochondrial permeability detection kit (BIOMOL, Plymouth Meeting, PA). Fluorescence was visualized with TRITC and FITC filters on an Olympus IX71 epifluorescent microscope and images were captured with QCapture Pro software.

The generation of reactive oxygen species (ROS) was measured with the cell permeable probe, 2'7'-dichlorodihydrofluorescein diacetate (H₂DCF-DA) as previously described (Wang and Joseph 1999, Hussain and Frazier 2002).

The relative fluorescent intensity related to the generation of ROS is measured on a fluorescent microplate reader SpectraMAX Gemini Plus (Molecular Devices, Sunnyvale, CA) after excitation at 485nm and emission at 530nm. Data are reported as a fold of increase compared to control. The validity of this assay was shown with the positive control, hydrogen peroxide (H_2O_2), which showed a dose-dependent increase in ROS production (Fig 2.4.5).

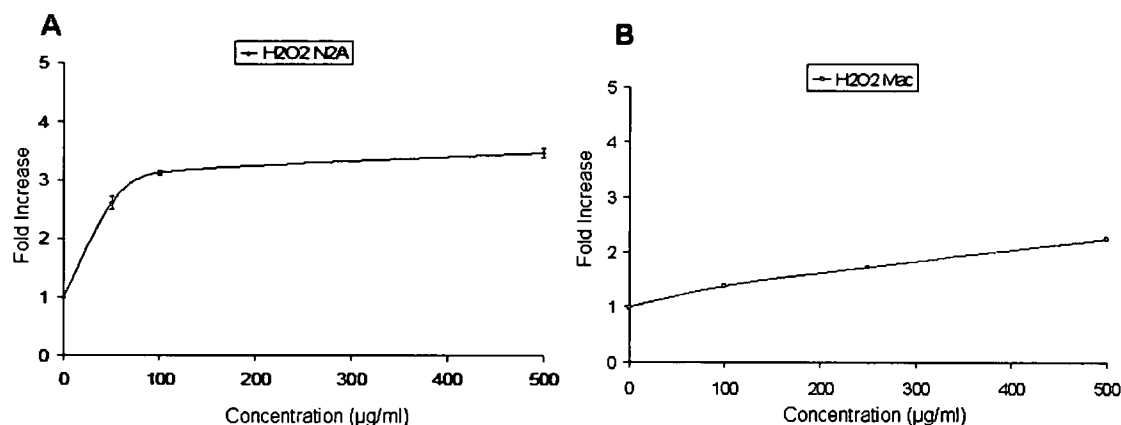


Figure 2.4.5. Production of reactive oxygen species (ROS) in cells incubated with H_2O_2 . (A) Neuroblastoma cells and (B) Macrophages after 24h.

For detection of the production of reactive oxygen species in the absence of cells, stock solutions of nanoparticles were incubated with a DCFH conjugated to horse radish peroxidase (HRP). The amount of resulting fluorescence is measured on a microplate reader.

2.5 Statistical Evaluation

The data were expressed as mean \pm standard deviation (SD) of three independent experiments. Wherever appropriate, the data were subjected to statistical analysis by one-way analysis of variance (ANOVA) followed by Tukey-Kramer's procedure for multiple comparisons. A value of $p < 0.05$ was considered significant. pHStat Excel add-in was used for the statistical analysis.

CHAPTER 3

CARBON NANOTUBES

3.1 Literature Review

Carbon is an essential part of living organisms and is abundant in nature in pure forms and in combination with other elements. For example, naturally occurring nano-sized carbons such as multi-walled carbon nanotubes and other fullerenic polyhedra have been ubiquitously found both indoors and outdoors as products of combustion (e.g. home gas stoves, forest fires, volcanic eruptions). Although carbon has long been recognized for its ability to exist in many structural forms (e.g. amorphous carbon, graphite, carbon nanotubes (CNT), fullerenes, nano-onions, nanodiamonds), it is the unique physico-chemical properties that of engineered carbon nanomaterials that has made them extremely attractive in industrial, environmental, military, and biomedical applications. These properties include their high tensile strength, resilience, flexibility, and other remarkable mechanical, electrical, thermal, and biological properties. For carbon nanotubes (CNTs), in particular, their unusual properties are directly related to the atomic arrangement of carbon atoms resulting in different diameters, helicities, and metal catalyst content (Dai, 2006). CNTs can be viewed as a graphene sheet rolled up into a nanoscale tube form to produce the so-called single-walled carbon nanotubes

(SWNTs). There may be additional graphene tubes around the core of a SWNT to form multi-walled carbon nanotubes (MWNTs). These elongated nanotubes usually have a diameter in the range of a few angstroms to tens of nanometers and a length of several micrometers up to millimeters with both ends of the tubes normally capped by fullerene-like structures containing pentagons. Schematics demonstrating the differences in carbon atom arrangement of different one, two, or three-dimensional forms of carbon nanomaterials are shown in Fig 3.1.1.

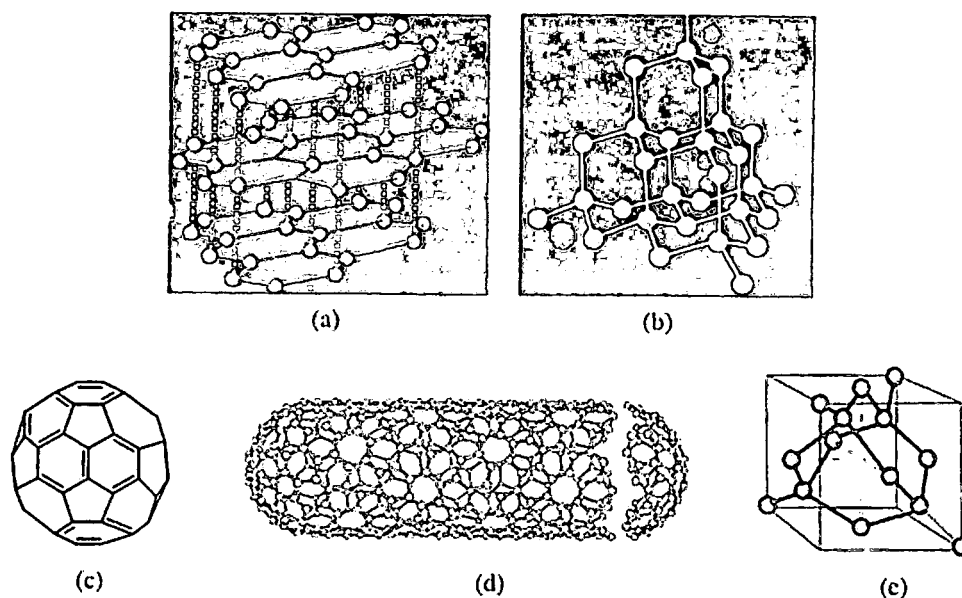


Figure 3.1.1. One-, two-, and three-dimensional carbon nanomaterials. (a) Graphite, (b) Diamond, (c) Buckminsterfullerene C₆₀, (d) [5,5] Armchair single-walled carbon nanotube, and (e) Nanodiamond (Dai 2006).

The widespread use of both SWNTs and MWNTs in many applications is now facilitated by their production and availability in relatively large quantities through simple, efficient, and inexpensive syntheses; for example in some large-scale military applications (Schrand and Benson-Tolle, in Dai 2006).

Because the world-wide production of SWNTs and MWNTs is projected to reach over 500 tons by 2008, exposure to carbon nanomaterials via occupational, consumer, environmental, or biomedical arenas is increasing at a rapid rate (Borm et al., 2006). Therefore, from a health perspective, determining the properties that contribute to carbon nanomaterial biocompatibility or toxicity are of great importance.

While bulk carbon is considered chemically inert with minimal reactivity towards cells of the body, nano-sized carbon, due to its small size, high surface-to-volume ratio, and reactive surface chemistry, is expected to greatly influence cellular permeability and dynamics (Dai, 2006, Hurt et al. 2006). However, there has been no direct link between carbon nanomaterials dimension and biocompatibility. Jia et al., 2005 found that MWNTs were more biocompatible than SWNTs whereas other studies have shown that smaller carbon nanotubes are more biocompatible than larger-sized carbon fibers (Price et al., 2004; Magrez et al., 2006). Therefore, many other factors must be taken into consideration before conclusions can be made regarding carbon nanomaterial biocompatibility.

Over the past year, the main property of carbon nanomaterials that became more heavily scrutinized in biocompatibility studies was the content of residual metal catalyst. Garibaldi et al., 2006 found that cardiac muscle cells incubated with highly purified SWNTs were only slightly modified in shape

due to SWNT binding to the cell membranes with cell viability remaining >90%. Kagan et al, 2006 demonstrated that SWNTs retaining 26 wt% Fe (from the catalyst used for the nanotube growth) caused significant loss of glutathione (GSH) and accumulation of lipid peroxidases compared to purified SWNTs (0.23 wt% Fe) in macrophages. Pulskamp et al., 2007 found that rat macrophages incubated with 100 µg/ml of MWNTs for 24h greatly reduced cell viability with increased ROS production compared to the control and purified SWNTs.

Another important factor in carbon nanomaterials biocompatibility studies that has been overlooked until recently is the differential biocompatibility of carbon nanomaterials to various cell types (Schrand et al., 2007b). A careful examination of the literature suggests that regardless of dimension (e.g. SWNT vs. MWNT), concentration, or duration of exposure, nanotubes are more toxic to immune (e.g. T-lymphocyte) and lung cells (e.g. macrophages).

Other studies demonstrate that surface functionalization of carbon nanotubes with carbonyl C=O, carboxyl (COOH), and/or hydroxyl (OH) played a role in the biocompatibility response (Magrez et al., 2006, Sato et al., 2005, Bottini et al., 2006). Bottini et al., 2006 examined the biocompatibility of pristine (purity > 95%) and acid oxidized MWNT in human T-cells at a high concentration of 400 µg/ml over 5 days and found that the pristine MWNTs reduced viability by 50% whereas the oxidized MWNT reduced the viability to < 20%. However,

other studies have reported that acid functionalization of nanomaterials such as hat-stacked carbon nanofibers, through the addition of carboxyl groups, leads to only weak changes in biocompatibility (Sato et al., 2005). On the other hand, human dermal fibroblasts incubated with water dispersible, functionalized SWNT (SWNT-phenyl-SO₃H, SWNT-phenyl-SO₃Na, or SWNT-phenyl-(COOH)₂) were found to be more biocompatible with an increased density of functional groups on their surfaces compared to unfunctionalized, surfactant stabilized SWNTs (Sayes et al., 2005). However, the acidic SWNT-(COOH)₂ produced a greater reduction in cell viability compared to SWNT-SO₃H. Therefore, the purpose of the functionalization, either through brief acid or base treatment to aid in removal of residual metal catalyst or to increase the density of particular functional groups on the surface must be further elaborated to understand its relationship to biocompatibility. A summary of some of the most current carbon nanomaterials biocompatibility or toxicity results are shown in Table 3.1.1.

Table 3.1.1. Summary of Carbon NM Biocompatibility or Toxicity.

NM	Properties	Cell Line/Animal	Dose	Time	Result	Reference
MWNT SWNT	SWNT purity 90%, 95% MWNT (0.6% Ni)	Alveolar Macrophage	0.38- 226 $\mu\text{g}/\text{cm}^2$	6h	Toxic	Jia et al., 2005
SWNT MWNT-1 MWNT-2	Carbon Nanotechnol- ogies, Inc. 5- 10%Fe (SWNT)	Murine Macrophage	0.005- 10 $\mu\text{g}/\text{ml}$	48-54h	Toxic	Murr et al., 2005
SWNT	phenyl-SO ₃ H, phenyl- SO ₃ Na, phenyl- (COOH) ₂	Human Dermal Fibroblast	3 - 30,000 $\mu\text{g}/\text{ml}$	48h	Non- toxic	Sayes et al., 2005
MWNT	Oxidized vs. Pristine (>95% purity)	T Lymphocyte	400 $\mu\text{g}/\text{ml}$	5 days	Toxic	Bottini et al., 2006
MWNT	CVD synthesis, HCl purified	Human Umbilical Vein Endothelial Cells	0.5-0.9 $\mu\text{g}/\text{ml}$	120h	Non- toxic	Flahaut et al., 2006
SWNT	Iron rich 26wt% vs. Iron-"free" 0.23wt%	RAW 264.7 Macrophages	120 - 500 $\mu\text{g}/\text{ml}$	up to 2.5h	Iron Rich - Toxic	Kagan et al., 2006
MWNT	HCl for purification, H ₂ SO ₄ for surface chemical groups C=O, COOH, OH	Lung Tumor Cells (H596, H446, Calu-1)	0.002- 0.2 $\mu\text{g}/\text{ml}$	4 days	Toxic	Magrez et al., 2006
MWNT SWNT SWNT- acid treated	0.6-2.8wt%Co (MWNT), 1.3wt%Co/1.2 wt% Ni (SWNT), 0.6wt%Co (purified SWNT)	Rat Macrophages (NR-8383) and human lung A549 cells	5-100 $\mu\text{g}/\text{ml}$	24h	Toxic	Pulskamp et al., 2007
SWNT MWNT CB ND	0.49wt%Fe (MWNT) 0.26wt%Fe (SWNT)	Murine Neuroblastoma, Rat Alveolar Macrophage	5-100 $\mu\text{g}/\text{ml}$	24h	Toxic to Macro- phage	Schrand et al., 2007b

Additional surface chemical modifications to untangle nanotubes bundles improving their stability, dispersion, and selectivity have provided further impetus for studying the impact of carbon nanotubes in both material and biological systems (Khabashesku et al., 2005; Osswald et al., 2006). Along with aiming to understand and improve carbon nanotube biocompatibility, covalent surface coupling of amino acids, bioactive peptides, proteins, carbohydrates, or nucleic acids are being pursued for delivery into cells (Georgakilas et al., 2003; Kam et al., 2004; Kam et al., 2005a; Bianco et al., 2005; Pantarotto et al., 2004; Pantarotto et al., 2003, Singh et al., 2005; Bianco et al., 2004). Nanotubes are particularly attractive for the targeted delivery of therapeutic agents or for cancer treatment due to the ability to functionalize both their inner and outer walls (Huang and Dai, 2002).

However, there is a great amount of caution in moving forward with medicinal uses of carbon nanotubes due to both cell culture and animal studies (Lam et al., 2004, Warheit et al., 2004, Shvedova et al., 2005), which are often divergent in their conclusions about the biocompatibility or toxicity of carbon nanotubes. While some studies suggest that carbon nanotubes are biocompatible (Flahaut et al., 2006, Fiorito et al., 2006), other studies suggest that carbon nanotubes, which are similar in size and morphology to asbestos, are potentially threatening to human health and the environment (Soto et al., 2005, Murr et al., 2005). For example, carbon nanotubes have been shown to inhibit cell growth or induce apoptosis (Cui et al., 2005), induce cell arrest

and apoptosis by activating genes involved in immune and inflammatory responses (Ding et al., 2005), activate nuclear transcription factors and stress-related kinases (Manna et al., 2005), and generate an irritant response to skin cells (Monteiro-Riviere et al., 2005). Because carbon nanomaterials are continuing to be engineered with varying properties and for a multitude of applications, the specific factors that contribute to biocompatibility are still under investigation. It is the goal of this chapter to relate the physico-chemical characteristics of carbon nanomaterials to their *in vitro* biocompatibility in multiple relevant cell types in order to rank the materials properties of greatest importance for the future engineering of biocompatible carbon nanomaterials.

3.2 Results for Characterization

The characteristics of carbon nanomaterials were evaluated for purity with ICP-OES; dimension, size distribution, and morphology with TEM; aggregate size in solution with DLS, and charge with zeta potential.

3.2.1 Purity of Carbon Nanotubes

Carbon nanomaterials were screened for elements present with x-ray fluorescence prior to quantitative analysis of elemental impurities with inductively-coupled plasma-optical emission spectroscopy (ICP-OES). The samples were attempted to be digested by vigorous boiling with strong mineral acids to extract acid-digestible trace elements. Despite this, the carbon nanomaterials were virtually indigestible leaving a considerable amount of undigested sample with an unknown extent of digestible trace elements extracted. The main impurity in the carbon nanotubes was iron (Fe) and was approximately 0.49 wt% Fe for MWNT compared to 0.26 wt% Fe for the SWNT with no detectable amounts of Fe in CB or ND. The source of this Fe impurity is from the catalysts used during the chemical vapor deposition synthesis. The impurity in the CB sample was approximately 0.43wt% S, which is from the hydrocarbon feedstock used in the furnace synthesis method. The surface chemical composition of functionalized MWNT-SO₃Na was verified with XPS showing a Fe catalyst content of 1.4 at% and S content of 2.1 at%.

3.2.2 Size and Morphology

The size distributions and morphologies of carbon nanomaterials were examined with TEM. Individual cubic nanodiamonds (ND-raw) had average sizes of 5.1 ± 1.7 nm (Fig 3.2.1A) and were smaller than spherical nano-sized carbon black nanoparticles, which had average sizes of 28.8 ± 8.4 nm (Fig 3.2.1B). The maximum lengths of both the single-walled (SWNT, Fig 3.2.1C) and multi-walled (MWNT, Fig 3.2.1D) carbon nanotubes were not as readily calculated due to bundling and tangling. The SWNTs existed in bundles that were greater than 3 μ m in length with bundle diameters of approximately 25nm whereas individual SWNT diameters were 1-3nm. The MWNTs were estimated to be from 0.5-40 μ m in length with diameters from 9-40nm. Micron-sized CdO nanoparticles (Fig 3.2.1E) were found typically in aggregates with an average size of 552.1 ± 238.8 and core particles of 179.3 ± 43.4 nm. Other carbon nanotubes MWNT-COOH had lengths ranging from 5-40 μ m and diameters from 6-40 nm, MWNT-SO₃Na and MWNT-2 had lengths of 6-7.5 μ m and diameters ranging from 14-52nm (average 33 nm) compared to 20-60nm (average 40 nm) for MWNT-2. For the cubic or spherical particles, the size distribution graphs are shown below the TEM images in Figure 3.2.1.

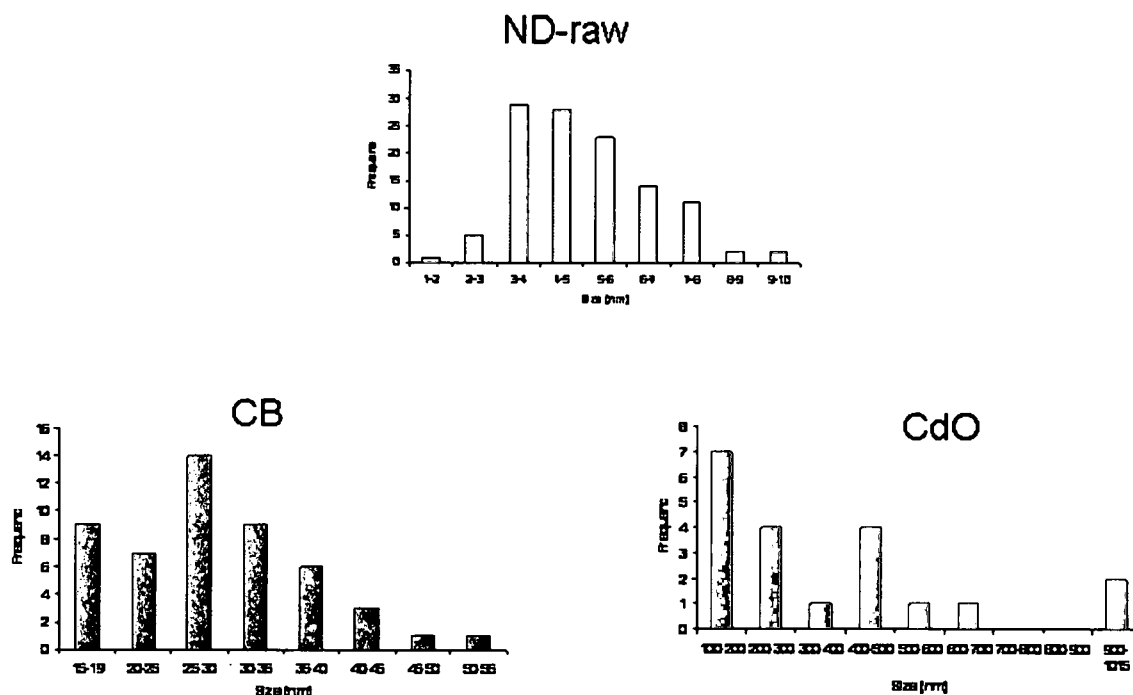
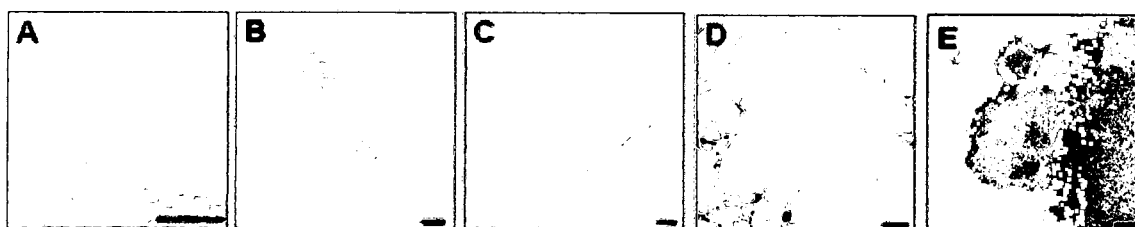


Figure 3.2.1. Size and morphology of carbon nanomaterials with TEM. (A) ND-raw, (B) CB, (C) SWNT, (D) MWNT, and (E) CdO. Scale bars are 100nm. Size Distribution graphs of nano-sized carbon black and positive control CdO obtained after counting nanoparticles from TEM images (Schrand et al., 2007a).

3.2.3 Dynamic Light Scattering and Zeta Potential

The solution properties of carbon nanomaterials in either water or cell culture media were examined for changes in size due to agglomeration with dynamic light scattering (Fig 3.2.2, Murdock et al., 2007). Because the calculation of nanomaterial size with light scattering is based upon spherical particles, the results for SWNT and MWNT were not as useful because both diameters and

lengths were analyzed by the machine as is shown for SWNT with several peaks at low and very high values (Fig 3.2.2). Additionally, the formation of very strong nanomaterials aggregates due to van der Waals forces is expected to occur for unmodified carbon nanomaterials in solution, which is shown for the nano-sized carbon black nanoparticles, which have much larger sizes than their primary size of approximately 30nm (Fig 3.2.2).

Dynamic light scattering (DLS) and laser doppler velocimetry (LDV) data for three types of carbon nanotubes and a spherical carbon black samples were measured at 25°C in water (Fig 3.2.2). For SWNT, MWNT-COOH, and CNT mean size values of 900nm, 825nm, and 821nm were found along with very high polydispersity index (PDI) readings. The nano-sized carbon black sample was analyzed in DMEM/F-12 cell culture media with and without serum to examine the effect of serum proteins on size in solution. The addition of 10% serum decreased the size from 2190nm to 970nm, but suspension in water produced less aggregation with an average agglomerate diameter of 396nm. SWNT had the largest zeta potential of the group at 50.2mV.

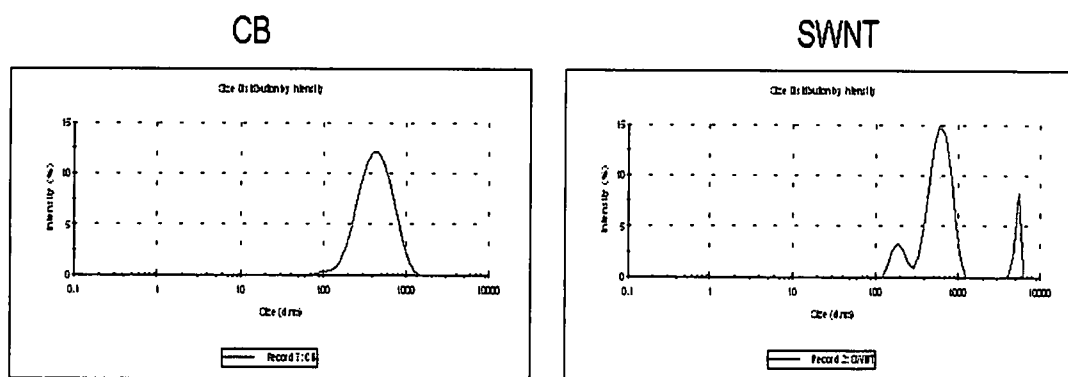


Figure 3.2.2. Dynamic light scattering (DLS) and zeta potential (ZP) data for carbon nanomaterials. Upper charts are representative size distributions for nano-sized carbon black particles and SWNTs. Lower charts show DLS and ZP data for various carbon nanomaterials used in these studies (adapted from Murdock et al., 2007).

Other changes in the dynamic agglomeration behavior of the carbon nanomaterials occurred with changes in temperature from 25°C to 37°C. As shown below in Fig 3.2.3 in the top row, the immediately applied carbon nanotubes to a cell culture of PC-12 cells are visually well-dispersed, but after 1 h of incubation at 37°C, the nanotubes are agglomerated and may not directly interact with the cells, which is shown in the lower rows. A summary of the characteristics of carbon nanomaterials in general and the properties of the carbon nanomaterials used in these studies is shown in Table 3.2.1.

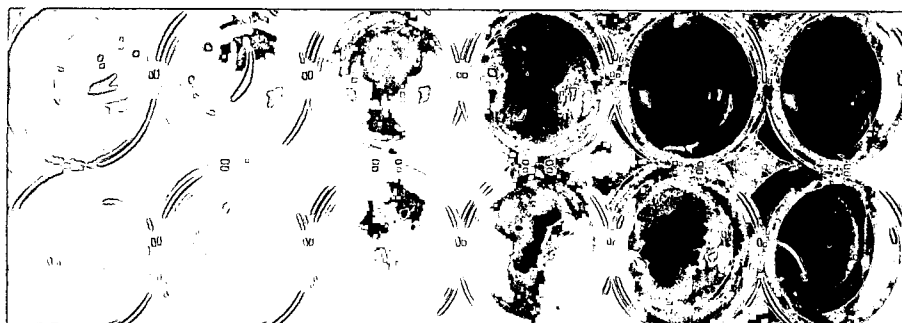


Figure 3.2.3. Change in dispersion of MWNTs. Top row: freshly prepared MWNTs at concentrations of 0, 5, 10, 25, 50, and 100 µg/ml in RMPI media. Bottom row: Change in the dispersion of MWNTs (same concentrations as above) after 1h at 37°C (Schrand et al., 2007c).

Table 3.2.1 Summary of Carbon Nanomaterial Characteristics.

	ND	CB
Synthesis Method	Detonation	Oil furnace
Color	Gray	Black
Morphology	Spherical/Cubic	Spherical
Carbon bond hybridization	sp ³	sp ²
Diameter	2-10 nm (~5nm)	~30 nm
Length	N/A	N/A
Price per gram	\$2-5/g	<\$0.01/g
% Fe or S Impurity	N/A	0.43 wt% S
Size in Water	158 nm	396 nm
Size in Cell Culture Media	2180 nm, DMEM-F12	2190 nm, DMEM-F12
Charge in Water	+42.8	-1.6

	SWNT	MWNT
Synthesis Method	CVD	CVD
Color	Black	Black
Morphology	Open or closed tube	Open or closed tube
Carbon bond hybridization	sp ⁿ	sp ⁿ
Diameter	1-10 nm (bundles ~25 nm)	2.5-30 nm (9-40 nm)
Length	50 nm-1 µm (bundles > 3µm)	> 10's of microns (0.5-40 µm)
Price per gram	up to \$2000/g	up to \$600/g
% Fe or S Impurity	0.26 wt% Fe	0.49 wt% Fe
Size in Water	900 nm	821 nm
Size in Cell Culture Media	N/A	N/A
Charge in Water	+50.2	-13.6

3.3 Results for Biocompatibility

Carbon nanomaterials were assessed for biocompatibility by morphological observation, MTT and ATP assays of viability, mitochondrial membrane permeability (MMP), lactase dehydrogenase (LDH) leakage, and generation of reactive oxygen species (ROS). The first set of experiments examined the biocompatibility of multi-walled carbon nanotubes in neuroendocrine (PC-12) cells; the second set of experiments investigated the differential biocompatibility of carbon nanomaterials in lung macrophages compared to neuroblastoma cells; the third set of experiments explored the effect of surface chemistry on CNT biocompatibility; and other several other factors that may impact biocompatibility were considered .

3.3.1 Biocompatibility of MWNTs in PC-12 Cells

Previous images showed the agglomeration of MWNTs after incubation with PC-12 cells in RPMI media after 1h at 37°C (Fig 3.2.3). Further observations with light microscopy showed that the nanotubes can remain highly agglomerated and may not always come into contact with the cells (Fig 3.3.1).

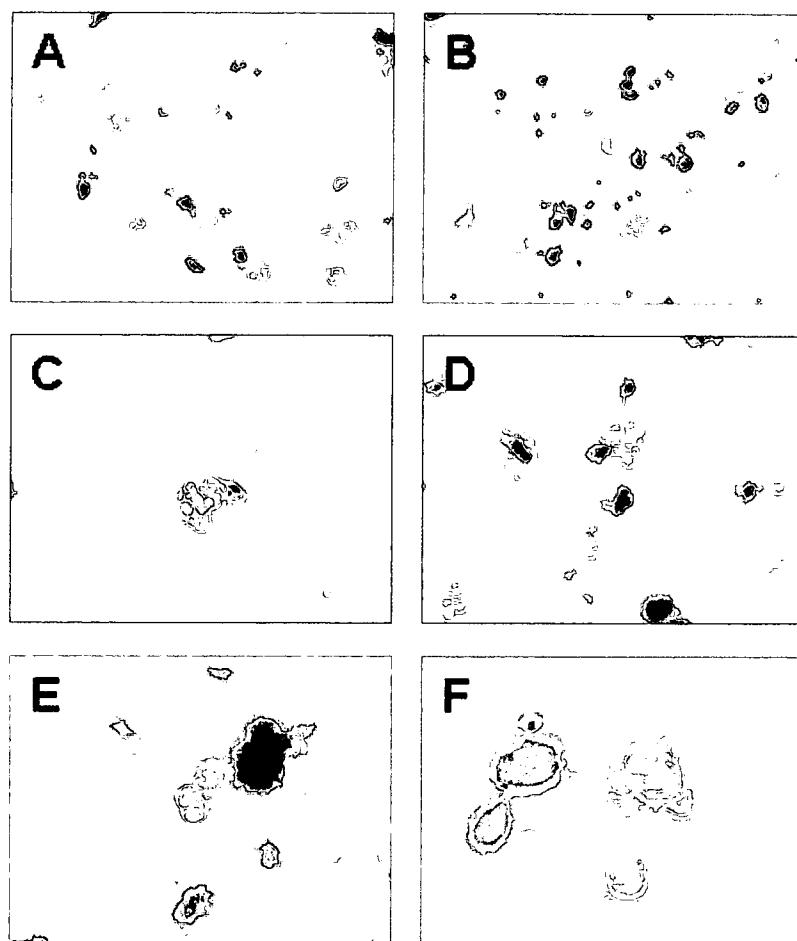


Figure 3.3.1. Light microscopy of PC-12 cell morphology after incubation with MWNTs. (A, C, E,) 25 $\mu\text{g/ml}$ or (B, D, F) 50 $\mu\text{g/ml}$ for 24h. Original magnifications were (A,B) 5.6x, (C,D) 12x, and (E, F) 32x taken on an Olympus IX71 inverted microscope (Schrand et al., 2007c).

However, shorter and better dispersed MWNTs examined with high illumination light microscopy are shown in close contact with cell membranes (Fig 3.3.2). At the highest concentration (100 $\mu\text{g/ml}$), the cells are barely visible due to membrane coverage with the MWNTs and fewer cells remained attached to the chambered slides compared to control cells, which made it difficult to find the cell amidst the suspended MWNTs.

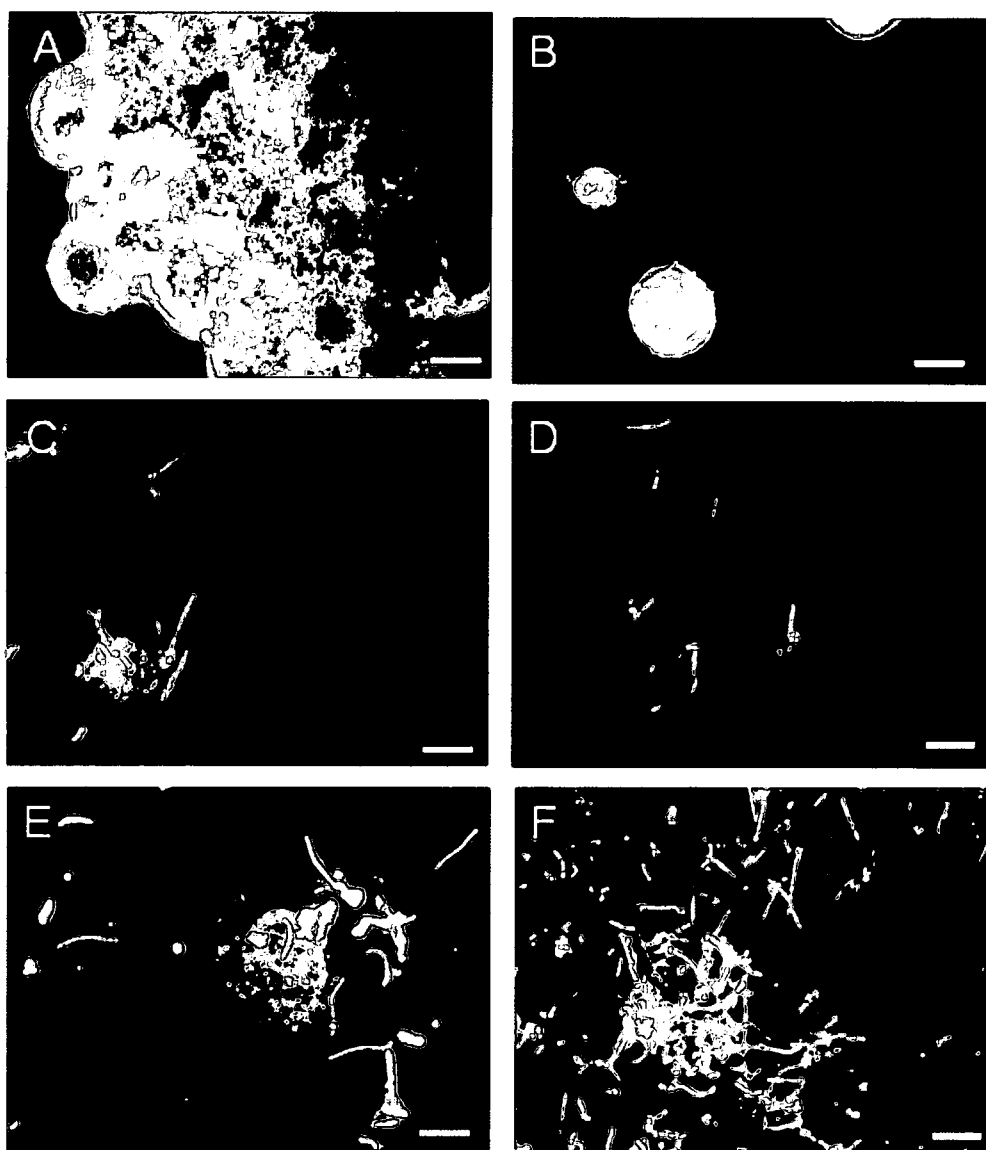
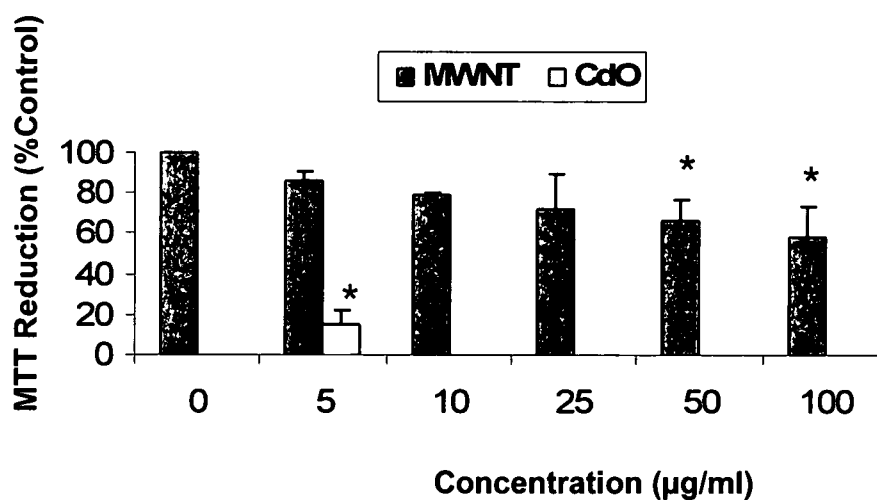


Figure 3.3.2. Ultrahigh resolution light microscopy of PC-12 cells incubated with MWNTs. (A-B) Control cells, (C-D) cell incubated with 25 $\mu\text{g/ml}$ MWNTs, and (E-F) cells incubated with 100 $\mu\text{g/ml}$ MWNTs after 24h. Scale bars are 10 μm .

Assessment of MWNT biocompatibility with the MTT assay showed that PC-12 cells incubated with 50-100 $\mu\text{g/ml}$ of MWNTs have significantly decreased viability compared to the untreated control (Fig 3.3.3A). The corresponding measurement of plasma membrane leakage with the LDH assay showed no significant increase in leakage compared to the control at any of the nanotube

concentrations tested (Fig 3.3.3B). Further examination of cell cross sections revealed the presence of nanotube bundles both outside the cell and beginning to penetrate the cell membrane, which are marked by black arrows in Figure 3.3.4. Other membrane features such as finger-like projections called filopodia (marked by white arrows) were preserved in some cells showing the similarity in morphology to the nanotubes. It is not known whether these membrane features further prevented nanotube internalization or if penetration of the nanotubes into the cell membranes was merely an artifact of the processing, which relies on centrifugation to pellet the cells before embedding and sectioning.

(A)



(B)

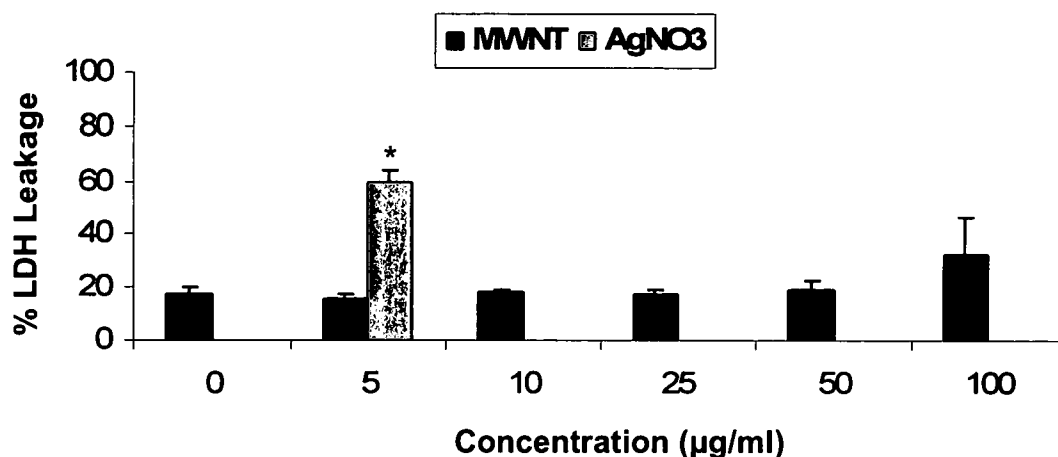


Figure 3.3.3. PC-12 cell viability and membrane leakage after incubation with 0-100 µg/ml of MWNT for 24h. (A) MTT assay viability results and (B) LDH assay results. Values that were significantly different from the control ($p < 0.05$) are denoted with asterisks (*). (Schrand et al., 2007c).

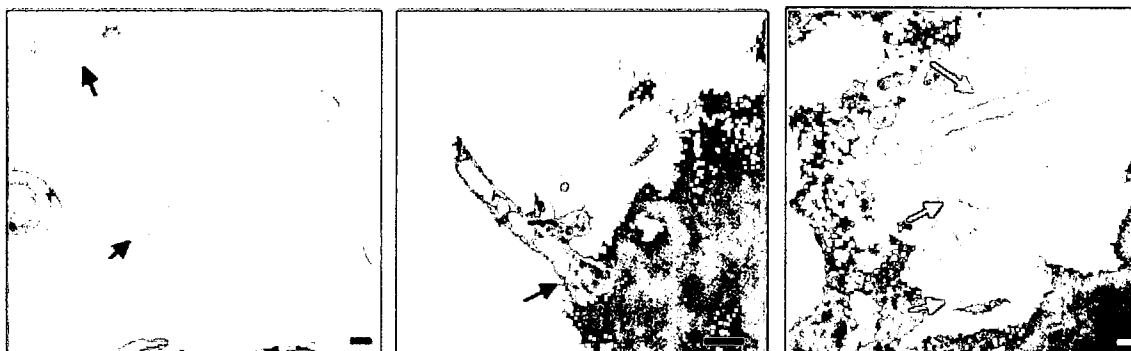


Figure 3.3.4. PC-12 cells and MWNTs. Transmission electron microscope (TEM) images show MWNTs both outside of the cell and barely inserting into the membrane (black arrows). The MWNTs are similar in morphology to membrane projections called filopodia (white arrows). Scale bars are 100 nm (Schrand et al., 2008b)

These results suggest that the aggregation behavior of MWNTs in cell culture media may effectively limit plasma membrane damage while cell viability is still reduced at high nanotube concentrations, which may be due to another mechanism such as blockage of plasma membrane receptors, binding and reduction of serum proteins from the cell culture media, release of soluble

catalyst ions into the cell solution, or other extracellular events. The effect of nanotube dispersion on biocompatibility was examined in later studies with functionalized carbon nanotubes.

3.3.2 Biocompatibility of Carbon Nanomaterials in N2A Cells and Macrophages

By comparing a neuronal cell line to a lung cell line, these studies help elucidate the impact of carbon nanomaterials based on cell-specific interactions. Morphological observations, the MTT assay of cell viability, mitochondrial membrane permeability (MMP), and reactive oxygen species (ROS) were examined to compare the effects of the carbon nanomaterials on biocompatibility. The positive control cadmium oxide (CdO) was used throughout the experiments to demonstrate toxicity. The choice of negative control was a fine carbon black nanoparticle (CB, 30nm), which has historically been used in inhalation studies as a fine particle control (Shvedova et al., 2005).

The morphology of both neuroblastoma cells and macrophages was round immediately after trypsinization. Upon attachment and growth, however, some of the neuroblastoma cells developed elongated extensions while others remained round, which is characteristic of these cells. On the other hand, the macrophages remained round, but could spread to larger sizes. There was a noticeable difference in internalization between the neuroblastoma cells and macrophages (Fig 3.3.5) after incubation with 100 µg/ml of various carbon

nanomaterials for 24h. The control neuroblastoma cells show neurite extensions (Fig 3.3.5A-E) while macrophages stayed round (Fig 3.3.5F-J). The clearly evident phagocytosis of carbon black completely filling the macrophages (Fig 3.3.5G) and accumulation of other carbon nanomaterials (Fig 3.3.5H-J) is markedly contrasted to the neuroblastoma cells (Fig 3.3.5B-E) where clusters of nanomaterials were found attached to the membrane with less obvious internalization.

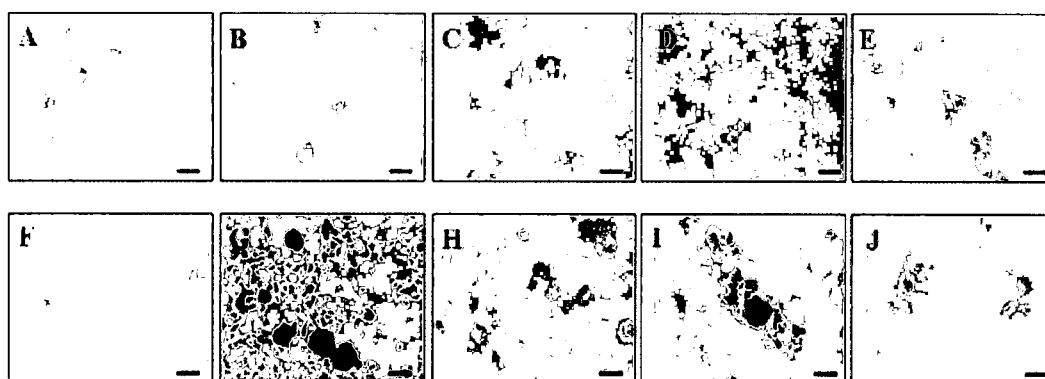


Figure 3.3.5. Phase contrast images of cells incubated with carbon nanomaterials. (A-E) Neuroblastoma and (F-J) Macrophage after 24h of incubation with 100 $\mu\text{g/ml}$ concentrations of carbon nanomaterials (A, F) Control, (B,G) CB, (C, H) ND-raw, (D, I) MWNT, and (E, J) SWNT. Notice the differential internalization. Scale bars are 100 microns. (Schrand et al., 2007b)

Additional light microscope images show that the nanomaterials are attached to the neuroblastoma cell membranes in an agglomerated form denoted by white arrows in Figure 3.3.6B-D. In contrast, alveolar macrophages incubated for 24h with a lower concentration (25 $\mu\text{g/ml}$) of multi-walled carbon nanotubes (MWNTs) or higher concentrations (100 $\mu\text{g/ml}$) of fine carbon black nanoparticles (CB) or nanodiamonds (NDs) show large agglomerates inside the cells (Fig 3.3.6F-H). The obvious exclusion of carbon

nanomaterials from the nucleus in the macrophages is denoted by black arrows while the cytoplasm is clearly filled (Fig 3.3.6F-G).

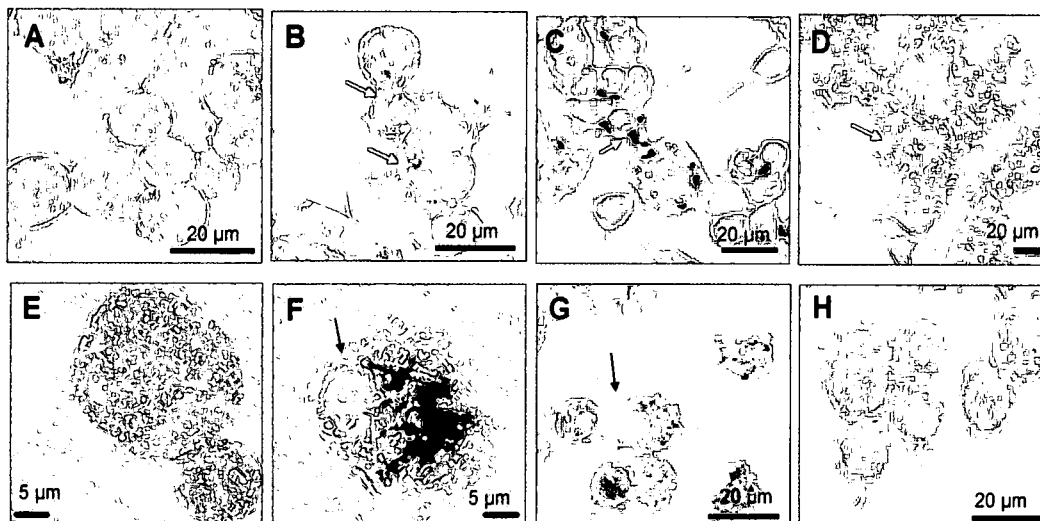


Figure 3.3.6. Examination of interactions between cells and carbon nanomaterials after 24h. (A-D) Neuroblastoma cells and (E-F) Macrophages. (A) Control neuroblastoma cells or cells incubated with 100 $\mu\text{g/ml}$ concentrations of (B) MWNTs, (C) CB, and (D) NDs. (E) Control macrophages or cells incubated with (F) 25 $\mu\text{g/ml}$ MWNTs, (G) 100 $\mu\text{g/ml}$ CB, and (H) 100 $\mu\text{g/ml}$ NDs. White arrows denote nanomaterials agglomerates and black arrows show the nucleus free from nanomaterials (Schrand et al., 2008b).

The primary mechanism of nanomaterial internalization was hypothesized to be different between neuroblastoma cells and macrophages because macrophages are known to internalize foreign debris as part of their role in the lung whereas neuroblastoma cells are not known to actively internalize materials, but may do so with a more general endocytosis mechanism. Although light microscopy clearly demonstrated the differential internalization of carbon nanomaterials by these two cell types, it was not clear if the carbon nanomaterials were internalized or if they merely were attached to the cell membrane in the neuroblastoma cells. Therefore, thin sections of the cells

were made and examined with TEM (Fig 3.3.7). It was discovered that the MWNTs (Fig 3.3.7A-C), SWNTs (Fig 3.3.7D-F), CB nanoparticles (Fig 3.3.7G-I), and NDs (Fig 3.3.7J-L) were consistently found inside cytoplasmic vacuoles.

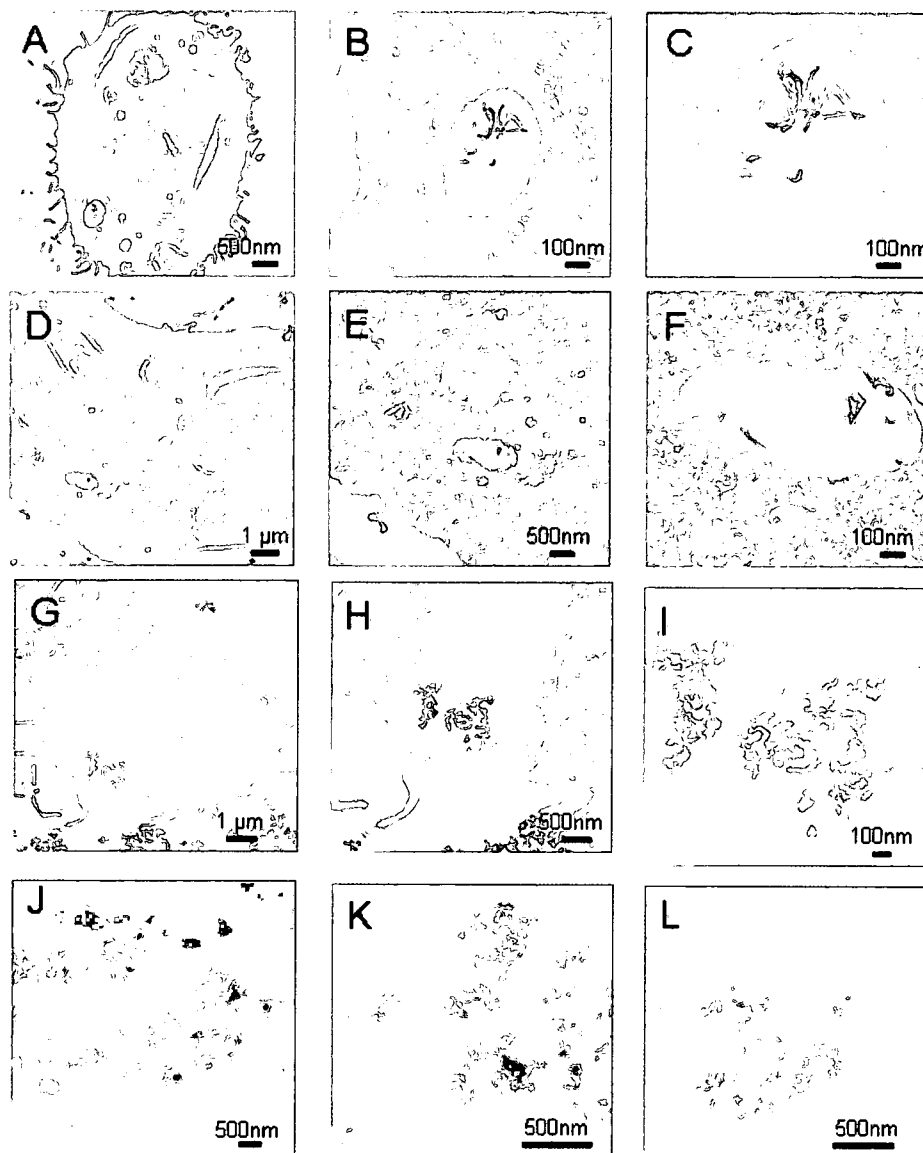


Figure 3.3.7. Transmission electron microscopy of the internalization of carbon nanomaterials into N2A cells. (A-C) Multi-walled carbon nanotubes, (D-F) single-walled carbon nanotubes, (G-I) nano-sized carbon black, and (J-L) nanodiamonds after 100 $\mu\text{g/ml}$ doses for 24h. Notice the presence of all of the different carbon nanomaterials localized into intracellular vacuoles (Schrand et al. 2008b).

For testing the differential biocompatibility of carbon nanomaterials after 24h in neuroblastoma cells and alveolar macrophages, the MTT assay was used. The results showed dose-dependent decreases in viability (Fig 3.3.8) for both cell types. For neuroblastoma cells, the interaction with SWNTs significantly decreased viability at concentrations from 50-100 $\mu\text{g/ml}$, whereas CB, MWNTs, and NDs did not decrease viability compared to the control (Fig 3.3.8A). In contrast, CdO severely reduced viability at the lowest concentration of 25 $\mu\text{g/ml}$.

The macrophages responded to the carbon nanomaterials in a similar manner as the neuroblastoma cells with the greatest biocompatibility for NDs (Fig 3.3.8B). In both cases, the following general trend of biocompatibility was observed: ND>CB>MWNT>SWNT. However, the decreases in viability were more pronounced for macrophages compared to neuroblastoma cells with significant decreases compared to the control after incubation with CB, SWNTs, and MWNTs at concentrations from 25-100 $\mu\text{g/ml}$.

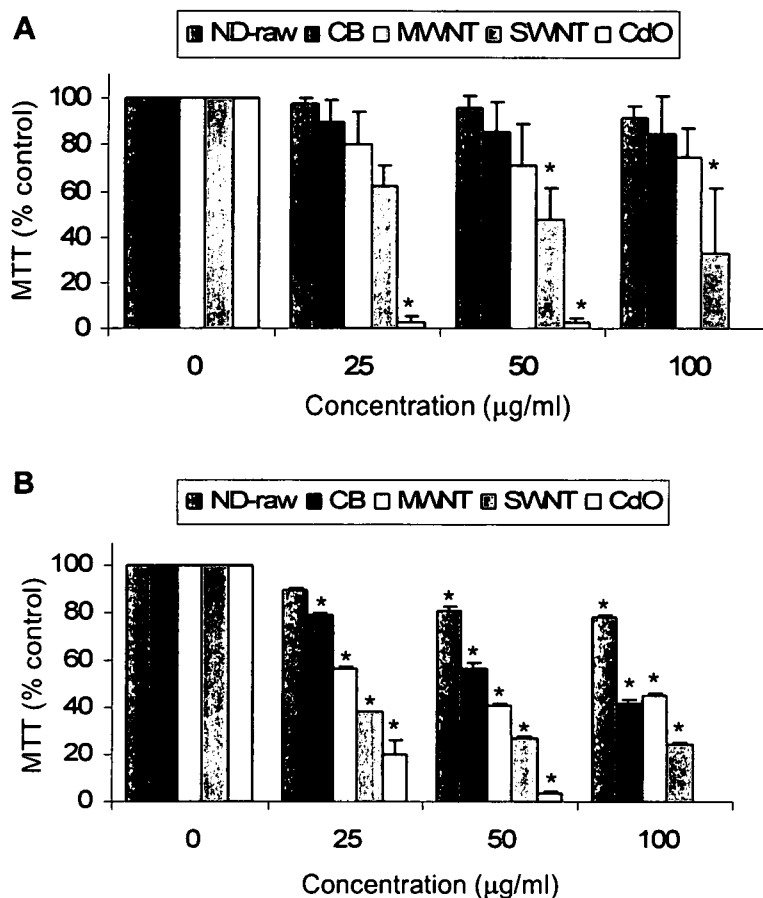


Figure 3.3.8. Biocompatibility evaluation of various carbon nanomaterials. (A) Neuroblastoma cells or (B) Macrophages. Notice the similar trends for biocompatibility ND>CB>MWNT>SWNT>CdO with macrophages being more sensitive to the carbon nanomaterials. Values that were significantly different from the control ($p<0.05$) are denoted with asterisks (*). (Schrand et al., 2007b)

To further examine interactions between the cells and carbon nanomaterials, changes in mitochondrial membrane permeability were examined with fluorescent microscopy (Fig. 3.3.9). The Mito-E-ΨTM fluorescent reagent, when aggregated inside healthy mitochondria fluoresces red whereas dispersion of the dye due to mitochondrial membrane leakage causes it to fluoresce green in the cytoplasm. Aggregation and retention of the

mitochondrial dye inside healthy cells was shown in control cells and cells incubated with 100 $\mu\text{g/ml}$ ND-raw for 24h. The dark color of the CNTs and CB tended to block the fluorescent signal in certain areas compared to cells incubated with NDs, but the dispersion of the dye to the green monomeric form in the cytoplasm was apparent for CB and MWNT (not shown) in addition to the positive control 2.5 $\mu\text{g/ml}$ CdO. It appears that macrophages incubated with 100 $\mu\text{g/ml}$ of MWNT had more dye leakage than cells incubated with 2.5 $\mu\text{g/ml}$ CdO (not shown). This along with the MTT viability assay, suggests that mitochondrial or apoptotic pathways may be influenced to a much greater extent by the presence of carbon nanotubes or CB compared to NDs.

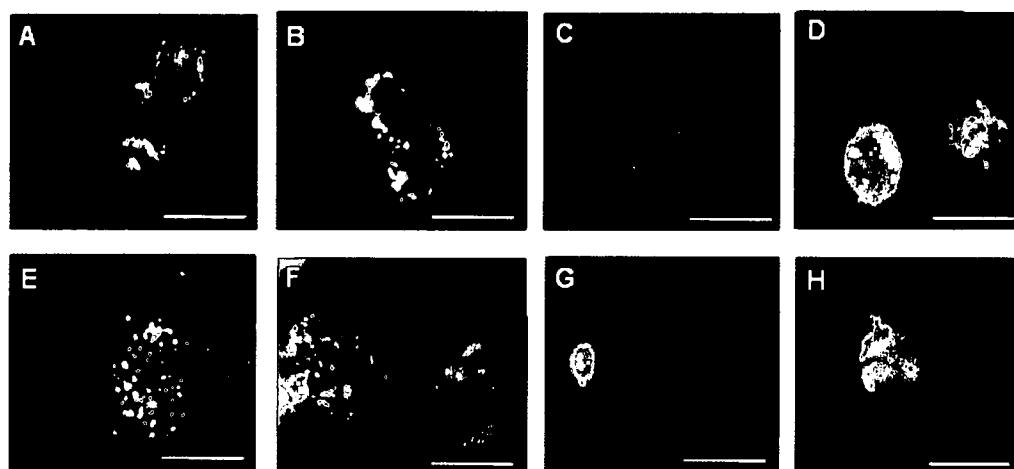


Figure 3.3.9. Mitochondrial membrane permeability of cells incubated with carbon NMs. (A-D) Neuroblastoma cells and (E-H) Macrophages. (A,E) Control, (B,F) 100 $\mu\text{g/ml}$ ND, (C,G) 100 $\mu\text{g/ml}$ CB, (D,H) 2.5 $\mu\text{g/ml}$ CdO after 24 h of incubation and fluorescent staining with the Mito-E- Ψ^{TM} stain for mitochondrial membrane permeability detection. Notice that the control cells and cells incubated with nanodiamonds showed intact mitochondrial membranes whereas cells incubated with carbon black or CdO may have been damaged after NM exposure indicative of mitochondrial membrane leakage and the initiation of apoptosis. Scale bars are 20 μm (Schrand et al. 2008b).

Nanomaterials that generate reactive oxygen species (ROS) induce oxidative stress and have been linked to a general toxic response (Nel et al., 2006). Although ROS can be natural by-products of cellular redox/enzymatic reactions (e.g. mitochondrial respiration, phagocytosis, and metabolism), ROS can also accumulate leading to various pathological conditions (Farber et al., 1990). We found that CNTs generated the greatest amount of ROS followed by CB, then ND in both neuroblastoma cells and macrophages (Fig 3.3.10).

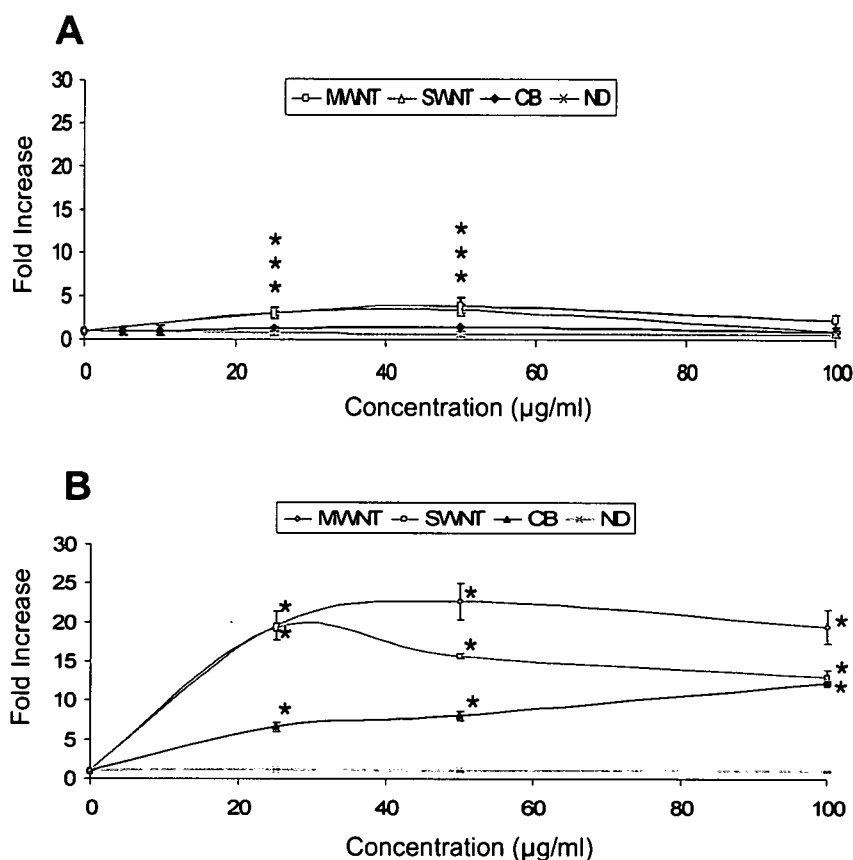


Figure 3.3.10. Generation of ROS after exposure to carbon NMs after 24h. (A) Neuroblastoma cells and (B) Macrophages. Notice that macrophages produce approximately five times the ROS when exposed to the same nanomaterials at the same concentrations as neuroblastoma cells. Significantly values ($p < 0.05$) are denoted by asterisks (*), but NDs do not show increases in ROS (Schrand et al., 2007b)

3.3.3 Biocompatibility of Functionalized Carbon Nanotubes in Neuroblastoma Cells

To demonstrate the influence of surface chemical functionalization, neuroblastoma cells were screened for biocompatibility after incubation with a variety of MWNTs and SWNTs. The visual dispersion of MWNT-COOH (Fig 3.3.11C) was better than other unfunctionalized carbon nanomaterials (Fig 3.3.11B,D).

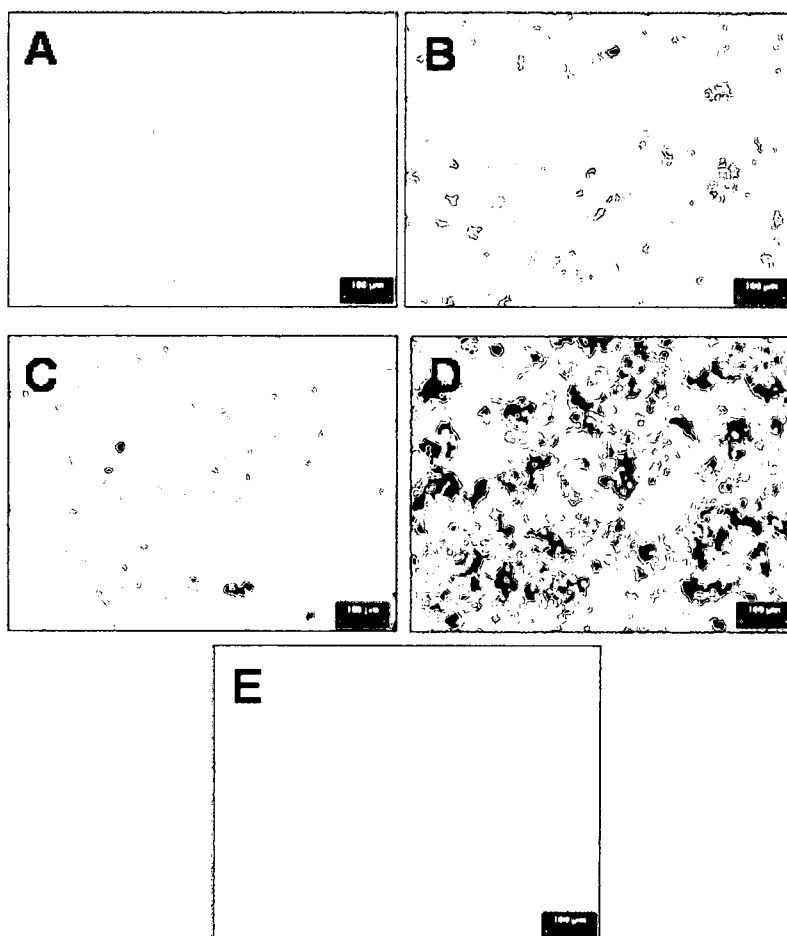
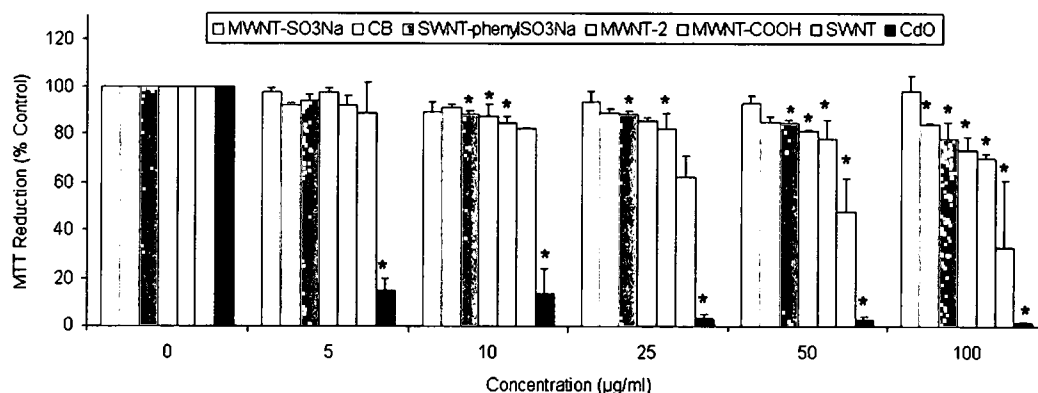


Figure 3.3.11. Morphological observation of N2A cells with carbon nanomaterials. (A) Control, (B) 100 µg/ml unmodified MWNT, (C) 100 µg/ml carboxylic acid-treated MWNT-COOH, (D) 100 µg/ml CB, and (E) 25 µg/ml positive control CdO after 24h of exposure. Scale bars are 100 µm.

When the biocompatibility of acidic MWNT-COOH was compared to the other carbon nanomaterials, with the MTT and ATP assays, MWNT-COOH decreased viability compared to MWNT or CB. However, other functional groups based on $-SO_3Na$ produced more biocompatible MWNTs and SWNTs with the general trend: MWNT- SO_3Na > MWNT and SWNT-phenyl SO_3Na > SWNT (Fig 3.3.12A). The positive control cadmium oxide, CdO, showed drastic decreases in viability at all concentrations in this study indicating the validity of the assay. Another viability assay based on luminescent ATP production showed similar results, but overall greater biocompatibility for the carbon nanomaterials suggesting that different biochemical tests for biocompatibility differ in their sensitivity (Fig 3.3.12B). Therefore, the differential biocompatibility of functionalized carbon nanomaterials may be explained by changes in surface chemistry, purity, and dispersion.

(A)



(B)

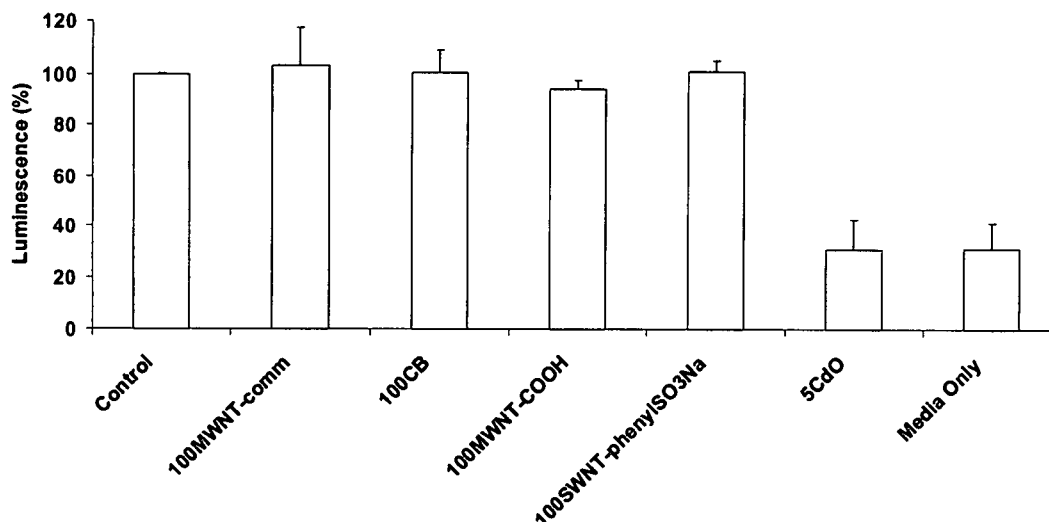


Figure 3.3.12. Viability assays in N2A cells incubated with various functionalized carbon nanomaterials (A) MTT and (B) ATP assays. Values that were significantly different from the control ($p < 0.05$) are denoted with asterisks (*). (Schrand et al. 2008b).

3.3.4 Factors that May Alter Carbon Nanomaterial Biocompatibility

Several other factors were considered in these studies for their impact on carbon nanomaterials biocompatibility: the amount of serum proteins present, interference with the biochemical assay probes, and cell growth on carbon nanotubes substrates compared to exposure of the nanotubes in solution. The presence of serum proteins in the cell culture media was found to directly impact the viability response (Fig 3.3.13). This was demonstrated by incubating macrophages with CB nanoparticles in growth media containing 20% serum compared to dosing media containing only 10% serum for 24h. The results show significant decreases in viability at concentrations from 25-100 $\mu\text{g/ml}$ compared to no significant difference from the control in the growth media. Similar increases in viability were found in keratinocytes after

exposure to Al₂O₃, Ag, and Cu nanoparticles in RPMI cell culture media containing serum compared to media without serum (Murdock et al., 2007).

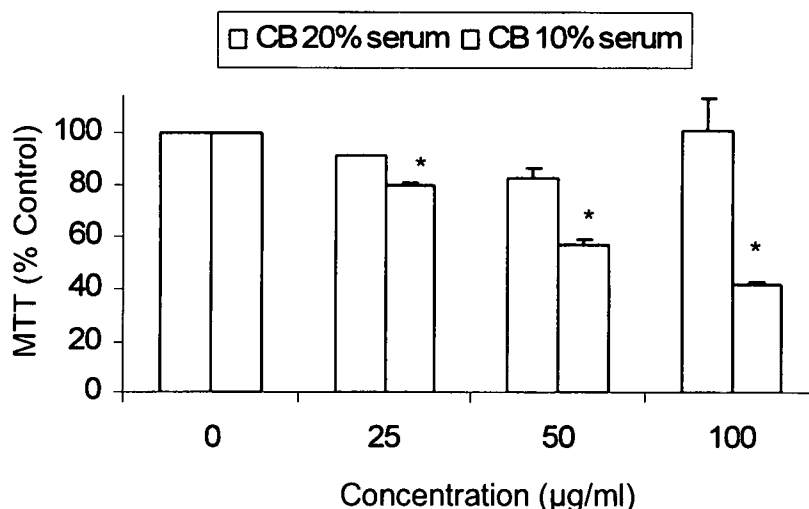
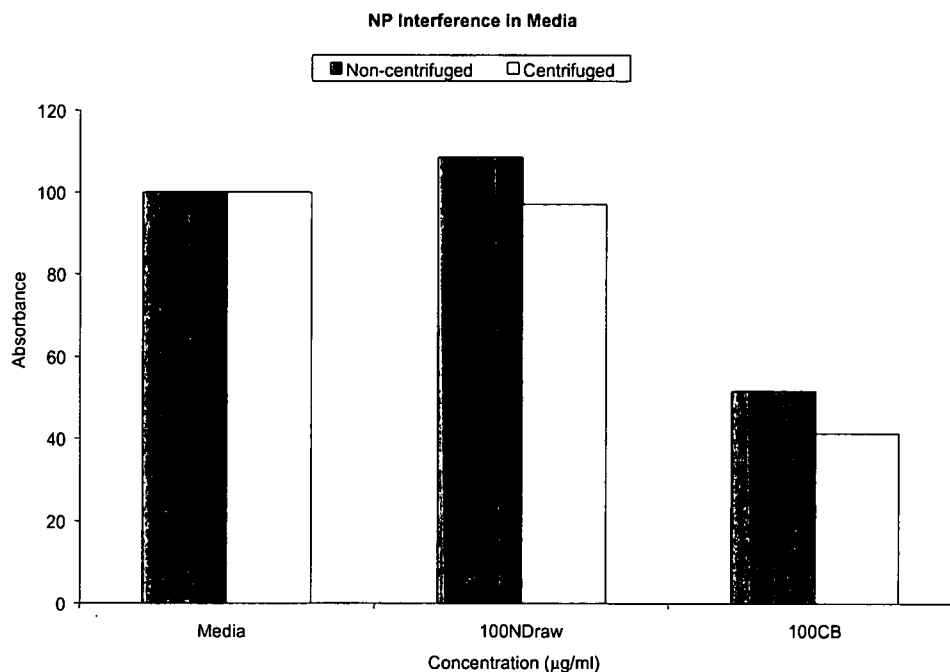


Figure 3.3.13. Effect of serum concentration on cell viability. Macrophages were dosed with carbon black nanoparticles (CB) in F12K cell culture media containing 10% or 20% FBS for 24h. Asterisks (*) denote a significant difference from the control at $p < 0.05$.

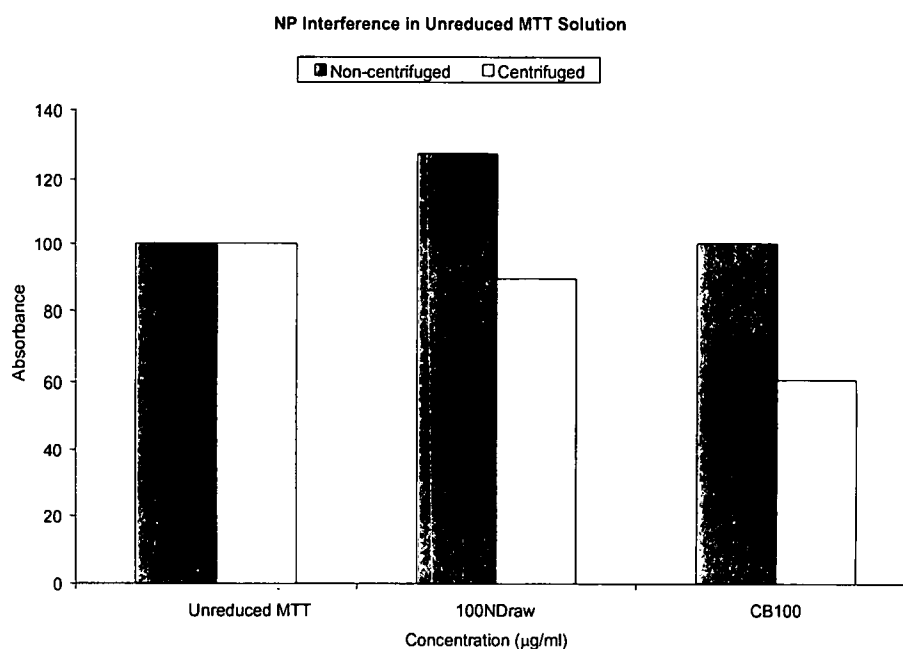
The interference of biochemical assay probes with carbon nanomaterials has been reported in previous *in vitro* biocompatibility studies (Monteiro-Riviere et al., 2005, Monteiro-Riviere and Inman, 2006). However, Wick et al., 2007 found that the binding of MTT-formazan to CNTs was negligible and did not influence their results (Wick et al., 2007). We also expect negligible binding of the reduced MTT product to the carbon nanomaterials used in our studies, but rather that the presence of the carbon nanomaterials could be responsible for changing the absorbance values. Therefore, in order to better understand the interference of the carbon nanomaterials with the biochemical assay probes, several experiments were performed.

Solutions of cell culture media (Fig. 3.3.14A), unreduced MTT solution (Fig. 3.3.14B), or reduced MTT solution (Fig. 3.3.14C) were examined for changes in absorbance after the addition of carbon nanomaterials and their removal by centrifugation. Centrifugation has been used in other studies to remove the nanoparticles and re-aliquoting to new microplates, but has not been adopted in all carbon nanomaterials biocompatibility studies (Jia et al., 2005). Nanodiamonds tended to increase the absorbance values when left in solution, likely due to their strong ability to diffract light. However, CB tended to reduce the absorbance both before and after centrifugation in cell culture media suggesting that some of the nanoparticles remained in solution.

(A)



(B)



(C)

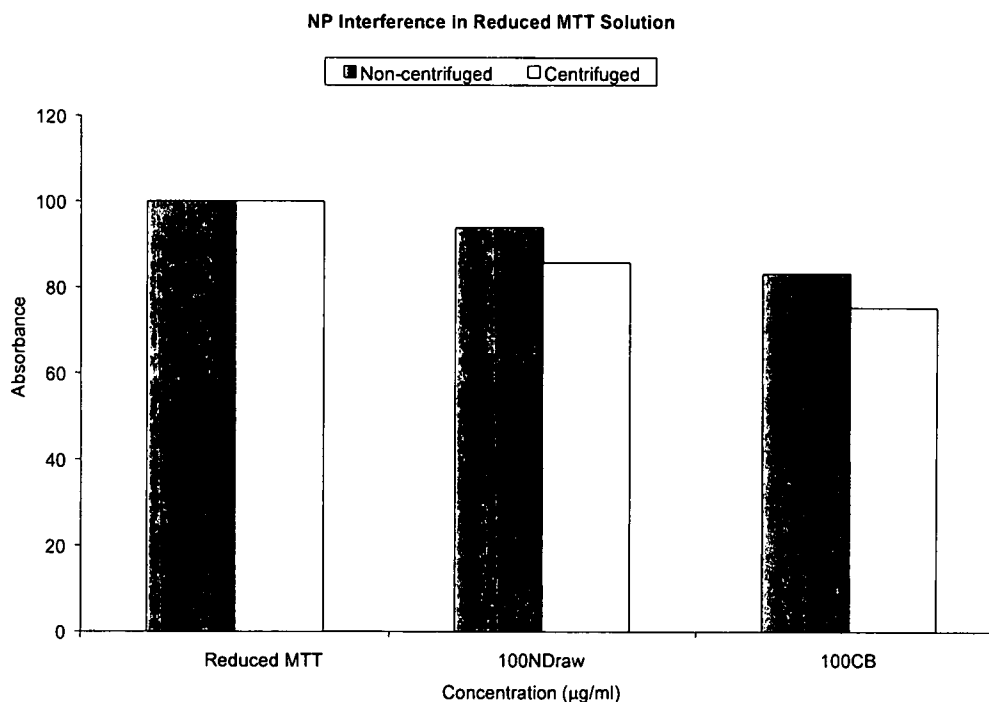


Figure 3.3.14. Effect of carbon nanomaterials on microplate reader absorbance. (A) Carbon nanomaterials in cell culture media, (B) Carbon nanomaterials in unreduced MTT solution, and (C) Carbon nanomaterials in reduced MTT solution (Schrand et al., 2007a).

Acellular ROS assays were conducted to assess the inherent ability of carbon nanomaterials to generate reactive oxygen species in the absence of cells. There was very little change from the 1.00 baseline after 1, 3, or 7 days (Fig 3.3.15). On Day 1, there was a slight decrease in ROS at the higher carbon nanomaterial concentrations (Fig 3.3.15A). On Day 2, there was a slight increase in ROS at 10 $\mu\text{g/ml}$ for the CB and MWNT (Fig 3.3.15B). On Day 3, there was a slight elevation for MWNT at the highest concentration of 150 $\mu\text{g/ml}$ (Figure 3.3.15C). Therefore, acellular ROS assays support the notion that the carbon nanomaterials used in our studies do not generate ROS in the absence of cells. This fact further implicates the cell-specific response of the macrophages to initiate an inflammatory cascade following certain nanomaterials internalization compared to the neuroblastoma cells.

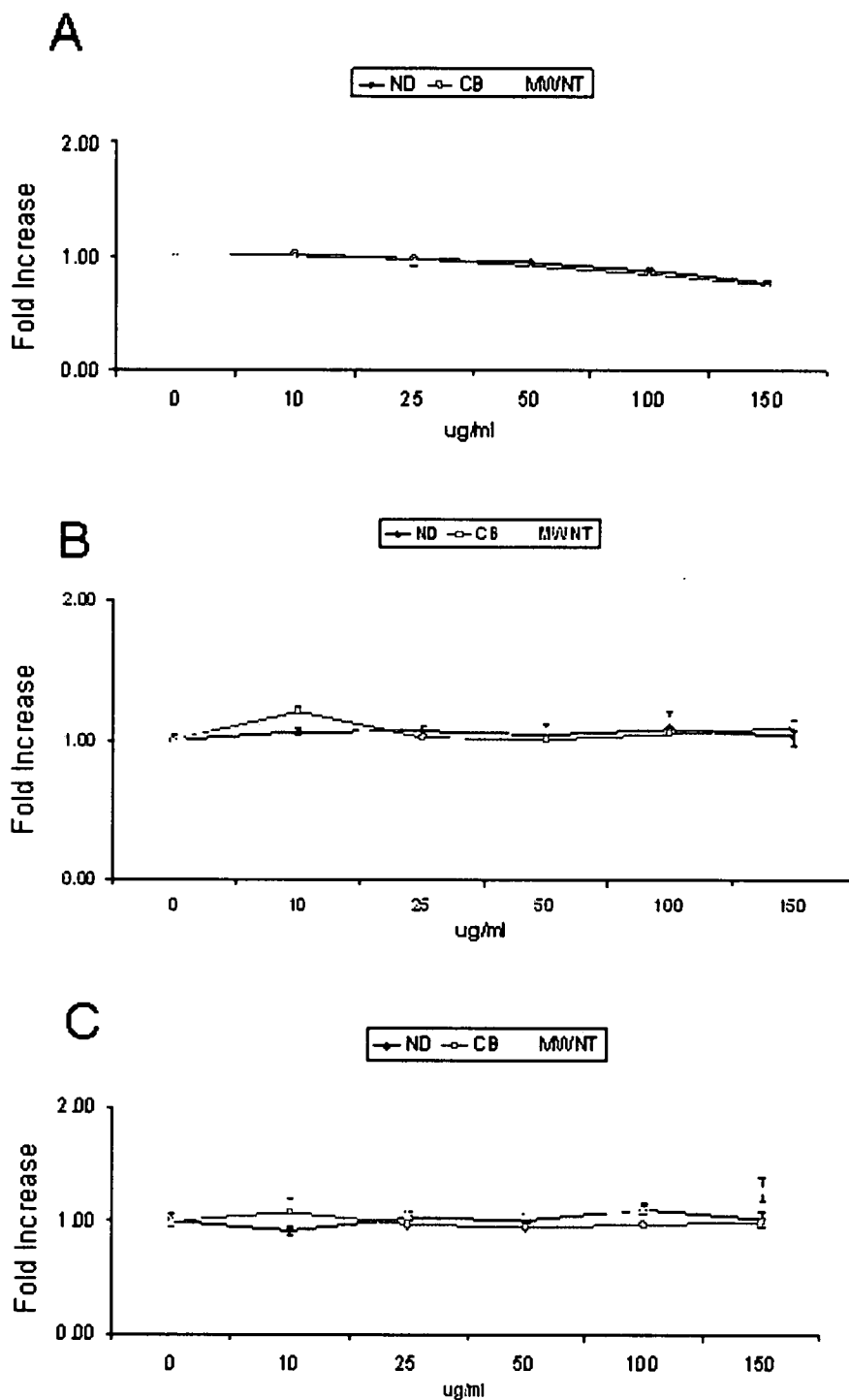


Figure 3.3.15. Acellular ROS response to carbon nanomaterials. (A) Day 1, (B) Day 2, and (C) Day 7.

It is expected that cells respond differently to growth on carbon nanotubes substrates compared to incubation with suspensions of freely floating nanotubes. Indeed, we have shown that neuroblastoma cells readily grow on single-walled carbon nanotube (SWNT) paper (Fig 3.3.16). No specific surface treatments were made to the substrate and the cells adhered and grew with normal morphological features such as extended neurites and intimate connections upon higher magnification with the SWNTs. These preliminary results suggest that SWNT in the form of paper could be used as a flexible, conductive biomaterial for cell growth or bio-sensing. Other studies with surface chemically functionalized carbon nanotubes as neuronal substrates are providing positive results for growth and stimulation, but efforts to optimize these substrates into multi-functional platforms or devices for implantation are still underway (Hu et al., 2004, Hu et al., 2005, Zhang et al., 2005b, Mattson et al., 2000).

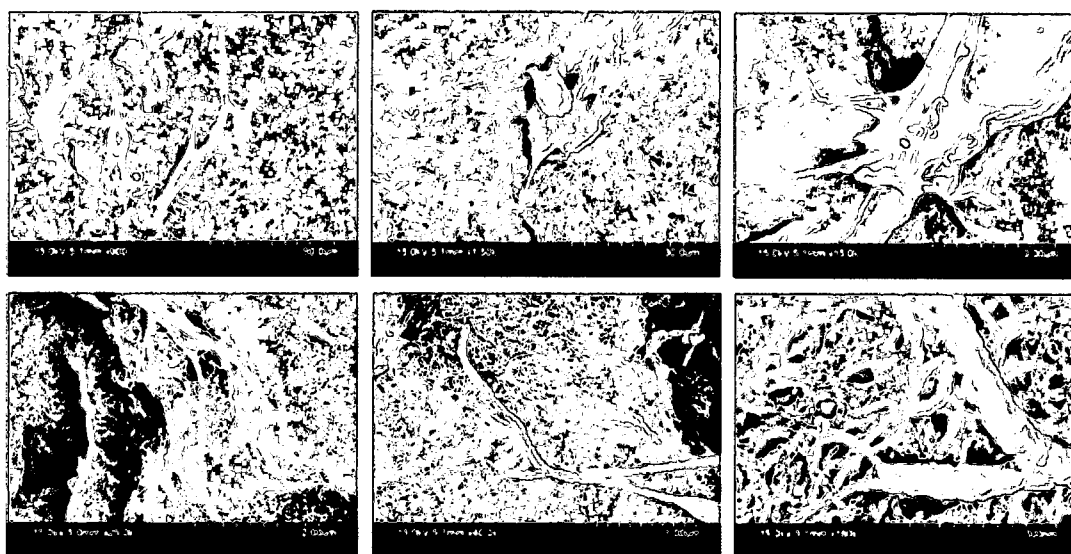


Figure 3.3.16. Cell growth on SWNT paper. Neuroblastoma cells grow and elongate on SWNT paper showing morphologies characteristic of cell attachment and spreading indicative of viability.

3.4 Discussion

Examining changes in cell morphology, decreases in cell viability, indicative of cell death, or increases in oxidative stress, measured by the increased formation of reactive oxygen or nitrogen species, in cells exposed to nanomaterials is important for establishing links between exposure and lung, cardiovascular, and autoimmune diseases. However, first understanding the characteristics responsible for the negative impact of nanomaterials on cell health must be revealed. In these studies, the main nanomaterial characteristic of carbon nanotubes, compared to CB or NDs, that is suspected to be responsible for the decreased cell viability, increased mitochondrial membrane potential, and increased ROS after exposure is the presence of transition metal catalysts that are used in the synthesis of the carbon nanotubes (e.g. Fe, Ni, Co). The estimated amount of solubilized Fe that could be extracted with nitric acid was 0.49 wt% Fe for MWNTs vs. 0.26 wt% Fe for SWNTs compared to levels below the detection limit for CB and NDs. In support of this notion, the highest ROS levels were produced by cells exposed to MWNTs followed by SWNTs, CB, and NDs for both N2A cells and macrophages.

Several other groups have recently produced similar results for the effect of Fe on cell viability after exposing cells to carbon nanotubes of varying purity (Garibaldi et al., 2006, Kagan et al, 2006, Pulskamp et al., 2007). Additionally, Wick et al., 2007 found that different fractions of CNTs, such as

those that are better dispersed with low carbonaceous material contamination, are more biocompatible than crocidolite asbestos, which has a higher Fe content than chrysotile asbestos, measured with the MTT assay or changes in cell proliferation after DNA analysis. Therefore, all of these studies support the conclusion that the metal catalyst residues are directly involved in the oxidative response.

The second factor found to greatly influence carbon nanomaterial biocompatibility was the cell type. The most noticeable difference between two cell types (neuroblastoma and macrophage) was in the amount of carbon nanomaterials internalized, which was likely related to the greater decreases in viability and increases in ROS in the macrophages. The inherent function of the macrophages to initiate an inflammatory response or programmed cell death may also occur to a greater extent in the immune cell (macrophage). However, despite these proposed cell-specific differences, there was a lack of ROS generation and retention of mitochondrial membrane integrity in cell lines incubated with NDs suggesting that the presence of impurities (e.g. Fe) has a greater influence the oxidative stress response of the cells. Although changes in morphology were difficult to assess in the N2A cells, due to their non-homogenous characteristics, the cells appeared to respond to the presence of nanomaterials by increased neurite extension. Other cells such as the PC-12 cells displayed irregular cell borders after contact with MWNTs

and macrophages tended to increase in size after accumulating nanomaterials throughout their cytoplasm.

The third nanomaterial characteristic suspected to greatly impact carbon nanomaterial biocompatibility was the size of the carbon nanomaterials, which is linked to the dispersion quality in solution, and factors such as temperature, surface chemistry, and charge. While all of the carbon materials examined in these studies were in the nanometer range, after suspension in cell culture media, they formed micron-sized agglomerates, which then come into contact with the cells. The smallest NDs were the most biocompatible carbon nanomaterials to multiple cell types, but as previously mentioned, this may be due to their purity or shape more than their size. The effect of temperature upon agglomeration behavior demonstrated that agglomeration increases over very short times such as 1h at 37°C compared to 25°C. This phenomenon was readily apparent in the studies with PC-12 cells where good biocompatibility was found and likely associated with decreased contact between the carbon nanotubes and cells. The differential biocompatibility of functionalized carbon nanomaterials may be explained by changes in size and dispersion related to surface chemistry. However, it was also suspected that the amorphous or graphitic carbon, fullerenes, metal catalysts, and other "contaminants" in nanotube samples were more fully removed after treatment with strong acids (e.g. hydrochloric, nitric, sulfuric) and high temperatures, which are typically used to generate the functional groups. Other chemical or

physical methods used to functionalize carbon nanomaterials may effectively prevent direct contact with the cell due to changes in hydrophobicity/hydrophilicity or charge and the resulting dispersion in cell culture media. Although surfactants and coatings were not examined in these studies, Wick et al., 2007 show that purified SWNTs well dispersed in a biocompatible surfactant; polyoxyethylene sorbitan monooleate (PS80) were more biocompatible than micron-sized agglomerates of purified SWNTs (Wick et al., 2007).

Other factors that can influence the size, dispersion, and apparent biocompatibility of carbon nanomaterials include the presence or absence of serum proteins, which were found to increase the biocompatibility of CB and other nanomaterials (Murdock et al., 2007), the binding of biochemical assay probes (e.g. MTT or ROS), direct interference with assay results due to increased or decreased absorbance in a microplate reader, the form of nanomaterials that the cell are exposed to (e.g. suspension or substrate), shape (Ding et al., 2005), surface reactivity, or degree of gravitational settling (Teeguarden et al., 2007). The subject of carbon nanomaterial interference with biochemical assay probes is still debatable as demonstrated by recent observations (Worle-Knirsch et al., 2006). However, it has been demonstrated that carbon nanomaterials in solution can decrease N2A cell viability while the same cells can readily grow on SWNT paper suggesting that the cells respond quite differently to the form of the carbon nanomaterials

(e.g. in suspension compared to growth on substrates). Therefore, it is imperative that the unique characteristics of carbon nanomaterials are optimized while at the same time engineering more biocompatible products.

CHAPTER 4

NANODIAMONDS

4.1 Literature Review

Interactions between diamond and biological systems have historically shown little reactivity due to the chemical inertness and high biocompatibility of diamond as both a substrate and in particulate form (Freitas, 2003, Table 4.1.1). Finely divided carbon particles are well tolerated by the body (Benson et al., 1969) and the passive nature of carbon in tissue has been known since ancient times as exemplified by the use of charcoal and lampblack nanomaterials for ornamental and official tattoos (Haubold, 1977). Early experimental work with cells exposed to micron-sized diamond particles further supports its low reactivity and high biocompatibility (Table 4.1.1). For example, several studies in polymorphonuclear (PMN) leukocytes have shown that micron-sized diamond particles can be used as an inert control because they do not stimulation the production of reactive oxygen species (Hedenborg and Klockars, 1989), can be phagocytosed without chemotactic activity (Tse and Phelps, 1970), and produce no effect on degranulation or secretion of cell motility factors (Higson and Jones, 1984). In other cell types such as macrophages, cells that readily ingest large amounts of debris, micron-sized diamond dust was found non-fibrogenic (Schmidt et al., 1984),

not affecting cell viability for at least 30h (Allison et al., 1966), and did not activate or change the cell morphology or production of interleukin 1-beta (Nordsletten et al., 1996). In fibroblasts, cells of the connective tissue, micron-sized diamond particles did not induce fibrogenic activity (Allison et al., 1966, Luhr, 1958), did not induce the release of proliferation factors (Schmidt et al., 1984), and had no mitogenic effect (Cheung et al., 1984). In animal studies, diamond particles did not contribute to inflammation when introduced or injected into implant traversing canals in rabbits (Per Aspenberg et al., 1996), canine knee joints (Tse and Phelps, 1970), or the complement system (Doherty et al., 1983). Blood exposed to diamond powder for 60 minutes did not produce detectable hemolysis (Dion et al., 1993). More recent studies with nano-sized diamonds also demonstrate that they are well tolerated by various cell types (Yu et al., 2005, Schrand et al., 2007a). Yu *et al.* investigated the biocompatibility of relatively large synthetic abrasive diamond powders (100 nm) in kidney cells and found good biocompatibility after incubation for 3h at concentrations up to 400 µg/ml (Yu et al., 2005). A summary of biocompatibility work with diamond particles is shown in Table 4.1.1.

Table 4.1.1. Biocompatibility Studies of Diamond Particles

Material	Dose/ Time	Cell Line/ Animal	Biocompatibility Results	Reference
2-4 μm diamond dust	10-100 $\mu\text{g/ml}$, 30h	Mouse peritoneal macrophages	Internalized, cells extended and mobile, lysosomal enzymes in phagosomes	Allison et al., 1966
3 μm diamond crystals	1-2 mg/ml , 45min	Human PMNs	No chemotactic activity, no change in motility, internalized	Tse & Phelps, 1970
3 μm diamond crystals	10 mg/ml , 4h	Canine knee joints	Low inflammation, low intra-articular pressure, low local cell count	Tse & Phelps, 1970
2-8 μm diamond crystals	4 mg/ml , 45min	Human peripheral blood neutrophils	Low chemotactic activity, internalized	Spilberg et al., 1982
2-7 μm diamond crystals	4 mg/ml , up to 12min	Horse and pig neutrophils	Internalized, but no respiratory burst, low oxygen consumption	Higson and Jones, 1984
<0.5 μm and 1-2 μm diamond dust	25-100 $\mu\text{g/ml}$, 24h	Human peripheral blood monocytes	No release of thymocyte (IL-1) or fibroblast proliferation factors	Schmidt et al., 1984
1-5 μm diamond crystals	100-400 $\mu\text{g/ml}$, 16h	Canine synovial fibroblasts	Internalized, but no mitogenic effect	Cheung et al., 1984
4-8 μm diamond dust	10-100 $\mu\text{g/ml}$	PMNs	No ROS generation	Hedenborg & Klockars, 1989
Diamond powder	0.5 g/cm^3 , 60 min	Diluted Blood	No detectible hemolysis	Dion et al., 1993
2-15 μm diamond particles	25 mg/ml , 3 weeks	Rabbit	No foreign body response, no decrease in bone formation	Aspenberg et al., 1996
2-15 μm diamond particles	500 $\mu\text{g/ml}$, 48h	Human monocytes	High viability, internalized, no IL-1 β production	Nordsletten et al., 1996
NDs	1.25 mg/ml , 90min	White Blood Cells	85-93% hemolysis	Puzyr et al., 2004
NDs	310 $\mu\text{g/ml}$, 90min	Red Blood Cells	3-50% hemolysis	Puzyr et al., 2004
Fluorescent NDs-100nm	20-400 $\mu\text{g/ml}$, 3h	Human kidney cells (293T)	Non-toxic, MTT assay	Yu et al., 2005
2-10nm NDs	5-100 $\mu\text{g/ml}$, 24h	Neuroblastoma cells	Internalized, no ROS, intact mitochondria, cytoskeletal alterations	Schrand et al., 2007a

However, the sharp, abrasive, jagged, splinter-like nature of shattered diamond particles is of particular concern for ingested or inhaled diamond particles. In this case, crude mechanical damage to human tissues and organs is expected while accumulation in the body due to the lack of degradation and elimination also warrant further investigation (Maxwell, 1988, Davies, 1984). Other well-known properties of diamond, in addition to its hardness and chemical inertness, change when it is reduced in size to the nano-scale.

Even smaller detonation nanodiamonds have many advantages over other carbon nanomaterials including their very small size, low cost synthesis, optical transparency, ability to be surface modified, and fluoresce after attachment of fluorophores or nitrogen-induced vacancies with electron beam irradiation (Treussart et al., 2006). The recent dispersion of 2-10nm detonation nanodiamonds in aqueous media by Ōsawa and co-workers has facilitated their use in physiological solutions (Krüger et al., 2005). However, NDs have been shown to efficiently adsorb proteins due to their high surface-to-volume ratio (Huang et al., 2004a, Huang et al., 2004b, Bondar et al., 2004), are able to translocate across the cell membrane due to their small size (Yu et al., 2005, Schrand et al., 2007a), can alter human gene expression responsible for cancer (Bakowicz-Mitura et al., 2007), and cause white cell destruction and erythrocyte hemolysis (Puzyr et al., 2004, Table 4.1.1). The same characteristics that contribute to potentially harmful effects

to the body are also considered useful for the development of therapeutic agents such as the transport of biological species (Bianco et al., 2005, Kam et al., 2005a); carriers for nucleic acids and biologically active molecules via bioloistic gene delivery into bacterial cells, yeast, insects, and plants (Grichko et al., 2006), for *in vitro* observation of growth hormone receptor molecules (Cheng et al., 2007), cellular biomarkers (Fu et al., 2007), and as scattering optical labels (Smith et al., 2007), the targeting of cancer cells for destructive purposes (Kam et al., 2005b), or the development of nanorobots (Freitas, 2003).

Therefore, it is critical to gain a better understanding of the biocompatibility of carbon nanomaterials, including nanodiamonds, due to the rapid world-wide production and use, which is increasing the exposure risk in occupational, consumer, environmental, and biomedical areas. In support of these studies, there is a great amount of evidence that some non-toxic micron-sized particles become toxic once they are reduced in size to the nano-scale (Heath et al. 1971, Oberdorster et al., 1992, Ferin et al., 1992, Donaldson et al, 1998, Johnston et al., 2000, Oberdorster et al., 2000). Therefore, it is the goal of this chapter to examine the interactions of mammalian cells with 2-10nm nanodiamonds, with various surface chemistries or fluorescence to reveal the relationship between their properties and biocompatibility.

4.2 Results for Characterization

The characteristics of nanodiamonds were chemically evaluated with FTIR and Raman; size distribution and morphology with TEM; aggregate size in solution with DLS, and charge with zeta potential. A summary of the characteristics of the nanodiamonds used in these studies is in Table 4.2.1.

4.2.1 Chemistry

The as-received nanodiamonds (ND-raw) were subjected to treatment with acid (70% HNO_3 and 98% H_2SO_4 at a ratio of 1:3) or strong base (NaOH, pH~14) in a sonication bath for 3 h and then stirred at 90°C for 10 h (Schrand et al., 2007a). The excess acids, bases, or impurities were removed by repeated sonication, centrifugation, and decantation. Raman, and FTIR were used to monitor the purification process to characterize the nanodiamonds before and after the purifications. The precipitates were readily dispersible in water once the pH of the nanodiamond suspension reached above ~4.5 for the acid-treated sample or below ~8.5 for the base-treated sample, which falls in the 7.2 - 7.6 pH range necessary for the media applied to cells. Example spectra for the NDs before and after the acid or base treatment are given in Fig. 4.2.1, which show an increase in the ND purity after the purifications, which also result in the formation of additional surface functional groups.

The FTIR spectrum of the as-received nanodiamond powder shows a strong absorption at 3430 cm^{-1} , weak intensity shoulder peaks at approximately 2928 cm^{-1} , and bands at 1720, 1630, 1334 (not labeled on graph) and 1117

cm^{-1} , which can be ascribed to the O-H, C-H, C=O, C=C, C-C and C-OH vibrational modes, respectively (Fig 4.2.1A). The FTIR data indicates the rich presence of hydroxyl and carboxylic acid functional groups on the nanodiamond surface. After the sonication-assisted acid treatment, the vibrational modes from C=O and C-H became more evident while those from C=C and C-C became weaker, indicating further functionalization of sp^2 and sp^3 carbons on the nanodiamond surface.

Raman scatterings show the diamond component peak at approximately 1327cm^{-1} for the as-received sample is not as prominent as the non-diamond component at approximately 1600cm^{-1} (Schrand et al., 2007a). The peak area ratio, $A_{\sim 1600\text{cm}^{-1}}/A_{\sim 1327\text{cm}^{-1}}$, is only approximately 0.11. After the acid purification, the peak area ratio increased to 0.56 for the supernatant obtained from at least ten cycles of sonication, centrifugation, and decantation. It should be noted that there is not a noticeable change in the peak area ratio after the first several centrifuged nanodiamond-contained supernatants, but only after several washings, does the peak area ratio become relatively high. Furthermore, a ratio value of 1.0 has not been reached in this work for either acid or base purified NDs. Therefore, non-diamond carbons generated from the stirred-media milling are not likely to be completely removed from the nanodiamond surfaces by the acid or base treatments, but the base treatment appears to more greatly remove the non-diamond carbons.

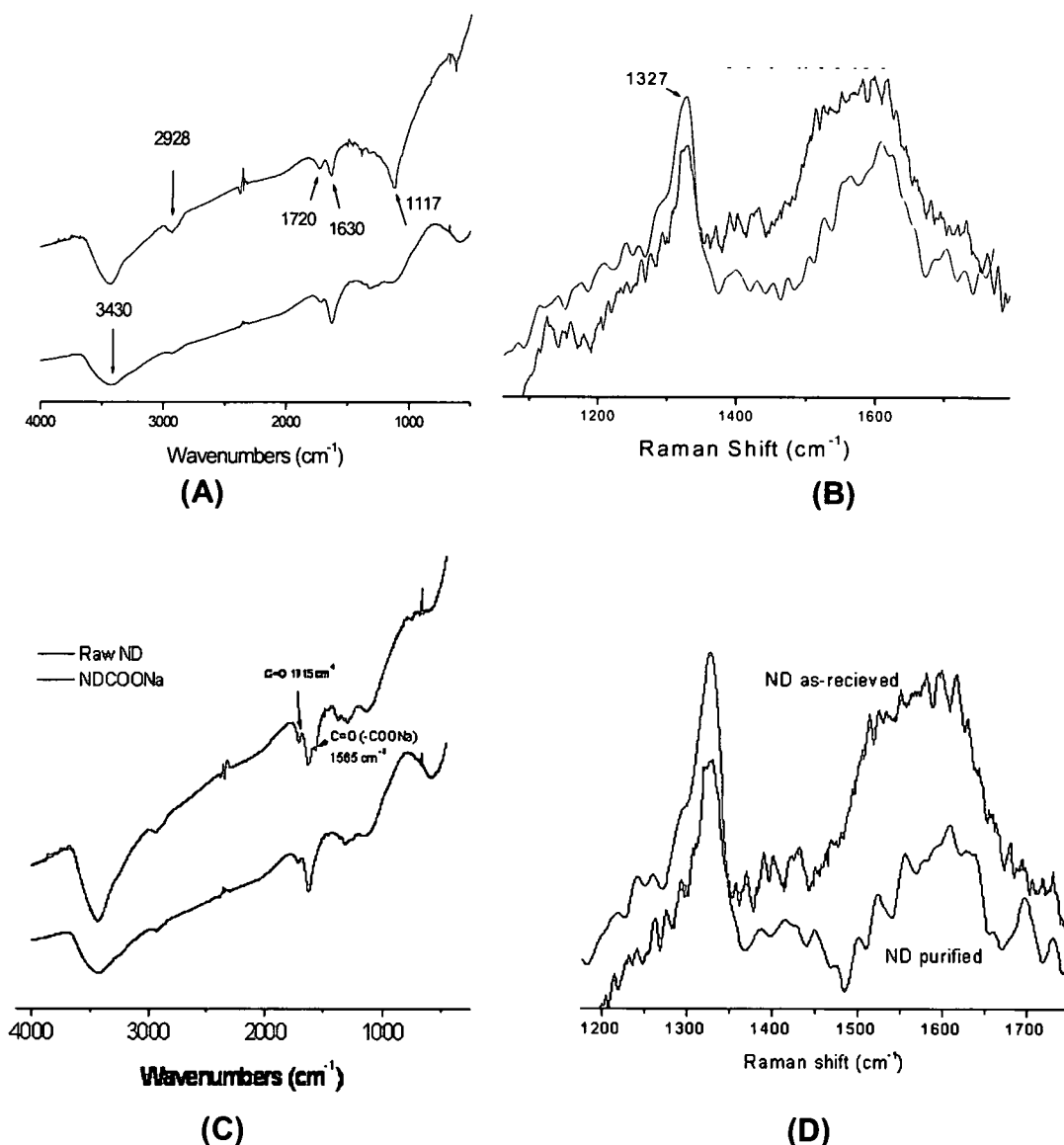


Figure 4.2.1. FTIR and Raman spectroscopy of NDs. (A) FTIR and (B) Raman spectra of NDs before (black) and after acid purification (red) and (C) FTIR and (D) Raman spectra of NDs before (black) and after base purification (red) (adapted from Schrand et al., 2007a).

4.2.2 Size and Morphology

Characterization of the size distributions and morphologies of nanodiamonds (NDs) was performed with transmission electron microscopy (TEM) from random fields of view. All NDs had cubic morphologies with primary particle

sizes ranging from 2-10 nm with the majority ~5 nm in size as shown with TEM and the associated size distribution graphs (Fig 4.2.2). ND-raw nanoparticles were on average 5.1 ± 1.7 nm in size (Fig 4.2.2), carboxylic acid purified nanodiamonds (ND-COOH) were 5.9 ± 1.6 nm (Fig 4.2.2B), base-purified nanodiamonds ND-COONa were 4.6 ± 1.1 nm, and ND-SO₃Na were 5.0 ± 1.7 nm.

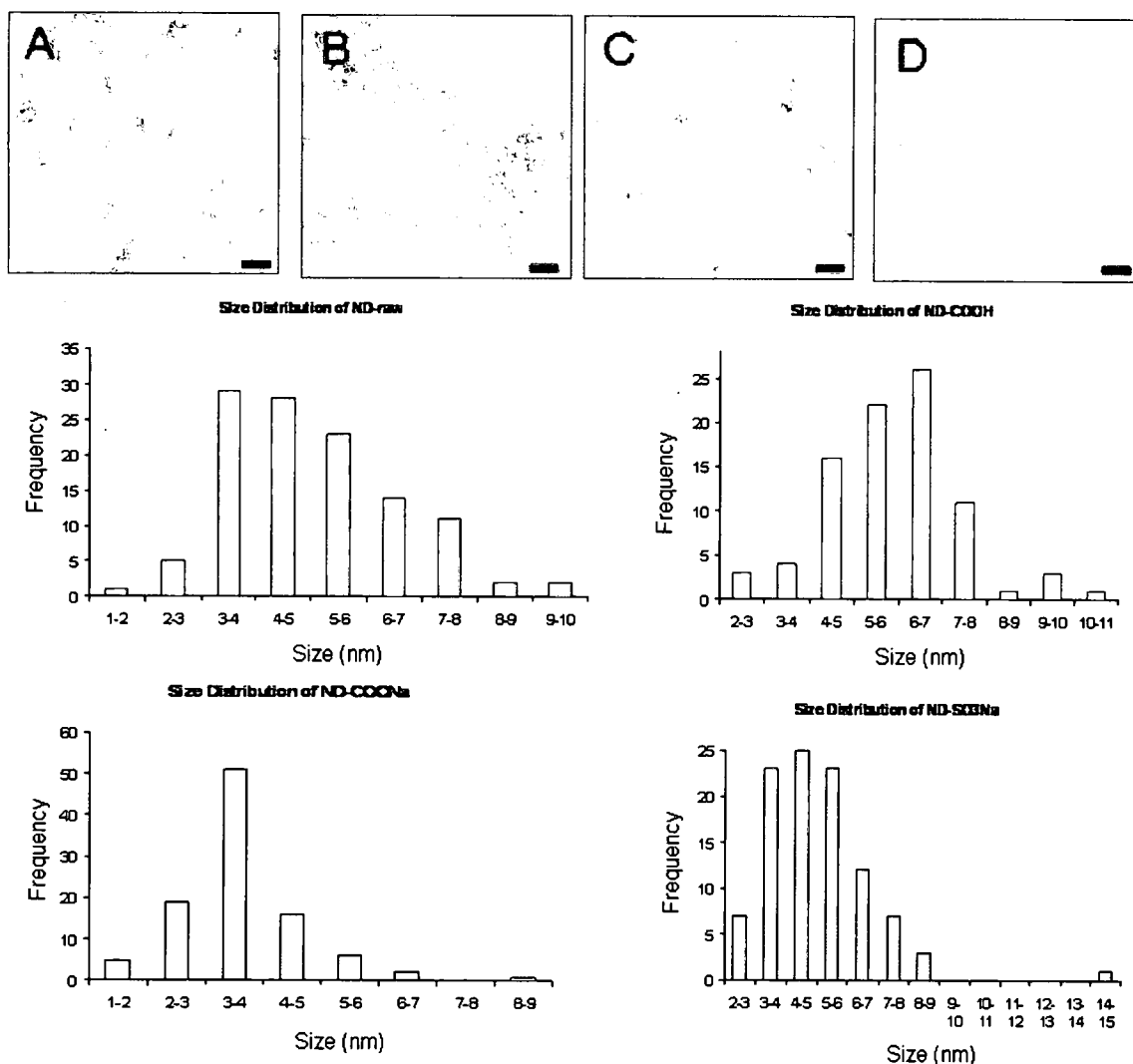


Figure 4.2.2. Size and morphology of NDs with transmission electron microscopy (TEM). (A) ND-raw, (B) ND-COOH, (C) ND-COONa, and (D) ND-SO₃Na. Scale bars are 100nm. Size distribution graphs of nanodiamonds after counting up to 100 nanoparticles from TEM images (Schrand et al., 2007a).

4.2.3 Dynamic Light Scattering and Zeta Potential

As-received NDs (ND-raw), acid purified (-COOH), or base purified (-COONa, -SO₃Na) nanodiamonds at concentrations of 1 mg/ml were briefly sonicated for 1 minute at approximately 30W with a probe tip sonicator before dispersion in DMEM/F12 cell culture media with or without 10% serum proteins. The roughly spherical (cubic) nanodiamonds formed aggregates ranging in size from approximately 20 nanometers to 2.5 microns depending on the type of solution (Fig 4.2.3), but the formation of very strong ND ranging in size from 25 to 100 nm is a well-known issue (Krüger et al., 2005). For ND-raw and ND-COONa, the smallest sizes were in water as represented by the intensity distribution from dynamic light scattering compared cell culture media with or without serum proteins. Both ND-COOH and ND-SO₃Na followed similar trends for lowest size in media with serum. Because the presence of serum in the media (blue spectra) appears to decrease the average ND size compared to media without serum (green spectra) in all samples, the serum proteins may encourage ND separation in solution. Preliminary protein binding experiments show the reduction of small molecular weight bands after the addition of nanoparticles to media containing serum, but further study is required to confirm the removal of serum proteins by the nanoparticles. Close examination of the control solutions of media with and without serum show that serum proteins contribute to <4% of the relative amount in sample volume at 15.6nm, which

may only be apparent in the ND-COOH spectra, but no other similar values are shown for the other ND solutions.

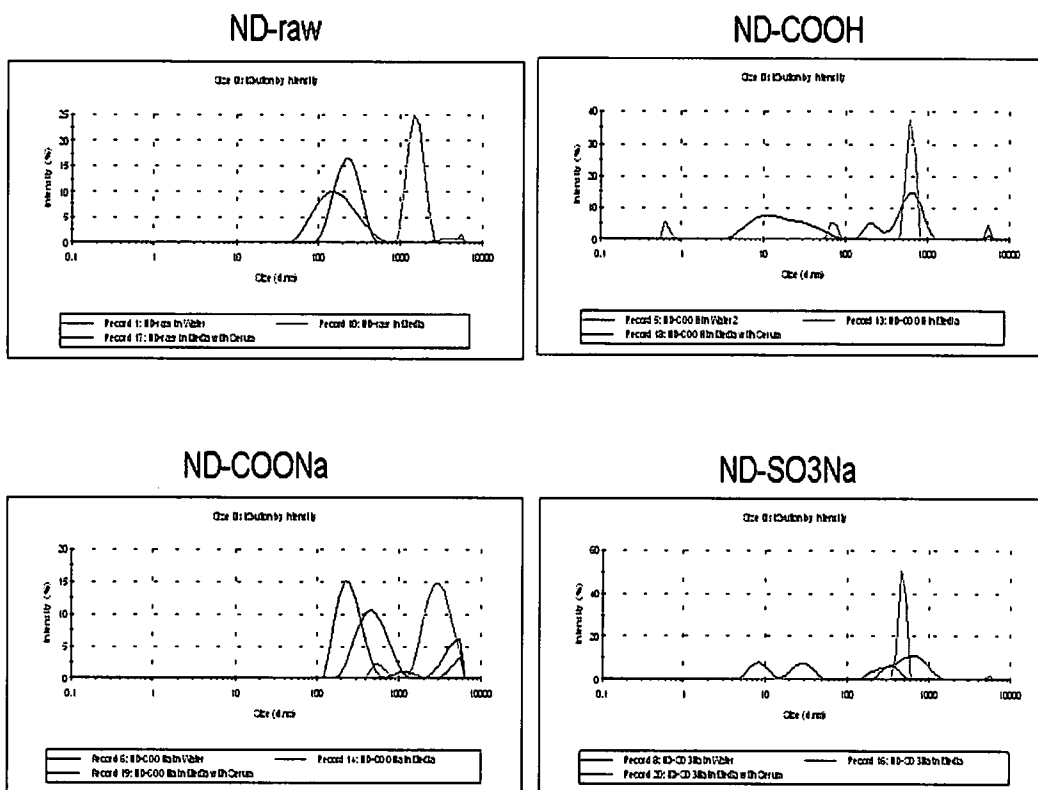


Figure 4.2.3. Dynamic light scattering (DLS) of nanodiamonds. Different color spectra indicate different solutions: red=water, green=media, and blue=media with serum.

The general reduction in size after the addition of serum may be explained by the zeta potential of the particles in solution. Zeta potential is a measurement of the charge which accumulates around the surface particle and gives an indication of the stability of the system. In general, a larger zeta potential, whether positive or negative, results in greater repulsive forces between the particles and therefore less agglomeration. Usually, a suspension with a zeta potential more positive than +30 mV or more negative than -30 mV is considered stable (Malvern Instruments 2005, Murdock et al., 2007).

Examination of the zeta potential of NDs in water showed a negative value (-14 mV) for the sodium sulfonic acid salt (base) purified ND-SO₃Na and increasingly positive values for ND-COOH (+6.49 mV), ND-COONa (+37 mV), and ND-raw (+42.8 mV) (Fig 4.2.4). Both ND-raw and ND-COONa were approximately +40 mV while the carboxylic acid purified NDs (ND-COOH) had a lower zeta potential of approximately +6.5 mV. Correlating the size values of NDs in water as compared to media with serum show the proposed high stability of ND-raw and ND-COONa with the highest zeta potentials in water as represented below in (size water, size media with serum, zeta potential in water). For ND-raw (158 nm, 246 nm, +42.8 mV) and ND-COONa (299 nm, 516 nm, +37 mV) the smallest ND size was in water and the zeta potential was quite high. In contrast, for ND-COOH (1000 nm, 18.2 nm, +6.49 mV) and ND-SO₃Na (559 nm, 162 nm, -14.3 mV), the smallest size was in media with serum and their corresponding zeta potentials in water had absolute values that were less than ND-raw and ND-COONa indicating a greater ability to agglomerate. Therefore, the NDs with the least variation from a zero charge/zeta potential were able to be better dispersed in cell culture media with serum proteins whereas NDs with highly positive charges/zeta potentials of approximately 40 were best dispersed in water. Other studies have shown that the electrostatic repulsion energy or zeta potential (ξ) for nanodiamond hydrosols can vary from -30 to -50mV (Bondar and Puzyr, 2004) and that electrostatic repulsion between negatively charged clusters of nanomaterials such as diamond, polystyrene latex, gold, clay, or fullerenes in water is

important for the stability of the solution (Ghosh et al., 2006, Deguchi et al., 2001).

Fluorescent rhodamine-labeled nanodiamonds (T-ND) were previously characterized as a stable aqueous colloidal suspension with a zeta potential of +40 mV, a primary size of ~4 nm, an average particle size of ~150 nm after suspension in water, and stable fluorescence for at least 8h. A comparison of the characteristics of the nanodiamonds used in these studies are shown below in Table 4.2.1.

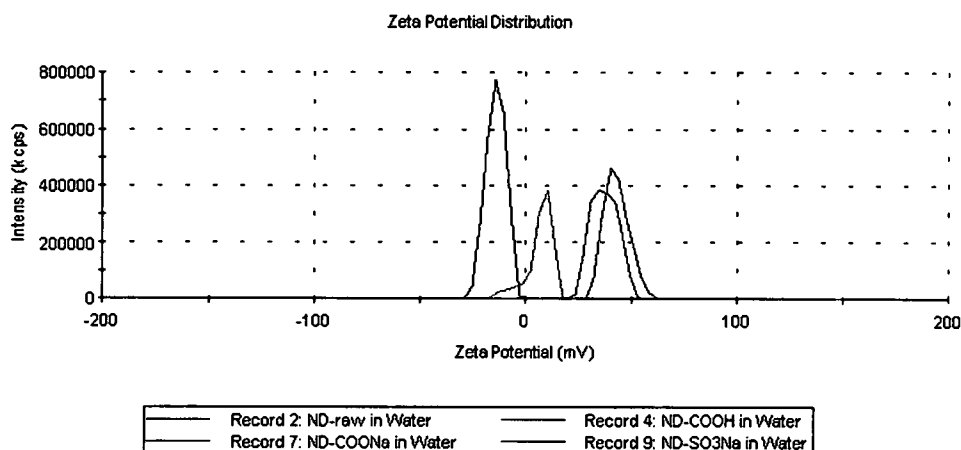


Figure 4.2.4. Zeta potential of nanodiamonds in water.

Table 4.2.1. Summary of Nanodiamond Characterization

Material	Avg. Diameter (TEM, nm)	Aggregate Size (DLS, Water, DMEM, DMEM+FBS, nm)	Charge (ZP, mV)
ND-raw	5.1 ± 1.7	158/2180/246	+ 43
ND-COOH	5.9 ± 1.6	1000/2710/18	+ 6.5
ND-COONa	4.6 ± 1.1	299/2390/516	+ 37
ND-SO ₃ Na	5.0 ± 1.7	559/1320/162	-14.3
T-ND	~4	~150/(N/A)	+ 40

4.3 Results for Biocompatibility

The biocompatibility of nanodiamonds was assessed by morphological examination, MTT assay for viability, mitochondrial membrane permeability (MMP), generation of reactive oxygen species (ROS), and cytoskeletal changes.

4.3.1 Morphological Observations

After 24 h of incubation with NDs, N2A cells appeared similar to controls with some cells displaying elongated neurites while others remained rounded, which is typical for this heterogeneous population of cells (Fig. 4.3.1A-E). Agglomerates of irregularly shaped NDs were visible in the surrounding media, agglomerated at cell borders, and along neurites at concentrations of ranging from 5-100 $\mu\text{g/ml}$ (Fig. 4.3.1B-E). In contrast, cells incubated with the positive control CdO (Fig. 4.3.1F) lacked cellular extensions, were reduced in size, had irregular cell borders, and formed vacuoles, which are morphological indicators of toxicity. Fluorescent nanodiamonds (T-ND) were further examined in three different cell types (N2A, macrophage, and human keratinocyte) and did not show morphological changes to any of the cells up to the highest concentration of 100 $\mu\text{g/ml}$ (data not shown).

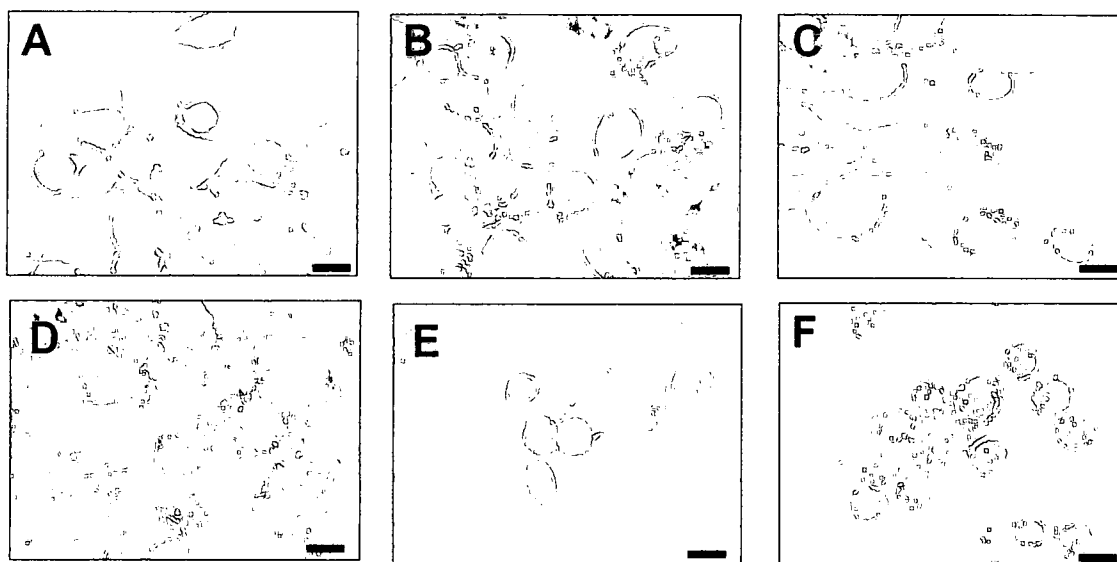


Figure 4.3.1. Morphological observation of N2A cells with nanodiamonds. (A) Control, (B) 100 µg/ml ND-raw, (C) 100 µg/ml ND-COOH, (D) 100 µg/ml ND-COONa, (E) 100 µg/ml ND-SO₃Na, and (F) 2.5 µg/ml CdO after 24h of exposure. Notice that agglomerates of nanodiamonds are seen surrounding the cell borders and attached to neurite extensions whereas cell morphology is unaffected by their presence compared to the control. However, CdO induces cell shrinkage and rounding indicative of toxicity. Scale bars are 20 microns (Schrand et al., 2007a).

Although nanodiamonds do not show gross morphological alterations, their ability to be internalized and have a high affinity for protein binding, may allow interactions with cellular proteins. Therefore, the architecture of the actin cytoskeleton was examined with fluorescent microscopy (Fig. 4.3.2). After neuroblastoma cells were incubated with 100 µg/ml of acid or base purified NDs for 24h, distinct branching and extension of multiple neurites were found compared to the control (Fig. 4.3.2). At low magnification, control cells show some neurites (Fig 4.3.2A), which were measured to be 19.7 ± 6.9 µm. At increasingly higher magnifications, the general cell morphology is shown (Fig 4.3.2B,C). In comparison, cells incubated with ND-raw for 24h (Fig. 4.3.2D-F)

show much longer neurites, which were measured from the low magnification image to be $82.0 \pm 13.27 \mu\text{m}$, approximately four times as long as the control neurites. In contrast, this increase in neurite extension was not shown with nano-sized carbon black particles (data not shown). Other purified nanodiamonds also show cytoskeletal disruption (Fig 4.3.2G-I).

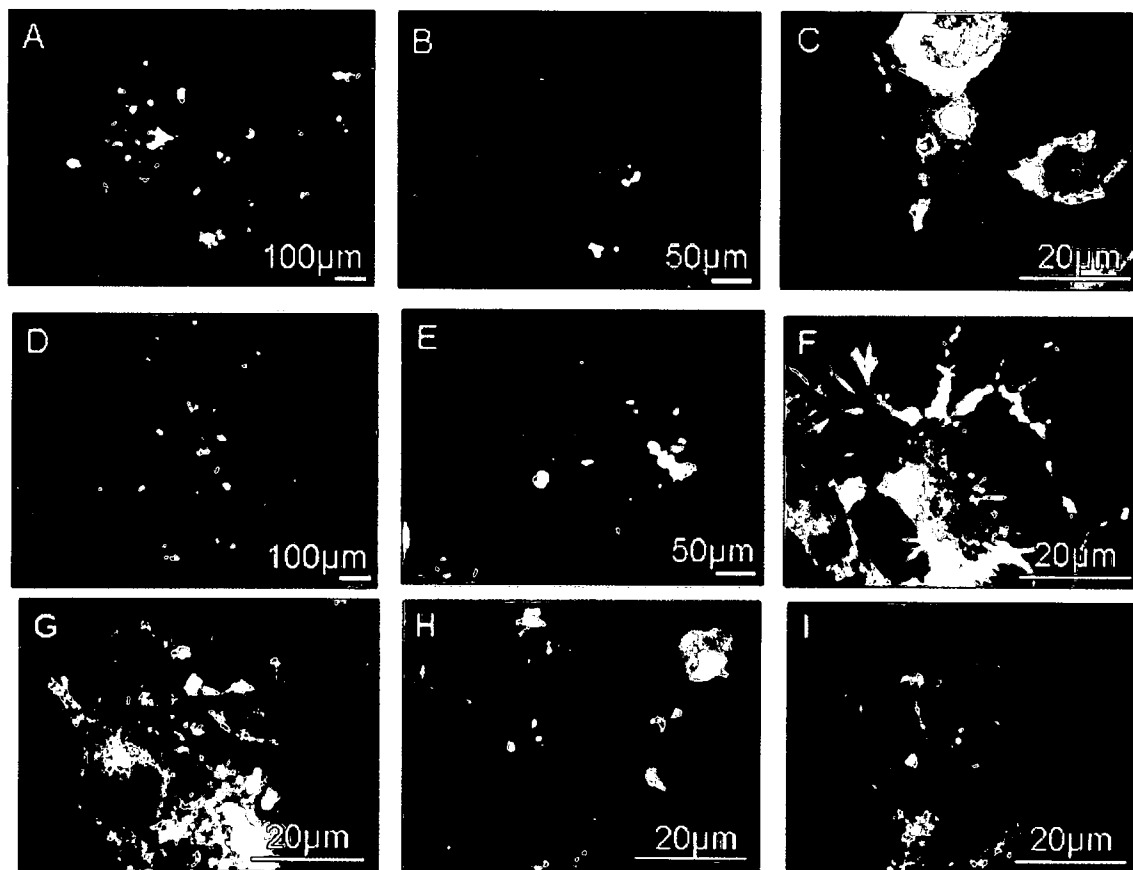


Figure 4.3.2. Cytoskeletal changes in N2A cells after exposure to NDs. (A-C) Control, (D-F) 100 $\mu\text{g/ml}$ of ND-raw, (G) 100 $\mu\text{g/ml}$ of ND-COOH, (H) 100 $\mu\text{g/ml}$ of ND-COONa, and (I) 100 $\mu\text{g/ml}$ of ND-SO₃Na for 24h. Notice the increase in branching after exposure to ND-raw (D-F) compared to control cells (A-C) at various magnifications (Schrand et al., 2008b).

After washing the cells, many of the nanodiamonds remained attached to the surface and the internalization of NDs was difficult to observe due to their transparency. Therefore, the internalization and localization of NDs into the

cells over time was examined with confocal microscopy for fluorescently-labeled NDs (T-ND) and with transmission electron microscopy (TEM). Before confocal images were obtained to observe T-ND internalization into N2A cells, the cells were examined for autofluorescence without staining. Representative unstained cells imaged with combined FITC, Rhodamine, and Hoechst filters showed non-specific fluorescence, but no true localization of any of the signals to specific cellular features (Fig 4.3.3A). In contrast, control cells stained with only Hoechst dye show localization to nuclei (Fig 4.3.3B). After incubation with 10 $\mu\text{g/ml}$ of T-ND, the fluorescent nanodiamonds show internalization into the cytoplasm after 1h with increasing accumulation from 1h to 24h (Fig 4.3.3C-D).

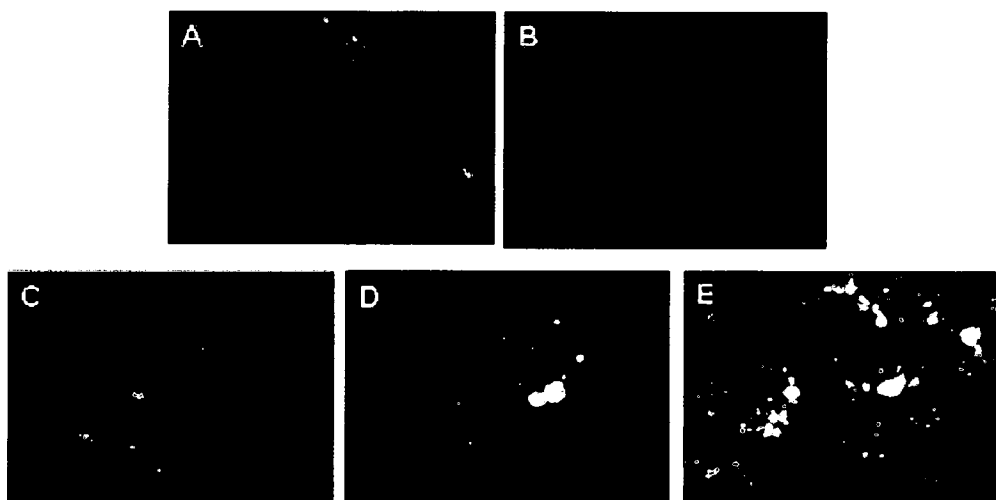


Figure 4.3.3. Representative confocal microscope images of control N2A cells or cells incubated with 10 $\mu\text{g/ml}$ T-ND from 1-24h. Cells were incubated with T-ND (red) and Hoechst dye (blue) for nuclear staining. (A) Unstained control, (B) Hoechst stained control, (C) 1h incubation with T-ND, (D) 3h incubation with T-ND, and (E) 24h incubation with T-ND. Notice that there is no localized cell autofluorescence (A) and that the amount of T-ND internalization increased over time. Images were taken at 60x magnification.

To more specifically examine the localization of the T-ND inside N2A cells, a lysosome stain was used. Lysosomes are single-membrane compartments found in most eukaryotic cells that are responsible for the breakdown of materials (<http://en.wikipedia.org/wiki/Organelle>). Lysosomes, in some cases, develop gradually from late endosomes, which are vesicles that carry materials brought into the cell by a process known as endocytosis (<http://micro.magnet.fsu.edu/cells/lysosomes/lysosomes.html>). The coalescence of the endosome with the low pH environment of the lysosome causes the degradation and release of the contents (<http://cellbio.utmb.edu/cellbio/lysosome.htm>). Control N2A cells show diffuse green staining with some very small punctuate spots indicative of lysosomes (Fig 4.3.4A). After incubation with 10 $\mu\text{g/ml}$ of T-ND for 1h, there was no

obvious localization to lysosomes, but T-NDs were found in the cytoplasm (Fig 4.3.4B). However, after 3-6h, there was an overlapping of the red signal from T-ND and the green signal representative of lysosomes resulting in yellow spots (Fig 4.3.4C-D). After 24h, most of the T-ND appeared to be released from the lysosomes and was back in the cytoplasm as red aggregates while the lysosomes remained stained in green (Fig 4.3.4E).

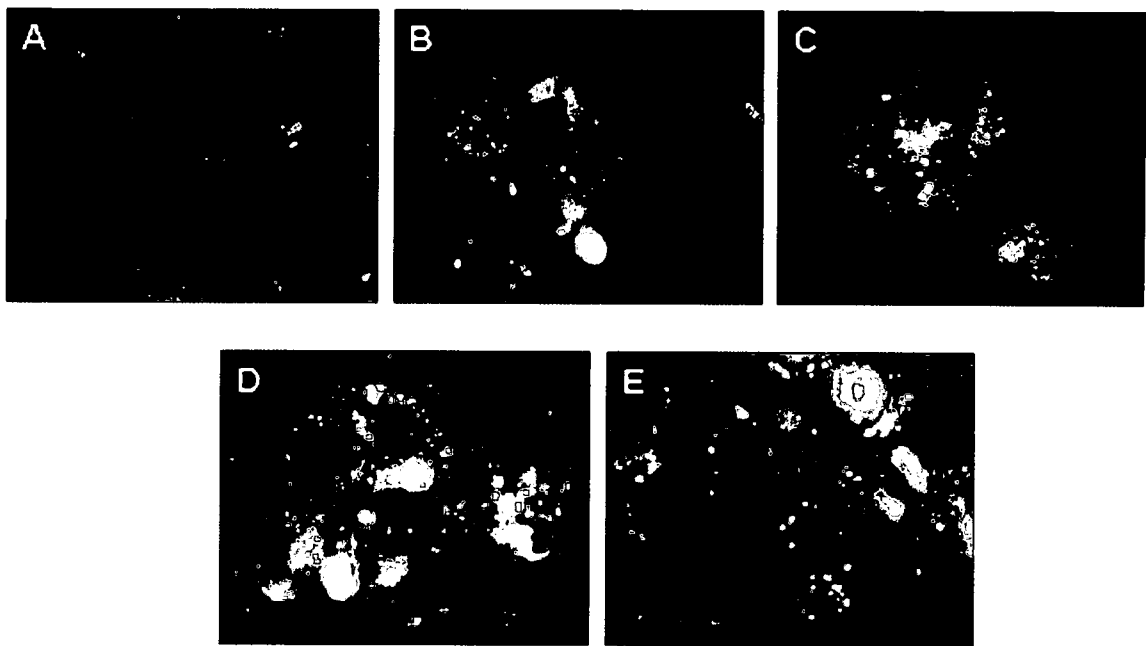


Figure 4.3.4. Confocal microscopy of N2A cells for co-localization of ND-TAMRA and lysosomes after various time points. Cells were incubated with 10 $\mu\text{g/ml}$ ND-TAMRA (red), then stained with Hoechst dye (blue) for nuclear staining and LysoTracker (green) for lysosomes. Combined red and green signals, indicative of co-localization of ND-TAMRA in lysosomes, appear in yellow. (A) Control, (B) 1h, (C) 3h, (D) 6h, (E) 24h. Notice that not all ND-TAMRA is localized to lysosomes, but some nanodiamonds are free in the cytoplasm and not all lysosomes contain ND-TAMRA. Images were taken at 60x magnification.

Examination of the differences in T-ND accumulation after 24h based on dosing concentration were examined after incubation with a low (10 $\mu\text{g/ml}$ T-ND) concentration and a high (50 $\mu\text{g/ml}$ T-ND) concentration. As shown in Fig 4.3.5, there were greater amounts of T-ND inside cells after exposure to the higher concentration (Fig 4.3.5C) compared to the lower concentration (Fig 4.3.5A). Similar trends in co-localization of T-ND with lysosomes were found after 24h when comparing the low (10 $\mu\text{g/ml}$ T-ND, Fig 4.3.5B) concentration to the high (50 $\mu\text{g/ml}$ T-ND, Fig 4.3.5D) concentration. At both concentrations, after 24h, many T-ND are found free in the cytoplasm and not isolated to lysosomes as was shown in the previous experiment suggesting that the T-ND may either be released by this time or have entered the cells without localization to lysosomes (Fig 4.3.4E). However, it appears that at the higher concentration, that there is more overlapping signals indicative of co-localization to lysosomes, so the cells may be trying to degrade the higher amount of NDs internalized.

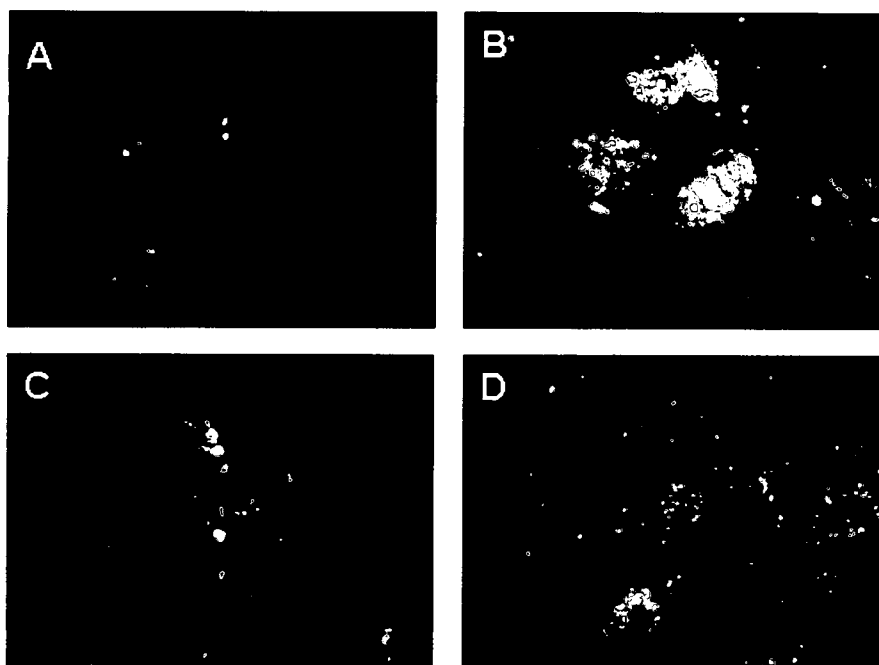


Figure 4.3.5. Confocal microscopy of N2A cells incubated with 10 µg/ml or 50 µg/ml of T-ND for 24h. Counterstain with Hoechst dye (blue) or Lysotracker (green) to label nuclei and lysosomes, respectively. (A,B) 10 µg/ml T-ND and (C,D) 50 µg/ml T-ND. Notice that the amount of T-ND internalization increases at the higher concentration of 50 µg/ml with some co-localization to lysosomes (overlapping red and green signals result in yellow color) at both concentrations after 24h. Images were taken at 60x magnification.

The verification of ND internalization and further localization was accomplished with TEM (Fig 4.3.6). Nanodiamonds were found both outside (white arrows) and inside the cells in intracellular vacuoles (black arrows), which are likely endosomes, after incubation for 1 to 24 h with N2A cells. The accumulation of NDs appears to increase over time with larger pockets of NDs found in cells incubated for 24h (Fig 4.3.6I-L) compared to 1h or 6h (Fig 4.3.6A-H). The size of the ND aggregates and intracellular vacuoles is ~500nm in size and several images suggest that the NDs, after coming into contact with the cell membrane, are brought inside by an endocytotic mechanism where they remain close to the edge of the membrane, but do not

appear to enter the nucleus. Additionally, the degradation of the membrane-bound structure containing the NDs was found in some areas after 24h, which may explain why there is a reduction in the co-localization of fluorescent signals for the NDs and the lysosome stain at 24h (Fig 4.3.6I, red arrow). Another explanation for the change in fluorescent signals could be the continued settling, contact, and internalization with the cells over time because at 24h the plasma membrane still appears to be invaginating to internalize more NDs and many pockets of NDs are still found close to the edge of the plasma membrane (Fig 4.3.6I-L).

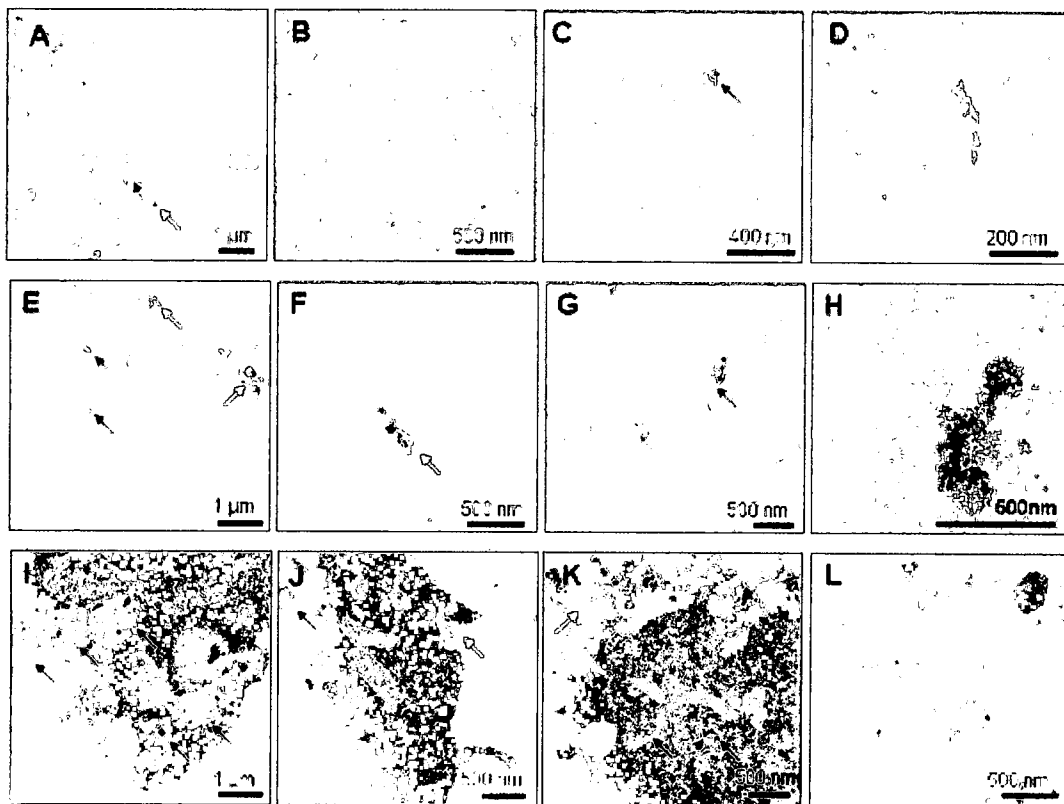
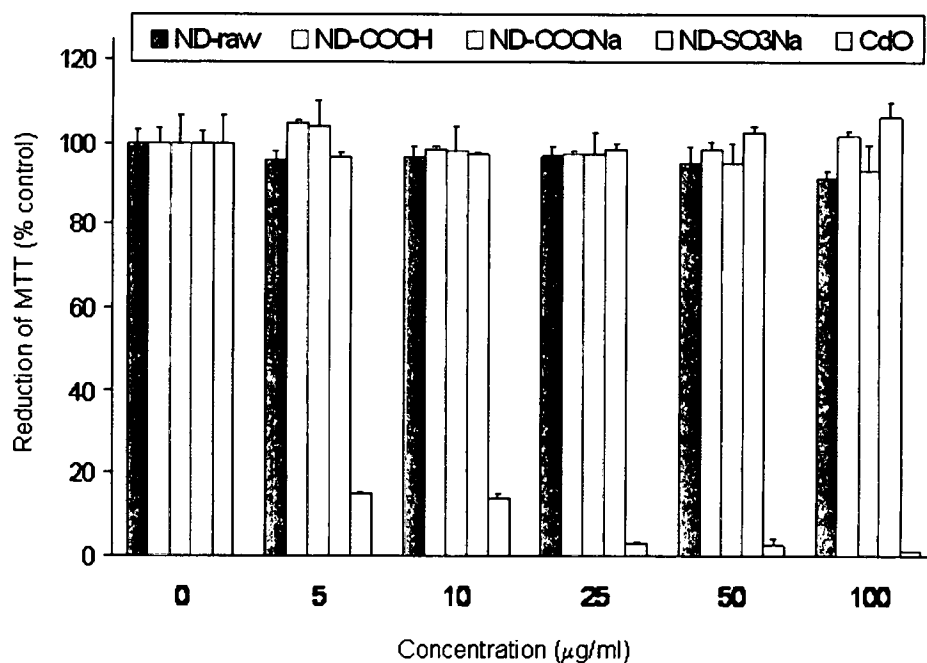


Figure 4.3.6. Internalization and localization of NDs into N2A cells with TEM. (A-D) After 1h incubation, (E-H) After 6h incubation, (I-L) After 24h incubation. Notice that the amount of internalization increases over time into both the cytoplasm and intracellular vacuoles up to 24h.

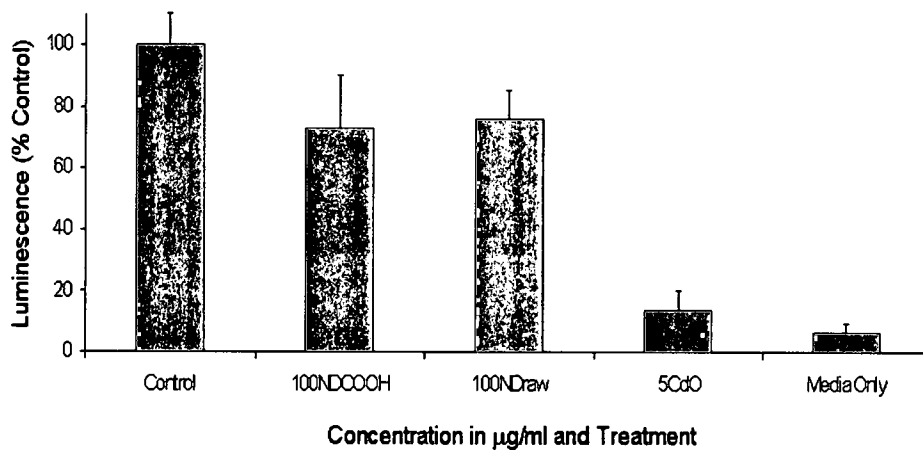
4.3.2 Biochemical Endpoints

Changes in the viability of neuroblastoma cells after exposure to NDs was assessed with the MTT colorimetric assay and luminescent ATP assay (Fig 4.3.8). The reduction of MTT dye occurs only in functional mitochondria, therefore, a decrease in MTT dye reduction is an indication of damage to mitochondria. Mitochondria are vulnerable targets for toxic injury by a variety of compounds because of their crucial role in maintaining cellular structure and function via aerobic ATP production (Hussain and Frazier, 2002). The positive control CdO exhibited strong toxicity with sharp decreases in cell viability compared to the control (Fig. 4.3.8A). However, cells incubated with various concentrations of NDs had some slightly higher viability values, but no significant difference in viability compared to controls at concentrations up to 100 $\mu\text{g/ml}$ (Fig. 4.3.8). To further confirm the low toxicity of NDs, several other cells types (macrophages, keratinocytes, and PC-12 cells) were investigated and found to display similar trends of biocompatibility at the same concentrations. An additional luminescent assay based on the ATP production of neuroblastoma cells after exposure to NDs showed similar, but slightly lower viability compared to the MTT assay (Fig 4.3.8B) demonstrating the usefulness of several cell lines and viability assays for nanomaterials biocompatibility studies. The functionalization of NDs with the fluorescent label rhodamine did not alter the biocompatibility (Fig 4.3.8C). Experiments over longer periods of time suggest that cells retain high viability for several days while exposed to nanodiamonds (data not shown).

(A)



(B)



(C)

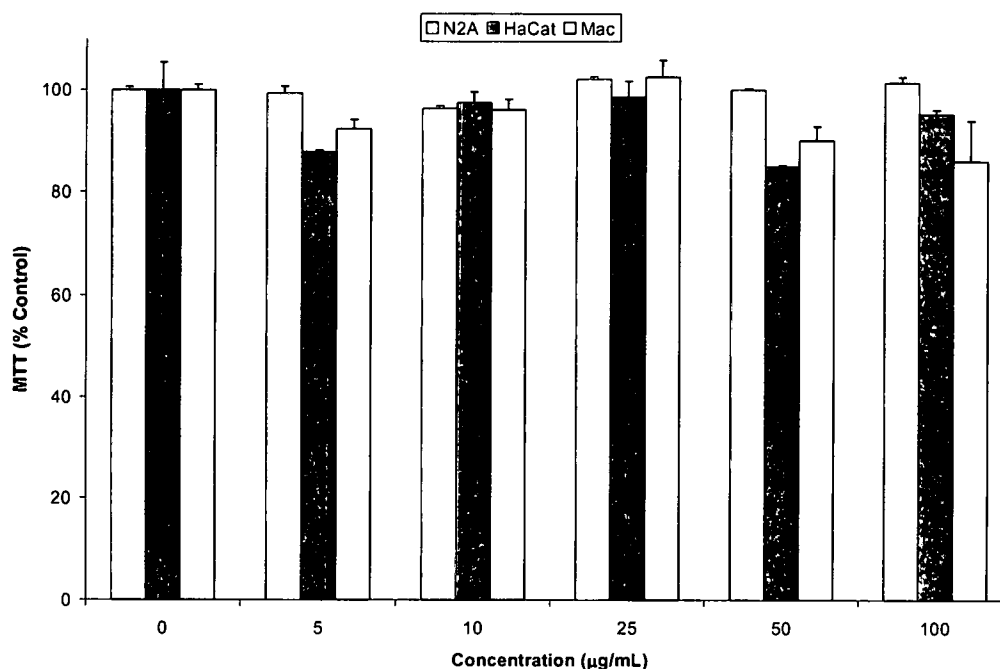


Figure 4.3.8. Viability assessment of NDs in cells. (A) Mitochondrial function was determined by the reduction of MTT after incubation with N2A cells, (B) ATP luminescent assay in N2A cells after nanodiamonds were removed by centrifugation after 24h, and (C) Comparison of viability assessment of fluorescent T-NDs by the MTT assay in three different cell types. No viability values were significantly reduced for any of the incubations with nanodiamonds (adapted from Schrand et al., 2007a).

Although nanodiamonds allowed cells to maintain high viabilities, it was unknown if after internalization they interfered with mitochondrial membranes. To assess changes in mitochondrial membrane permeability, two different fluorescent dyes (Rhodamine 123 and Mito-E- Ψ^{TM}) were used. Neuroblastoma cells were incubated with 100 µg/ml of ND-raw or 50 µg/ml CdO for 24 h and retention of Rhodamine dye within intact mitochondrial membranes showing similar staining patterns in control and ND-raw treated cells regardless of the excitation wavelength used to fluoresce the Rhodamine dye either red or green (Fig 4.3.9A-B, E-F). However, after the

cells were incubated with CdO, there was leakage of the Rhodamine dye (Fig 4.3.9D, G) from the mitochondrial membranes into the cytoplasm resulting in a diffuse red or green. For the M_{it}-E-ΨTM dye, the dispersion of the dye into the cytoplasm results in a green monomeric form in contrast to the red packaged form of the dye, which is shown for intact mitochondrial membranes for control and ND-raw treated cells compared to CdO treated cells (Fig 4.3.9H-J).

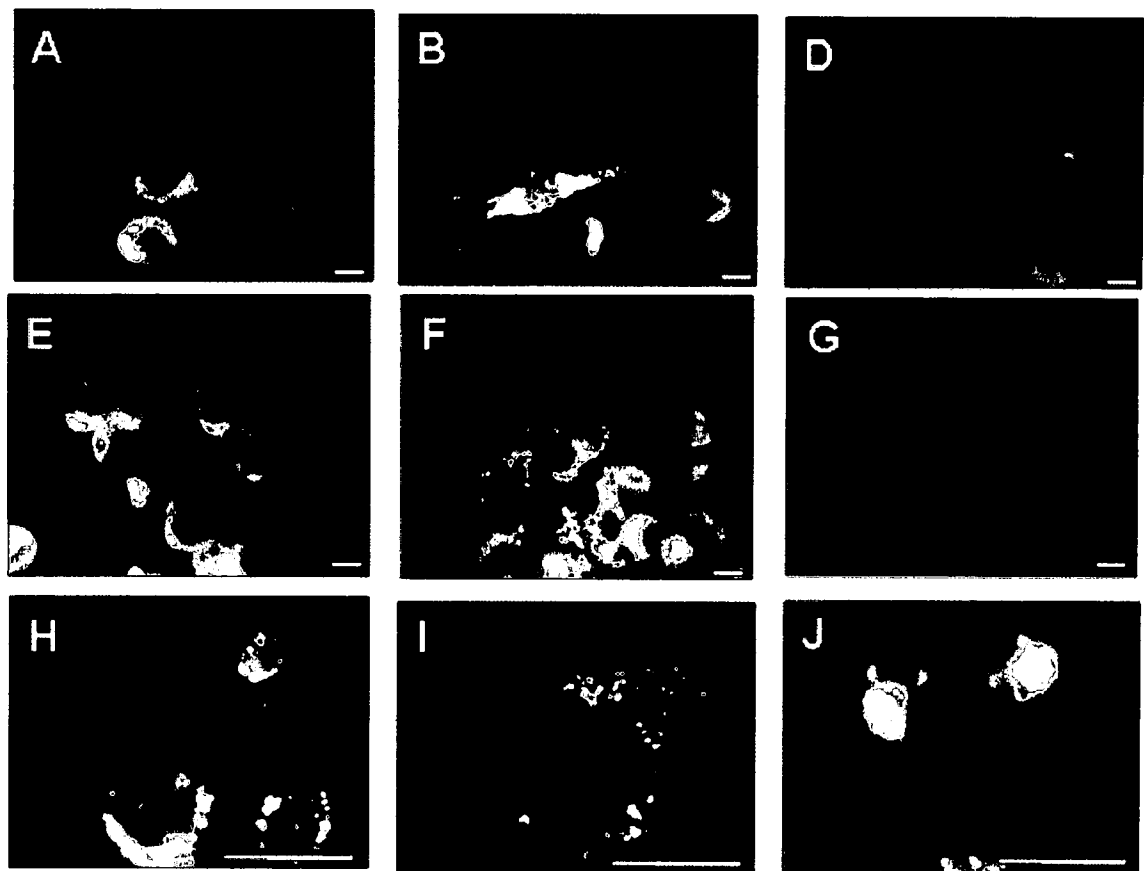


Figure 4.3.9. Mitochondrial membrane permeability of N2A cells incubated with NDs. (A-G) Rhodamine 123 and (H-J) M_{it}-E-ΨTM after 24h of exposure to 100 μg/ml of ND-raw or 50 μg/ml CdO. (A, E, H) Controls, (B, F, I) 100 μg/ml of ND-raw, and (D, G, J) 50 μg/ml CdO. Scale bars are 20 μm.

In order to investigate nanoparticle-induced oxidative stress as mechanistic changes, we assessed the generation of reactive oxygen species (ROS) (Nel et al., 2006). The cumulative production of ROS due to nanoparticle exposure was assessed after fluorescence of dichlorofluorescein (DCF), an oxidized form of 2',7'-dichlorofluorescein (DCFH). Figure 4.3.10 shows that nanodiamonds did not initiate an oxidative stress response shown by the lack of reactive oxygen species (ROS) generation compared to fine carbon black nanoparticles (Fig 4.3.10). Some of the ROS values for cells incubated with NDs are even lower than the control with the exception of ND-SO₃Na, which was slightly greater than the control (Fig 4.3.10). The only significant increase in ROS compared to the control was for CB at 25 µg/ml, but then the values decrease likely due to decreases in cell viability, which were shown with the MTT assay at concentrations from 50-100 µg/ml. The lack of ROS generation by cells incubated with NDs is consistent with the MTT and ATP results. Therefore, these results further support the biocompatibility of NDs and suggest that ND does not induce ROS generation in this *in vitro* cell model system.

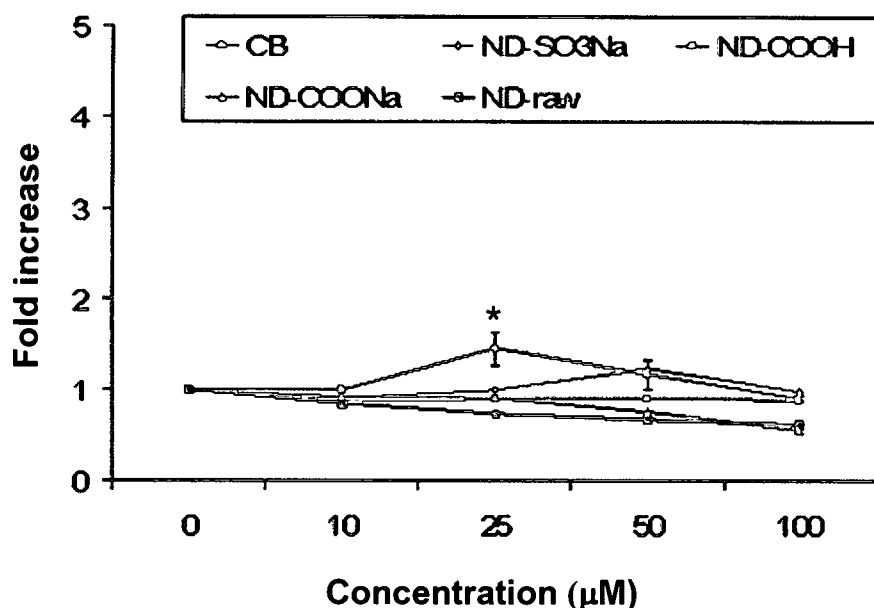


Figure 4.3.10. Reactive oxygen species (ROS) generation after exposure to NDs. There is low ROS for all of the purified nanodiamonds in neuroblastoma cells after 24h (Schrand et al., 2008b). Values that were significantly different from the control ($p < 0.05$) are denoted with asterisks (*).

4.3.3 Changes in Cell Proliferation and Growth on ND Substrates

Further observations of changes in cell growth in culture or on ND substrates were performed. Low magnification light microscope images show the confluence of control cells, but ND-treated cells tend to cluster and localize to aggregates of NDs (Fig 4.3.11). When cell counts were performed under similar experimental conditions, we found that cell growth continued over 96h, but was reduced in the cells incubated with NDs compared to the control suggesting that the clustering behavior of the cells around the NDs may contribute to reduced cell proliferation.

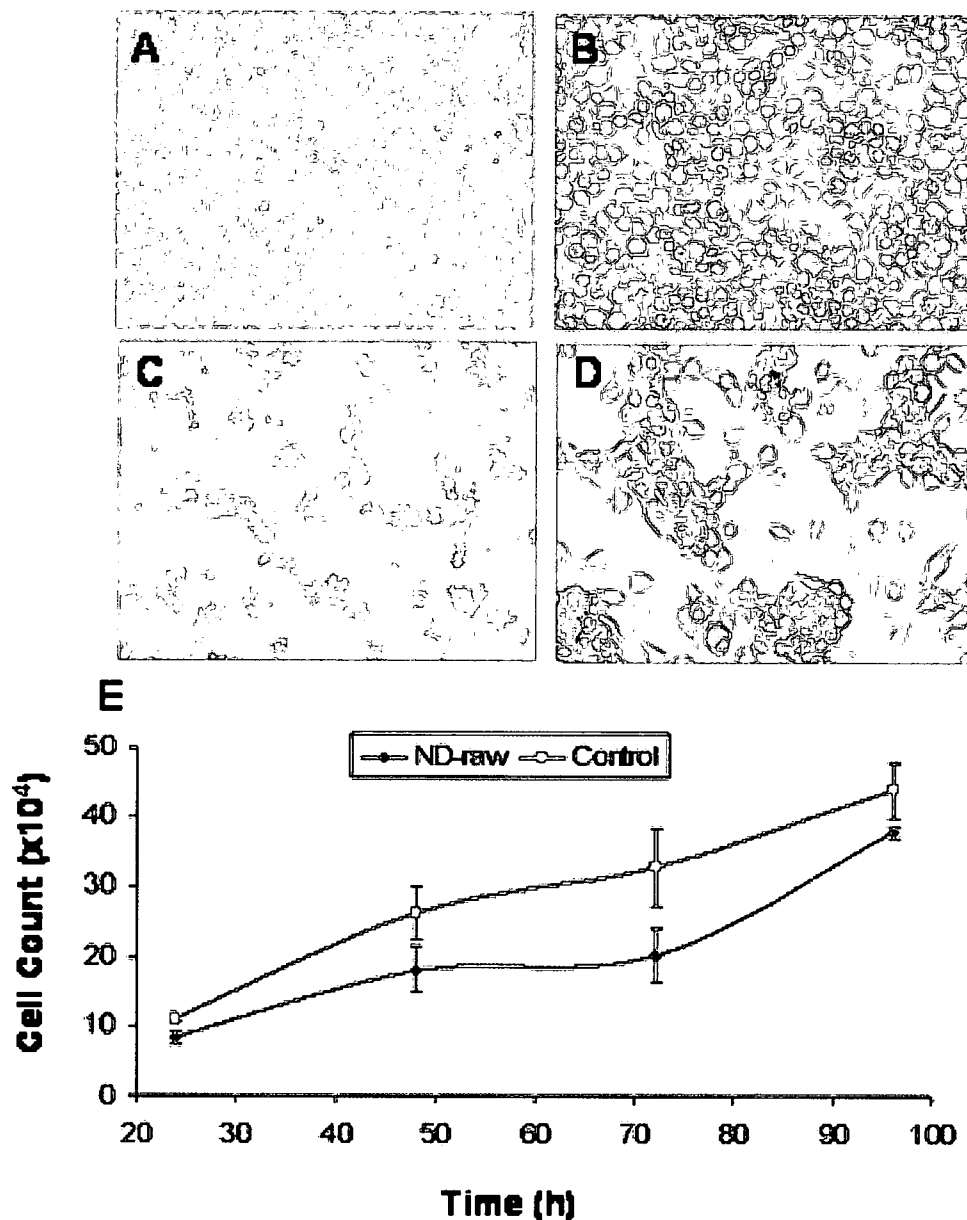


Figure 4.3.11. Morphology and cell proliferation changes in N2A cells after exposure to NDs. (A-D) Low magnification light microscopy images (taken at 6x and 12x) of (A-B) Control cells and (C-D) Cells incubated with 100 µg/ml NDs for 24h. Notice the aggregation behavior of the cells and NDs. (E) Changes in cell proliferation over 96h in control or cells incubated with 100 µg/ml NDs. Notice that both sets of cell continue to proliferate, but the cells incubated with NDs have reduced cell growth.

To study the behavior of neuroblastoma cells on ND substrates, cells were grown on both control (collagen or poly-l-lysine) substrates and ND-coated substrates for 96 h (Fig 4.3.12). Cells grown on both control and ND-coated substrates showed attachment and neurite extension with similar morphologies visualized with scanning electron microscopy (Fig. 4.3.12). Cell viability and growth were examined after 168h showing continued trypan blue dye exclusion (data not shown) and visual increases in proliferation suggesting that these substrates would support long-term cell attachment and growth.

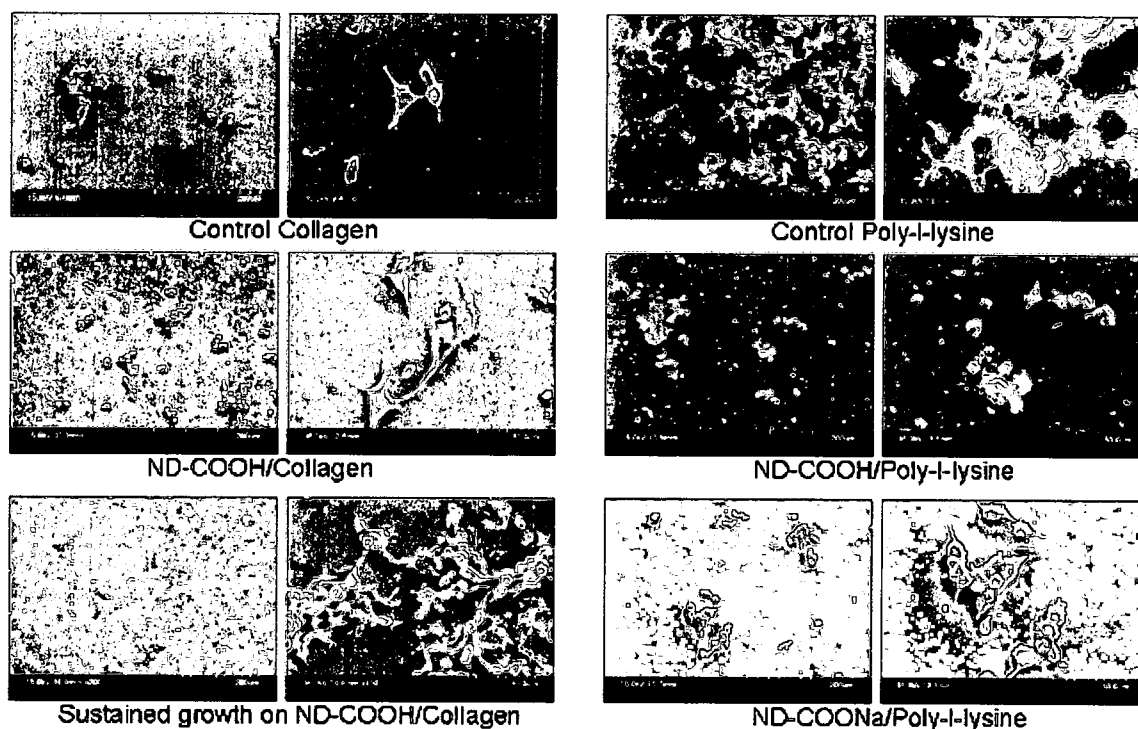


Figure 4.3.12. Cell growth on ND substrates. Scanning electron micrographs showing cell growth on ND substrates over 24h or the sustained viability and growth of cells after 168h (Schrand et al., 2008b).

4.4 Discussion

Many nanomaterials are being examined for use in biological systems as biological probes or substrates, but they face many limitations for practical use. For example, nanomaterials for bio-labeling should ideally be composed of very small primary sized nanoparticles with good dispersion quality and retention of their small sizes in physiological solutions. Additionally, factors such as pH stability, low photobleaching over time, photostability through covalent or protected fluorophores, lack of reactive oxygen species (ROS) generation, biocompatibility, high internalization efficiency, and thermal insulation would provide maximum therapeutic benefits and avoid damage to living cells or tissues. In this regard, NDs appear to ideal candidates for use in biological systems due to their small size (~4-5 nm), purity, ability to be functionalized, and retention of high cellular viability. However, further characterization reveals that there are still non-diamond carbons that remain on the ND surface, but these impurities can be reduced with acid or base purification as shown with FTIR and Raman spectroscopy. Other results with the size and charge in solution demonstrate that maintaining higher surface charges (~40 mV) creates smaller agglomerates of NDs ~150-158nm for ND-raw and fluorescently modified T-ND in water. However, once NDs are introduced into cell culture media, their size greatly increases up to 2 microns, so it is difficult to predict the effect of size on biocompatibility for any nanomaterial based upon the primary size as measured with TEM or size in non-physiological solvents. Additionally, greater dispersion in cell culture

media will be required to overcome membrane barriers such as nuclear pores for gene therapy. However, in these studies, regardless of the size of the NDs in cell culture media, further purification, or fluorescent labeling, there was high viability for a variety of cells with maintenance of mitochondrial membrane integrity and no indication of ROS after exposure and internalization at concentrations up to 100 µg/ml over 24h. Therefore, the properties that contribute to the biocompatibility of NDs may be their original purity and low reactivity.

While many other types of nanomaterials have been found biocompatible, the pathway for internalization and degradation at the cellular level is still not known for different types of nanomaterials and has not yet become controllable. Recent results suggest that quantum dot-multi-walled carbon nanotube conjugates (Jia et al., 2007) or multi-photon carbon dots (Cao et al., 2007) are internalized by temperature/energy-dependent endocytosis after 1h at 37°C compared to little or no uptake at 4°C. Other studies suggest that nanomaterials can achieve target specific localization after modification with antibodies or TAT (Cao et al., 2007, Lu et al., 2007). However, to complicate the situation, the entrapment of most nanoparticles in endosomes and then to lysosomes leads to a low pH environment where many nanoparticles can lose their desirable properties or are prevented from targeting specific cellular components. An additional factor to consider in the mechanism of nanoparticle uptake, accumulation, and localization is cell-specific

differences, which have been shown between N2A and macrophages (Schrand et al., 2007b) and HeLa, MSC, KGla, and Jurkat cells (Ricarda-Lorenz et al., 2006).

In order to better understand the kinetics of ND entry and localization inside cells, both non-fluorescent and fluorescent NDs were examined with microscopic techniques. It was expected that internalized NDs would localize to the cytoplasm, but not to the nucleus, as has recently been shown with both non-fluorescent or fluorescent electron-beam irradiated diamond particles (Schrand et al., 2007a, Fu et al., 2007, Yu et al., 2005). In these studies, NDs were rapidly internalized by 1h and continued to accumulate in the cytoplasm as visualized with confocal microscopy up to 24h. Closer examination at intermediate time points with a stain for lysosomes shows co-localization to lysosomes between 3h to 6h with subsequent release back into the cytoplasm or new ND internalization after 24h, which were not consistently localized to lysosomes. The influence of concentration on internalization and localization was also examined. After 24h of incubation with higher concentrations of NDs, there were larger accumulations of NDs inside the cells. However, it appeared that at the higher concentration that there was more localization to lysosomes than at the lower concentration suggesting that the cells may more actively be trying to degrade the internalized NDs if internalized at sufficiently high concentrations.

Therefore, the main properties that were found to influence the internalization of NDs were concentration and duration of exposure although surface charge was also expected to play a role. Although the differences in uptake between the different NDs in these studies was not quantified, other studies have found that cationic groups on the surface of fluorescently-labeled polymeric particles enhance their uptake compared to uncharged particles (Ricarda-Lorenz et al., 2006). In contrast, other coatings, such as bovine serum albumin (BSA), which has a negative charge and has been shown to strongly bind to NDs (Kong et al., 2005) is implicated in reducing cellular entry, increased biocompatibility, and enhanced solution dispersion/stability. Because NDs can efficiently bind proteins, caution should be used. For example, changes in the internal support structure, composed primarily of the protein actin, were shown in these studies after 24h of exposure to the highest dose of ND particles (100 µg/ml).

In related studies, the growth of N2A cells on ND substrates demonstrated cell attachment, growth, and morphologies similar to control cells over 168h. However, morphological changes, in general, were difficult to assess in the N2A cells, due to their non-homogenous characteristics. N2A cells appeared to respond to the presence of nanomaterials in solution by increased neurite extension or branching and decreased proliferation. Other cells such as macrophages tended to increase in size after accumulating NDs throughout their cytoplasm. It is suspected that the accumulation of nanomaterials inside

cells over time, although they are may appear biocompatible, could itself lead to decreases in cell viability due to the inability of the cell to degrade or release them. Therefore, it will be important to monitor the long-term interactions of both implantable composites containing nanomaterials as reinforcement fillers or coatings, which could lead to the production of wear debris and accumulation in the body, as well as nanomaterials used in solution form. In conclusion, some of the same properties that make carbon nanomaterials, including nanodiamonds, useful can also contribute to unknown biological and environmental consequences and further studies should be performed before they are accepted in biomedical applications.

CHAPTER 5

SILVER NANOPARTICLES

5.1 Literature Review

Colloidal forms of silver have been used for medicinal purposes for hundreds of years with the belief that they were safe and capable of preventing disease. However, the more recent incorporation of silver (Ag) nanoparticles into many common household products (e.g., band aids, topical products, soaps, refrigerators, washing machines, countertops, food storage containers, and clothing) due to their increased anti-microbial effectiveness has raised some health concerns. Meanwhile, the production of nano-sized Ag particles, which is now on the order of kg's per month, is expected to increase to tons over the next 2-3 years in applications such as the large-scale production of printable electronics, photonics, sensors, catalysts, and thin films, which rely on their incorporation into polymers (Goia, 2004, Suvorova et al., 2005). Therefore, it is imperative that studies begin to address the exposure risks, benefits, and overall relationship between Ag nanoparticle characteristics and their interactions with biological systems.

The high anti-microbial impact of Ag nanoparticles compared to bulk silver is well known and hypothesized to be due to the large surface area, porosity, and reactivity of the nanoparticles, which can deactivate oxygen metabolism enzymes or directly bind to viruses (Alt et al., 2004, Morones et al., 2005, Elechiguerra et al., 2005). As antiviral agents, silver nanoparticles have shown the ability to effectively disrupt the reproductive capabilities of viruses including HIV-1 with increasing effectiveness at smaller sizes (e.g. 1-10 nm nanoparticles strongly attach to the virus) (<http://www.nanoscale.com>, Elechiguerra et al., 2005). Due to the strong affinity of Ag with –SH groups, it is hypothesized that Ag nanoparticles are potentially harmful to all cells through protein binding (Hussain et al. 1994). However, it is not known how much more resistant mammalian cells are to different forms and concentrations of Ag compared to bacteria or viruses. For example, in skin cells, the toxic dose of silver nitrate was shown to be similar for both skin cells and bacteria (Poon and Burd 2004). Other studies have suggested that bacteria are more sensitive to Ag nanoparticles compared to eukaryotic cells due to the increased sized, complexity of architecture, and redundancy of organelles such as mitochondria in mammalian cells where it may take a larger concentration of nanoparticles or ions to produce the same toxic effect (Alt et al., 2004). Additionally, the protein complexes associated with bacterial electron transport are located on the cell exterior unlike in eukaryotic cells where these structures can only be accessed after overcoming the

plasma membrane barrier and translocation to the interior of the cell (Alt et al., 2004).

Studies are only beginning to examine the effects of Ag nanoparticles in mammalian cells and systems. Our recent *in vitro* reports on the toxicity of Ag NPs in liver cells, germ-line stem cells, neuroendocrine cells, and alveolar macrophages have found that Ag nanoparticles induce greater toxicity than carbon nanomaterials and many other metal nanoparticles including aluminum (Al-30nm), molybdenum (MoO₃-30nm), iron (Fe₃O₄), and titanium (TiO₂) (Hussain et al 2005, Braydich-Stolle et al., 2005, Hussain et al., 2006, Murdock et al., 2007). Similar to bacterial or viral studies (Morones et al., 2005, Elichiguerra et al., 2005), the toxicity of silver nanoparticles increased with decreasing size and with increasing concentration through the generation of oxidative stress (Hussain et al 2005, Braydich-Stolle et al., 2005). C18-4 germ line stem cells were more sensitive to Ag nanoparticles (Ag-15nm) than either BRL-3A liver cells or CRL-2192 alveolar macrophages (Braydich-Stolle et al., 2005, Hussain et al., 2005). In BRL-3A cells and macrophages, there were also significant increases in reactive oxygen species (ROS) generation after 6 or 24 h, respectively, of exposure to 10-50 µg/ml of Ag-15nm suggesting that the mechanism of toxicity is through an oxidative stress pathway. Other signs of toxicity included reductions in mitochondrial membrane potential, reduced glutathione (GSH) levels, and the activation of pro-inflammatory cytokines after exposure to Ag-15nm (Hussain et al., 2005).

These results raise concerns in using Ag NPs for the imaging of neural tissue and cells, in particular, due to the possibility of contributing to neurodegenerative diseases (e.g. Parkinson's and Alzheimer's) due to their ability to produce reactive oxygen species and oxidative stress (Kedar, 2003, Jendelova et al., 2004).

In an effort to prevent the direct interaction between the nanoparticle surface and the cell and at the same time increase dispersion, the surface chemistry of metal and other nanoparticles, such as quantum dots or carbon nanotubes, can be engineered. This technique has proven to be an effective method preventing any inherent toxicity derived from the core nanomaterial (Dumortier et al., 2006, Hoshino et al., 2004, Chen et al., 2005, Lesniak et al., 2005, Wilhelm et al., 2003, Gupta and Curtis, 2002). The formation of a protective interfacial barrier between the metal core and cells is especially important for preventing damage to the surrounding healthy cells and tissues for applications where nanoparticles are targeted to certain cells such as photodynamic/thermolysis cancer cell destruction or the delivery of drugs/diagnostic agents (Gupta and Gupta 2005, Berry et al., 2003, Berry et al., 2004, Jordan et al., 1999). It has been shown that the incorporation of Ag nanoparticles into polymers (Balogh et al., 2001, Yeo et al. 2003, Jeong et al., 2005, Chou et al., 2005) or other materials for biomedical applications such as bone cement (Alt et al., 2004) does not alter its toxic effect on bacteria and viruses. Other studies have found that the incorporation of Ag nanoparticles

into polymers creates more stable dispersions in solution, which is important for applications such as imaging probes or for the deposition of thin films (Lesniak et al., 2005, Balogh et al., 2001, Suvorova et al., 2005).

In these studies, we examined the potential of Ag nanoparticles to act as cellular labels while closely monitoring the relationship between their characteristics and biocompatibility. First, the characteristics that were considered for an ideal nanomedical label include a: lack of photobleaching or blinking, biocompatibility, stability in various environments, small size, and no thermal perturbation or catalytic effects. Because Ag nanoparticles are noble metal plasmon resonant particles (e.g. Au, Ag, Pt, Pd), the production of an optical signal occurs upon the excitation of surface plasmon resonances, which are collective oscillations of free electrons at the surface of metals (Lesniak et al., 2005; Skebo et al., 2007; Kumar et al., 2007). These oscillations give rise to the intense colors of solutions of plasmon resonant nanoparticles as well as very intense light scattering properties. The intense light scattering properties of plasmon-resonant nanoparticles such as silver have recently been examined for agglomeration, internalization, and interaction in a variety of live cells with a high illumination system (Skebo et al., 2007). The maximum detection limit of this system was experimentally determined to be approximately 60-90nm nm, or a 6000x increase in magnification, in comparison to the 180nm or less obtainable resolution in modern confocal instruments (Foster, 2004; Vodyanoy, 2005; Vainrub et al.,

2006). Therefore, taking advantage of both the intense light scattering properties of Ag nanoparticles and the enhanced resolution obtainable with the high illumination system in physiological solutions, studies on the interactions between Ag nanoparticles and live cells have been made possible.

However, the health effects of exposure to Ag nanoparticles, in particular, are not fully understood and their applications in biomedical arenas are still being explored. Therefore, with the potential for human exposure to Ag nanoparticles increasing in common products, it the goal of this chapter to elucidate some of the critical nanomaterials characteristics related to the biocompatibility of Ag nanoparticles in mammalian cells.

5.2 Results for Characterization

In this study, two types of Ag nanoparticles synthesized by different methods (hydrocarbons in plasma vs. wet chemical synthesis with polysaccharides) were characterized and examined for their potential use as biocompatible biological labels in neuroblastoma (N2A) cells. Variations in the properties of the two different Ag nanoparticles properties are attributed to differences in their synthesis methods and processing. According to the manufacturer, hydrocarbon synthesized Ag nanoparticles were synthesized out of a plasma gas, which includes silver and a mixture of other gases in a proprietary form including hydrocarbons. As the plasma cools, graphitic carbon and silver are both concurrently formed, with the resulting hydrocarbons reducing the ability of the silver nanoparticles to sinter together. The approximately 2% amorphous carbon (confirmed with XRD and EDS) in the final product is not chemically bound to the silver, but rather surrounds it as a matrix to prevent agglomeration. In contrast to the hydrocarbon synthesized Ag nanoparticles, the polysaccharide synthesized Ag nanoparticles were produced through a reduction of silver ions in an aqueous solution by a naturally occurring polysaccharide polymer (MW ~250,000). In this case, the Ag is reduced by the functional groups inserted on the extended polysaccharide chains. The nanoparticles formed are wrapped into the polymer and separated from the surrounding environment. In this study, the term 'nanoparticle' denotes the primary particle and 'agglomerates' are considered tightly bound collections of

primary nanoparticles, which are not uniformly dispersed. An overview of the Ag nanoparticles used in these studies is shown below (Table 5.2.0).

Table 5.2.0. Overview of Ag Nanoparticles and Controls. Abbreviations are: NC=Novacentrix Co., CU=Clarkson University, S=Sigma Co., HC=hydrocarbon, and PS=acacia gum polysaccharide.

Co.	Description	Abbreviation	Form
NC	HC, 13nm	Ag13	Powder
NC	HC, 28nm	Ag28	Powder
NC	HC, 43nm	Ag43	Powder
CU	PS, 10nm	Ag10Disp	Solution
CU	PS, 26nm	Ag26Disp	Solution
CU	PS, 52nm	Ag52Disp	Solution
CU	Acacia gum, PS	PS	Powder
S	AgNO ₃	AgNO ₃	Solution

Characterization of the elemental compositions, concentrations, and impurities was performed with XRF, AAS, and ICP-OES. Examination of the morphologies and size distributions of the silver nanomaterials was performed with transmission electron microscopy (TEM). Chemistry was examined with FTIR, Raman, and XPS. The dispersion state and corresponding size and charge of the silver nanoparticles in water or cell culture media was examined with dynamic light scattering (DLS) and zeta potential, respectively. Combining these techniques provides multiple methods for verifying the critical nanomaterials properties for a variety of materials engineering and bioengineering studies.

5.2.1 Concentration and Purity

Concentrations of the silver nanoparticles in solution were obtained after weighing dry powders in mg amounts (100mg) on a scale and then suspending them in water (100mL) to a final concentration of 1 mg/ml. Polysaccharide synthesized silver nanoparticles were received in aqueous solution at a specified concentration, then diluted to 1 mg/ml by adding additional deionized water. For quality control purposes, aliquots (1ml) were verified for elemental composition, concentration, and impurities before use in *in vitro* experiments with XRF, AAS, and ICP-OES.

The samples were first screened with x-ray fluorescence (XRF) to determine the elements present. For all of the Ag samples, the XRF results demonstrated that Ag was the major element present. However, The XRF technique does not take into account the presence of elements, such as carbon, below atomic number 11 (EDAX Eagle II micro-fluorescence instrument).

Most of the solutions appeared to have lower actual concentrations of Ag than the expected 1000 µg/ml for the stock 1 mg/ml solutions in water when examined independently with both AAS and ICP-OES (Table 5.2.1). For example, Ag10Disp only showed an average concentration of ~150 µg/ml; Ag26Disp and Ag28, ~325-364 µg/ml compared to Ag52Disp, which showed a slightly greater than 1000 µg/ml concentration, and Ag13, which was almost

twice the expected concentration. A control sample consisting only of sterile water did not show any presence of Ag. Quantitative analysis for elemental impurities with inductively-coupled plasma-optical emission spectroscopy (ICP-OES) showed no other detectable elements.

Table 5.2.1. Ag Nanoparticle Concentration Analysis with atomic absorption spectroscopy (AAS) and inductively-coupled plasma optical emission spectroscopy (ICP-OES).

Abbreviation	Average Concentration (AAS)	Average Concentration (ICP-OES)
Ag13	1862.7	1858.2
Ag28	324.9	336.65
Ag43	646.8	661.6
Ag10Disp	146.45	136.5
Ag26Disp	363.6	373.9
Ag52Disp	1052.8	1041.25

5.2.2 Size and Morphology

The different Ag nanoparticles used in these studies were received and examined with transmission electron microscopy for size distributions and morphologies (Fig 5.2.1-5.2.2). The smallest primary size of Ag was ~10nm, the largest nanoparticles were ~50nm, and all of the Ag nanoparticles were polydisperse in size and spherical in morphology. Measurement of 100 randomly selected individual nanoparticles from TEM images was used to determine the size distributions (Fig 5.2.2, Table 5.2.2).

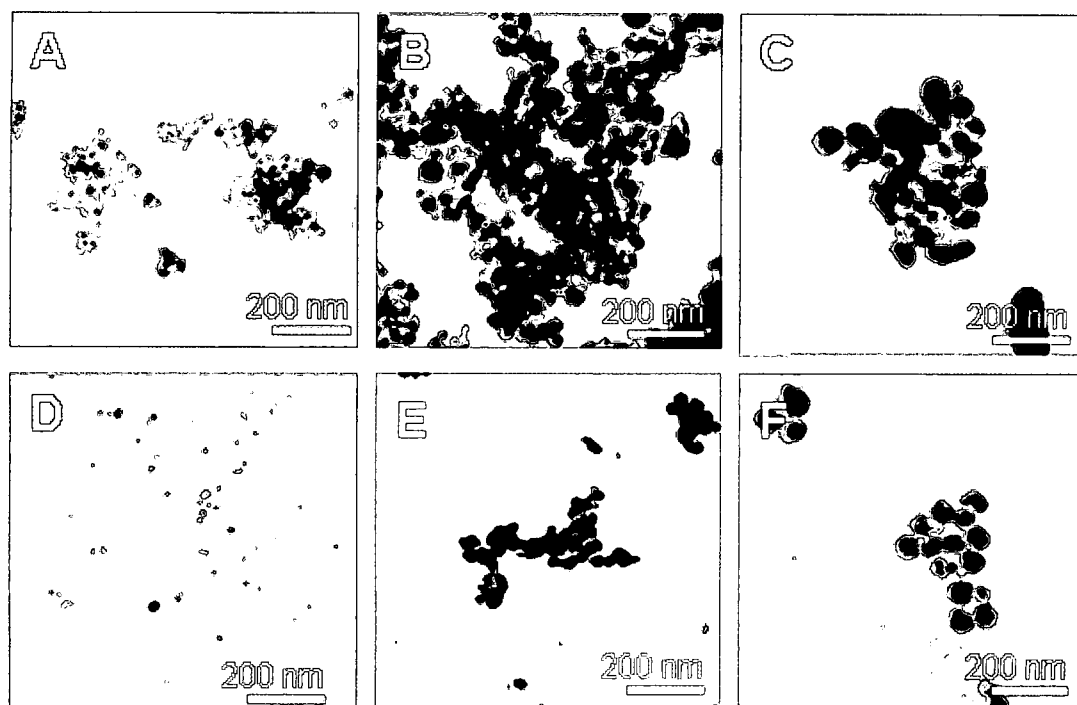


Figure 5.2.1. Size and morphology of Ag nanoparticles with TEM. (A) Ag13, (B) Ag28, (C) Ag43, (D) Ag10Disp, (E) Ag26Disp, and (F) Ag52Disp. All images were taken at a magnification of 50kx and scale bars are 200nm.

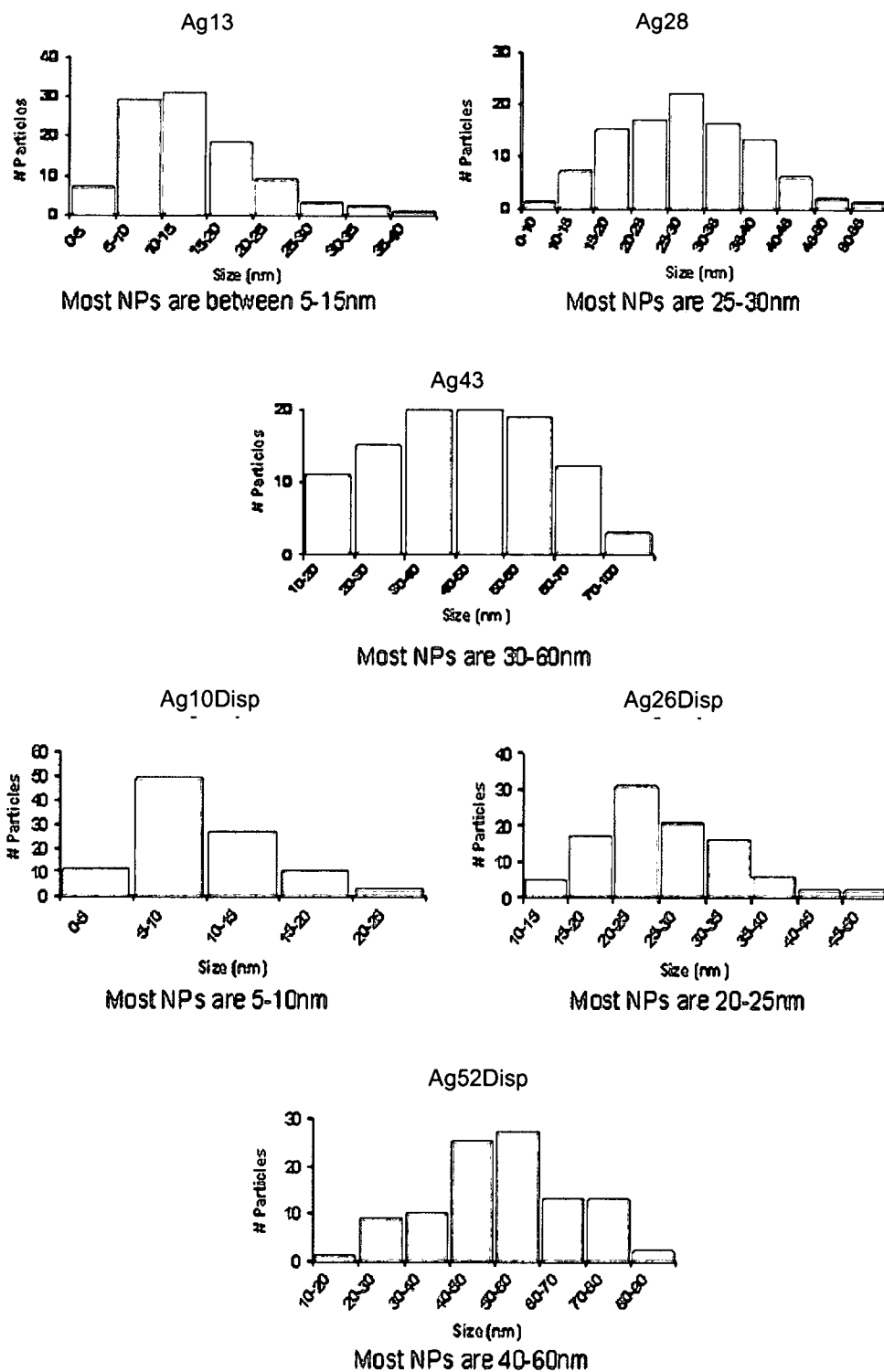


Figure 5.2.2. Size distributions of Ag nanoparticles from TEM. Polydisperse distributions were plotted in Excel after randomly counting 100 nanoparticles per sample.

Table 5.2.2. Summary of Primary Ag Nanoparticle Size.

Abbreviation	TEM Size	Avg Size	Majority Size Distribution
Ag13	13.3 ± 7.0nm	13	5-15
Ag28	27.5 ± 9.1nm	28	25-30
Ag43	42.5 ± 17.1nm	43	30-60
Ag10Disp	9.5 ± 4.3nm	10	5-10
Ag26Disp	26.0 ± 8.4nm	26	20-25
Ag52Disp	52.4 ± 15.2nm	52	40-60

Further electron microscopy characterization to compare Ag28 to Ag26Disp demonstrated that the two types of Ag nanoparticles show similarities in their crystalline diffraction patterns predominantly silver elemental composition (Fig 5.2.3A-J). Scanning electron micrographs of the two types of Ag nanoparticles show very few morphological differences except that the appearance of Ag28 (Fig 5.2.3A) is somewhat more clustered compared to Ag26Disp (Fig 5.2.3F). This can be attributed to the formation of large, dry powder aggregates for Ag28 nanoparticles compared to the synthesis and sample preparation of Ag26Disp in aqueous solution. The use of SEM reveals similarities between the size and morphology of the two different Ag nanoparticles, but cannot reveal the presence of surface hydrocarbons or the polysaccharide coating. However, brightfield TEM can reveal the size, morphology, and surface coating of the Ag nanoparticles. For example, the lacey appearance of the amorphous carbon on and surrounding the Ag28 nanoparticles is shown in Figure 5.2.3B. The polysaccharide coating of Ag26Disp is also shown with brightfield TEM (Fig 5.2.3G). Selected area

diffraction patterns (SADP) show the 111, 200, 220, and 113 planes in both samples demonstrating the similar crystalline structures (Fig 5.2.3D,I), but there are slight differences in the EDX spectra demonstrating elemental differences between the compositions of the Ag nanoparticles (Fig 5.2.3E,J). Because the hydrocarbon Ag nanoparticles were synthesized in a powder form without a uniform surface coating, the surface areas exposed to air readily bind with sulfur as part of the oxidative corrosion process, known as tarnishing, and a peak for sulfur is shown in the EDX spectra of Ag28 (Fig 5.2.3E). Another difference between the spectra of the two types of Ag nanoparticles used in this study was the increased C peak in Ag26Disp, which is attributed to the carbon-rich polysaccharide. The presence of Cu, and trace amounts of Fe and Co, in both spectra are from the elements present in Cu alloy TEM grid. All of data obtained for electron microscopy and associated techniques is performed under high vacuum and constitutes the size, morphology, electron diffraction, and composition analysis characteristics of the primary nanoparticles. However, more detailed analysis of the surface chemical groups present the Ag nanoparticle surface can contribute to understanding the mechanism of toxicity or biocompatibility because these surfaces are to come into direct contact with the cell, which will be described in the subsequent section.

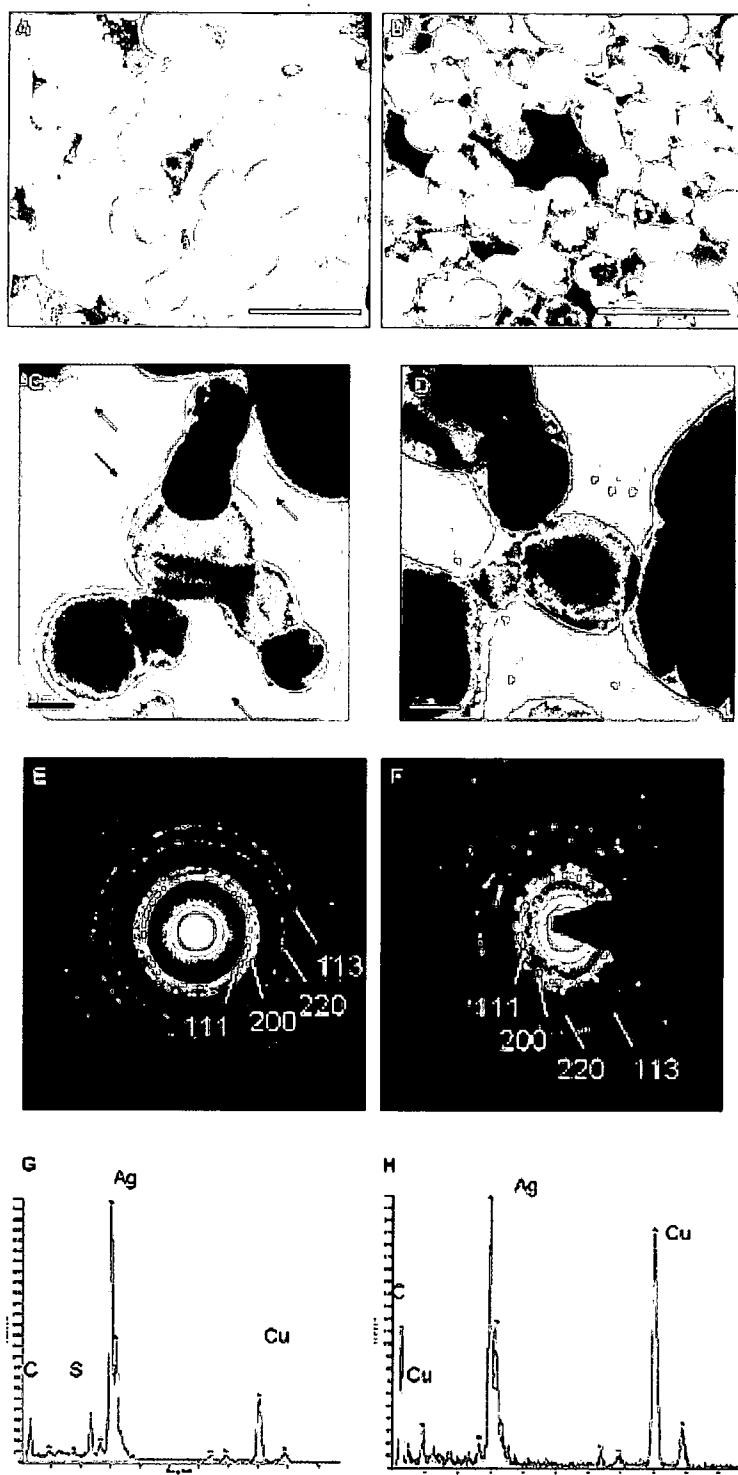


Figure 5.2.3. Electron microscopy characterization of Ag nanoparticles. Scanning electron microscopy of (A) Ag28 and (B) Ag26Disp. Transmission electron microscopy of (C) Ag28 and (D) Ag26Disp. The presence of hydrocarbons (black arrows) or polysaccharide coating (white arrows) are shown. Selected area electron diffraction patterns of (E) Ag28 and (F) Ag26Disp. Energy dispersive x-ray analysis (EDS) of (G) Ag28 and (H) Ag26Disp. Scale bars are 100nm in A-B and 20nm in C-D.

5.2.4 Chemistry

The chemical surface properties of nanoparticles are critical for understanding the possible attractive/repulsive forces or ability of certain functional groups to affect the interface between nanoparticles and cells. Therefore, a combination of FTIR, Raman, and X-ray photoelectron (XPS) spectroscopy were performed to characterize the Ag nanoparticle surfaces prior to introduction into cell culture.

A comparison between one of the hydrocarbon synthesized Ag nanoparticles (Ag28) and one of the polysaccharide synthesized Ag nanoparticles (Ag26Disp) of similar size is shown in Fig 5.2.4. The FTIR spectra show strong absorption peaks at $\sim 3430\text{ cm}^{-1}$ and weaker intensity peaks at $\sim 2925\text{ cm}^{-1}$, $\sim 1630\text{ cm}^{-1}$, and $\sim 770\text{ cm}^{-1}$ (Fig 5.2.4). The rich presence of hydroxyl groups bound to the surface of the Ag nanoparticles and broadening of the peaks due to hydrogen bonding are well known phenomena of hydrated compounds (Hummel, 1982, Coates, 2000). The peak at $\sim 3430\text{ cm}^{-1}$ and $\sim 1630\text{ cm}^{-1}$ can be ascribed to the O-H vibrational mode. The peak at $\sim 2925\text{ cm}^{-1}$ can be assigned to aliphatic C-H groups, which are most noticeable in the Ag10Disp spectra. The peak at $\sim 760\text{--}775\text{ cm}^{-1}$ can be assigned to C-O groups. Both C-H stretch and C-O groups are well known for polysaccharides (Bellamy, 1975). Differences between the polysaccharide synthesized Ag nanoparticles were further examined with FTIR (Fig 5.2.5).

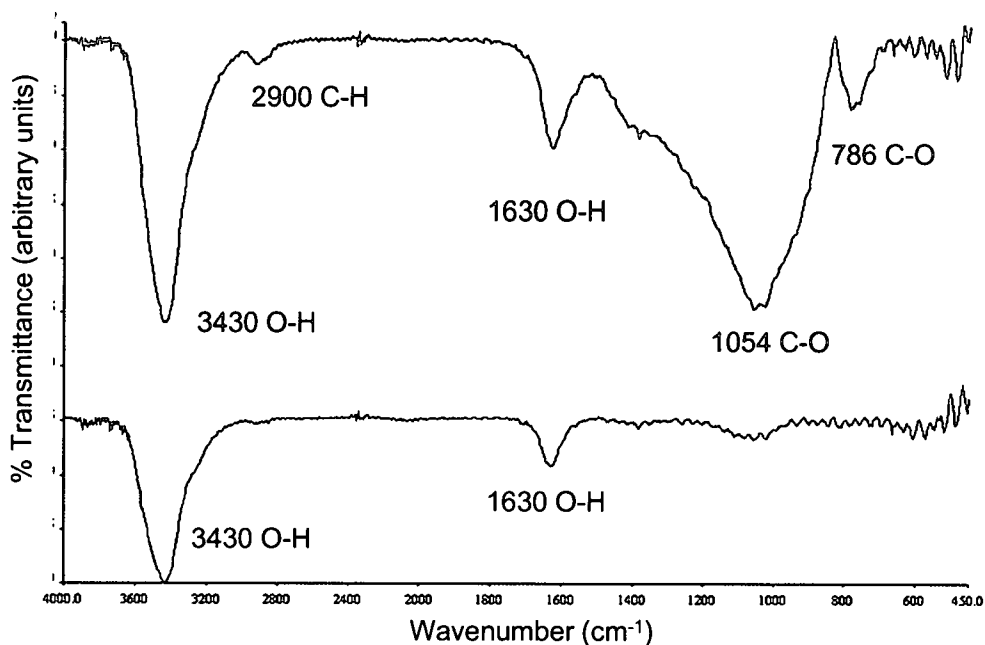


Figure 5.2.4. FTIR spectra of Ag nanoparticles. Notice the difference in chemical makeup of the hydrocarbon synthesized and polysaccharide synthesized Ag nanoparticles. Upper spectra is Ag26Disp with a large and broad C-O peak characteristic for the polysaccharide coating and lower spectra is Ag28, which lacks this peak.

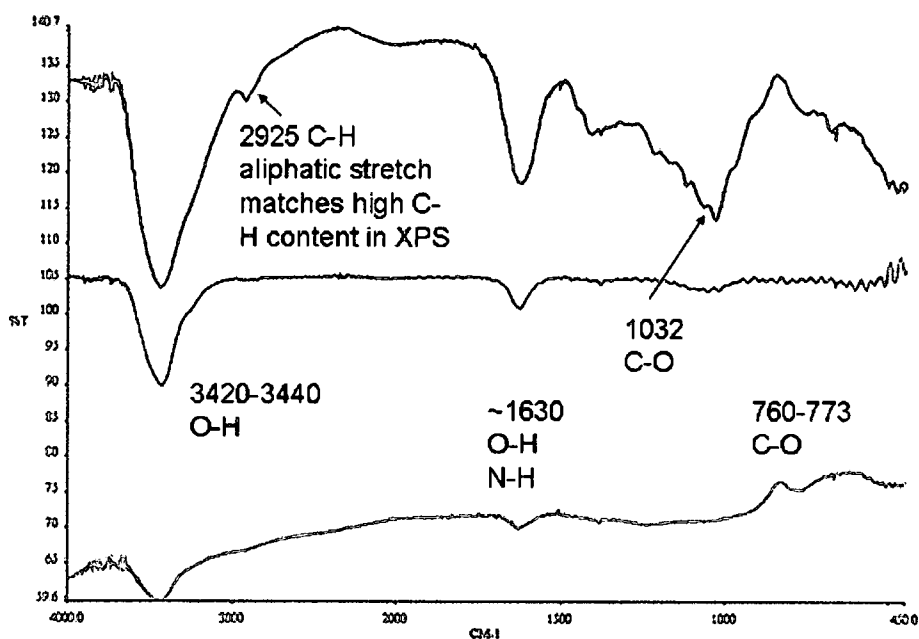


Figure 5.2.5. FTIR of polysaccharide-synthesized Ag nanoparticles. Ag10Disp: blue curve, Ag26Disp: black curve, Ag52Disp: red curve.

Raman spectra support the greater presence of carbonaceous coating on the polysaccharide synthesized Ag26Disp sample (Fig 5.2.6). As shown in Figure 5.2.6, there are two large peaks at approximately 1590 cm^{-1} and 1360 cm^{-1} compared to much smaller scatterings for the hydrocarbon synthesized Ag28 sample.

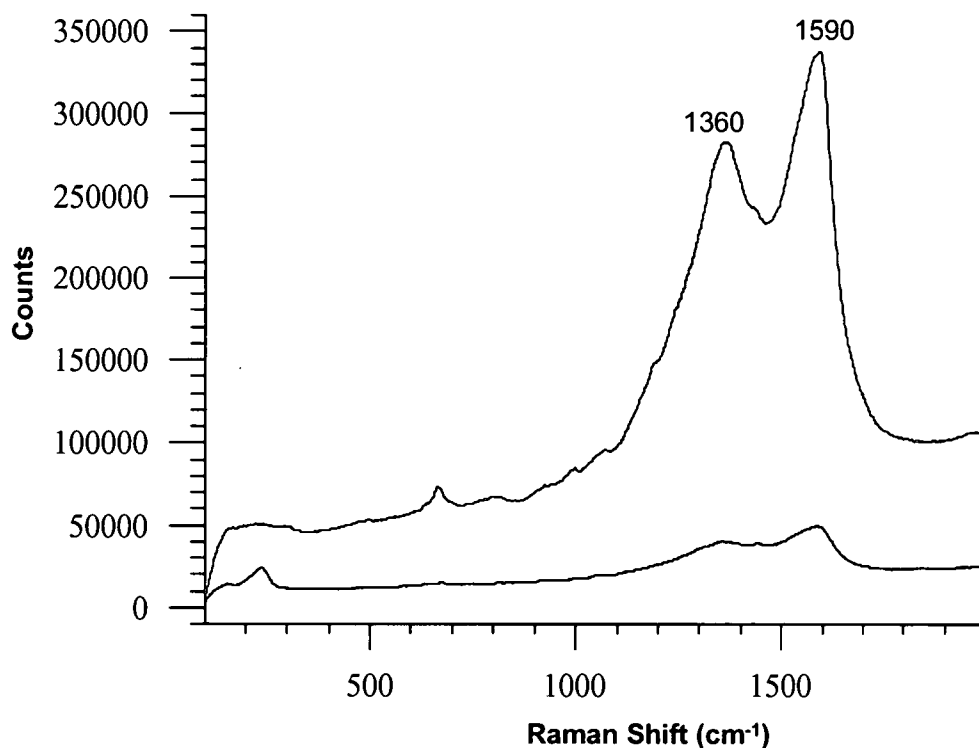


Figure 5.2.6. Raman spectra of Ag nanoparticles. Notice the difference in the chemical surface states of hydrocarbon synthesized and polysaccharide synthesized Ag nanoparticles. Upper spectra is Ag26Disp showing two prominent C-based peaks and lower spectra is Ag28 with low scattering.

X-ray photoelectron spectroscopy (XPS) was used to further characterize the chemical composition of the very outermost layers (e.g. 1-3nm) of the Ag nanoparticles used in these studies (Table 5.2.3). All of the Ag nanoparticle surfaces contained C, O, and N with the exception of the plasma gas/hydrocarbon synthesized Ag nanoparticles, which did not contain N. In the Ag28 sample, the Ag signal was not blocked because there was not an effective surface coating. However, the synthesis of Ag nanoparticles by polysaccharide reduction of Ag ions in aqueous solution, led to effective blockage of the Ag signal in most samples. The control polysaccharide (acacia gum) powder is primarily composed of C, O, and a small amount of N. These elements are found as intense C-O bonds due to C-OH or C-O groups in the polysaccharide, and the low level of nitrogen is likely due to the protein component. The total C content for the polysaccharide synthesized samples ranged from 35 at% for Ag52Disp up to 68 at% for Ag10Disp with the control polysaccharide and Ag26Disp having approximately 60 at% C. The aliphatic C-H groups, which were most noticeable in the Ag10Disp FTIR spectra also corresponds to the higher C-H content shown with XPS for the Ag10Disp sample. The Ag26Disp sample has an increased amount of N compared to the other polysaccharide synthesized Ag nanoparticle samples. More of the Ag nanoparticle surface appears to be exposed for the Ag52Disp sample as demonstrated by the higher Ag signal compared to the other polysaccharide synthesized samples. However, the oxygen content is also high and similar to the polysaccharide alone, which makes it difficult to determine if the oxygen

signal is from oxidation or free floating polysaccharide. The Na and N content in the Ag52Disp sample are also the lowest out of all of the polysaccharide synthesized Ag nanoparticle samples. Because the samples are first dried on Al foil, there may be some underlying Al signal if the sample is not fully covering the foil surface. Therefore, these results are consistent with the FTIR and Raman spectra demonstrating surface chemistry differences between the different Ag nanoparticles.

Table 5.2.3. Atom % Surface Compositions of Ag Nanoparticles Determined by X-ray Photoelectron Spectroscopy. *Ag28 is representative of other sizes of hydrocarbon-synthesized Ag nanoparticles.

Sample	C			O	Na	N	Ag	Al	S
	C=O, OCO	C-O	C- H,C						
Hydrocarbon									
Ag 28*	4.9	7.6	28	33.5	---	---	22.4	3.7	---
Polysaccharide									
Acacia gum (Polysaccharide)	10.8	38.1	8.8	39.1	---	3.1	---	---	---
Ag10Disp									
-1	1.2	3.8	62.6	20	9	0.5	0.2	---	2.7
-2	1.2	4.3	61.8	20.2	8.8	0.7	< 0.1	---	2.9
Ag 26Disp									
-1	12.2	23.9	25.5	28.1	3.8	5.9	0.6	---	---
-2	12.7	24.9	22.5	27.6	4.7	6.2	1.4	---	---
Ag52Disp	4.6	5.5	24.9	43	1.5	1.2	11	8.4	---

5.2.3 Solution Properties

Nanoparticle dispersion has recently been investigated with an ultrahigh resolution system attached to a standard research grade inverted microscope (Skebo et al., 2007). This method provides a rapid, simple visual representation of nanoparticle aggregates greater than 100 nm while in aqueous suspension without the need for additional specialized sizing instruments, which may be limited in detecting aggregates greater than 5-6 microns in size (Malvern Instruments 2005; Murdock et al., 2007). However, in these studies, the size and charge of the Ag nanoparticles was systematically examined with dynamic light scattering and zeta potential. Dynamic light scattering (DLS) size measurements were used to compare primary Ag nanoparticle sizes with TEM and show a great increase in agglomeration once introduced into water or cell culture media (Table 5.2.4). The average agglomerate diameter for Ag nanoparticles suspended in water corresponded to the primary TEM nanoparticle sizes, however, with an ~10X increases in size. However, once the Ag nanoparticles were suspended in cell culture media, the hydrocarbon synthesized Ag nanoparticles did not show consistent size-dependent increases relative to the primary TEM size (Table 5.2.4). The corresponding charge of the Ag nanoparticles was somewhat correlated to the resulting size in cell culture media with Ag10Disp and Ag26Disp having the most negative zeta potentials and smallest agglomerate sizes of 188 nm and 278 nm in media. However, Ag nanoparticles with charges between -17.8 to -26.2 produced larger

agglomerates in media ranging in size from 384-1010nm. This data supports the general observation that a larger zeta potential (e.g. more positive than +30mV or more negative than -30mV) results in greater repulsive forces between the particles and therefore less agglomeration (Malvern Instruments 2005).

Table 5.2.4. Summary of Ag Size and Charge Characteristics

Abbreviation	TEM			
	Average Size	DLS Average Size in Water	DLS Average Size in Media	Charge
Ag13	13 nm	148 nm	1010 nm	-19.6
Ag28	28 nm	208 nm	384 nm	-26.2
Ag43	43 nm	630 nm	605 nm	-18.9
Ag10Disp	10 nm	64 nm	188 nm	-59.4
Ag26Disp	26 nm	126 nm	278 nm	-39.4
Ag52Disp	52 nm	250 nm	576 nm	-17.8

5.3 Results for Biocompatibility

5.3.1 Morphological Observations

Neuroblastoma cells were untreated or incubated with Ag nanoparticles for 24h before visualization with high illumination light microscopy or scanning electron microscopy for observations of morphological changes or Ag nanoparticle binding (Fig 5.3.1). Control neuroblastoma cells prepared for imaging with high illumination light microscopy typically appear elongated in morphology with a diffuse blue tint characteristic of illumination and reflectance from endogenous scattering associated with internal cellular organelles such as mitochondria, endosomes, or vesicles (Fig 5.3.1A). However, cells that were incubated with 25 $\mu\text{g/ml}$ of Ag28 nanoparticles for 24h, then washed with cell culture media to remove unbound nanoparticles, show similar cell morphologies to the control cells (Fig 5.3.1B-C). However, the Ag28 nanoparticles are brightly illuminated and distinctly rounded nanoparticle agglomerates that were noticeably distinguishable from the background cellular illumination with a strong interaction to the cell membrane and neurites (Fig 5.3.1B-C). The Ag nanoparticles (Fig 5.3.1B) appear to more agglomerated than the Ag26Disp nanoparticles (Fig 5.3.1C). Although this procedure of nanoparticle incubation and washing before high illumination imaging is a quick and convenient technique that does not require the use of extra chemicals for sample preparation, which allows the imaging of interactions between nanoparticles and live cells. However, it is not certain whether the nanoparticles are solely located on the surface of the cells or if

they have been internalized and what long-term effects the nanoparticles may have on cellular function.

To verify that the Ag nanoparticles were truly attached to the outer portion of the plasma membrane, the cells were examined with scanning electron microscopy and presence of the Ag nanoparticles was confirmed with energy dispersive x-ray analysis (EDS). Control cells lacked the presence of any higher atomic contrast materials on the surface with an overall gray appearance (Fig 5.3.1D). The lack of Ag was also verified with EDS and shows only the presence of C, O, Na, Mg, and Si (Fig 5.3.1G). The Si signal is from the underlying substrate. However, the Ag28 nanoparticles on the surface of the dosed cells were easily distinguishable from any sample preparation artifacts and cellular membrane irregularities due to their higher atomic contrast than the carbonaceous cellular material (Fig 5.3.1E-F). In the cells dosed with 25 µg/ml of Ag28 nanoparticles, large aggregates of Ag nanoparticles up to 5 microns in size were found on the surface of the cells (Fig 5.3.1E, H). In contrast, cells dosed with 25 µg/ml of Ag26Disp nanoparticles had a more uniform surface binding of the Ag nanoparticles and were morphologically different than either the control cells or Ag28-treated cells with what appeared to be more neurite extensions (Fig 5.3.1F,I). One difference between the Ag28 and Ag26Disp nanoparticles was the presence of a S peak in Ag26Disp, which is due to an added stabilizing agent (Daxad),

which is a sodium salt of a high-molecular-weight naphthalene sulfonate formaldehyde condensate (Sondi et al., 2003).

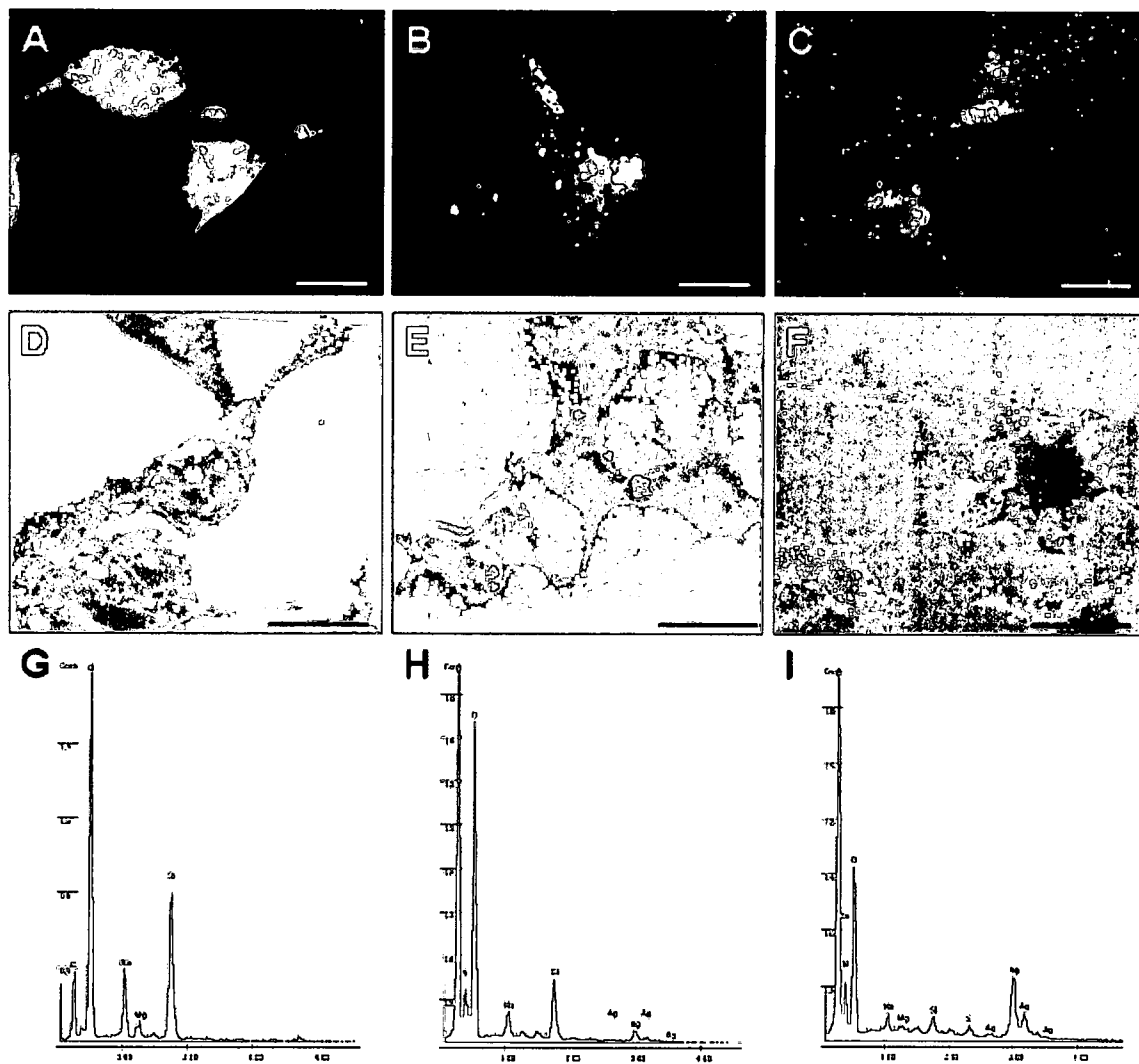


Figure 5.3.1. Binding of Ag nanoparticles to cells. (A-C) High illumination light microscopy of (A) Control N2A cells, (B) 25 µg/ml Ag28, (C) 25 µg/ml Ag26Disp. (D-F) Scanning electron microscopy of (D) Control N2A cells, (E) 25 µg/ml Ag28, (F) 25 µg/ml Ag26Disp. (G-I) Energy dispersive x-ray analysis of (G) Control N2A cells, (H) Cells incubated with Ag28nm, and (I) Cells incubated with Ag26Disp.

To determine if either type of Ag nanoparticles were internalized by the cells after 24h, the cells were incubated with 25 µg/ml of Ag28 or polysaccharide synthesized Ag nanoparticles, embedded in LR White resin, thin sectioned with an ultramicrotome, and examined with transmission electron microscopy (TEM). Silver nanoparticles were found in membrane-bound intracellular vacuoles that appear to be endosomes by their size, shape, and location near the surface of the plasma membrane after 24h (Fig 5.3.2). Endosomes are typically acidic reservoirs that are responsible for transporting material for further degradation by lysosomes (Alberts et. al., 2004). Inside the intracellular compartments, individual Ag28 nanoparticles ranging in size from 15-50 nm were found in relatively loose aggregates (Fig 5.3.2B). In contrast, polysaccharide synthesized Ag26Disp nanoparticles appeared aggregated once inside the cell (Fig 5.3.2C-D). Multiple images suggest that the polysaccharide coating is maintained after 24h of incubation with cells and after internalization by the appearance of a lower contrast matrix surrounding multiple Ag26Disp nanoparticles.

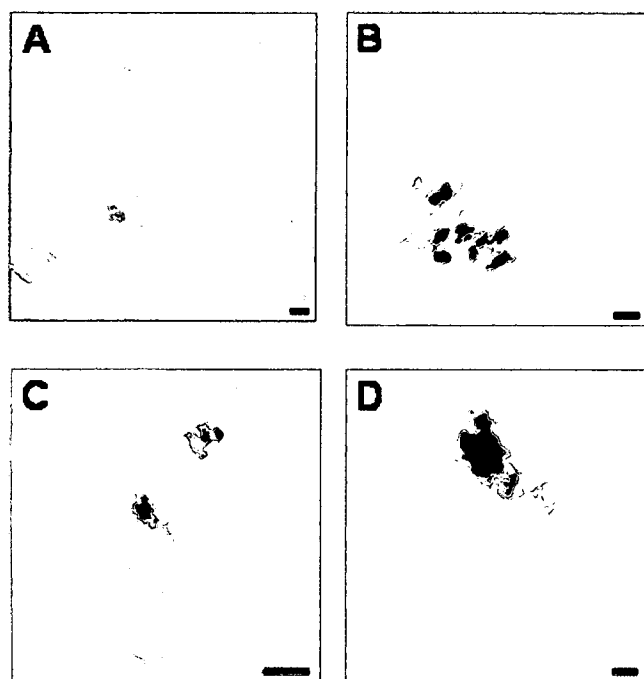


Figure 5.3.2. TEM of Ag nanoparticles inside N2A cells. Internalization and localization of Ag nanoparticles to intracellular vacuoles after 24h of incubation with 25 $\mu\text{g/ml}$ of Ag nanoparticles. (A) Ag28, (B) higher magnification image of (A), (C) Ag26Disp, and (D) higher magnification of lower intracellular vacuole in (C). Scale bars are (A,C) 500nm and (B,D) 100nm.

Because both types of the Ag nanoparticles were internalized after 24h, subcellular effects were further examined. It is hypothesized that the small size of nanoparticles may allow their translocation into critical organelles such as mitochondria (Foley et al., 2002) or that they may interact with cellular proteins of the cytoskeleton (Schrand et al., 2007a). Therefore, after cells were incubated with Ag nanoparticles for 24 h, fluorescent microscopy was used to examine the effect of the nanoparticles on mitochondrial membrane permeability and cytoskeletal architecture (Fig 5.3.3). The use of the Mito-E- Ψ^{TM} fluorescent reagent allows the visualization of healthy mitochondria, which aggregate the dye and emit red fluorescence, compared to cells with damaged mitochondrial membranes where the dye fluoresces

green in the cytoplasm (Fig 5.3.3A-D). Aggregation and retention of the mitochondrial dye inside healthy control cells is shown in Fig 5.3.3A and leakage of the dye in cells incubated with the positive control CdO is shown in Fig 5.3.3D. A representative image of cells incubated with 25 $\mu\text{g}/\text{ml}$ of Ag28 nanoparticles showed reduced mitochondrial membrane integrity compared to Ag26Disp as indicated by predominantly green dispersion of the dye in the cytoplasm compared to punctuate areas of red and green overlap (Fig 5.3.3B-C). Fluorescent staining and microscopy of the actin cytoskeleton and nuclei of cells incubated Ag nanoparticles showed similar changes in internal structure (Fig 5.3.35E-H). Cells incubated with Ag28 nanoparticles (Fig 5.3.3F) or the positive control CdO (Fig 5.3.3H) did not retain intact cytoskeleton in comparison to control cells (Fig 5.3.3E) or cells incubated with Ag26Disp nanoparticles (Fig 5.3.3G).

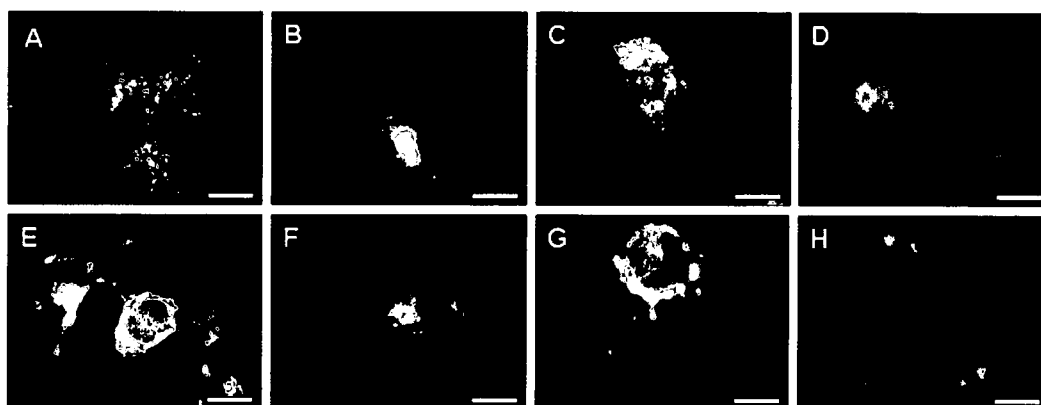
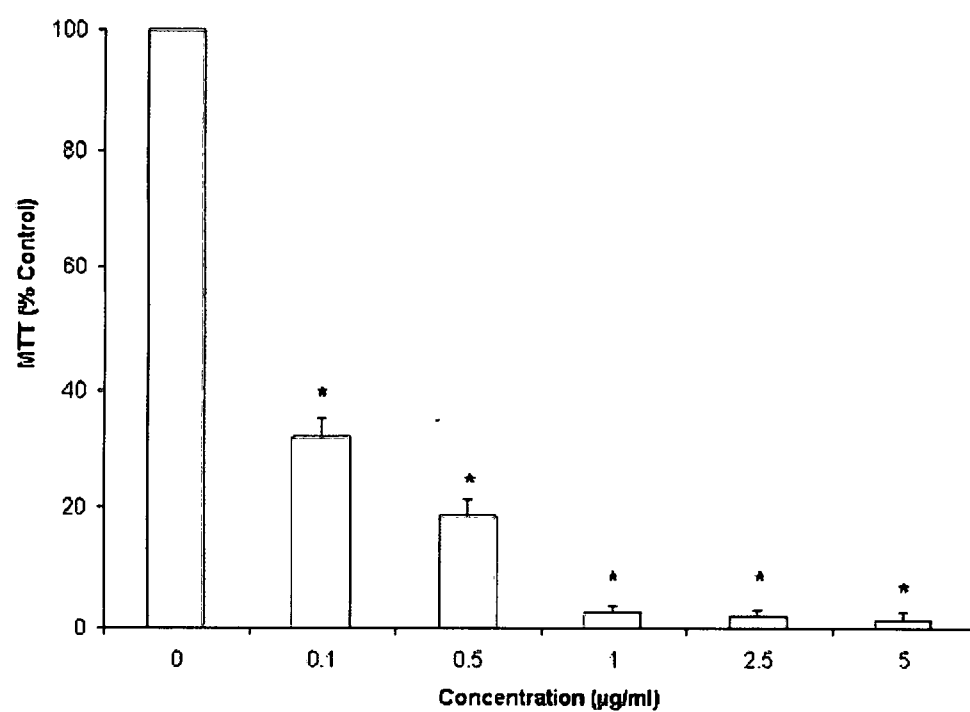


Figure 5.3.3. N2A cell interactions with Ag nanoparticles. (A-D) Fluorescent microscopy demonstrating mitochondrial membrane permeability after 24h. (E-H) Fluorescent microscopy for cytoskeletal architecture after 24h. (A) Control, (B) 25 $\mu\text{g}/\text{ml}$ Ag28, (C) 25 $\mu\text{g}/\text{ml}$ Ag26Disp, (D) 2.5 $\mu\text{g}/\text{ml}$ CdO, (E) Control, (F) 25 $\mu\text{g}/\text{ml}$ Ag28, (G) 25 $\mu\text{g}/\text{ml}$ Ag26Disp, and (H) 2.5 $\mu\text{g}/\text{ml}$ CdO. Scale bars are 20 microns.

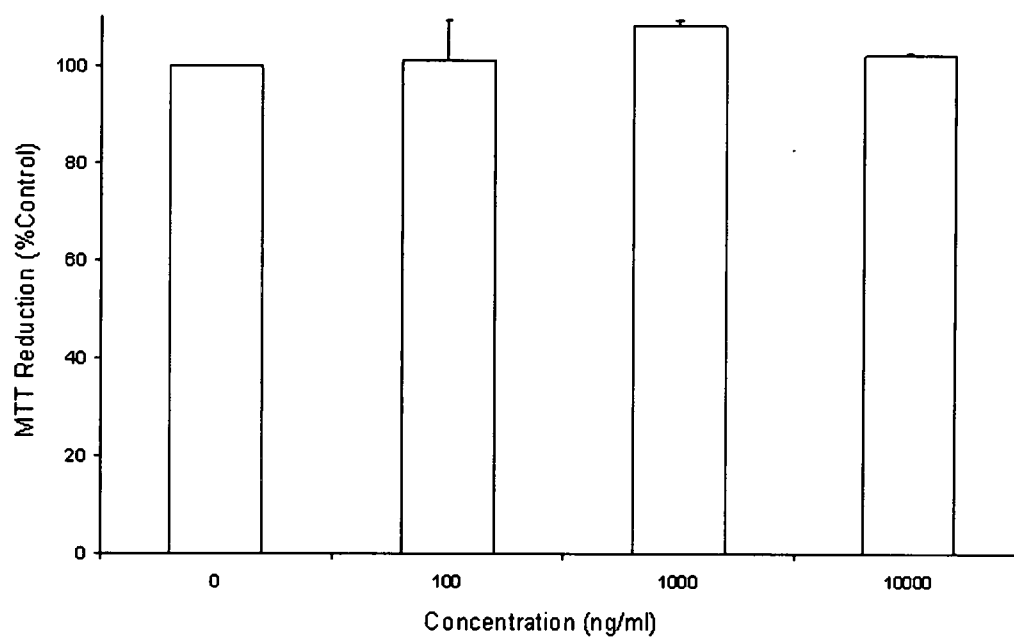
5.3.2 Biochemical Endpoints

It was hypothesized that the polysaccharide synthesis and subsequent surface chemistry changes would increase the biocompatibility of Ag nanoparticles. Therefore, in order to assess the differences in the biocompatibility of the two types of Ag nanoparticles, the MTT assay was performed (Fig 5.3.4). First, the validity of the MTT assay for studies with silver in N2A cells was assessed with the soluble silver compound silver nitrate (AgNO_3) as the positive control. Silver nitrate shows dose-dependent decreases in viability at very low concentrations ($\sim 0.1 \mu\text{g/ml}$) after 24h (Fig 5.3.4A). Additionally, the effect of polysaccharide alone was tested at concentrations up to 10,000 ng/ml ($10 \mu\text{g/ml}$), but did not have any impact on cell viability compared to the control (Fig 5.3.4B). However, exposure to either hydrocarbon synthesized Ag nanoparticles or polysaccharide synthesized Ag nanoparticles produced slightly different toxicities based on both the size and synthesis technique (Fig 5.3.4C,D). In general, the smaller sized Ag nanoparticles (Ag13 and Ag10Disp) were more toxic than the larger Ag nanoparticles. The polysaccharide synthesis also lends some additional protection to the cells increasing the viability compared to the hydrocarbon synthesized Ag nanoparticles at the comparable sizes (Fig 5.3.4E). Therefore, these MTT viability results support the prior fluorescent microscopic images for greater biocompatibility of the Ag26Disp nanoparticles compared to the Ag28 nanoparticles.

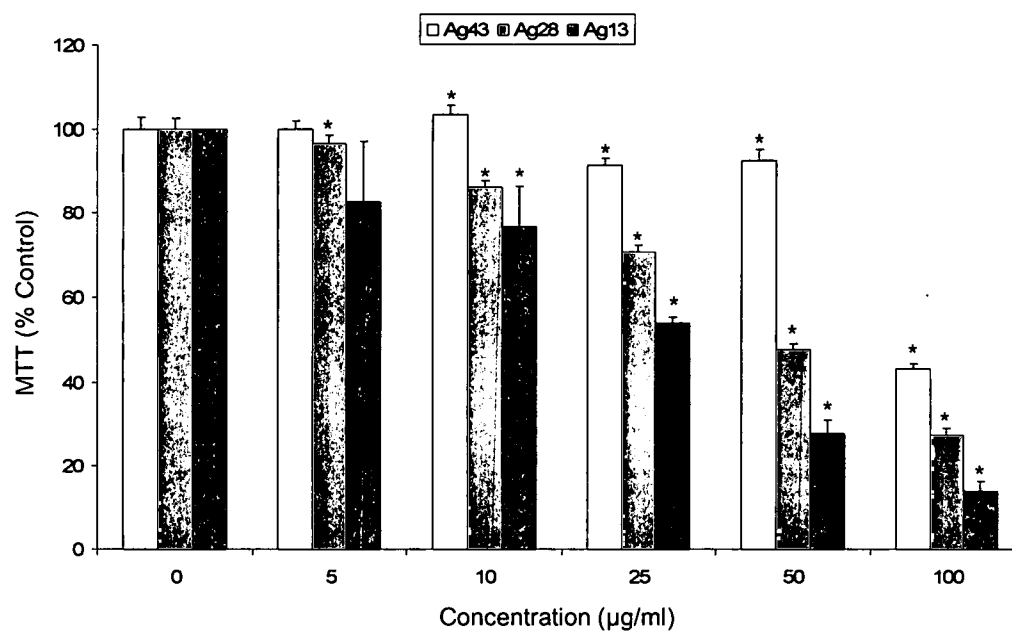
(A)



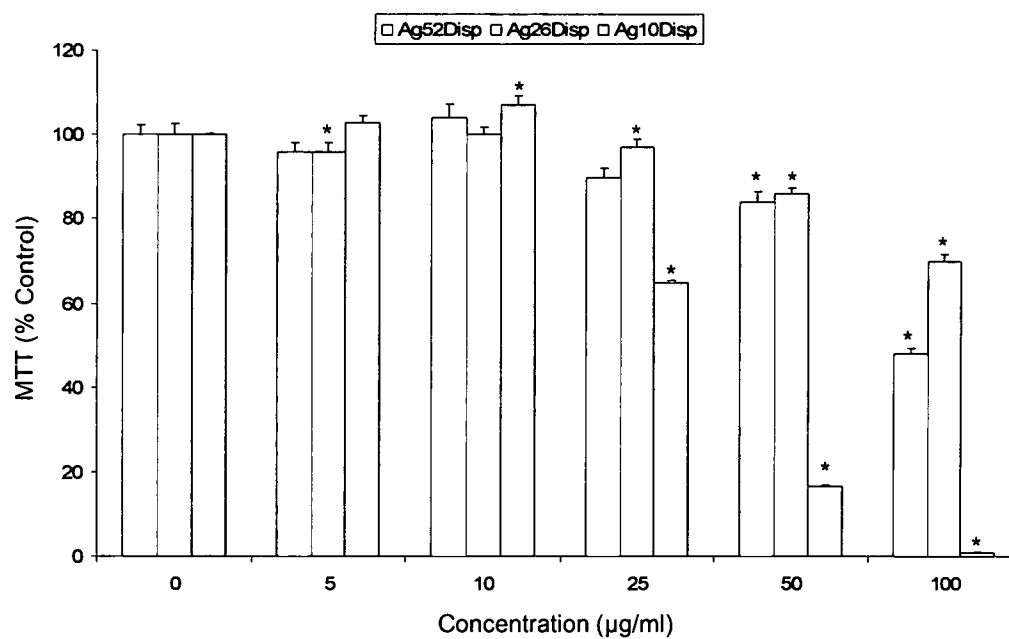
(B)



(C)



(D)



(E)

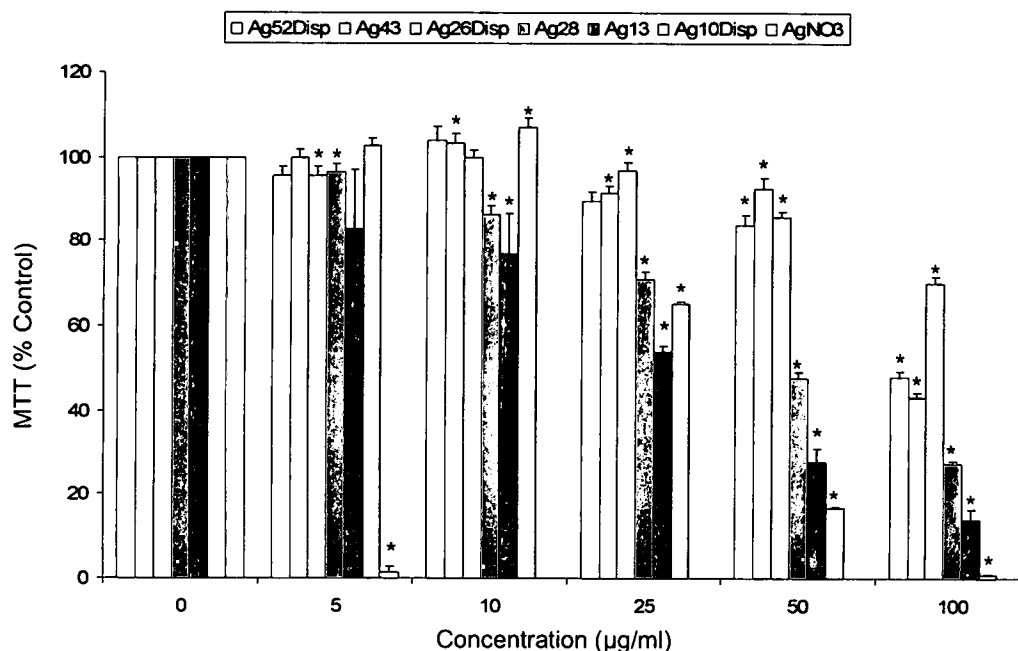
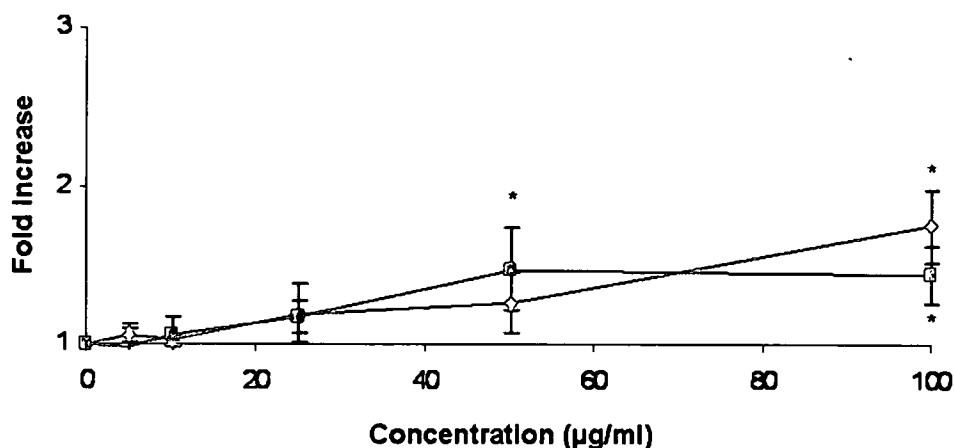


Figure 5.3.4. MTT viability assay. N2A cells incubated with various concentrations of Ag nanoparticles for 24h. (A) AgNO₃, (B) Polysaccharide, (C) Hydrocarbon synthesized Ag nanoparticles, (D) Polysaccharide synthesized Ag nanoparticles, and (E) All Ag nanoparticles tested. Values that were significantly different from the control ($p < 0.05$) are denoted with asterisks (*).

To investigate the potential role of oxidative stress after 24h of cell exposure to the Ag nanoparticles, the increase in fluorescent intensity of the probe DCFH compared to control cells was observed. Increases in cell fluorescence are expressed as a fold-increase relative to control cells, which are equal to 1-fold. Therefore, an increase in cell fluorescence indicates an increase in the generation of reactive oxygen species (ROS) or oxidative stress to the cells (Fig 5.3.5A). Cells incubated with Ag28 nanoparticles show dose-dependent increases in ROS generation up to approximately 1.5-2 times the control with significant increases at 50-100 µg/ml concentrations (Fig 5.3.5A). However, the Ag26Disp nanoparticles do not induce a significant

increase in ROS compared to the control until the highest concentration of 100 $\mu\text{g/ml}$. The positive control for the generation of ROS was hydrogen peroxide (H_2O_2), which shows a dose-dependent linear correlation ($R^2 = 0.9986$) in ROS production from cells incubated with concentrations from 0 to 2000 μM indicating the validity of the assay (Fig 5.3.5B). Further, the endogenous ability of the Ag nanoparticles to react with the DCFH probe in an acellular environment and produce fluorescence indicative of ROS was also investigated and found to be negative (data not shown).

(A)



(B)

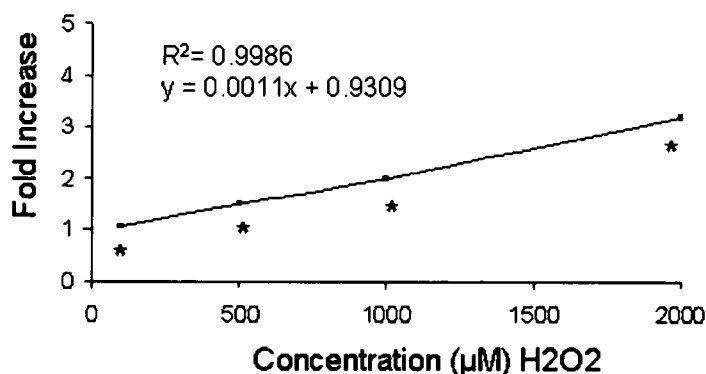


Figure 5.3.5. Reactive oxygen species (ROS) generation after exposure to Ag nanoparticles. (A) ROS generation in N2A cells incubated with Ag28 (blue) or Ag26Disp (red) nanoparticles for 24h. (B) Positive control hydrogen peroxide. Values that were significantly different from the control ($p < 0.05$) are denoted with asterisks (*).

5.4 Discussion

Spherical polydisperse Ag nanoparticles synthesized by different methods (e.g. hydrocarbon plasma vs. polysaccharide reduction), but with similar average primary sizes as verified by TEM, were further characterized and tested for biocompatibility in N2A cells. The main difference between the Ag nanoparticles was the presence of polysaccharides on the surface of the AgDisp samples as chemically verified with FTIR, Raman, and XPS. Once in solution, Ag10Disp and Ag26Disp had the lowest average sizes, which were reflected in their zeta potentials $< -30\text{mV}$. Therefore, synthesizing the Ag nanoparticles by polysaccharide reduction not only led to the presence of an organic coating, but increased the dispersion of the AgDisp nanoparticles in cell culture media compared to the hydrocarbon synthesized Ag nanoparticles.

Overall, the polysaccharide synthesized Ag nanoparticles were more biocompatible than similarly-sized hydrocarbon synthesized Ag nanoparticles as demonstrated by the MTT assay, retention of mitochondrial membrane integrity, and lower generation of ROS. However, the morphology of the cells exposed to the AgDisp nanoparticles appeared altered with increased neurite branching compared to controls or cells incubated with hydrocarbon synthesized Ag nanoparticles, as was shown with other nanomaterials such as NDs, which may be a generic response of N2A cells to nanomaterials and not a composition-specific response. An explanation for the differential

biocompatibility between the hydrocarbon and polysaccharide synthesized Ag nanoparticles can be explained by the lack of surface coating on the hydrocarbon synthesized Ag samples, which did not effectively block direct contact between the Ag nanoparticle and the cell. This was shown with surface chemistry analysis (FTIR and XPS) where in the Ag28 sample, the Ag signal was not blocked because there was not an effective surface coating, although hydrocarbons were present as evidenced by carbon content and TEM imaging. In contrast, the synthesis of Ag nanoparticles by polysaccharide reduction of Ag ions in aqueous solution led to effectively blockage of the XPS Ag signal in most samples due to the coverage of the surface by polysaccharides. The Ag10Disp solution also contained a surfactant, which was evident by the higher levels of Na and S (DAXAD dispersant). This additive, in addition to its small size and increased dispersion, may be why it was the most toxic of the Ag nanoparticles at the higher 50-100 $\mu\text{g/ml}$ concentrations.

However, if size was truly the primary factor influencing toxicity, the above characterization would predict that the Ag10Disp nanoparticles, which show the lowest size distributions in cell culture media, should be more toxic to the cells at all of the concentrations tested. However, Ag10Disp nanoparticles were not the most toxic Ag nanoparticle until the highest concentrations of 50-100 $\mu\text{g/ml}$ (Fig 5.3.4E). Additionally, Ag13 nanoparticles once introduced into cell culture media had the largest average size of 1010nm compared to any of

the other Ag nanoparticles, but still more greatly reduced cell viability compared to other larger nanoparticles, regardless of the synthesis method (Table 5.2.4). Therefore, the size-dependent toxicity previously reported in bacteria (Morones et al., 2005) and other studies (Hussain et al., 2005, Braydich-Stolle et al., 2005) may be more closely linked to the increased surface reactivity of the smaller nanoparticles, the number dose of nanoparticles coming into contact with the cell rather than the equivalent mass dose for different sized nanoparticles, variations in the concentration of the nanoparticles, the size of the nanoparticles in solution, and other factors such as better dispersion of the nanoparticles, which again, can influence the number of nanoparticles coming into contact with and internalized by the cell through decreased agglomeration and reduced gravitational settling.

Although Ag nanoparticles are continuing to be synthesized in great amounts for incorporation into many consumer products, questions remain regarding the maximum Ag nanoparticle exposure levels and pathways for elimination from the body. The EPA recommended limit for silver exposure is 1.09 mg/day for a 160 pound individual, but there are currently no studies examining the average amount of Ag nanoparticles released from products that are aerosolized or in direct contact with the skin such as wound dressing or topical ointments containing silver. Because the toxic dose of silver nitrate to skin cells was similar to that of bacteria (Poon and Burd 2004), the dynamics of silver toxicity at the cellular level are particularly important to

provide the desired anti-microbial effect while protecting the body from unwanted side effects. In this regard, further investigations should better define optimal administration routes, the ability of the nanoparticles to translocate to systems other than the sites of administration (such as cells of the nervous system), and the accumulation and degradation of nanoparticles in cells and tissues.

If Ag nanoparticles, similar to the ones used in these studies, are used as biological labels, the concentration should be kept low, dispersion further increased to allow effective internalization into the cell possible transport into the nuclear region, and additional functionalities added to modify the mechanism of internalization by different cell types. In these studies, although both forms of Ag nanoparticles were internalized into intracellular vacuoles, the lack of internalization into the nucleus was expected because passive transport into the nucleus is limited to particles with diameters of 9 nm or less (Paine et al., 1975). The predominant mechanism of internalization for N2A cells in these studies appeared to be non-specific endocytosis, but other mechanisms can occur and accumulation has been shown to vary by cell type (Schrand et al., 2007b). Although, the results of these studies did not show a large increase in ROS after exposure to Ag28 or Ag26Disp nanoparticles (~2X), it was significantly different from the control at 50-100 µg/ml for Ag28 compared to 100 µg/ml for Ag26Disp. Therefore, the history of metals in neurodegenerative disease must be weighed against the

benefits of therapeutic use when oxidative stress has been shown in these and other *in vitro* experiments (Hussain et al., 2005).

In conclusion, taking advantage of the highly desirable properties of Ag nanoparticles while protecting the body from harmful side effects is a worthwhile long-term goal, and surface modification of nanoparticles seems to be one of the keys to achieving that goal.

CHAPTER 6

SUMMARY AND CONCLUSIONS

6.1 Summary

These studies were conducted to assess the relationship between engineered carbon and metal nanomaterials and biocompatibility in cell types that are relevant targets for nanomaterial exposure or therapeutic applications. The nanomaterial characteristics that most greatly impacted the biocompatibility were composition, presence of impurities, size-related properties (*e.g.* primary size, agglomerate size in solution, charge, temperature, serum proteins, shape), surface chemistry, and cell-specific responses (*e.g.* internalization amount and mechanism). The biocompatibility results related to the material properties and cell response are shown below for carbon and silver nanomaterials (Table 6.1.1 and 6.1.2).

Table 6.1.1 Summary of Carbon Nanomaterial Biocompatibility.

	SWNT	MWNT	CB	ND
Impurities	Fe from catalyst	↑Fe content :ROS	No Fe, but S	No Fe, more pure
Size/Shape	Smaller diameter than MWNT, Tube	Size in water ~ same as SWNT	Size in media ~ same as ND, Spherical	Smallest primary size, Cubic
Charge	High + charge, Greatest reduction in viability	- Charge, SO ₃ Na more - than COOH	- Charge	High + charge, Large accumulation over 24h
Surface Chemistry	phenylSO ₃ Na group > SWNT	SO ₃ Na group > COOH group	N/A	No Effect
Localization	Vacuole, not nucleus	Vacuole, not nucleus	Vacuole, not nucleus	Also Lysosomes
Contact and Internalization	Yes, Endocytosis	Yes, Endocytosis	Yes, Endocytosis	Yes, Endocytosis
Morphology	No change	No change	No change	↑ Branching
Mitochondrial Membranes	Increased leakage	Increased leakage	Increased leakage	Unaffected
Oxidative Stress	Up to 5-20X ↑ROS	Up to 5-20X ↑ROS	~2-10X ↑ROS	None
Cell Specific Response	Greater decreases in viability in Lung immune cells	Increased internalization phagocytosis in Lung immune cells	Endocytosis in Neuroblastoma cells	Neurite branching in Neuroblastoma cells

Table 6.1.2. Summary of Ag Nanoparticle Biocompatibility.

	Ag28	Ag26Disp
Size Effects	43>28>13	52>26>10
Charge	-26.2	-39.4
Surface Chemistry	No Na/N, strong Ag signal	C-O, C=O, COC
Morphological Alterations	Membrane binding, rounding	Membrane binding, retention of neurites
Contact and Internalization	Yes, endocytosis	Yes, endocytosis
Localization	Intracellular Vacuole, not nucleus	Intracellular Vacuole, not nucleus
Mitochondrial Membranes	Increased leakage	Slight increase in leakage
Oxidative Stress	Up to ~2X, Significant @ 50-100 µg/ml	Significant @ 100 µg/ml
Cell Specific Response	Reduced viability in Lung immune cells	NT

The objectives of this research that were accomplished were:

1. Nanomaterial Characterization – thorough examination of the size, morphology, composition, concentration, purity, agglomeration state, charge, and inherent reactivity of carbon and metal-based nanomaterials were assessed.
2. Cell-Nanomaterial Interactions – demonstration of NM contact and morphological changes after exposure to nanomaterials including internalization and localization in cells after 24h.
3. Nanomaterial Biocompatibility – changes in cell viability and associated biochemical endpoints were determined after 24h of exposure to carbon and metal-based nanomaterials in solution.

The results of this research satisfy all three research objectives and provide a model for other *in vitro* studies with an emphasis on thoroughly characterized nanomaterials and relationships to their properties in the cell culture environment. The importance of these studies is warranted and timely because nanotoxicity research is a new and emerging field and there are not well-established guidelines or references. Therefore, modifications and careful consideration of each assay were required due to the differences between chemical biocompatibility or toxicity studies compared to those involving nanomaterials. In these studies, a variety of microscopic (e.g. light, fluorescent, electron), analytical (e.g. ICP-OES, AAS, XPS) and biochemical assays (e.g. MTT, MMP, ROS, etc.) were used to expand the current knowledge about *in vitro* nanomaterials biocompatibility. Therefore, these studies provide technical information on several different nanomaterials and cell types, which are highly valuable to other researchers. In particular, these studies emphasize that the surface chemistry, purity, dimension, size distribution, morphology, aggregate size in solution, and charge are critical parameters for understanding the biocompatibility or toxicity of nanomaterials to cells.

6.2 Conclusions

Results in the contained studies significantly contribute to understanding the materials characteristics that are related to *in vitro* biocompatibility. The following important conclusions and discoveries were made:

1) Nanomaterial Characterization – It was essential to have consistent quality control procedures for verifying the size, morphology, concentration, charge, and chemical properties (e.g. purity, surface chemistry) of nanomaterials before use in cellular systems. An emphasis on an engineering interpretation of nanomaterial properties and changes related to the cell culture environment (e.g. changes in dispersion/size) was critical for understanding the relationship between nanomaterial characteristics and their resultant biocompatibility. For example, the size of all of the nanomaterials increased upon suspension in solution, but nanomaterials retaining a very large positive or negative charge ($> 30\text{mV}$) demonstrated the smallest sizes and best dispersion.

2) Cell-Nanomaterial Interactions – Multiple imaging techniques suggest that nanomaterials contact plated cells in culture after gravitational settling or through Brownian motion, are internalized, and localize to areas within the cytoplasm, but not nucleus. Both skin and neuroblastoma cells examined in these studies showed internalization of nanomaterials after 24h into intracellular vacuoles (e.g. endosomes) and the suggested mechanism of

entry was non-specific endocytosis. Further support for this mechanism was found through time-dependent internalization studies with fluorescent NDs showing localization to lysosomes, which are responsible for degrading contents found in endosomes. In comparison, lung immune cells internalized nanomaterials in larger amounts by phagocytosis. Other important morphological changes that were discovered in these studies after cells were incubated with nanomaterials included increased neurite branching, reductions in proliferation, and alterations in membrane labeling based on surface coatings.

3) Nanomaterial Biocompatibility – These studies are the first to examine the differential biocompatibility of carbon nanomaterials in multiple cell types with studies on neuronal cells being of particular value due to the lack of published biocompatibility data on this cell type. Other new findings include examination of the biocompatibility of Ag nanoparticles in mammalian cells compared to most studies, which use microbes, and the first reports of the testing of very small 2-10nm NDs in cells. Of all the nanomaterials studied, NDs were the most biocompatible, did not disrupt mitochondrial membranes, and lacked ROS. In contrast, carbon nanotubes and Ag nanoparticles caused mitochondrial membrane leakage and the generation of ROS, which is likely based on the presence of residual metal (Fe) catalysts and the surface reactivity, respectively. Overall, the data suggest that the biocompatibility of nanomaterials is primarily based on composition, size,

surface chemistry, and cell type with smaller Ag nanoparticles demonstrating greater toxicity to cells than carbon nanomaterials and lung immune cells showing greater sensitivity to nanomaterials likely due to their innate inflammatory response to foreign materials. Therefore, on the basis of these results, one immediate suggested application of NDs in biocompatibility studies would be as a replacement for the fine CB presently used in some studies as a negative nanoparticle control.

In summary, the effective concentrations where 50% of the cells died (EC₅₀ values) for the nanomaterials examined in these studies are summarized below in Table 6.2.1. Because some nanomaterials failed to reduce mitochondrial function by at least 50% at their highest doses, exact EC₅₀ values could not be calculated. Therefore, the EC₅₀ values for these nanomaterials are stated as >100 µg/ml.

Table 6.2.1. Summary of effective concentrations that reduced cell viability by 50% after 24h (EC50 values).

	Neuroblastoma	Macrophage	PC-12	HaCat/ HEL-30
ND-raw	>100 µg/ml	>100 µg/ml	>100 µg/ml	>100 µg/ml
T-ND	>100 µg/ml	>100 µg/ml		>100 µg/ml
ND-COOH	>100 µg/ml			
ND-COONa	>100 µg/ml			
ND-SO₃Na	>100 µg/ml			
SWNT	>100 µg/ml	20 µg/ml		
MWNT	46 µg/ml	35 µg/ml	>100 µg/ml	
CB	>100 µg/ml	73 µg/ml	>100 µg/ml	
MWNT-SO₃Na	>100 µg/ml			
SWNT-phenylSO₃Na	>100 µg/ml			
MWNT-2	>100 µg/ml			
MWNT-COOH	>100 µg/ml			
Ag43	47 µg/ml			
Ag28	47 µg/ml			
Ag13	29 µg/ml			
Ag52Disp	97 µg/ml			
Ag26Disp	>100 µg/ml			
Ag10Disp	33 µg/ml			
CdO	0.44 µg/ml	6.8 µg/ml	3 µg/ml	
AgNO₃	0.07 µg/ml			

CHAPTER 7

CHALLENGES AND SUGGESTED FUTURE RESEARCH

Although a detailed study of carbon and metal-based NMs has been conducted to elucidate the relationship between their properties and biocompatibility, the investigation of novel materials and their effects on biological systems is a complex field. Several of the remaining challenges in studying the relationship between engineered NM characteristics and their resultant *in vitro* biocompatibility include accurately estimating the degree of NM interaction with living cells, subsequent NM internalization, localization, and accumulation over time. In these studies, several characterization methods were established in addition to multiple microscopic methods (e.g. light, fluorescent, electron), to characterize and quantify the internalization and accumulation of NMs into cells. This chapter will focus on the challenges and suggested further research in order to: 1) preserve the most accurate state of cells after NM exposure by avoiding artifacts and toxic chemicals while obtaining high resolution images (e.g. TEM, STEM, Wet SEM) providing details on NM internalization, localization, and mechanism of entry, 2) determine the NM properties responsible for cell recognition, binding, localization, internalization, and accumulation (e.g. charge, surface chemistry, size), 3) elaborate on the mechanism of NM entry into cells, localization, and

physico-chemical state of nanomaterials once inside cells, and 4) quantify the amount of NMs internalized into cells with spectroscopic techniques.

The evaluation of NM uptake with *in vitro* cell culture can be monitored with a variety of techniques such as fluorescent microscopy, flow cytometry, fluorescent-activated cell sorting (FACS), confocal microscopy, inductively coupled plasma mass spectroscopy, radio-active labeling, photoluminescence, and AFM. While the majority of research in this area relies on the use of fluorescent nanomaterials, the emphasis of this chapter will be on carbon and metal-based nanomaterials.

7.1 Preservation of the Most Natural State for High Resolution Imaging

Light, fluorescent, and confocal microscopy are very attractive options for studying the interactions of NMs with living cells, but cannot resolve individual nanoparticles or detailed localization within cells. Although higher resolution optics have been developed as attachments to light or fluorescent microscopes (*e.g.* Cytoviva system), without serial sectioning capabilities, it is difficult to distinguish NMs residing outside compared to inside the cell. In order to obtain nanometer resolution, electron microscopy is used, but the sample preparation can generate many artifacts due to the crosslinking of proteins and dehydration before embedment in resin, thin sectioning, and viewing under high vacuum/high electron beam energy conditions. In addition, the use of toxic heavy metal stains are used to provide contrast, thereby leading to dramatic changes from the original living cell sample. Lower voltage imaging with scanning transmission electron microscopy (STEM) in a standard SEM may generate greater contrast without the use of heavy metal stains, but still requires an electron transparent sample. By comparison, the use of high vacuum capsules for wet imaging in SEM (*e.g.* Quantomix capsules) lends itself to more realistic observations of hydrated samples, but may still require that the cells are stained, and therefore in an altered state, to provide adequate contrast.

In these studies, three different electron microscopy techniques (TEM, STEM, and Wet SEM) were compared for their ability to effectively demonstrate Ag nanoparticle internalization, localization, and clues to the mechanism of internalization in three different cell types (lung, neuroblastoma, and skin).

Traditional Transmission Electron Microscopy (TEM)

Macrophages incubated with 25 µg/ml of Ag₂₈ nanoparticles for 24h show internalization of the Ag nanoparticles, which is likely accomplished through phagocytosis, their primary function of engulfing solid, foreign debris after contact with the cell membrane (Fig 7.1.1A-B, white arrows). After phagocytosis of the debris, an internal vacuole or phagosome, is formed, which is usually delivered to the lysosome, an organelle involved in the breakdown of cellular components. The contents are subsequently degraded and either released extracellularly via exocytosis, or released intracellularly to undergo further processing (<http://en.wikipedia.org/wiki/Phagocytosis>). However, some agglomerated Ag nanoparticles were also found outside of the cells suggesting that the nanoparticles did not effectively come into contact with the cells, the nanoparticles were removed from the cell membranes during sample processing, or that there are limitations on the size of nanoparticle agglomerates that can be actively phagocytosed (black arrows, Fig 7.1.1A).

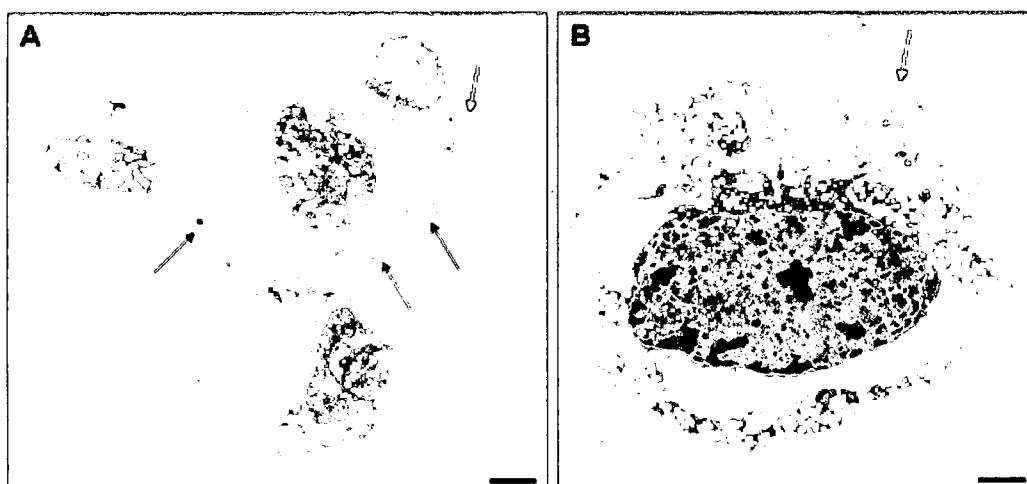


Figure 7.1.1. TEM of macrophages incubated with 25 $\mu\text{g/ml}$ Ag28 for 24h. (A) Four macrophages showing different degrees of Ag nanoparticle internalization (see white arrow). Notice that some Ag nanoparticles remain outside the cells (black arrows). (B) Higher magnification images of a single macrophage with Ag nanoparticles enclosed in an intracellular vacuole or phagosome (white arrow). Scale bars are 2 μm .

Scanning Transmission Electron Microscopy (STEM)

Although SEM is typically used to generate topographical images, in the case of STEM imaging, the electron beam passes through the sample instead of scanning only its surface. In addition observing the internal features of the cells, STEM can make use of a lower electron voltage of 5kV, compared to 80-200kV for TEM, with very good contrast due to the small interaction volume of the thin (<70nm) section of resin embedded cells. Additionally, there is no need for additional heavy metal staining with toxic chemicals such as uranyl acetate and lead citrate. The visualization of Ag26Disp nanoparticle internalization by neuroblastoma cells after 24h is shown in Figure 7.1.2. The low magnification image in Fig 7.1.2A shows an entire cell with a prominent round nucleus and many other cytoplasmic organelles, which display greater contrast than the previously imaged macrophages with high voltage TEM (Fig

7.1.1). At higher magnification, the presence of Ag nanoparticles inside small intracellular vesicles is evident (Fig 7.1.2B-C, black arrows).

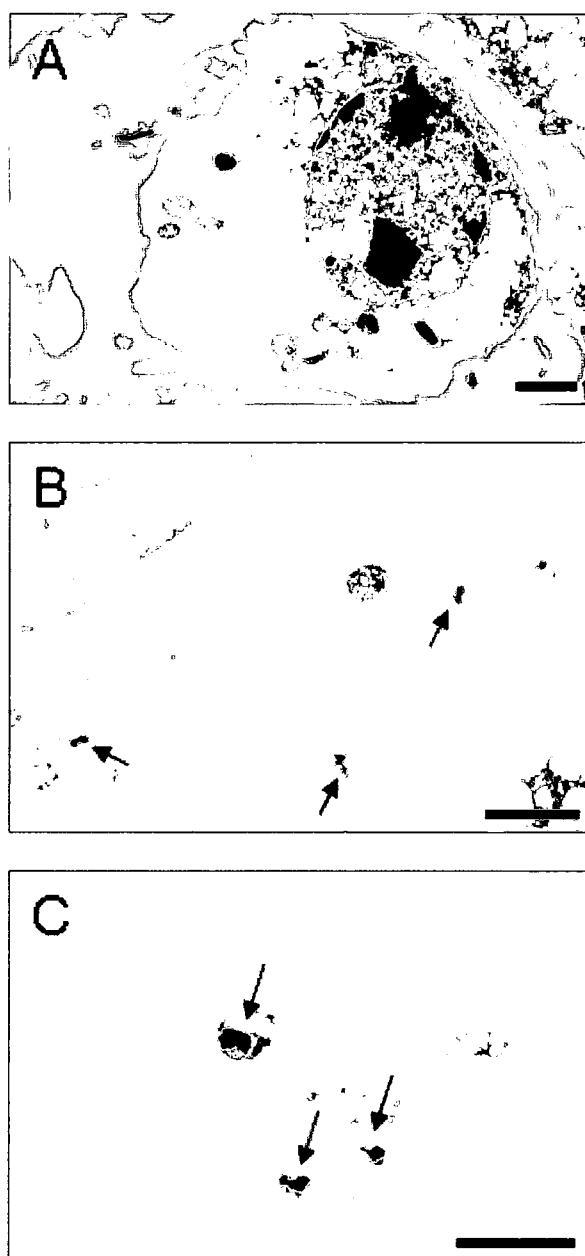


Figure 7.1.2. Scanning transmission electron microscopy (STEM) of N2A cells. Cells were incubated with 25 $\mu\text{g/ml}$ polysaccharide synthesized Ag26Disp nanoparticles for 24h. Black arrows denote the presence of the Ag nanoparticles in round intracellular vesicles. Scale bars are 2 μm in (A) and (B) and 500nm in (C).

Wet Imaging with Scanning Electron Microscopy (SEM)

SEM of cells attached to a polymer membrane and contained within air tight capsules allowed the penetration of the electron beam through the polymer membrane of the capsule while maintaining a high vacuum between the wet cell sample and the microscope sample chamber. Although, under some circumstances, living cells have been imaged in this manner, in these studies it was necessary to generate cell contrast with a heavy metal stain (osmium tetroxide), which leads to cell death, but also preserves the state of interaction between the cells and Ag nanoparticles. Other required conditions for imaging with the wet capsules included use of the maximum voltage available in the SEM (30kV) in backscatter mode in order to generate the appropriate signal contrast.

Visualization of the internalization of 25 $\mu\text{g/ml}$ Ag28 nanoparticles into keratinocytes after 24h with conventional light microscopy is shown in Figure 7.1.3A-B. Some of the Ag28 nanoparticles formed large, dark aggregates outside of the cells as depicted with black arrows in Figure 7.1.3B, which is characteristic of their aggregation in cell culture media. In SEM, the high atomic contrast of the Ag28 nanoparticles generates a bright signal showing dense agglomerates both inside and outside the cells (Fig 7.1.3C-E). White arrows in Fig 7.1.3D denote the presence of agglomerates outside the cell similar to Fig 7.1.3B. Because the electron image is generated from an interaction volume of only a few microns deep between the polymer

membrane and the attached cell surface, only particles that have been effectively bound to the membrane or internalized contribute to the image signal (Behar, 2005). Additionally, the nanoparticle contrast is reduced when the signal is scattered through the cell membrane (Fig 7.1.3E, black arrow) compared to a nanoparticle agglomerate outside the cell shown (Fig 7.1.3E, white arrow).

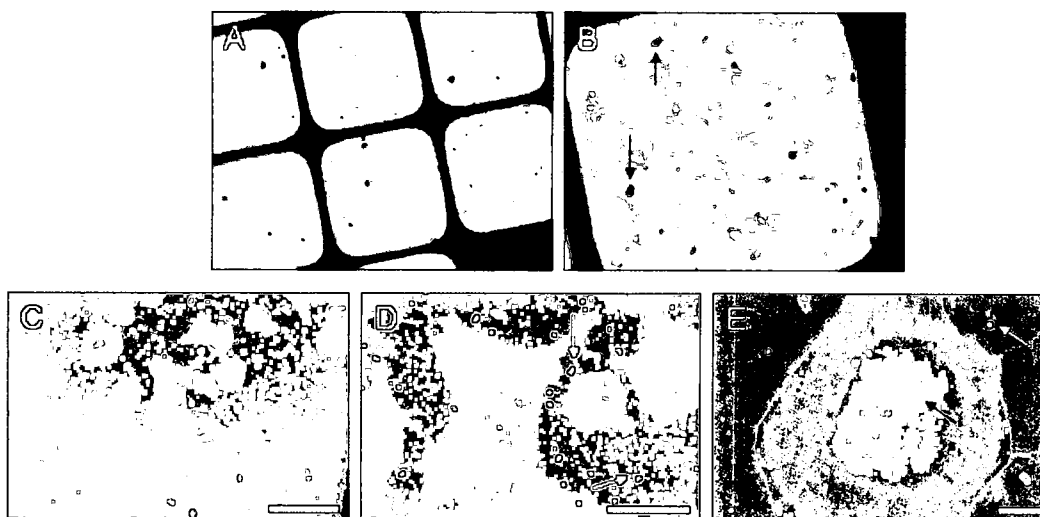


Figure 7.1.3. Wet imaging of cells under high vacuum. Interaction and internalization of 25 $\mu\text{g/ml}$ Ag28 after 24h incubation with keratinocytes. (A, B) Low magnification light microscope images (6x, 12x) of cells and Ag nanoparticles on the polymer wet imaging capsule membrane. Black arrows in (B) denote Ag28 nanoparticle agglomerates outside of the cells. (C-E) Scanning electron microscope (SEM) images of cells showing Ag28 nanoparticles both inside and outside of the cells at increasing magnifications. White arrows in (D) and (E) show nanoparticle agglomerates outside of the cells. Black arrow in (E) demonstrates reduced contrast due to signal generation through the cell plasma membrane. Scale bars are 50, 20, and 5 microns for (C), (D), and (E), respectively.

Therefore, a comparison of these three electron microscopic techniques reveals that traditional TEM preparation is most useful to obtain high resolution images of cells and NMs. However, future studies should strive to preserve the quality of the cells in the most natural state.

7.2 Nanomaterial Properties Responsible for Cell Attraction, Binding, Internalization, Localization, and Accumulation

The way cells communicate with their environment through chemical, electrical, or mechanical signals is a highly sophisticated and regulated process (Chenevier et al., 2000). Nevertheless, the whole process leading to signal transmission and cell response usually involves an initial and limiting step that entails some sort of recognition at the cell surface. Most common mechanisms of recognition require specific binding of ligands such as sugars or proteins to membrane receptors by a lock and key mechanism. However, it is unclear how cells bind nanomaterials, which may not be recognized by the cell receptors. One possible explanation is the electrostatic attraction between nanomaterials and the negative charge density of the cell surface, which is due to the presence of sulfated glycosaminoglycans, polysaccharide acids, membrane glycoproteins bearing sialic acid residues and membrane lipids (Chenevier et al., 2000).

In these studies, the effect of NM surface charge, surface chemistry, and size were considered as properties that could effect the interaction of NMs with the cell surface. For example, although the two different types of Ag nanoparticles with different surface chemistries were both found to bind cell surfaces, the greater degree of agglomeration in the hydrocarbon synthesized Ag nanoparticles may reduce the internalization amount compared to the polysaccharide synthesized Ag nanoparticles. Alternatively, the polysaccharide moieties on the surface of the AgDisp nanoparticles may

more strongly bind the membrane surface and reduce the internalization amount compared to the hydrocarbon synthesized Ag nanoparticles. However, the specific effect of surface chemistry on internalization has not been confirmed and both types of Ag nanoparticles had similar negative charge values (-26 mV vs. -39 mV) and were internalized after 24h into intracellular vacuoles. In order to determine if there is differential binding and internalization of the Ag nanoparticles, suggested experiments include examining the direct binding of Ag nanoparticles to specific cell receptors or surface proteins (e.g. polysaccharides, glycoproteins) and a combination of 3-D cell reconstruction with AFM of TEM sections made on an ultramicrotome aided with the development of a computer-based program for nanoparticle recognition for quantification.

The effect of charge on surface attraction and subsequent internalization appeared to be greater for the highly positively charged (+40 mV) NDs than any of the other nanomaterials tested (e.g. carbon nanotubes, carbon black, Ag nanoparticles). However, quantifying the amount of carbon NMs inside the cells is still a technical hurdle. An additional factor to consider for the possibly greater accumulation was the small primary size of the NDs compared to the other NMs tested. However, once suspended in cell culture media, both the NDs (2-10 nm) and the smallest Ag nanoparticles (15 nm) produced the largest agglomerates between 1-2 microns in average diameter in comparison. In contrast, the smallest polysaccharide synthesized

Ag10Disp nanoparticles produced the smallest agglomerates in cell culture media of 188nm, which suggests that surface chemistry has a profound influence on dispersion and may also contribute to differential cell binding, internalization, and accumulation.

In order to systematically examine the effects of charge, surface chemistry, or size on Ag nanoparticle accumulation, further surface modifications (e.g. coating, charge, fluorescence) could be made. For example, amino-modified polystyrene particles with varied surface charge and resultant size (168-1290 nm) have demonstrated differential internalization into various cell lines (Ricarda-Lorenz et al., 2006). A fluorescent activated cell sorter (FACS) was used to detect the uptake of the particles and confocal and transmission electron microscopy revealed differences in their subcellular localization. The cationic polymeric particles had enhanced uptake compared to uncharged particles and the differences in intracellular localization between the different cell types was explained by different endocytotic/pinocytotic properties. Another study showed that colloids with positively charged surfaces bound much more efficiently those with neutral surfaces (Chenevier et al., 2000). The issues involved in the quantification of NM binding or internalization will be discussed in a separate section.

7.3 Elaboration on Mechanism of Nanomaterial Entry into Cells and Subsequent Physico-Chemical Changes

Once the nanomaterials are in close proximity to the cell surface (based on the NM properties discussed in the previous section: charge, surface chemistry, or size), mechanisms such as passive diffusion or active transport could lead to internalization. This section will discuss the general mechanisms involved in ligand entry, some experimental techniques such as changes in temperature or the addition of chemicals that can be used to modify the uptake response, and what physico-chemical changes may occur to the NMs once internalized by cells.

The general endocytic mechanisms by which ligands (e.g. viruses) can be taken into the cell are clathrin-mediated endocytosis, uptake via caveolae, macropinocytosis, and phagocytosis (Parker and Parrish, 2000). Ligands that are taken into cells by receptor-mediated endocytosis are trafficked to early sorting endosomes where the low-pH environment causes many ligands to dissociate from their receptors. Receptor-dissociated ligands are rapidly trafficked to late endosomes and then to lysosomes, where they are degraded. Specific signals on the cytoplasmic tail of some receptors may cause them to be sorted and returned to the plasma membrane for reuse, while in other cases both the receptor and ligand are targeted to the late endosome/lysosome for degradation (Rajasekaran et al. 2003). The fate of internalized ligands and receptors is complex, and other pathways exist,

which target receptors and receptor-bound ligands to a perinuclear recycling endosomal compartment and in some cases to the Golgi network (Parker and Parrish, 2000).

In these studies, it was discovered that all of the nanomaterials localized to cytoplasmic vacuoles, which resembled endosomes after 24h. However, further examination of fluorescent NDs suggested possible attempts at degradation by co-localization in lysosomes. However, difficulties in rinsing away settled NDs from the cell surface and glass slides occurred when the temperature-dependent internalization of NDs was examined. Therefore, modifications to certain NMs to enhance their dispersion and isolation from the cell surface should be optimized before future kinetic and chemical studies examine NM energy-dependent uptake, and more specifically, whether it occurs through caveolae or clathrin-coated pits. These data could then assist in determining the rate limiting steps for the optimization of nanomaterial delivery. For example, several studies by Dr. Lim and colleagues examined the uptake of the fluorescently labeled, cationic polymer chitosan into A549 cells derived from human respiratory epithelium (Huang et al., 2002, Ma and Lim, 2003). Nanoparticle uptake increased with increasing concentration, as verified with confocal microscopy and quantified with fluorometry, but was a saturable and temperature-dependent event with greater uptake at 37°C compared to 4°C (Huang et al., 2002). The suggested mechanism of uptake was absorptive endocytosis initiated by non-specific

interactions between the nanoparticles and cell membranes in part mediated by a clathrin-mediated process (Huang et al., 2002).

Other studies have used chemical metabolic inhibitors and actin/endocytosis such as sodium azide, 2,4-dinitrophenol, and cytochalasin D to elaborate on the mechanism of uptake into cells. For example, the *in vitro* delivery of nano- and micro-sized particles (20nm, 2000 nm) to human retinal pigment epithelial cells was examined by Aukunuru et al. in the presence of colchicine, cytochalasin B, and sodium azide (<http://www.drugdeliverytech.com/cgi-bin/articles.cgi?idArticle=33>). Colchicine reduced the uptake of both of the particles by ~30% while cytochalasin B reduced the uptake of the 20 nm particles by 51% and sodium azide reduced the uptake of the 2000-nm particles by 30%. Another study with biodegradable poly(D,L-lactide-co-glycolide) (PLGA) nanoparticles containing 6-coumarin as a fluorescent maker were used to study the effect of different sizes (100nm, 800nm, and 10 microns) on uptake by primary cultured rabbit conjunctival epithelial cells (Qaddoumi et al., 2004). Uptake was inhibited by lower incubation temperature (4°C vs. 37°C), sodium azide, 2,4-dinitrophenol, or cytochalasin D with uptake hypothesized to occur by adsorptive-type endocytosis.

Regarding the physical and chemical state of internalized NMs, many questions still remain based on the properties of the living cellular environment (e.g. variations in pH, corrosive ability). In these studies it

appeared that the AgDisp nanoparticles were more agglomerated inside the intracellular vacuoles, but this may be due to the extensive sample preparation or cellular degradation of the polysaccharide. Using separation techniques to isolate fractions of the cell for further analysis may provide additional insight into both the localization of nanoparticles to certain organelles as well as possible physical and chemical changes. Additionally, the impact of the metal catalyst on carbon nanotube biocompatibility or toxicity should be further examined to determine the mechanism of action. It is possible that soluble metal species are released into the cellular environment, nano-scale corrosion is occurring, or electrochemical signals are being produced. These in-depth studies are expected to greatly contribute to a variety of studies involving physiological solutions and systems.

7.4 Quantifying NM Internalization with Spectroscopic Techniques

Although visualizing the internalization and localization of both carbon and silver NMs inside the cells was demonstrated in this research with various forms of microscopy, quantifying the kinetics of accumulation over time remains a challenge to this research due to factors such as NM size, agglomeration state in solution, and diffusional or gravitational effects. The main challenge with quantifying the uptake of carbon nanomaterials resides in the fact that cells are also primarily composed of carbon and there is not currently an effective method to isolate, characterize, and quantify these different forms of carbon. Another variable that deserves careful consideration is the choice of cell type. In these studies, measures were taken to obtain an adequate signal and avoid interference from detached cells or media components. Therefore, macrophages, which are known to rapidly ingest large quantities of debris and NMs compared to neuroblastoma cells or skin cells, were used to examine the accumulation of Ag nanoparticles over time with UV-visible (UV-Vis) spectroscopy and atomic absorption spectroscopy (AAS).

UV-Visible Spectroscopy to Quantify Metal Nanoparticle Uptake

One study examined the use of UV-Vis in addition to TEM for the uptake of 18nm Au nanoparticles in human leukemia cells demonstrating rapid internalization over a 1 hour period (Connor et al., 2005). However, the ability of UV-Vis to detect very small mass per volume changes is limited and also dependent upon the dispersion quality of the NMs. In our studies, a

microplate reader for UV-Vis measurements made it possible to examine small volumes of solution incubated with or without cells. First, known concentrations of Ag26Disp nanoparticles in physiologically relevant solutions (water and PBS) were measured for absorbance values at the characteristics peak for Ag at ~390nm. The signal obtained from low concentrations of Ag26Disp (5-25 $\mu\text{g/ml}$) was not distinguishable from the water or PBS solutions and concentrations greater than 250 $\mu\text{g/ml}$ were required to more than double the signal from 0.039 to 0.098 (Fig 7.4.1). However, these high concentrations are not suitable for further uptake studies because they are toxic to the cells.

Further examination of Ag nanoparticle UV-Vis characteristics in cell culture media demonstrated increased agglomeration in addition to background signals from the media, itself (e.g. pH indicators if present), which effectively blocked the Ag signal up to concentrations of 500 $\mu\text{g/ml}$. Although higher concentrations were not measured to determine if a signal could be obtained, these higher concentrations would likely be toxic to the cells and of little practical application. Therefore, future studies with solutions of Ag or other plasmon resonant metal nanoparticles should be well dispersed in an appropriate physiological solution that does not significantly contribute to the background signal in UV-Vis or reduce cell viability.

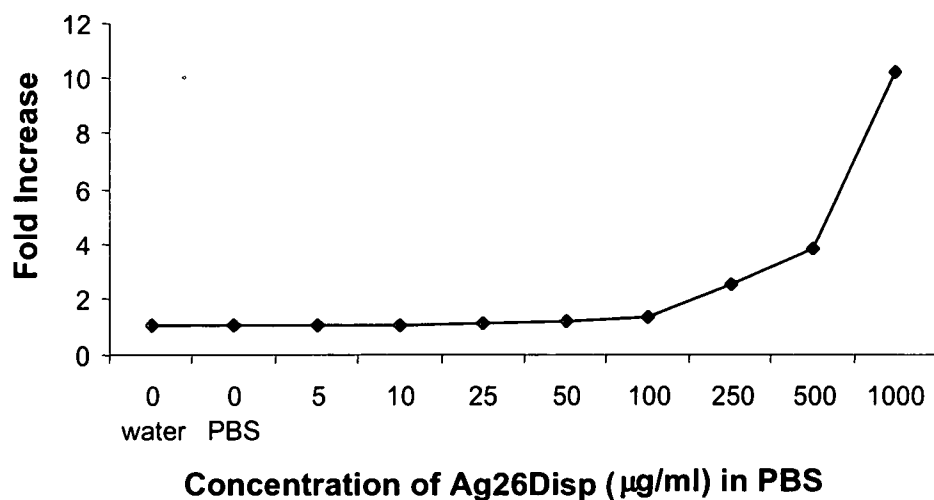


Figure 7.4.1. Summary of UV-Vis spectroscopy of Ag26Disp in PBS. Notice that there is an increase in absorbance at relatively high nanoparticle concentrations.

Furthermore, the effects of gravitational settling, floating cells, centrifugation, and temperature were considered for obtaining a successful Ag UV-Vis signature. After 24h of incubation, Ag nanoparticles in PBS were found to adhere to the bottom of cell culture plates and were not easily dislodged. This suggests that when aliquots are taken of the nanoparticle solution that some nanoparticles will not be accounted for thereby skewing the concentration remaining "in solution" and not internalized by the cells. The influence of floating cells increased the absorbance compared to solutions without cells. However, a simple technique such as centrifugation at 1000 rpm to preferentially spin out the larger, heavier cells while keeping well suspended nanoparticles in solution was not successful as both the cells and nanoparticles were spun out. This is likely due to the larger sized agglomerates of nanoparticles present in solution after 24h of incubation at

37°C. Further proof for the temperature-dependent change in dispersion was found when aliquots taken from plates containing both 250 µg/ml and 500 µg/ml solutions of Ag26Disp nanoparticles in PBS had greater absorbances after 24h of incubation at 4°C compared to decreased absorbances after incubation at 37°C with no change in PBS alone at either temperature.

Atomic Absorption Spectroscopy (AAS) to Quantify Metal Nanoparticle Uptake

One study demonstrated the uptake of cerium oxide into human lung fibroblasts with inductively coupled plasma mass spectroscopy and the amount of internalization of the nanoparticles found to be dependent on their size while number density or surface area were of less effect (Limbach et al., 2005). This study suggested that the rapid formation of nanoparticle aggregates occurs greatly in small particles due to a high number density while larger nanoparticles stay primarily unagglomerated. They also suggest that diffusion limits the uptake of smaller particles while sedimentation limits the transport of the nanoparticles into the cells.

In these studies, in order to comparatively estimate the amount of Ag nanoparticles internalized by macrophages, time points from 2-24h were examined with atomic absorption spectroscopy (AAS). An average uptake of 1.27 µg Ag/10⁵ cells for three separate experiments was obtained after dosing with 25 µg/ml Ag28 nanoparticles for 24h. In this case, the cells internalized approximately 8.5% of the originally applied Ag dose. However, experiments

at shorter time points (0min-2.5h) showed little change in the amount of ~ 0.5 $\mu\text{g Ag}/10^5$ cells.

Effect of Gravity on Internalization and Toxicity

One caveat to examining the internalization of agglomerated NMs into cells is the effect of gravitational settling, which can not only have a major impact on cell viability over 24h, but may arbitrarily cause some large nanoparticle agglomerates to settle onto the bottom of the cell culture dishes skewing the amount of NMs associated with the cells. To demonstrate these effects, macrophages were incubated with Ag nanoparticles either in an upright position, which shows nanoparticle settling (Fig 7.4.2A) or in an inverted or upside down (UD) position where very few Ag nanoparticles are found associated with the cells (Fig 7.4.2B). The presence of large amounts of Ag nanoparticles changes the cell morphology to more irregular compared to rounded, which was also evidenced by less MTT reduction (decreased purple color) and reduced viability. However, there was some reduction in viability after simply sealing and inverting the chambered slides.

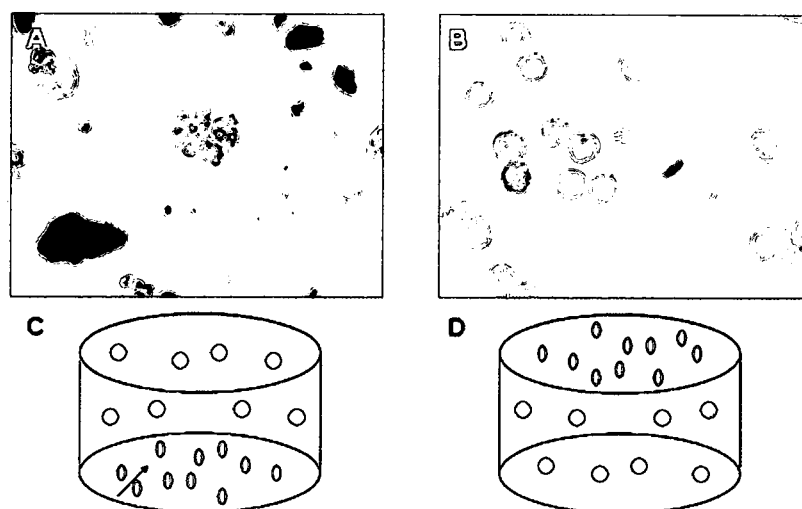


Figure 7.4.2. The effect of gravitational settling on cell-NM contact. The interaction of 25 $\mu\text{g/ml}$ concentrations of Ag28 in macrophages was increased due to gravitational settling after 24h compared to inverted set-ups. (A,C) Cells incubated upright showing settling of large Ag agglomerates and (B,D) Cells incubated upside-down showing very few Ag agglomerates. Lower schematics demonstrate how the cell chambers were set-up corresponding to the above images. Images were taken with phase contrast light microscopy at 32x magnification.

Suggestions for future research to better quantify the amount of NMs internalized by cells include developing NMs with optimal dispersion in cell culture media that do not agglomerate and settle due to chemical or gravitational constraints. Additionally, the development of techniques to effectively separate the suspended, membrane-bound, and internalized NMs by differential centrifugation or special washing procedures with chemicals such as sodium azide (Maselli et al., 2002) could aid in quantifying the relative amounts of NMs associated with cells.

7.5 Discussion

Many studies are beginning to evaluate the biocompatibility or toxicity of engineered NMs with *in vitro* systems. However, it is important to perform further systematic studies to better understand the critical NM properties (e.g. charge, surface chemistry, size) and cellular environment factors (e.g. temperature, pH) involved in NM attraction, binding, internalization, localization, accumulation, and the resultant physico-chemical that occur within different cell types. The optimization of sample preparation techniques to retain the most natural and accurate representation of cell-NM interactions for microscopic, spectroscopic, and other relevant analysis methods will continue to be a major portion of this research.

A comparison of three different electron microscopy imaging techniques revealed that traditional TEM sample preparation was more useful than wet imaging in SEM of non-metal nanomaterials due to issues with generating substantial atomic contrast in backscattering mode compared to metal nanoparticles. However, STEM had the advantage of observing the internal features of the cells with greater contrast at lower electron voltage of 5 kV than both the wet imaging technique (30 kV in Quantomix capsules) or traditional TEM (80-200 kV in for TEM). Both STEM and TEM demonstrated better localization of Ag nanoparticles inside the cells compared to the wet imaging capsules. However, the sample preparation is more time consuming and requires embedding and thin sectioning of the cells before imaging is

performed. Additionally, distinguishing individual nanomaterials amongst the background cellular features, which can be similar in size and contrast (e.g. granules), can be difficult. For example, if individual nanoparticles existed inside the cell, they could bind to certain proteins or organelles and effectively hide from view. Otherwise, if they translocated through the nuclear pores (<9nm) into the nucleus, they could bind between the double helix lattices of DNA.

Elucidation of the mechanisms responsible for NM internalization, localization, and possible degradation are also very important in order to effectively engineer NMs for practical use in biological systems. Currently, the entrapment of most nanoparticles in endosomes, and then association with lysosomes, exposes the NMs to a confined, low pH environment where many nanoparticles can lose their desirable properties or be prevented from targeting specific cellular components. Therefore, altering the cellular transport mechanisms either through changes in the NM properties or the cell culture environment (e.g. temperature, chemical additives) can lead to the development novel NM applications such as diagnostic tools or targeted delivery systems.

Spectroscopic methods provide complementary information to microscopic observations of NM internalization by cells. Two techniques (UV-Vis and AAS) were compared for their suitability in quantitatively estimating

nanoparticle accumulation over time. The major limitation of the UV-Vis studies was the stability of the Ag nanoparticles. Although small volumes could be read in a microplate reader (100-200 μ L), the low concentrations (<100 μ g/ml) required for biocompatibility studies were not readily distinguished from the background signal. Additionally, suspension in media completely disrupted the plasmon peak likely due to agglomeration of the nanoparticles. Other issues that confounded the results included: gravitational settling, which reduced the absorbance when aliquots were removed from the plates, increases in absorbance due to floating cells, removal of both cells and nanoparticles after centrifugation, and larger sized agglomerates after incubation at 37°C compared to storage at 4°C. Although further tagging of the nanomaterials with fluorescent labels to follow their internalization and localization appears as to be an attractive alternative, the fluorescent signal of T-NDs was also indistinguishable from the background autofluorescence of cell culture media until concentrations greater than 500 μ g/ml. In comparison, AAS studies were more promising demonstrating an increase in cell-associated Ag after 24h, but could be improved through better nanoparticle dispersion and separation from the cells.

In conclusion, the invaluable expertise of a multidisciplinary team will be required to develop new techniques and interpret the ultimate effect of NMs on human health and in future therapeutic applications.

REFERENCES

- Alberts B, Johnson A, Lewis J, Raff M, Bray D, Hopkin K, Roberts K, Walter P (2004) *Essential Cell Biology*, 2nd Edition (in English), New York, NY: Garland Science; <http://en.wikipedia.org/wiki/Endosomes>.
- Allison AC, Harington JS, Birbeck M (1966) An examination of the cytotoxic effects of silica on macrophages. *J Exp Med* 124: 141-154.
- Alt V, Bechert T, Steinrucker P, Wagener M, Seidel P, Dingeldein E, Domann E, Schnettler R (2004) An in vitro assessment of the antibacterial properties and cytotoxicity of nanoparticulate silver bone cement. *Biomaterials* 25: 4383-4391.
- Bakowicz-Mitura K, Bartosz G, Mitura S (2007) Influence of Diamond Powder Particles on Human Gene Expression. *Surface & Coatings Technology* 201: 6131-6135.
- Balogh L, Swanson DR, Tomalia DA, Hagnauer GL, McManus AT (2001) Dendrimer-Silver Complexes and Nanocomposites as Antimicrobial Agents. *Nano Letters* 1:1:18-21.
- Barile FA Introduction to In Vitro Cytotoxicology: Mechanisms and Methods, First Edition, CRC Press, Boca Raton, 1994.
- Barratt MD (1996) Quantitative structure-activity relationships (QSARs) for skin corrosivity of organic acids, bases and phenols: principal components and neural network analysis of extended datasets. *Toxicology in Vitro* 10: 85-94.
- Beck-Speier I, Dayal N, Karg E, Maier KL, Schumann G, Schulz H, Semmler M, Takenaka S, Stettmaier K, Bors W, Ghio A, Samet JM, Heyder J (2005) Oxidative Stress and Lipid Mediators Induced in Alveolar Macrophages by Ultrafine Particles. *Free Radical Biology & Medicine* 38: 1080-1092.
- Bellamy LJ. The Infrared Spectra of Complex Molecules. Chapman and Hall, London, 1975.
- Bene L, Szentesi G, Matyus L, Gaspar R, Damjanovich S (2005) Nanoparticle energy transfer on the cell surface. *J. Mol. Recognit.* 3: 236-253.

Benigni R, Andreoli C, Giuliani A (1994) QSAR Models for Both Mutagenic Potency and Activity: Application to Nitroarenes and Aromatic Amines. *Environmental and Molecular Mutagenesis* 24: 208-219.

Benson J, Pre-Survey on Biomedical Applications of Carbon, North American Rockwell Corp. (1969).

Bergamaschi E, Bussolati O, Magrini A, Bottini M, Migliore L, Bellucci S, Iavicoli I, Bergamaschi A (2006). Nanomaterials and lung toxicity: interactions with airways cells and relevance for occupational health risk assessment. *Int.J.Immunopathol.Pharmacol.* 19: 3-10.

Berry CC, Wells S, Charles S, Curtis ASG (2003) Dextran and Albumin Derivatised Iron Oxide Nanoparticles: Influence on Fibroblasts In Vitro. *Biomaterials* 24: 4551-4557.

Berry CC, Wells S, Charles S, Aitchison G, Curtis ASG (2004) Cell Response to Dextran-derivatised Iron Oxide Nanoparticles Post Internalization. *Biomaterials* 25: 5405-5413.

Bianco A, Hoebeke J, Godefroy S, Chaloin O, Pantarotto D, Briand J-P, Muller S, Prato M, Partidos CD (2004) Cationic Carbon Nanotubes Bind to CpG Oligodeoxynucleotides and Enhance Their Immunostimulatory Properties. *J. Am. Chem. Soc.* 127: 58-59.

Bianco A, Kostarelos K, Partidos C, Prato M (2005) Biomedical Applications of Functionalised Carbon Nanotubes. *Chem. Comm* 571-577.

Bondar V and Puzyr A (2004) Nanodiamonds for Biological Applications. *Physics of the Solid State* 46:4: 716-719.

Borm PJA, Robbins D, Haubold S, Kuhlbusch T, Fissan H, Donaldson K, Schins R, Stone V, Kreyling W, Lademann J, Krutmann J, Warheit D, Oberdorster E (2006) The Potential Risks of Nanomaterials: A Review Carried Out for ECETOC. *Particle and Fibre Toxicology* 3:11:1-35.

Bottini M, Bruckner S, Nika K, Bottini N, Bellucci S, Magrini A, Bergamaschi A, Mustelin T (2006) Multi-walled Carbon nanotubes induce T lymphocyte apoptosis. *Toxicology Letters* 160 (2) 121-126.

Braydich-Stolle L, Hussain S, Schlager J.J., and Claude-Hofmann M (2005) In Vitro Cytotoxicity of Nanoparticles in Mammalian Germline Stem Cells. *Toxicological Sciences* 1-8.

Brown DM, Stone V, Findlay P, MacNee W, Donaldson K (2000). Increased inflammation and intracellular calcium caused by ultrafine carbon black is independent of transition metals or other soluble components. *Occup. Environ. Med.* 57: 685-691

Brown DM, Wilson MR, MacNee W, Stone, V, Donaldson K (2001) Size-dependent proinflammatory effects of ultrafine polystyrene particles: A role for surface area and oxidative stress in the enhanced activity of ultrafines. *Toxicol. Appl. Pharmacol.* 191-199.

Burns A, Ow H, Wiesner U (2006) Fluorescent Core-shell Silica Nanoparticles: Towards "Lab on a Particle" Architectures for Nanobiotechnology. *Chemical Society Reviews* 35: 1028-1042.

Cao L, Wang X, Meziani MJ, Lu F, Wang H, Luo PG, Lin Y, Harruff BA, Veca LM, Murray D, Xie SY, Sun YP (2007) Carbon Dots for Multiphoton Bioimaging. *JACS*.

Carbon Black User's Guide, International Carbon Black Association, 2004

Carmichael J, DeGraff WD, Gazdar AF, Minna JB, Mitchell JB (1987) Evaluation of a tetrazolium-based semiautomated colorimetric assay: Assessment of chemosensitivity testing. *Cancer Research* 47: 936-942.

Casarett, LJ, Doull, J, Klaassen CD (2001) Casarett and Doull's toxicology : The basic science of poisons. New York: McGraw-Hill Medical Pub. Division.

Chen C, Xing G, Wang J, Zhao Y, Li B, Tang J, Jian G, Wang T, Sun J, Xing L, Yuan H, Gao Y, Meng H, Chen Z, Zhao F, Chai Z, Fang X (2005) Multihydroxylated [Gd@C82(OH)22]n Nanoparticles: Antineoplastic Activity of High Efficiency and Low Toxicity. *Nano Letters* 5: 10: 2050-2057.

Chenevier P, Veyret B, Roux D, Henry-Toulme N (2000) Interaction of Cationic Colloids at the Surface of J774 Cells: A Kinetic Analysis. *Biophysical Journal* 79: 1298-1309.

Cheng CY, Perevedentseva E, Tu JS, Chung PH, Cheng CL, Liu KK, Chao JI, Chen PH, Chang CC (2007) Direct and In Vitro Observation of Growth Hormone Receptor Molecules in A549 Human Lung Epithelial Cells by Nanodiamond Labeling. *Applied Physics Letters* 90: 163903.

Cheung HS, Story MT, McCarty DJ (1984) Mitogenic effects of hydroxyapatite and calcium pyrophosphate dihydrate crystals on cultured mammalian cells. *Arthritis Rheum* 27: 668-674.

Chien, CT, Lin, WH, Yu, SL, Chou, CC, Chen, JJ, Yang, PC (2006) Titanium dioxide nanoparticles induce emphysema-like lung injury in mice. *FASEB J.* 20: 2393-2395.

Chithrani BD, Ghazani AA, Chan WCW (2006) Determining the Size and Shape Dependence of Gold Nanoparticle Uptake into Mammalian Cells. *Nano Letters* 6: 4: 662-668.

Chlopek, J, Czajkowska B, Szaraniec B, Frackowiak E, Szostak K Beguin F (2006) In Vitro Studies of Carbon Nanotubes Biocompatibility. *Carbon* 44:106-1111.

Chou W-L, Yu D-G, Yang M-C (2005) The Preparation and Characterization of Silver-loading Cellulose Acetate Hollow Fiber Membrane for Water Treatment. *Polymers for Advanced Technologies* 16: 600-607.

Clemedson C, Barile F, Chesne C, Cottin M, Curren R, Exkwall B, Ferro M, Gomez-Lechon M, Imai K, Janus J, Kemp R, Kerszman G, Kjellstrand P, Lavrijsen K, Logemann P, McFarlane-Abdulla E, Roguet R, Segner H, Thusvander A, Walum E, Ekwall, B (2000) MEIC Evaluation of Acute Systemic Toxicity. Part VII. Prediction of Human Toxicity By Results from Testing of the First 30 Reference Chemicals with 27 Further In Vitro Assays. *ATLA* 28: 159-200.

Coates J. Interpretation of Infrared Spectra, A Practical Approach in Encyclopedia of Analytical Chemistry R.A. Meyers (Ed.) pp. 10815-10837, John Wiley & Sons Ltd, Chichester, 2000.

Connor EE, Mwamuka J, Gole A, Murphy CJ, Wyatt MD (2005) Gold Nanoparticles Are Taken Up by Human Cells but Do Not Cause Acute Cytotoxicity. *Small* 1:3: 325-327.

Cool DR, Fenger M, Snell CR, Loh YP (1995) Identification of the sorting signal motif within pro-opiomelanocortin for the regulated secretory pathway. *J. Biol. Chem.* 270: 8723-8729.

Cool DR, Normant E, Shen F, Chen HC, Pannel L, Zhang Y, Loh YP (1997) Carboxypeptidase E is a regulated secretory pathway sorting receptor: genetic obliteration leads to endocrinological disorders in the Cpefat mouse. *Cell* 88:1-11.

Cronin MT and Basketter DA (1994) Multivariate analysis of a Skin Sensitization Database. *SAR and QSAR in Environmental Research* 2: 159-179.

Cui D, Tian F, Ozkan C, Wang M, Gao H (2005) Effect of Single Wall Carbon Nanotubes on Human HEK293 Cells. *Toxicology Letters* 155: 73-85.

Dai L, Ed.; Elsevier: Amsterdam, 2006, Carbon Nanotechnology: *Recent Developments in Chemistry, Physics, Materials Science and Device Applications*.

Davies G. Diamond, Adam Hilger Ltd., Bristol (1984).

Deguchi S, Alargove RG, Tsujii K (2001) Stable Dispersions of Fullerenes, C60 and C70 in Water. Preparation and Characterization. *Langmuir* 17: 6013-6017.

Dieter O. Hummel. Atlas of Polymer and Plastics Analysis, 2nd completely revised edition, Deerfield Beach, Fla.: Verlag Chemie International, 1982. v.1, Polymers, structures and spectra. v.2, Plastics, fibres, rubbers, resins; starting and auxiliary materials, degradation products. v.3, Additives and processing aids.

Ding L, Stilwell J, Zhang T, Elboudwrej O, Jiang H, Selegue J, Cooke P, Gray J, Chen F (2005) Molecular Characterization of the Cytotoxic Mechanism of Multi-wall Carbon Nanotubes and Nano-onions on Human Skin Fibroblast *Nano Lett.* 5: 12: 2448-2464.

Dion I, Roques X, Baquey C, Baudet E, Basse Cathalinat B, More N (1993) Hemocompatibility of diamond-like carbon coating. *Biomed Mater Eng* 3: 51-55.

Doherty M, Whicher JT, Dieppe PA (1983) Activation of the alternative pathway of complement by monosodium urate monohydrate crystals and other inflammatory particles. *Ann Rheum Dis* 42: 285-291.

Dolmatov VY (2001) Detonation Synthesis Ultradispersed Diamonds: Properties and Applications. *Russian Chemical Reviews* 70: 607-626.

Donaldson K, Li XY, MacNee W. (1998) Ultrafine (nanometer) particle mediated lung injury. *J. Aerosol. Sci.* 29: 553-560.

Donaldson K and Tran CL (2002) Inflammation caused by particles and fibers. *Inhalation Toxicology* 14: 5-27.

Drake PL and Hazelwood KJ (2005) Exposure-related health effects of silver and silver compounds: a review. *Ann. Occup. Hyg.* :7 575-585.

Dumortier H, Lacotte S, Pastorin G, Marega R, Wu W, Bonifazi D, Brian J.-P., Prato M, Muller S, Bianco A (2006) Functionalized Carbon Nanotubes are Non-toxic and preserve the Functionality of primary immune Cells. *NanoLett* 6: 7: 1522-1528.

Eisenbrand G, Pool-Zobel B, Baker V, Balls M, Blaauboer B, Boobis A, Carere A, Kevekordes S, Lhuguenot J-C, Pieters R, Kleiner J (2002) Methods of In Vitro Toxicology. *Food and Chemical Toxicology* 40: 193-226.

Elechiguerra J, Burt J, Morones J, Camacho-Bragado A, Gao X, Lara H, Yacaman M (2005) Interaction of silver nanoparticles with HIV-1. *Journal of Nanobiotechnology* 3:6: 1-14.

Farber JL, Kyle ME, Coleman JB (1990) Mechanisms of cell injury by activated oxygen species. *J Lab Invest* 62: 670-679.

Ferin J, Oberdorster G, Penney DP (1992) Pulmonary retention of ultrafine and fine particles in rats. *Am. J. Respir. Cell. Mol. Biol.* 6: 535-542.

Fiorito S, Serafino A, Andreola F, Bernier P (2006) Effects of Fullerenes and Single-wall Carbon Nanotubes on Murine and Human Macrophages. *Carbon* 44: 1100-1105.

Flauhaut E, Durrieu M, Remy-Zolghadri M, Bareille R, Baquey C (2006) Investigation of the cytotoxicity of CCVD carbon nanotubes towards human umbilical vein endothelial cells. *Carbon* 44: 1093-1099.

Foley S, Crowley C, Smaih M, Bonfils C, Elanger B, Seta P, Larroque C (2002) Cellular Localisation of a Water-soluble Fullerene Derivative. *Biochemical and Biophysical Research Communications* 294: 116-119.

Foster B (2004) Focus on microscopy: A technique for imaging live cell interactions and mechanisms. *American Laboratory* 11: 21-27.

Freitas RA, Jr, Nanomedicine Volume IIA: Biocompatibility, Landes Bioscience, Georgetown, TX, (2003).

Fu CC, Lee HY, Chen K, Lim TS, Wu HY, Lin PK, Wei PK, Tsao PH, Chang HC, Fann W (2007) Characterization and Application of Single Fluorescent Nanodiamonds as Cellular Biomarkers. *PNAS* 104:3:727-732.

Garibaldi S, Brunelli C, Bavastrello V, Ghigliotti G, Nicolini C (2006) Carbon nanotube biocompatibility with cardiac muscle cells. *Nanotechnology* 17: 391-397.

Georgakilas V, Tagmatarchis N, Pantarotto D, Bianco A, Briand J-P, Prato M. (2003) Amino Acid Functionalisation of Water Soluble Carbon Nanotubes. *Chemical Communications* 24: 3050-3051.

Ghosh SK, Alargova RG, Deguchi S, Tsujii K (2006) Dispersion Stability of Colloids in Sub- and Supercritical Water. *J. Phys. Chem B* 110: 25901-25907.

Goia DV (2004) Preparation and Formation Mechanism of Uniform Metallic Particles in Homogenous Solutions. *J. Mater. Chem* 14: 1-9.

Greiner N, Phillips D, Johnson J, Volk F (1988) *Nature* 333: 6172: 440-442.

Grichko V, Grishko V, Shenderova O (2006) Nanodiamond Bullets and Their Biological Targets. *NanoBiotechnology* 2:1:1.

Gupta AK and Curtis ASG (2004) Lactoferrin and Ceruloplasmin Derivatized Superparamagnetic Iron Oxide Nanoparticles for Targeting Cell Surface Receptors. *Biomaterials* 25: 3029-3040.

Gupta AK and Gupta M. (2005) Synthesis and Surface Engineering of Iron Oxide Nanoparticles for Biomedical Applications. *Biomaterials* 26: 3995-4021.

Halliwell B, Gutteridge J, Cross C J (1992) Free Radicals, Antioxidants and Human Disease: Where Are We Now? *J Lab Clin Med* 119: 598-620.

Haubold A, Carbon in Prosthetics, 283: 383-395 (1977).

Heath JC, Freeman MAR, Swanson SAV, Carcinogenic properties of wear particles from prostheses made in cobalt-chromium alloy, *Lancet*, 564-566 (1971).

Hedenborg M, Klockars M (1989) Quartz dust-induced production of reactive oxygen metabolites by human granulocytes. *Lung* 167: 23-32.

Higson FK, Jones OT (1984) Oxygen radical production by horse and pig neutrophils induced by a range of crystals. *J Rheumatol* 11: 735-740.

Hoet P, Bruske-Hohlfeld I, Salata O (2004) Nanoparticles: known and unknown health risks. *Journal of Nanobiotechnology* 2:12.

Hohr D, Steinfartz Y, Schins RP, Knaapen AM, Martra G, Fubini B, Borm PJ (2002) The surface area rather than the surface coating determines the acute inflammatory response after instillation of fine and ultrafine TiO₂ in the rat *Int. J. Hyg. Environ. Health* 205:239-244.

Hoshino A, Kujioka F, Oku T, Suga M, Sasaki YF, Ohta T, Yasuhara M, Suzuki K, Yamamoto K (2004) Physicochemical Properties and Cellular Toxicity of Nanocrystal Quantum Dots Depend on Their Surface Modification. *Nano Letters* 4: 11: 2163-2169.

<http://cellbio.utmb.edu/cellbio/lysosome.htm>

<http://en.wikipedia.org/wiki/Organelle>

<http://en.wikipedia.org/wiki/Phagocytosis>

http://en.wikipedia.org/wiki/UV-visible_spectroscopy

<http://micro.magnet.fsu.edu/cells/lysosomes/lysomes.html>

<http://pathology.emory.edu/images>

<http://serc.carleton.edu/images/usingdata/nasaimages/periodic-table.gif>

<http://students.chem.tue.nl/ifp03/synthesis.html>

<http://www.cabot-corp.com>

<http://www.drugdeliverytech.com/cgi-bin/articles.cgi?idArticle=33>

<http://www.gmu.edu/departments/SRIF/tutorial/aas/aas3.htm>

http://www.icp-oes.net/detection_limits.htm

<http://www.icp-oes.net/Instruments.html>

<http://www.nano.gov/html/facts/appsprod.html>

<http://www.nano.gov/html/facts/whatIsNano.html>

<http://www.nanoscale.com>

<http://www.nanotek.org.uk>

<http://www.sciencenewsforkids.org/articles/20030820/refs.asp>

<http://www.scottcamazine.com/photos/AIDS>

<http://www.smalltimes.com>

<http://www.theorator.com/bills108/s189.html>

<http://www.unl.edu/CMRAcfem/em.htm>

<http://www.unl.edu/CMRAcfem/interact.htm>

Hu H, Ni Y, Montana V, Haddon RC, Parpura V (2004) Chemically Functionalized Carbon Nanotubes as Substrates for Neuronal Growth. *Nano Letters*, 4 (3): 507-511.

Hu H, Ni Y, Mandal SK, Montana V, Zhao B, Haddon RC, Parpura V (2005) Polyethyleneimine Functionalized Single-walled Carbon Nanotubes as a Substrated for Neuronal Growth. *J. Phys. Chem. B*, 109: 4285-4289.

Huang S and Dai L (2002) Plasma Etching for Purification and Controlled Opening of Aligned Carbon Nanotubes. *Journal of Physical Chemistry B* 106: 3543-3545.

Huang LCL, Chang H (2004a) Adsorption and Immobilization of Cytochrome c on Nanodiamonds. *Langmuir* 20: 5879-5884.

Huang TS, Tzeng Y, Liu Y, Chen Y, Walker K, Guntupalli R, Liu C (2004b) Immobilization of Antibodies and Bacterial Binding on Nanodiamond and Carbon Nanotubes for Biosensor Applications. *Diamond and Rel Mat* 13: 1098-1102.

Hurt RH, Monthieux M, Kane A (2006) Toxicology of Carbon Nanomaterials: Status, Trends, and Perspectives on the Special Issue. *Carbon* 44, 1028-1033.

Hussain S, Meneghini E, Moosmayer M, Lacotte D, Anner BM (1994) Potent and reversible interaction of silver with pure Na,K ATPase and Na,K ATPase liposomes. *Biochim. Biophys. Acta* 1190: 402-408.

Hussain SM and Frazier JM (2002) Cellular toxicity of hydrazine in primary hepatocytes. *Toxicological Sciences* 69: 424-432.

Hussain SM, Hess KL, Gearhart JM, Geiss KT, Schlager JJ (2005) In Vitro Toxicity of Nanoparticles in BRL-3A Rat Liver Cells. *Toxicology In Vitro* 19: 975-983.

Hussain S; Javorina A, Schrand A, Duhart H, Ali S, Schlager J (2006) The Interaction of Manganese Nanotubes with PC-12 Cells Induces Dopamine Depletion. *J. Tox. Sci.* 92(2): 456-463.

Jendelova P, Herynek V, Urdzikova L, Glogarova K, Kroupova J, Bryja V., Andersson B, Burian M., Hajek M, Sykova E (2004) Magnetic Resonance Tracking of Transplanted bone marrow and embryonic stem cells labeled by iron oxide nanoparticles in rat brain and spinal cord. *J Neurosci Res* 76: 232-243.

Jeong SH, Hwang YH, Yi SC (2005) Antibacterial Properties of Padded PP/PE Nonwovens Incorporating Nano-sized Silver Colloids. *Journal of Materials Science* 40: 5413-5418.

Jia G, Wang H, Yan L, Wang X, Pei R, Yan T, Zhao Y, Guo, X (2005) Cytotoxicity of Carbon Nanomaterials: Single-wall Nanotube, Multi-wall Nanotube, and Fullerene. *Environmental Science and Technology* 39:5:1378-1383.

Jia N, Lian Q, Shen H, Wang C, Li X, Yang Z (2007) Intracellular Delivery of Quantum Dots Tagged Antisense Oligodeoxynucleotides by Functionalized Multiwalled Carbon Nanotubes. *NanoLetters*.

Johnston CJ, Finkelstein JN, Mercer P, Corson N, Gelein R, Oberdorster G (2000) Pulmonary effects induced by ultrafine PTFE particles. *Toxicol. Appl. Pharmacol.* 168: 208-215.

Jordan A, Scholz R, Wust P, Schirra H, Schiestel T, Schmidt H, Felix R (1999) Endocytosis of Detran and Silan-coated Magnetite Nanoparticles and the Effect of Intracellular Hyperthermia on Human Mammary Carcinoma Cells In Vitro. *Journal of Magnetism and Magnetic Materials* 194: 185-196.

Kagan VE, Tyurina YY, Tyurin VA, Konduru NV, Potapovich AI, Osipov AN, Kisin ER, Schwegler-Berry D, Mercer R, Castranova V, Shvedova AA (2006) Direct and Indirect Effects of Single Walled Carbon Nanotubes on RAW 264.7 Macrophages: Role of Iron. *Toxicology Letters* 165: 88-100.

Kam NWS, Jessop TC, Wender PA, Dai H (2004) Nanotube Molecular Transporters: Internalization of Carbon Nanotube-Protein Conjugates into Mammalian Cells. *Journal of the American Chemical Society* 126: 6850-6851.

Kam NWS, O'Connell M, Wisdom JA, Dai H (2005a) Carbon Nanotubes as Multifunctional Biological Transporters and Near-Infrared Agents for Selective Cancer Cell Destruction. *Proceedings of the National Academy of Sciences* 102 (33): 11600-11605.

Kam NWS, O'Connell M, Wisdom JA, Dai HJ (2005b) Carbon Nanotubes as Intracellular Protein Transporters: Generality and Biological Functionality. *Journal of the American Chemical Society* 127: (16): 6021-6026.

Kamysny A, Ben-Moshe M, Aviezer S, Magdassi S (2005) Ink-Jet Printing of Metallic Nanoparticles and Microemulsions. *Macromolecular Rapid Communications* 4: 281-288.

Kano H and Kawata S (1996), Fine-pitch metallic grating for sensing liquid characteristics *Optics Letters* 21: 1848-1850.

Kedar NP (2003) Can we Prevent Parkinson's and Alzheimer's Disease? *J Postgrad Med* 49: 236-245.

Khabashesku V, Margrave J, Barrera E (2005) Functionalized Carbon Nanotubes and Nanodiamonds for Engineering and Biomedical Applications. *Diamond and Related Materials* 14: 859-866.

Kim JS, Yoon TJ, Yu KN, Kim BG, Park SJ, Kim HW, Lee KH, Park SB, Lee JK, Cho MH (2006) Toxicity and tissue distribution of magnetic nanoparticles in mice. *Toxicol.Sci.* 89: 338-347.

Kleinman MT, Sioutas C, Chang MC, Boere AJF, Cassee FR (2003) Ambient Fine and coarse particles suppression of alveolar macrophage functions *Toxicology Letters* 137: 151-158.

Kneipp K, Kneipp H, Itzkan I, Dasari R, Feld, MS (1999) Ultrasensitive Chemical Analysis by Raman Spectroscopy. *Chemical Reviews* 99: (10): 2957-2976.

Kneuer C, Sameti M, Bakowsky U, Schiestel T, Schirra H, Schmidt H, Lehr CM (2000) A Non-viral DNA Delivery System Based on Surface Modified Silica Nanoparticles Can Efficiently Transfect Cells In Vitro. *Bioconjugate Chemistry* 11: 926-932.

Kong XL, Huang LCL, Hsu CM, Chen WH, Han CC, Chang HC (2005) High Affinity Capture of Proteins by Diamond Nanoparticles for Mass Spectroscopic Analysis. *Anal. Chem.* 77: 259-265.

Krüger A, Kataoka F, Ozawa M, Fujino T, Suzuki Y, Aleksenskii AE, Vul A-Ya., Ōsawa E (2005) Unusually tight Aggregation in Detonation Nanodiamond: Identification and Disintegration. *Carbon* 43: 1722-1730.

Kumar S, Harrison N, Richards-Kortum R, Sokolov K (2007) Plasmonic Nanosensors for Imaging Intracellular Biomarkers in Live Cells. *Nano Letters* 7: 5: 1338-1343.

Lam CJ, McCluskey R, Hunter RL (2004) Pulmonary Toxicity of Single-Wall Carbon Nanotubes in Mice 7 and 90 Days After Intratracheal Instillation *Toxicological Sciences* 77: 1: 126-134.

Lamprecht B, Krenn JR, Leitner A, Aussenegg FR (1999) Resonant and Off-Resonant Light-Driven Plasmons in Metal Nanoparticles Studied by Femtosecond-Resolution Third-Harmonic Generation. *Physical Review Letters* 83: 21: 4421-4424.

Lee JH, Jun YW, Yeon SI, Shin JS, Cheon J (2006) Dual-mode nanoparticle probes for high-performance magnetic resonance and fluorescence imaging of neuroblastoma. *Angew Chem Int Ed* 45: 8160-8162.

Lesniak W, Bielinska AU, Sun K, Janczak KW, Shi X, Baker JR Jr., Balogh LP (2005) Silver/Dendrimer Nanocomposites as Biomarkers: Fabrication, Characterization, In Vitro Toxicity, and Intracellular Detection. *Nano Letters* 5:11:2123-2130.

Limbach LK, Li Y, Grass RN, Brunner TJ, Hintermann MA, Muller M, Gunther D, Stark W (2005) Oxide Nanoparticle Uptake in Human Lung Fibroblasts: Effects of Particle Size, Agglomeration, and Diffusion at Low Concentrations. *Environmental Science and Technology* 39: 9370-9376.

Lipscomb MF and Masten BJ (2002) Dendritic Cells: Immune Regulators in Health and Disease. *Physiol. Rev.* 82: 97-130.

Loft S, Poulsen H (1999) Markers of Oxidative Damage to DNA: Antioxidants and Molecular Damage. *Methods Enzymol* 300: 166-184.

Lu H, Yi G, Zhao S, chen D, Guo LH, Cheng J (2004) Synthesis and Characterization of Multi-functional Nanoparticles possessing magnetic, up-conversion fluorescence, and bio-affinity properties. *Journal of Materials Chemistry* 14: 1336-1341.

Lu CW, Hung Y, Hsiao JK, Yao M, chung TH, Lin YS, Wu SH, Hsu SC, Liu HM, Mou CY, Yang CS, Huang DM, Chen YC (2007) Bifunctional Magnetic Silica Nanoparticles for Highly Efficient Human Stem Cell Labeling. *NanoLetters* 7:1: 149-154.

Luhr HG (1958) Comparative studies on phagocytosis of coal powders of various carbonification grades, also of quartz and diamond powders in tissue cultures. *Arch Gewerbepath* 16: 355-374.

Magdassi S, Bassa A, Vinetsky Y, Kamyshny A (2003) Silver Nanoparticles as Pigments for Water-based Ink-Jet Inks. *Chemistry of Materials* 11: 2208-2217.

Magrez A, Kasas S, Salicio V, Pasquier N, Seo J, Celio M, Catsicas, S, Schwaller B, Forro L (2006) Cellular Toxicity of Carbon-Based Nanomaterials. *Nano Letters* 6:6: 1121-1125.

Malvern Instruments ZetaSizer NanoSizer, Instruction Manual, Man0317 Issue 2.2, (2005).

Manna S, Sarkar S, Barr J, Wise K, Barrera E, Jejelowo O, Rice-Ficht A, Ramesh G (2005) Single-walled Carbon Nanotube Induces Oxidative Stress and Activates Nuclear Transcription Factor- κ B in Human Keratinocytes. *Nano Letters* 5:9: 1676-1684.

Maselli A, Laevsky G, Knecht DA (2002) Kinetics of Binding, Uptake, and Degradation of Live Fluorescent (DsRed) Bacteria by *Dictyostelium discoideum*. *Microbiology* 148: 413-420.

Mattson M, Haddon R, Rao A (2000) Molecular Functionalization of Carbon Nanotubes and Use as Substrates for Neuronal Growth. *Journal of Molecular Neuroscience* 14: 175-182.

Maxwell H. The Poisoner's Handbook, Loompanics Unlimited, Port Townsend, WA, 1988.

Maynard A, Baron P, Foley M, Shvedova A, Kisin E, Castronova V (2004) Exposure to Carbon Nanotube Material: Aerosol Release During the Handling of Unrefined Single-walled Carbon Nanotube Material. *Journal of Toxicology and Environmental Health* 67: 87-107.24

Monteiro-Riviere N, Nemanich R, Inman A, Wang Y, Riviere J (2005) Multi-walled Carbon Nanotube Interactions with Human Epidermal Keratinocytes. *Toxicology Letters* 155: 377-384.

Monteiro-Riviere N and Inman A (2006) Challenges for Assessing Carbon Nanomaterial Toxicity to the Skin. *Carbon* 44: 1070-1078.

Morones JR, Elechiguerra JL, Camacho A, Holt K, Kouri JB, Ramirez JT, Yacaman MJ. (2005) The bactericidal effect of silver nanoparticles. *Nanotechnology* 16: 2346-2353.

Muller M, Mackeben S, Muller-Goymann CC (2004) Physicochemical characterisation of liposomes with encapsulated local anaesthetics. *Int. J. Pharm.* 1-2: 139-148.

Murdock RC, Braydich-Stolle L, Schrand AM, Schlager JJ, and Hussain SM (2007) Characterization of Nanomaterial Dispersion in Solution Prior to In Vitro Exposure Using Dynamic Light Scattering Technique *Toxicological Sciences Online* September 13.

Murr L, Garza K, Soto K, Carrasco A, Powell T, Ramirez D, Guerrero P, Lopez D, Venzor III J (2005) Cytotoxicity Assessment of Some Carbon Nanotubes and Related Carbon Nanoparticle Aggregates and the Implications for Anthropogenic Carbon Nanotube Aggregates in the Environment. *Int. J. Environ. Res. Public Health* 2:1, 31-42.

Murray PT. Course Notes, MAT 601- Surface Chemistry of Solids, University of Dayton, Dayton, OH, 2004.

Nel A, Xia T, Madler L, Li N (2006) Toxic Potential of Materials at the Nanolevel. *Science* 311: 622-627.

Nordsletten L, Hogasen AK, Konttinen YT, Santavirta S, Aspenberg P, Aasen AO (1996) Human monocytes stimulation by particles of hydroxyapatite, silicon carbide and diamond: in vitro studies of new prosthesis coatings. *Biomaterials* 17: 1521-1527.

Oberdorster G, Ferin J, Gelein R, Soderholm SC, Finkelstein J (1992) Role of the alveolar macrophage in lung injury-studies with ultrafine particles. *Environ. Health Perspect.* 97: 193-199.

Oberdorster G. Toxicology of Ultrafine Partilces: *In Vivo* Studies. Phil. Trans. R. Soc. Lond. A (2000) 358 : 2719-2740.

Oberdorster E (2004a) Manufactured Nanomaterials (Fullerenes, C60) Induce Oxidative Stress in the Brain of Juvenile Largemouth Bass. *Environmental Health Perspectives* 112 (10): 1058-1062.

Oberdorster G, Sharp Z, Elder AP, Gelein R, Kreyling W, Cox C. (2004b) Translocation of Inhaled Ultrafine Particles to the Brain. *Inhal Toxicol* 16: 437-445.

Oberdorster G, Oberdorster E, Oberdorster J (2005a) Nanotoxicology: An Emerging Discipline Evolving from Studies of Ultrafine Particles. *Environmental Health Perspectives* 113: 7: 823-839.

Oberdorster G, Maynard A, Donaldson K, Castranova V, Fitzpatrick J, Carter J, Karn B, Kreyling W, Lai D, Olin S, Monteiro-Riviere N, Warheit D, Yang H, "Particle and Fibre Toxicology, Review: *Principles for characterizing the potential human health effects from exposure to nanomaterials: elements of a screening strategy*", BioMed Central (2005b) <http://www.particleandfibretoxicology.com/content/pdf/1743-8977-2-8.pdf>

Olanow CW (2004) Manganese-induced Parkinsonism and Parkinson's Disease 26.

Osswald S, Yushin G, Mochalin V, Kucheyev SO, Gogotsi Y (2006) Control of sp²/sp³ carbon ratio and surface chemistry of nanodiamond powders by selective oxidation in air. *J Am Chem Soc* 128: 11635-11642.

Paine PL, Moore LC, Horowitz SB (1975) Nuclear envelope permeability *Nature* 254 (5496):109-114.

Pal S, Tak YK, Song JM (2007) Does Antibacterial Activity of Silver Nanoparticle Depend on Shape of Nanoparticle? A Study on Gram-negative *E. coli*. *Appl. Environ. Microbiol.* 2007; 73: 1712-1720.

Pantarotto D, Briand JP, Prato M, Bianco A (2004) Translocation of Bioactive Peptides Across Cell Membranes by Carbon Nanotubes. *Chem. Commun.* 16-17.

Pantarotto D, Partidos CD, Graff R, Hoebeke J, Bri JP, Prato M, Bianco A (2003) Synthesis, Structural Characterization, and Immunological Properties of Carbon Nanotubes Functionalized with Peptides. *Journal of the American Chemical Society* 125: 6160-6164.

Parker JSL and Parish CR (2000) Cellular Uptake and Infection by Canine Parvovirus Involves Rapid Dynamin-Regulated Clathrin-Mediated Endocytosis, Followed by Slower Intracellular Trafficking. *Journal of Virology*.

Per Aspenberg, Anttila A, Konttinen YT, Lappalainen R, Goodman SB, Nordsletten L, Santavirta S (1996) Benign response to particles of diamond and SiC: bone chamber studies of new joint replacement coating materials in rabbits *Biomaterials* 17:807-812.

Podlipensky JL, Seifert G, Graener H, Cravetchi I (2003) Second-harmonic generation from ellipsoidal silver nanoparticles embedded in silica glass *Optics Letters* 28: 9: 716-718.

Poh W and Loh K (2004) Biosensing Properties of Diamond and Carbon Nanotubes. *Langmuir* 20: 5484-5492.

Poon VKM and Burd A (2004) In Vitro Cytotoxicity of Silver: Implication for Clinical Wound Care. *Burns* 30: 140-147.

Preece N, Timbrell J (1989) Investigation of Lipid Peroxidation Induced by Hydrazine Compounds *In Vivo* in the Rat. *Pharmacol Toxicol* 64: 282-285.

Price RL, Haberstroh KM, Webster TJ (2004) Improved Osteoblast Viability in the Presence of Smaller Nanometer Dimensioned Carbon Fibres. *Nanotechnology* 15: 8: 892-900.

Pulskamp K, Diabaté, Krug HF (2007) Carbon Nanotubes Show No Sign of Acute Toxicity but Induce Intracellular Reactive Oxygen Species in Dependence on Contaminants. *Toxicology Letters* 168: 58-74.

Puzyr AP, Neshumayev DA, Tarskikh SV, Makarskaya GV, Dolmatov V.-Yu, Bondar VS (2004) Destruction of Human Blood Cells in Interaction with Detonation Nanodiamonds in Experiments In Vitro. *Diamond and Related Materials* 13: 2020-2023.

Qaddoumi MG, Ueda H, Yang J, Davda J, Labhasetwar V, Lee VHL (2004) The Characteristics and Mechanisms of Uptake of PLGA Nanoparticles in Rabbit Conjunctival Epithelial Cell Layers. *Pharmaceutical Research* 21:4: 641-648.

Rajasekaran SA, Anilkumar G, Oshima E, Bowie JU, Liu H, Heston W, Bander NH, Rajasekaran AK (2003) A Novel Cytoplasmic Tail MXXXL Motif Mediates the Internalization of Prostate-specific Membrane Antigen. *Molecular Biology of the Cell* 14: 4835-4845.

Rehn B, Seiler F, Rehn S, Bruch J, Maier M (2003) Investigations on the Inflammatory and Genotoxic Lung effects of two types of titanium dioxide: Untreated and Surface Treated. *Toxicol Appl Pharmacol* 189: 84-95.

Ricarda-Lorenz M, Holzapfel V, Musyanovych A, Nothelfer K, Walther P, Frank H, Landfester K, Schrezenmeier H, Mailander V (2006) Uptake of Functionalized, Fluorescent-labeled Polymeric Particles in Different Cell Lines and Stem Cells. *Biomaterials* 27: 2820-2828.

Rosenman KD, Moss A, Kon S (1979) Argyria: clinical implications of exposure to silver nitrate and silver oxide. *J. Occup. Med.* 6: 430-435.

Salgueiriño-Maceira V, Correa-Duarte MA, Spasova M, Liz-Marzan LM, Farle M (2006) Composite silica spheres with magnetic and luminescent functionalities. *Advanced Functional Materials* 16: 509-514.

Sato Y, Shibata K-I, Kataoka H, Ogino S-I, Bunshi F, Yokoyama A, Tamura K, Akasaka T, Uo M, Motomiya K, Jeyadevan B, Hatakeyama R, Watari F, Tohji K (2005b) Strict Preparation and Evaluation of Water-soluble Hat-stacked Carbon Nanofibers for Biomedical Application and Their High Biocompatibility: Influence of Nanofiber Surface Functional Groups on Cytotoxicity. *Molecular BioSystems* 1: 142-145.

Sayes C, Liang F, Hudson J, Mendez J, Guo W, Beach J, Moore V, Doyle C, West J, Billups W, Ausman K, Colvin V (2005) Functionalization Density Dependence of Single-walled Carbon Nanotubes Cytotoxicity In Vitro. *Toxicology Letters* 161:2: 135-142.

Schmidt JA, Oliver CN, Lepe-Zuniga JL, Green I, Gery I (1984) Silica-stimulated monocytes release fibroblast proliferation factors identical to interleukin 1. A potential role for interleukin 1 in the pathogenesis of silicosis. *J Clin Invest* 73: 1462-1472.

Schrand AM and Benson-Tolle T "Carbon Nanotube and Epoxy Composites for Military Applications" in Carbon Nanotechnology Ed. Dai 2006.

Schrand AM, Huang H, Carlson C, Schlager JJ, Ōsawa E, Hussain SM, Dai L (2007a) Are Diamond Nanoparticles Cytotoxic? *The Journal of Physical Chemistry B Letters* 111(1): 2-7.

Schrand AM, Dai L, Schlager JJ, Hussain SM, Ōsawa E (2007b) Differential Biocompatibility of Carbon Nanotubes and Nanodiamonds. *Diamond & Related Materials* 16: 12: 2118-2123.

Schrand AM, Szcublewski K, Schlager JJ, Dai L, Hussain SM (2007c) Interaction and Biocompatibility of Multi-walled Carbon Nanotubes in PC-12 Cells *International Journal of Neuroprotection and Neuroregeneration* 3 (2): 115-121.

Schrand AM, Dai L, Schlager JJ, Hussain SM (2008a) Recent Advances in Toxicity Testing of Nanomaterials: Characteristics, Uptake, and Mechanisms in Book entitled 'New Technologies for Toxicity Testing' Ed. Nirmala Bhoghal (Landes Bioscience, Georgetown, TX, USA). In Press

Schrand AM, Johnson J, Dai L, Hussain SM, Schlager JJ, Zhu L, Hong Y, Ōsawa E (2008b) Cytotoxicity and Genotoxicity of Carbon Nanomaterials in Book entitled 'Safety of Nanoparticles: From Manufacturing to Clinical Applications' Ed. Prof. Thomas Webster, Brown University (Springer Publishing). In Press

Shenderova O, Zhirnov V, Brenner D (2002) Carbon Nanostructures. *Crit Rev Solid State Mat Sci* 27¼: 227-356.

Shvedova AA, Kisin ER, Mercer R, Murray AR, Johnson VJ, Potapovich AI, Tyurina YY, Gorelik O, Arepalli S, Schwegler-Berry D, Hubbs AF, Antonini J, Evans DE, Ku B, Ramsey D, Maynard A, Kagan VE, Castranova V, Baron P (2005) Unusual inflammatory and fibrogenic pulmonary responses to single-walled carbon nanotubes in mice. *American Journal of Physiology-Lung Cellular and Molecular Physiology* 289: 5: L698-L708.

Siesjo B, Agardh C, Bengtsson F (1989) Free radicals and brain damage. *Cerebrovasc Brain Metab Rev* 1: 165-211.

Singh R, Pantarotto D, McCarthy D, Chaloin O, Hoebeke J, Partidos CD, Bri JP, Prato M, Bianco A, Kostarelos K. (2005) Binding and Condensation of Plasmid DNA onto Functionalized Carbon Nanotubes: Toward the Construction of Nanotube-Based Gene Delivery Vectors. *Journal of the American Chemical Society* 127:12: 4388-4396.

Skebo JE, Grabinski CM, Schrand AM, Schlager JJ, Hussain SM (2007) Assessment of Metal Nanoparticle Agglomeration, Uptake, and Interaction Using a High Illuminating System *Int. J. Tox.* 26: 135-141.

Smiley ST, Reers M, Mottola-Hartshorn C, Lin M, Chen A, Smith TW, Steele GD Jr., Chen LB (1991) Intracellular Heterogeneity in Mitochondrial Membrane Potentials Revealed by a J-aggregate-forming Lipophilic Cation JC-1. *Proceedings of the National Academy of Science USA* 88: 3671-3675.

Smith BR, Niebert M, Plakhotnik T, Zvyagin AV (2007) Transfection and Imaging of Diamond Nanocrystals as Scattering Optical Labels. *Journal of Luminescence* 260-263.

Sondi I, Goia DV, Matijevic E (2003) Preparation of Highly Concentrated Stable Dispersions of Uniform Silver Nanoparticles. *Journal of Colloid and Interface Science* 260: 75-81.

Soto K, Carrasco A, Powell T, Garza K, Murr L (2005) Comparative In Vitro Cytotoxicity Assessment of Some Manufactured Nanoparticulate Materials Characterized by Transmission Electron Microscopy. *J. Nanopart. Res.* 7: 145-169.

Spilberg I, Mehta J, Simchowitz L (1982) Induction of a Chemotactic Factor From Human Neutrophils by Diverse Crystals. *J Lab Clin Med* 100: 399-404.

Stupp S, Donners J, Li L, Mata A. (2005). Expanding Frontiers in Biomaterials. *MRS Bulletin* 30: 864.

Suvorova EI, Klechkovskaya VV, Kopeikin VV, Buffat PA (2005) Stability of Ag Nanoparticles Dispersed in Amphiphilic Organic Matrix. *Journal of Crystal Growth* 275: 2351-2356.

Tan W, Wang K, He X, Zhao XJ, Drake T, Wang L, Bagwe RP (2004) Bionanotechnology Based on Silica Nanoparticles. *Medicinal Research Reviews* 24: 5: 621-638.

Teeguarden JG, Hinderliter, PM, Orr, G, Thrall BD, Pounds JG (2007) Particokinetics *In Vitro*: Dosimetry Considerations for *In Vitro* Nanoparticle Toxicity Assessments. *Toxicological Sciences* 95(2):300-312.

Thomas K and Sayre P (2005) Research strategies for safety evaluation of nanomaterials, Part I: evaluating the human health implications of exposure to nanoscale materials. *Toxicol. Sci.* 2: 316-321.

Treussart F, Jacques V, Wu E, Gacoin T, Grangier P, Roch JF (2006) Photoluminescence of Single Colour Defects in 50nm Diamond Nanocrystals. *Physica B* 376-377: 926-929.

Trohalaki S, Zellmer R, Pachter R, Hussain S, Frazier J (2002) *Toxicol. Sci.* 68: 498-507.

Tse RL and Phelps P (1970) Polymorphonuclear leukocyte motility in vitro. V. Release of chemotactic activity following phagocytosis of calcium pyrophosphate crystals, diamond dust, and urate crystals. *J Lab Clin Med* 76: 403-415.

Vainrub A, Pustovyy O, Vodyanoy V (2006) Resolution of 90nm ($\lambda/5$) in an Optical Transmission Microscope with an Annular Condenser. *Optics Letters* 31: (19) 2855-2857.

Vodyanoy V (2005) High resolution light microscopy of live cells. *Microscopy Today* 13:26-28, 17.

Wagner AJ, Bleckmann CA, Murdock RC, Schrand AM, Schlager JJ, Hussain SM (2007) Cellular Interaction of Different Forms of Aluminum Nanoparticles in Rat Alveolar Macrophages. *Journal of Physical Chemistry B* 111 (25) 7353-7359.

Wang W, Ruan C, Gu B (2006) Development of Gold-silica composite nanoparticle substrates for perchlorate detection by surface-enhanced Raman spectroscopy. *Analytica Chimica Acta* 567: 121-126.

Wang F, Jiang X-G, Lu W (2004) Intranasal Delivery of Methotrexate to the Brain in Rats Bypassing the Blood-Brain Barrier *Drug Delivery Technology* 4:1. <http://www.drugdeliverytech.com/cgi-bin/articles.cgi?idArticle=205>.

Wang H and Joseph JA (1999) Quantifying Cellular Oxidative Stress by Dichlorofluorescein Assay Using Microplate Reader. *Free Radical. Biol. and Med.* 27: 612-616.

Warheit DB, Webb TR, Sayes CM, Colvin VL, Reed, KL (2006) Pulmonary instillation studies with nanoscale TiO₂ rods and dots in rats: toxicity is not dependent upon particle size and surface area. *Toxicol. Sci.* 1: 227-236.

Wick P, Manser P, Limbach LK, Dettlaff-Weglikowska U, Krumeidch F, Roth S, Stark WJ, Bruinink A (2007) The Degree and Kind of Agglomeration Affect Carbon Nanotube Cytotoxicity. *Toxicology Letters* 168: 121-131.

Wieder ME, Hone DC, Cook MJ, Handsley MM, Gavrilovic J, Russell DA (2006) Intracellular Photodynamic Therapy with Photosensitizer-nanoparticle Conjugates: Cancer Therapy Using a 'Trojan horse'. *Photochemical and Photobiological Sciences* 5: 727-734.

Wilhelm C, Billotey C, Roger J, Pons JN, Bacri J.-C., Gazeau F (2003) Intracellular Uptake of Anionic Superparamagnetic Nanoparticles as a Function of Their Surface Coating. *Biomaterials* 24: 1001-1011.

Worle-Knirsch JM, Pulskamp K, Krug HF (2006) Oops They Did It Again! Carbon Nanotubes Hoax Scientists in Viability Assays. *Nano Letters* 6 (6): 1261-1268.

Xu ZP, Zeng QH, Lu GQ, Ui AB (2006) Inorganice Nanoparticles as Carriers for Efficient Cellular Delivery. *Chemical Engineering Science* 61: 1027-1040.

Yang W, Auciello O, Butler J, Cai W, Carlisle J, Gerbi J, Gruen D, Knickerbocker T, Lasseter T, Russell J, Smith L, Hamers R (2002) DNA-modified Nanocrystalline Diamond Thin-films as Stable, Biologically Active Substrates. *Nat Mat* 1: 253-257 .

Yang W, Zhang CG, Qu HY, Yang HH, Xu JG (2004) Novel Fluorescent Silica Nanoparticle Probe for Ultrasensitive Immunoassays. *Analytica Chimica Acta* 503: 163-169.

Yeo SY, Lee HJ, Jeong SH (2003) Preparation of Nanocomposite Fibers for Permanent Antibacterial Effect. *Journal of Materials Science* 38: 2143-2147.

Yu B (1994) Cellular Defenses Against Damage From Reactive Oxygen Species. *Physiol Rev* 74: 139-162.

Yu S, Kang M, Chang H, Chen K, Yu Y (2005) Bright Fluorescent Nanodiamonds: No Photobleaching and Low Cytotoxicity. *J. Am. Chem. Soc.* 127: 17604-17605.

Zhang Q, Kusaka Y, Sato K, Mo Y, Fukuda M, Donaldson K (1998) Toxicity of ultrafine nickel particles in lungs after intratracheal instillation. *Journal of Occupational Health* 40:3: 171-176.

Zhang Q, Kusaka Y, Zhu X, Sato K, Mo Y, Kluz T, Donaldson K (2003) Comparative toxicity of standard nickel and ultrafine nickel in lung after intratracheal instillation. *J. Occup. Health.* 1: 23-30.

Zhang Z, Kleinstreuer C, Donohue JF, Kim CS (2005a) Comparison of micro- and nano-size particle depositions in a human upper airway model. *Aerosol Science* 211-233.

Zhang X Prasad S, Niyogi S, Morgan A, Ozkan M, Ozkan C (2005b) Guided Neurite Growth on Patterned Carbon Nanotubes. *Sensors and Actuators* 106: 843-850.

Zharov VP, Galitovskaya EN, Johnson C, Kelly T (2005) Syntergistic Enhancement of Selective Nanophotothermolysis with Gold Nanoclusters: Potential for Cancer Therapy. *Lasers in Surgery and Medicine* 37: 219-226.

APPENDIX A
Statistics for MTT and LDH Assays for PC-12 Cells with MWNTs and Controls

MTT PC-12/MWNT Concentrations:

1-0 µg/ml
2-5 µg/ml
3-10 µg/ml
4-25 µg/ml
5-50 µg/ml
6-100 µg/ml

Tukey Kramer Multiple Comparisons							
Group	Sample Mean	Sample Size	Comparison	Absolute Difference	Std. Error of Difference	Critical Range	Results
1	100	3	Group 1 to Group 2	14.43668	6.01909004	28.591	Means are not different
2	85.56332	3	Group 1 to Group 3	20.74991	6.01909004	28.591	Means are not different
3	79.25009	3	Group 1 to Group 4	27.52468	6.01909004	28.591	Means are not different
4	72.47532	3	Group 1 to Group 5	34.01796	6.01909004	28.591	Means are different
5	65.98204	3	Group 1 to Group 6	42.07705	6.01909004	28.591	Means are different
6	57.92295	3	Group 2 to Group 3	6.313231	6.01909004	28.591	Means are not different
			Group 2 to Group 4	13.088	6.01909004	28.591	Means are not different
Other Data			Group 2 to Group 5	19.58129	6.01909004	28.591	Means are not different
Level of significance	0.05		Group 2 to Group 6	27.64037	6.01909004	28.591	Means are not different
Numerator d.f.	6		Group 3 to Group 4	6.77477	6.01909004	28.591	Means are not different
Denominator d.f.	12		Group 3 to Group 5	13.26806	6.01909004	28.591	Means are not different
MSW	108.6883		Group 3 to Group 6	21.32714	6.01909004	28.591	Means are not different
Q Statistic	4.75		Group 4 to Group 5	6.493287	6.01909004	28.591	Means are not different
			Group 4 to Group 6	14.55237	6.01909004	28.591	Means are not different
			Group 5 to Group 6	8.059082	6.01909004	28.591	Means are not different
Anova: Single Factor							
SUMMARY							
Groups		Count	Sum	Average	Variance		
Column 1		3	300	100	0		
Column 2		3	256.6899707	85.56332358	26.99983336		
Column 3		3	237.7502784	79.25009281	1.372100598		
Column 4		3	217.4259693	72.47532311	271.557304		
Column 5		3	197.9461088	65.98203628	121.0246372		
Column 6		3	173.7688625	57.92295418	231.1761332		
ANOVA							
Source of Variation		SS	df	MS	F	P-value	F crit
Between Groups		3339.260957	5	667.8521915	6.144653823	0.004766936	3.105875239
Within Groups		1304.260017	12	108.6883347			
Total		4643.520974	17				

MTT PC-12/CdO Concentrations:

1-0 µg/ml
2-0.1 µg/ml
3-0.5 µg/ml
4-1 µg/ml
5-2.5 µg/ml
6-5 µg/ml

CdO							
Group	Sample Mean	Sample Size	Comparison	Absolute Difference	Std. Error of Difference	Critical Range	Results
1	100	3	Group 1 to Group 2	0.120025	7.96995082	37.857	Means are not different
2	100.12	3	Group 1 to Group 3	0.077985	7.96995082	37.857	Means are not different
3	99.92201	3	Group 1 to Group 4	15.77625	7.96995082	37.857	Means are not different
4	84.22375	3	Group 1 to Group 5	50.6554	7.96995082	37.857	Means are different
5	49.3446	3	Group 1 to Group 6	85.13555	7.96995082	37.857	Means are different
6	14.86445	3	Group 2 to Group 3	0.19801	7.96995082	37.857	Means are not different
			Group 2 to Group 4	15.89628	7.96995082	37.857	Means are not different
			Group 2 to Group 5	50.77543	7.96995082	37.857	Means are different
			Group 2 to Group 6	85.25558	7.96995082	37.857	Means are different
			Group 3 to Group 4	15.69827	7.96995082	37.857	Means are not different
			Group 3 to Group 5	50.57742	7.96995082	37.857	Means are different
			Group 3 to Group 6	85.05757	7.96995082	37.857	Means are different
			Group 4 to Group 5	34.87915	7.96995082	37.857	Means are not different
			Group 4 to Group 6	69.3593	7.96995082	37.857	Means are different
			Group 5 to Group 6	34.48015	7.96995082	37.857	Means are not different
Other Data							
Level of significance	0.05						
Numerator d.f.	6						
Denominator d.f.	12						
MSW	190.5603						
Q Statistic	4.75						

Anova: Single Factor						
SUMMARY						
Groups	Count	Sum	Average	Variance		
Column 1	3	300	100	0		
Column 2	3	300.3600747	100.1200249	168.083423		
Column 3	3	299.7660448	99.92201494	292.8657452		
Column 4	3	252.6712388	84.22374625	72.54987188		
Column 5	3	148.0337914	49.34459714	549.9185459		
Column 6	3	44.59334439	14.86444813	59.94450381		
ANOVA						
Source of Variation	SS	df	MS	F	P-value	F crit
Between Groups	18708.88974	5	3741.777948	19.63565863	2.11314E-05	3.105875239
Within Groups	2286.72418	12	190.5603483			
Total	20995.61392	17				

LDH PC-12/MWNT concentrations:

1-0 µg/ml
2-5 µg/ml
3-10 µg/ml
4-25 µg/ml
5-50 µg/ml
6-100 µg/ml

MWNT							
Group	Sample Mean	Sample Size	Comparison	Absolute Difference	Std. Error of Difference	Critical Range	Results
1	17.36562	3	Group 1 to Group 2	1.623644	3.44140174	16.347	Means are not different
2	15.74198	3	Group 1 to Group 3	0.910856	3.44140174	16.347	Means are not different
3	18.27648	3	Group 1 to Group 4	0.578941	3.44140174	16.347	Means are not different
4	17.94456	3	Group 1 to Group 5	2.325941	3.44140174	16.347	Means are not different
5	19.69156	3	Group 1 to Group 6	15.14403	3.44140174	16.347	Means are not different
6	32.50965	3	Group 2 to Group 3	2.5345	3.44140174	16.347	Means are not different
			Group 2 to Group 4	2.202585	3.44140174	16.347	Means are not different
			Group 2 to Group 5	3.949585	3.44140174	16.347	Means are not different
			Group 2 to Group 6	16.76767	3.44140174	16.347	Means are different
			Group 3 to Group 4	0.331915	3.44140174	16.347	Means are not different
			Group 3 to Group 5	1.415085	3.44140174	16.347	Means are not different
			Group 3 to Group 6	14.23317	3.44140174	16.347	Means are not different
			Group 4 to Group 5	1.747	3.44140174	16.347	Means are not different
			Group 4 to Group 6	14.56509	3.44140174	16.347	Means are not different
			Group 5 to Group 6	12.81809	3.44140174	16.347	Means are not different
Other Data							
Level of significance	0.05						
Numerator d.f.	6						
Denominator d.f.	12						
MSW	35.52974						
Q Statistic	4.75						

Anova: Single Factor						
SUMMARY						
Groups	Count	Sum	Average	Variance		
Column 1	3	52.09686688	17.36562229	7.878120267		
Column 2	3	47.22593426	15.74197809	4.198285678		
Column 3	3	54.82943506	18.27647835	0.835705739		
Column 4	3	53.83368937	17.94456312	2.957717882		
Column 5	3	59.07468975	19.69156325	11.87387161		
Column 6	3	97.52895039	32.50965013	185.4347259		
ANOVA						
Source of Variation	SS	df	MS	F	P-value	F crit
Between Groups	565.3873427	5	113.0774685	3.182614772	0.04657698	3.105874669
Within Groups	426.3568542	12	35.52973785			
Total	991.7441969	17				

APPENDIX B
Statistics for MTT and ROS Assays for N2A Cells with CNMs, NDs, Ag
NPs, and Controls

MTT N2A/CdO concentrations:

1-0 µg/ml
2-0.1 µg/ml
3-0.5 µg/ml
4-1 µg/ml
5- 2.5 µg/ml
6- 5 µg/ml
7-10 µg/ml
8-25 µg/ml
9-50 µg/ml

Combined CdO									
Group	Sample Mean	Sample Size	Comparison	Absolute Difference	Std. Error of Difference	Critical Range	Results		
1	100	3	Group 1 to Group 2	25.26111	3.6610796	18.159	Means are different		
2	74.73889	3	Group 1 to Group 3	54.79097	3.6610796	18.159	Means are different		
3	45.20903	3	Group 1 to Group 4	67.70328	3.6610796	18.159	Means are different		
4	32.29672	3	Group 1 to Group 5	85.37333	3.6610796	18.159	Means are different		
5	14.62667	3	Group 1 to Group 6	86.29	3.6610796	18.159	Means are different		
6	13.71	3	Group 1 to Group 7	98.47134	3.6610796	18.159	Means are different		
7	1.528661	3	Group 1 to Group 8	98.4355	3.6610796	18.159	Means are different		
8	1.564498	3	Group 1 to Group 9	98.95333	3.6610796	18.159	Means are different		
9	1.046667	3	Group 2 to Group 3	29.52986	3.6610796	18.159	Means are different		
Other Data			Group 2 to Group 4	42.44217	3.6610796	18.159	Means are different		
Level of significance	0.05		Group 2 to Group 5	60.11222	3.6610796	18.159	Means are different		
Numerator d.f.	9		Group 2 to Group 6	61.02889	3.6610796	18.159	Means are different		
Denominator d.f.	18		Group 2 to Group 7	73.21023	3.6610796	18.159	Means are different		
MSW	40.21051		Group 2 to Group 8	73.17439	3.6610796	18.159	Means are different		
Q Statistic	4.96		Group 2 to Group 9	73.69222	3.6610796	18.159	Means are different		
			Group 3 to Group 4	12.9123	3.6610796	18.159	Means are not different		
			Group 3 to Group 5	30.58236	3.6610796	18.159	Means are different		
			Group 3 to Group 6	31.49903	3.6610796	18.159	Means are different		
			Group 3 to Group 7	43.68036	3.6610796	18.159	Means are different		
			Group 3 to Group 8	43.64453	3.6610796	18.159	Means are different		
			Group 3 to Group 9	44.16236	3.6610796	18.159	Means are different		
			Group 4 to Group 5	17.67006	3.6610796	18.159	Means are not different		
			Group 4 to Group 6	18.58672	3.6610796	18.159	Means are different		
			Group 4 to Group 7	30.76806	3.6610796	18.159	Means are different		
			Group 4 to Group 8	30.73222	3.6610796	18.159	Means are different		
			Group 4 to Group 9	31.25006	3.6610796	18.159	Means are different		
			Group 5 to Group 6	0.916667	3.6610796	18.159	Means are not different		
			Group 5 to Group 7	13.09801	3.6610796	18.159	Means are not different		
			Group 5 to Group 8	13.06217	3.6610796	18.159	Means are not different		
			Group 5 to Group 9	13.58	3.6610796	18.159	Means are not different		
			Group 6 to Group 7	12.18134	3.6610796	18.159	Means are not different		
			Group 6 to Group 8	12.1455	3.6610796	18.159	Means are not different		
			Group 6 to Group 9	12.66333	3.6610796	18.159	Means are not different		
			Group 7 to Group 8	0.035837	3.6610796	18.159	Means are not different		
			Group 7 to Group 9	0.481994	3.6610796	18.159	Means are not different		
			Group 8 to Group 9	0.517832	3.6610796	18.159	Means are not different		

Anova: Single Factor						
SUMMARY						
<i>Groups</i>	<i>Count</i>	<i>Sum</i>	<i>Average</i>	<i>Variance</i>		
Column 1	3	300	100	0		
Column 2	3	224.2166692	74.73888974	191.6117124		
Column 3	3	135.627075	45.209025	4.277895069		
Column 4	3	96.89016866	32.29672289	32.80319421		
Column 5	3	43.88	14.62666667	27.20343333		
Column 6	3	41.13	13.71	105.8623		
Column 7	3	4.585982767	1.528660922	0.015451056		
Column 8	3	4.693494601	1.5644982	0.028384323		
Column 9	3	3.14	1.046666667	0.092233333		
ANOVA						
<i>Source of Variation</i>	<i>SS</i>	<i>df</i>	<i>MS</i>	<i>F</i>	<i>P-value</i>	<i>F crit</i>
Between Groups	30219.81738	8	3777.477172	93.94252968	4.32592E-13	2.510157895
Within Groups	723.7892074	18	40.21051152			
Total	30943.60658	26				

MTT N2A/ND-row concentrations:

1-0 µg/ml
2-25 µg/ml
3-50 µg/ml
4-100 µg/ml

ND-row									
	Sample	Sample		Absolute	Std. Error	Critical			
Group	Mean	Size	Comparison	Difference	of Difference	Range	Results		
1	100	3	Group 1 to Group 2	3.174096	2.25725682	10.225	Means are not different		
2	96.8259	3	Group 1 to Group 3	5.043904	2.25725682	10.225	Means are not different		
3	94.9561	3	Group 1 to Group 4	8.723523	2.25725682	10.225	Means are not different		
4	91.27648	3	Group 2 to Group 3	1.869809	2.25725682	10.225	Means are not different		
			Group 2 to Group 4	5.549428	2.25725682	10.225	Means are not different		
Other Data			Group 3 to Group 4	3.679619	2.25725682	10.225	Means are not different		
Level of significance		0.05							
Numerator d.f.		4							
Denominator d.f.		8							
MSW		15.28563							
Q Statistic		4.53							

Anova: Single Factor						
SUMMARY						
Groups	Count	Sum	Average	Variance		
Column 1	3	300	100	0		
Column 2	3	290.4777133	96.82590442	7.295727028		
Column 3	3	284.8682866	94.95609552	33.5589242		
Column 4	3	273.82943	91.27647666	20.28784891		
ANOVA						
Source of Variation	SS	df	MS	F	P-value	F crit
Between Groups	119.5857326	3	39.86191086	2.607803788	0.123801651	4.066180557
Within Groups	122.2850003	8	15.28562503			
Total	241.8707328	11				

MTT N2A/CB Concentrations:

1-0 µg/ml
2-25 µg/ml
3-50 µg/ml
4-100 µg/ml

CB									
Group	Sample Mean	Sample Size	Comparison	Absolute Difference	Std. Error of Difference	Critical Range	Results		
1	100	3	Group 1 to Group 2	11.13178	6.73360326	30.503	Means are not different		
2	88.86822	3	Group 1 to Group 3	14.94213	6.73360326	30.503	Means are not different		
3	85.05787	3	Group 1 to Group 4	15.94494	6.73360326	30.503	Means are not different		
4	84.05506	3	Group 2 to Group 3	3.810355	6.73360326	30.503	Means are not different		
			Group 2 to Group 4	4.813162	6.73360326	30.503	Means are not different		
			Group 3 to Group 4	1.002807	6.73360326	30.503	Means are not different		
Other Data									
Level of significance	0.05								
Numerator d.f.	4								
Denominator d.f.	8								
MSW	136.0242								
Q Statistic	4.53								

Anova: Single Factor						
SUMMARY						
Groups	Count	Sum	Average	Variance		
Column 1	3	300	100	0		
Column 2	3	266.6046732	88.8682244	105.2589741		
Column 3	3	255.173607	85.057869	163.8526343		
Column 4	3	252.1651875	84.05506249	274.9853465		
ANOVA						
Source of Variation	SS	df	MS	F	P-value	F crit
Between Groups	480.0867716	3	160.0289239	1.176473586	0.377663344	4.066180557
Within Groups	1088.19391	8	136.0242387			
Total	1568.280681	11				

MTT N2A/MWNT Concentrations:

1-0 µg/ml
2-25 µg/ml
3-50 µg/ml
4-100 µg/ml

MWNT							
Group	Sample Mean	Sample Size	Comparison	Absolute Difference	Std. Error of Difference	Critical Range	Results
1	100	3	Group 1 to Group 2	20.41752	7.26696452	32.919	Means are not different
2	79.58248	3	Group 1 to Group 3	29.08409	7.26696452	32.919	Means are not different
3	70.91591	3	Group 1 to Group 4	25.92711	7.26696452	32.919	Means are not different
4	74.07289	3	Group 2 to Group 3	8.666568	7.26696452	32.919	Means are not different
Other Data			Group 2 to Group 4	5.509594	7.26696452	32.919	Means are not different
			Group 3 to Group 4	3.156974	7.26696452	32.919	Means are not different
Level of significance	0.05						
Numerator d.f.	4						
Denominator d.f.	8						
MSW	158.4263						
Q Statistic	4.53						

Anova: Single Factor						
SUMMARY						
Groups	Count	Sum	Average	Variance		
Column 1	3	300	100	0		
Column 2	3	238.7474371	79.58247905	188.1780799		
Column 3	3	212.7477322	70.91591073	296.4610507		
Column 4	3	222.218655	74.072885	149.0661501		
ANOVA						
Source of Variation	SS	df	MS	F	P-value	F crit
Between Groups	1537.804667	3	512.6015555	3.235583298	0.081811396	4.066180557
Within Groups	1267.410561	8	158.4263202			
Total	2805.215228	11				

MTT N2A/SWNT Concentrations:

1-0 µg/ml
2-25 µg/ml
3-50 µg/ml
4-100 µg/ml

SWNT						
Group	Sample Mean	Sample Size	Comparison	Absolute Difference	Std. Error of Difference	Critical Range Results
1	100	3	Group 1 to Group 2	37.43747	9.44167076	42.771 Means are not different
2	62.56253	3	Group 1 to Group 3	52.11813	9.44167076	42.771 Means are different
3	47.88187	3	Group 1 to Group 4	67.29293	9.44167076	42.771 Means are different
4	32.70707	3	Group 2 to Group 3	14.68066	9.44167076	42.771 Means are not different
			Group 2 to Group 4	29.85546	9.44167076	42.771 Means are not different
			Group 3 to Group 4	15.17479	9.44167076	42.771 Means are not different
Other Data						
Level of significance	0.05					
Numerator d.f.	4					
Denominator d.f.	8					
MSW	267.4354					
Q Statistic	4.53					

Anova: Single Factor						
SUMMARY						
Groups	Count	Sum	Average	Variance		
Column 1	3	300	100	0		
Column 2	3	187.6875934	62.56253113	69.84555594		
Column 3	3	143.6456016	47.88186721	194.3239208		
Column 4	3	98.12122319	32.7070744	805.5722842		
ANOVA						
Source of Variation	SS	df	MS	F	P-value	F crit
Between Groups	7487.509653	3	2495.836551	9.332482445	0.005442036	4.066180557
Within Groups	2139.483522	8	267.4354402			
Total	9626.993174	11				

MTT N2A/CdO Concentrations:

1-0 µg/ml

2-25 µg/ml

3-50 µg/ml

CdO							
Group	Sample Mean	Sample Size	Comparison	Absolute Difference	Std. Error of Difference	Critical Range	Results
1	100	3	Group 1 to Group 2	97.51661	0.52785252	2.2909	Means are different
2	2.483389	3	Group 1 to Group 3	98.95254	0.52785252	2.2909	Means are different
3	1.047463	3	Group 2 to Group 3	1.435926	0.52785252	2.2909	Means are not different
Other Data							
Level of significance	0.05						
Numerator d.f.	3						
Denominator d.f.	6						
MSW	0.835885						
Q Statistic	4.34						

Anova: Single Factor						
SUMMARY						
Groups	Count	Sum	Average	Variance		
Column 1	3	300	100	0		
Column 2	3	7.450166152	2.483388717	2.415034602		
Column 3	3	3.142388975	1.047462992	0.092619986		
ANOVA						
Source of Variation	SS	df	MS	F	P-value	F crit
Between Groups	19303.15594	2	9651.57797	11546.53996	1.75255E-11	5.14325285
Within Groups	5.015309175	6	0.835884862			
Total	19308.17125	8				

MTT N2A/MWNT-SO₃Na Concentrations:

1-0 µg/ml
 2-5 µg/ml
 3-10 µg/ml
 4-25 µg/ml
 5-50 µg/ml
 6-100 µg/ml

MWNT-SO ₃ Na							
Group	Sample Mean	Sample Size	Comparison	Absolute Difference	Std. Error of Difference	Critical Range	Results
1	100	3	Group 1 to Group 2	4.211474	4.19699688	19.936	Means are not different
2	95.78853	3	Group 1 to Group 3	0.290001	4.19699688	19.936	Means are not different
3	99.71	3	Group 1 to Group 4	1.742169	4.19699688	19.936	Means are not different
4	98.25783	3	Group 1 to Group 5	5.130762	4.19699688	19.936	Means are not different
5	94.86924	3	Group 1 to Group 6	5.764574	4.19699688	19.936	Means are not different
6	94.23543	3	Group 2 to Group 3	3.921473	4.19699688	19.936	Means are not different
Other Data			Group 2 to Group 4	2.469305	4.19699688	19.936	Means are not different
			Group 2 to Group 5	0.919289	4.19699688	19.936	Means are not different
			Group 2 to Group 6	1.553101	4.19699688	19.936	Means are not different
			Group 3 to Group 4	1.452168	4.19699688	19.936	Means are not different
			Group 3 to Group 5	4.840761	4.19699688	19.936	Means are not different
			Group 3 to Group 6	5.474573	4.19699688	19.936	Means are not different
			Group 4 to Group 5	3.388593	4.19699688	19.936	Means are not different
			Group 4 to Group 6	4.022405	4.19699688	19.936	Means are not different
			Group 5 to Group 6	0.633812	4.19699688	19.936	Means are not different
Anova: Single Factor							
SUMMARY							
Groups	Count	Sum	Average	Variance			
Column 1	3	300	100	0			
Column 2	3	287.3655793	95.78852642	12.98171488			
Column 3	3	299.1299969	99.70999896	34.61828124			
Column 4	3	294.773494	98.25783132	22.95580298			
Column 5	3	284.6077136	94.86923786	83.19081356			
Column 6	3	282.7062773	94.23542578	163.3194776			
ANOVA							
Source of Variation	SS	df	MS	F	P-value	F crit	
Between Groups	94.3600825	5	18.8720165	0.357124595	0.86798653	3.105875239	
Within Groups	634.1321806	12	52.84434838				
Total	728.4922631	17					

MTT N2A/CB Concentrations:

1-0 µg/ml
2-5 µg/ml
3-10 µg/ml
4-25 µg/ml
5-50 µg/ml
6-100 µg/ml

CB						
Group	Sample Mean	Sample Size	Comparison	Absolute Difference	Std. Error of Difference	Critical Range Results
1	100	3	Group 1 to Group 2	8.324136	6.23290145	29.606 Means are not different
2	91.67586	3	Group 1 to Group 3	8.794331	6.23290145	29.606 Means are not different
3	91.20567	3	Group 1 to Group 4	11.13178	6.23290145	29.606 Means are not different
4	88.86822	3	Group 1 to Group 5	14.94213	6.23290145	29.606 Means are not different
5	85.05787	3	Group 1 to Group 6	15.94494	6.23290145	29.606 Means are not different
6	84.05506	3	Group 2 to Group 3	0.470195	6.23290145	29.606 Means are not different
Other Data			Group 2 to Group 4	2.80764	6.23290145	29.606 Means are not different
			Group 2 to Group 5	6.617995	6.23290145	29.606 Means are not different
			Group 2 to Group 6	7.620801	6.23290145	29.606 Means are not different
			Group 3 to Group 4	2.337445	6.23290145	29.606 Means are not different
			Group 3 to Group 5	6.1478	6.23290145	29.606 Means are not different
			Group 3 to Group 6	7.150607	6.23290145	29.606 Means are not different
			Group 4 to Group 5	3.810355	6.23290145	29.606 Means are not different
Level of significance	0.05		Group 4 to Group 6	4.813162	6.23290145	29.606 Means are not different
Numerator d.f.	6		Group 5 to Group 6	1.002807	6.23290145	29.606 Means are not different
Denominator d.f.	12					
MSW	116.5472					
Q Statistic	4.75					

Anova: Single Factor						
SUMMARY						
Groups	Count	Sum	Average	Variance		
Column 1	3	300	100	0		
Column 2	3	275.0275917	91.6758639	36.87992554		
Column 3	3	273.6170072	91.20566907	118.3062093		
Column 4	3	266.6046732	88.8682244	105.2589741		
Column 5	3	255.173607	85.057869	163.8526343		
Column 6	3	252.1651875	84.05506249	274.9853465		
ANOVA						
Source of Variation	SS	df	MS	F	P-value	F crit
Between Groups	495.5579274	5	99.11158547	0.850398818	0.540313963	3.105875239
Within Groups	1398.56618	12	116.5471816			
Total	1894.124107	17				

MTT N2A/SWNT-phenyl-SO3Na Concentrations:

1-0 µg/ml
 2-5 µg/ml
 3-10 µg/ml
 4-25 µg/ml
 5-50 µg/ml
 6-100 µg/ml

SWNT-phenylSO3Na						
Group	Sample Mean	Sample Size	Comparison	Absolute Difference	Std. Error of Difference	Critical Range Results
1	100	3	Group 1 to Group 2	6.044862	1.77429241	8.4279 Means are not different
2	93.95514	3	Group 1 to Group 3	11.50245	1.77429241	8.4279 Means are different
3	88.49755	3	Group 1 to Group 4	11.72784	1.77429241	8.4279 Means are different
4	88.27216	3	Group 1 to Group 5	15.28315	1.77429241	8.4279 Means are different
5	84.71685	3	Group 1 to Group 6	21.58214	1.77429241	8.4279 Means are different
6	78.41786	3	Group 2 to Group 3	5.457592	1.77429241	8.4279 Means are not different
			Group 2 to Group 4	5.68298	1.77429241	8.4279 Means are not different
Other Data			Group 2 to Group 5	9.238287	1.77429241	8.4279 Means are different
Level of significance			Group 2 to Group 6	15.53728	1.77429241	8.4279 Means are different
Numerator d.f.			Group 3 to Group 4	0.225388	1.77429241	8.4279 Means are not different
Denominator d.f.			Group 3 to Group 5	3.780695	1.77429241	8.4279 Means are not different
MSW			Group 3 to Group 6	10.07969	1.77429241	8.4279 Means are different
Q Statistic			Group 4 to Group 5	3.555307	1.77429241	8.4279 Means are not different
			Group 4 to Group 6	9.854299	1.77429241	8.4279 Means are different
			Group 5 to Group 6	6.298992	1.77429241	8.4279 Means are not different

Anova: Single Factor					
SUMMARY					
Groups	Count	Sum	Average	Variance	
Column 1	3	300	100	0	
Column 2	3	281.8654139	93.95513798	6.465732094	
Column 3	3	265.4926373	88.49754577	1.891338951	
Column 4	3	264.8164737	88.27215789	1.906400656	
Column 5	3	254.1505527	84.7168509	1.734042178	
Column 6	3	235.2535771	78.41785904	44.66852985	
ANOVA					
Source of Variation	SS	df	MS	F	P-value F crit
Between Groups	829.9781784	5	165.9956357	17.5762017	3.74682E-05 3.105875239
Within Groups	113.3320875	12	9.444340621		
Total	943.3102659	17			

MTT N2A/MWNT-2 Concentrations:

1-0 µg/ml
 2-5 µg/ml
 3-10 µg/ml
 4-25 µg/ml
 5-50 µg/ml
 6-100 µg/ml

MWNT-2									
Group	Sample Mean	Sample Size	Comparison	Absolute Difference	Std. Error of Difference	Critical Range	Results		
1	100	3	Group 1 to Group 2	7.557188	2.89830472	13.767	Means are not different		
2	92.44281	3	Group 1 to Group 3	12.68574	2.89830472	13.767	Means are not different		
3	87.31426	3	Group 1 to Group 4	4.854303	2.89830472	13.767	Means are not different		
4	104.8543	3	Group 1 to Group 5	15.70591	2.89830472	13.767	Means are different		
5	84.29409	3	Group 1 to Group 6	26.6662	2.89830472	13.767	Means are different		
6	73.3338	3	Group 2 to Group 3	5.128549	2.89830472	13.767	Means are not different		
Other Data			Group 2 to Group 4	12.41149	2.89830472	13.767	Means are not different		
			Group 2 to Group 5	8.148723	2.89830472	13.767	Means are not different		
Level of significance	0.05		Group 2 to Group 6	19.10901	2.89830472	13.767	Means are different		
Numerator d.f.	6		Group 3 to Group 4	17.54004	2.89830472	13.767	Means are different		
Denominator d.f.	12		Group 3 to Group 5	3.020174	2.89830472	13.767	Means are not different		
MSW	25.20051		Group 3 to Group 6	13.98046	2.89830472	13.767	Means are different		
Q Statistic	4.75		Group 4 to Group 5	20.56021	2.89830472	13.767	Means are different		
			Group 4 to Group 6	31.5205	2.89830472	13.767	Means are different		
			Group 5 to Group 6	10.96029	2.89830472	13.767	Means are not different		

Anova: Single Factor						
SUMMARY						
Groups	Count	Sum	Average	Variance		
Column 1	3	300	100	0		
Column 2	3	277.3284354	92.44281181	64.77312363		
Column 3	3	261.9427886	87.31426288	26.27793692		
Column 4	3	314.5629086	104.8543029	5.604397072		
Column 5	3	252.8822671	84.29408902	24.94074605		
Column 6	3	220.0013988	73.3337996	29.60686108		
ANOVA						
Source of Variation	SS	df	MS	F	P-value	F crit
Between Groups	1929.944291	5	385.9888581	15.31670772	7.53092E-05	3.105875239
Within Groups	302.4061295	12	25.20051079			
Total	2232.35042	17				

MTT N2A/MWNT-COOH Concentrations:

1-0 µg/ml
 2-5 µg/ml
 3-10 µg/ml
 4-25 µg/ml
 5-50 µg/ml
 6-100 µg/ml

MWNT-COOH								
Group	Sample Mean	Sample Size	Comparison	Absolute Difference	Std. Error of Difference	Critical Range	Results	
1	100	3	Group 1 to Group 2	5.210638	5.83779078	27.73	Means are not different	
2	94.78936	3	Group 1 to Group 3	13.98413	5.83779078	27.73	Means are not different	
3	86.01587	3	Group 1 to Group 4	34.6095	5.83779078	27.73	Means are different	
4	65.3905	3	Group 1 to Group 5	5.233288	5.83779078	27.73	Means are not different	
5	105.2333	3	Group 1 to Group 6	16.0552	5.83779078	27.73	Means are not different	
6	83.9448	3	Group 2 to Group 3	8.77349	5.83779078	27.73	Means are not different	
Other Data			Group 2 to Group 4	29.39886	5.83779078	27.73	Means are different	
			Group 2 to Group 5	10.44393	5.83779078	27.73	Means are not different	
			Group 2 to Group 6	10.84456	5.83779078	27.73	Means are not different	
			Group 3 to Group 4	20.62537	5.83779078	27.73	Means are not different	
			Group 3 to Group 5	19.21742	5.83779078	27.73	Means are not different	
			Group 3 to Group 6	2.071073	5.83779078	27.73	Means are not different	
Level of significance	0.05		Group 4 to Group 5	39.84279	5.83779078	27.73	Means are different	
Numerator d.f.	6		Group 4 to Group 6	18.5543	5.83779078	27.73	Means are not different	
Denominator d.f.	12		Group 5 to Group 6	21.28849	5.83779078	27.73	Means are not different	
MSW	102.2394							
Q Statistic	4.75							

Anova: Single Factor							
SUMMARY							
Groups	Count	Sum	Average	Variance			
Column 1	3	300	100	0			
Column 2	3	284.368085	94.78936166	214.8197542			
Column 3	3	258.047614	86.01587134	14.94506659			
Column 4	3	196.1714908	65.39049695	41.00468924			
Column 5	3	315.699865	105.2332883	162.6323567			
Column 6	3	251.8343956	83.94479853	180.0345541			
ANOVA							
Source of Variation	SS	df	MS	F	P-value	F crit	
Between Groups	3028.771549	5	605.7543098	5.924861543	0.005504163	3.105875239	
Within Groups	1226.872842	12	102.2394035				
Total	4255.644391	17					

MTT N2A/SWNT Concentrations:

1-0 µg/ml
 2-5 µg/ml
 3-10 µg/ml
 4-25 µg/ml
 5-50 µg/ml
 6-100 µg/ml

SWNT						
Group	Sample Mean	Sample Size	Comparison	Absolute Difference	Std. Error of Difference	Critical Range Results
1	100	3	Group 1 to Group 2	6.291541	8.93914517	42.461 Means are not different
2	93.70846	3	Group 1 to Group 3	17.87464	8.93914517	42.461 Means are not different
3	82.12536	3	Group 1 to Group 4	37.43747	8.93914517	42.461 Means are not different
4	62.56253	3	Group 1 to Group 5	52.11813	8.93914517	42.461 Means are different
5	47.88187	3	Group 1 to Group 6	67.29293	8.93914517	42.461 Means are different
6	32.70707	3	Group 2 to Group 3	11.5831	8.93914517	42.461 Means are not different
Other Data			Group 2 to Group 4	31.14593	8.93914517	42.461 Means are not different
			Group 2 to Group 5	45.82659	8.93914517	42.461 Means are different
			Group 2 to Group 6	61.00138	8.93914517	42.461 Means are different
			Group 3 to Group 4	19.56282	8.93914517	42.461 Means are not different
			Group 3 to Group 5	34.24349	8.93914517	42.461 Means are not different
			Group 3 to Group 6	49.41828	8.93914517	42.461 Means are different
			Group 4 to Group 5	14.68066	8.93914517	42.461 Means are not different
Level of significance	0.05		Group 4 to Group 6	29.85546	8.93914517	42.461 Means are not different
Numerator d.f.	6		Group 5 to Group 6	15.17479	8.93914517	42.461 Means are not different
Denominator d.f.	12					
MSW	239.7249					
Q Statistic	4.75					

Anova: Single Factor						
SUMMARY						
Groups	Count	Sum	Average	Variance		
Column 1	3	300	100	0		
Column 2	3	281.1253782	93.70845939	368.3911113		
Column 3	3	246.3760658	82.12535525	0.21682392		
Column 4	3	187.6875934	62.56253113	69.84555594		
Column 5	3	143.6456016	47.88186721	194.3239208		
Column 6	3	98.12122319	32.7070744	805.5722842		
ANOVA						
Source of Variation	SS	df	MS	F	P-value	F crit
Between Groups	10632.70116	5	2126.540233	8.870750576	0.001010786	3.105875239
Within Groups	2876.699392	12	239.7249494			
Total	13509.40055	17				

ROS N2A/ND-raw Concentrations:

1-0 µg/ml

2-25 µg/ml

3-50 µg/ml

4-100 µg/ml

ND-raw							
Group	Sample Mean	Sample Size	Comparison	Absolute Difference	Std. Error of Difference	Critical Range	Results
1	1	3	Group 1 to Group 2	0.269304	0.15357003	0.6957	Means are not different
2	0.730696	3	Group 1 to Group 3	0.33073	0.15357003	0.6957	Means are not different
3	0.66927	3	Group 1 to Group 4	0.378634	0.15357003	0.6957	Means are not different
4	0.621366	3	Group 2 to Group 3	0.061426	0.15357003	0.6957	Means are not different
			Group 2 to Group 4	0.10933	0.15357003	0.6957	Means are not different
			Group 3 to Group 4	0.047904	0.15357003	0.6957	Means are not different
Other Data							
Level of significance	0.05						
Numerator d.f.	4						
Denominator d.f.	8						
MSW	0.070751						
Q Statistic	4.53						

Anova: Single Factor						
SUMMARY						
Groups	Count	Sum	Average	Variance		
Column 1	3	3	1	0		
Column 2	3	2.192088288	0.730696096	0.058983406		
Column 3	3	2.007809898	0.669269966	0.105130678		
Column 4	3	1.86409907	0.621366357	0.118890948		
ANOVA						
Source of Variation	SS	df	MS	F	P-value	F crit
Between Groups	0.257468476	3	0.085822825	1.213021899	0.365874789	4.066180557
Within Groups	0.566010064	8	0.070751258			
Total	0.82347854	11				

ROS N2A/CB concentrations:

1-0 µg/ml
2-25 µg/ml
3-50 µg/ml
4-100 µg/ml

CB									
Group	Sample Mean	Sample Size	Comparison	Absolute Difference	Std. Error of Difference	Critical Range	Results		
1	1	3	Group 1 to Group 2	6.104673	1.83244481	8.301	Means are not different		
2	7.104673	3	Group 1 to Group 3	5.783267	1.83244481	8.301	Means are not different		
3	6.783267	3	Group 1 to Group 4	11.77088	1.83244481	8.301	Means are different		
4	12.77088	3	Group 2 to Group 3	0.321406	1.83244481	8.301	Means are not different		
			Group 2 to Group 4	5.666209	1.83244481	8.301	Means are not different		
			Group 3 to Group 4	5.987615	1.83244481	8.301	Means are not different		
Other Data									
Level of significance	0.05								
Numerator d.f.	4								
Denominator d.f.	8								
MSW	10.07356								
Q Statistic	4.53								

Anova: Single Factor						
SUMMARY						
Groups	Count	Sum	Average	Variance		
Column 1	3	3	1	0		
Column 2	3	21.31401965	7.104673218	3.502082674		
Column 3	3	20.34980057	6.783266856	5.919108162		
Column 4	3	38.31264558	12.77088186	30.87305686		
ANOVA						
Source of Variation	SS	df	MS	F	P-value	F crit
Between Groups	207.9957196	3	69.33190654	6.88256121	0.013183114	4.066180557
Within Groups	80.58849538	8	10.07356192			
Total	288.584215	11				

ROS/N2A SWNT Concentrations:

1-0 µg/ml
2-25 µg/ml
3-50 µg/ml
4-100 µg/ml

SWNT							
Group	Sample Mean	Sample Size	Comparison	Absolute Difference	Std. Error of Difference	Critical Range	Results
1		3	Group 1 to Group 2	2.061399	0.19832417	0.8984	Means are different
2	3.061399	3	Group 1 to Group 3	2.406967	0.19832417	0.8984	Means are different
3	3.406967	3	Group 1 to Group 4	0.030443	0.19832417	0.8984	Means are not different
4	0.969557	3	Group 2 to Group 3	0.345569	0.19832417	0.8984	Means are not different
			Group 2 to Group 4	2.091842	0.19832417	0.8984	Means are different
			Group 3 to Group 4	2.43741	0.19832417	0.8984	Means are different
Other Data							
Level of significance	0.05						
Numerator d.f.	4						
Denominator d.f.	8						
MSW	0.117997						
Q Statistic	4.53						

Anova: Single Factor						
SUMMARY						
Groups	Count	Sum	Average	Variance		
Column 1	3	3	1	0		
Column 2	3	9.184196016	3.061398672	0.067155749		
Column 3	3	10.22090208	3.40696736	0.371950479		
Column 4	3	2.908671432	0.969557144	0.032883495		
ANOVA						
Source of Variation	SS	df	MS	F	P-value	F crit
Between Groups	15.35997779	3	5.119992597	43.39071252	2.70069E-05	4.066180557
Within Groups	0.943979446	8	0.117997431			
Total	16.30395724	11				

ROS N2A/MWNT concentrations:

1-0 µg/ml
2-25 µg/ml
3-50 µg/ml
4-100 µg/ml

MWNT						
Group	Sample Mean	Sample Size	Comparison	Absolute Difference	Std. Error of Difference	Critical Range Results
1	1	3	Group 1 to Group 2	2.067503	0.37464886	1.6972 Means are different
2	3.067503	3	Group 1 to Group 3	2.968205	0.37464886	1.6972 Means are different
3	3.968205	3	Group 1 to Group 4	1.250936	0.37464886	1.6972 Means are not different
4	2.250936	3	Group 2 to Group 3	0.900702	0.37464886	1.6972 Means are not different
			Group 2 to Group 4	0.816568	0.37464886	1.6972 Means are not different
			Group 3 to Group 4	1.717269	0.37464886	1.6972 Means are different
Other Data						
Level of significance	0.05					
Numerator d.f.	4					
Denominator d.f.	8					
MSW	0.421085					
Q Statistic	4.53					

Anova: Single Factor						
SUMMARY						
Groups	Count	Sum	Average	Variance		
Column 1	3	3	1	0		
Column 2	3	9.202509958	3.067503319	0.40522428		
Column 3	3	11.9046147	3.968204901	0.76554007		
Column 4	3	6.752807092	2.250935697	0.513576901		
ANOVA						
Source of Variation	SS	df	MS	F	P-value	F crit
Between Groups	14.30753247	3	4.769177491	11.32591745	0.002988076	4.066180557
Within Groups	3.368682502	8	0.421085313			
Total	17.67621497	11				

MTT N2A/ND-row Concentrations:

1-0 µg/ml
 2-5 µg/ml
 3-10 µg/ml
 4-25 µg/ml
 5-50 µg/ml
 6-100 µg/ml

ANOVA Table									
ND-row									
Group	Sample Mean	Sample Size	Comparison	Absolute Difference	Std. Error of Difference	Critical Range	Results		
1	100	3	Group 1 to Group 2	4.148757	2.05290196	9.7513	Means are not different		
2	95.85124	3	Group 1 to Group 3	3.780717	2.05290196	9.7513	Means are not different		
3	96.21928	3	Group 1 to Group 4	3.174096	2.05290196	9.7513	Means are not different		
4	96.8259	3	Group 1 to Group 5	5.043904	2.05290196	9.7513	Means are not different		
5	94.9561	3	Group 1 to Group 6	8.723523	2.05290196	9.7513	Means are not different		
6	91.27648	3	Group 2 to Group 3	0.36804	2.05290196	9.7513	Means are not different		
			Group 2 to Group 4	0.974662	2.05290196	9.7513	Means are not different		
			Group 2 to Group 5	0.895147	2.05290196	9.7513	Means are not different		
			Group 2 to Group 6	4.574766	2.05290196	9.7513	Means are not different		
Other Data			Group 3 to Group 4	0.606621	2.05290196	9.7513	Means are not different		
Level of significance			Group 3 to Group 5	1.263188	2.05290196	9.7513	Means are not different		
Numerator d.f.			Group 3 to Group 6	4.942806	2.05290196	9.7513	Means are not different		
Denominator d.f.			Group 4 to Group 5	1.869809	2.05290196	9.7513	Means are not different		
MSW			Group 4 to Group 6	5.549428	2.05290196	9.7513	Means are not different		
Q Statistic			Group 5 to Group 6	3.679619	2.05290196	9.7513	Means are not different		

Anova: Single Factor						
SUMMARY						
Groups	Count	Sum	Average	Variance		
Column 1	3	300	100	0		
Column 2	3	287.5537287	95.85124292	6.032471095		
Column 3	3	288.6578492	96.21928307	8.684345046		
Column 4	3	290.4777133	96.82590442	7.295727028		
Column 5	3	284.8682866	94.95609552	33.5589242		
Column 6	3	273.82943	91.27647666	20.28784891		
ANOVA						
Source of Variation	SS	df	MS	F	P-value	F crit
Between Groups	120.0819053	5	24.01638105	1.899546337	0.168140248	3.105875239
Within Groups	151.7186325	12	12.64321938			
Total	271.8005378	17				

MTT N2A/ND-COOH Concentrations:

1-0 µg/ml
2-5 µg/ml
3-10 µg/ml
4-25 µg/ml
5-50 µg/ml
6-100 µg/ml

ND-COOH									
Group	Sample Mean	Sample Size	Comparison	Absolute Difference	Std. Error of Difference	Critical Range	Results		
1	100	3	Group 1 to Group 2	4.473239	8.43629042	40.072	Means are not different		
2	104.4732	3	Group 1 to Group 3	1.544249	8.43629042	40.072	Means are not different		
3	98.45575	3	Group 1 to Group 4	2.995159	8.43629042	40.072	Means are not different		
4	97.00484	3	Group 1 to Group 5	1.591654	8.43629042	40.072	Means are not different		
5	98.40835	3	Group 1 to Group 6	1.540029	8.43629042	40.072	Means are not different		
6	101.54	3	Group 2 to Group 3	6.017488	8.43629042	40.072	Means are not different		
Other Data			Group 2 to Group 4	7.468398	8.43629042	40.072	Means are not different		
			Group 2 to Group 5	6.064893	8.43629042	40.072	Means are not different		
Level of significance	0.05		Group 2 to Group 6	2.93321	8.43629042	40.072	Means are not different		
Numerator d.f.	6		Group 3 to Group 4	1.450911	8.43629042	40.072	Means are not different		
Denominator d.f.	12		Group 3 to Group 5	0.047406	8.43629042	40.072	Means are not different		
MSW	213.513		Group 3 to Group 6	3.084278	8.43629042	40.072	Means are not different		
Q Statistic	4.75		Group 4 to Group 5	1.403505	8.43629042	40.072	Means are not different		
			Group 4 to Group 6	4.535189	8.43629042	40.072	Means are not different		
			Group 5 to Group 6	3.131684	8.43629042	40.072	Means are not different		

Anova: Single Factor						
SUMMARY						
Groups	Count	Sum	Average	Variance		
Column 1	3	300	100	0		
Column 2	3	313.4197169	104.473239	47.63410679		
Column 3	3	295.3672535	98.45575115	101.3895932		
Column 4	3	291.0145216	97.00484053	218.5048053		
Column 5	3	295.2250367	98.40834556	462.5940795		
Column 6	3	304.6200884	101.5400295	450.9553442		
ANOVA						
Source of Variation	SS	df	MS	F	P-value	F crit
Between Groups	108.8048813	5	21.76097626	0.101918747	0.989823083	3.105875239
Within Groups	2562.155858	12	213.5129882			
Total	2670.960739	17				

MTT N2A/ND-COONa Concentrations:

1-0 µg/ml
2-5 µg/ml
3-10 µg/ml
4-25 µg/ml
5-50 µg/ml
6-100 µg/ml

ND-COONa								
Group	Sample Mean	Sample Size	Comparison	Absolute Difference	Std. Error of Difference	Critical Range	Results	
1	100	3	Group 1 to Group 2	3.658353	3.50603126	16.654	Means are not different	
2	103.6584	3	Group 1 to Group 3	2.089857	3.50603126	16.654	Means are not different	
3	97.91014	3	Group 1 to Group 4	2.800836	3.50603126	16.654	Means are not different	
4	97.19916	3	Group 1 to Group 5	4.970652	3.50603126	16.654	Means are not different	
5	95.02935	3	Group 1 to Group 6	7.030229	3.50603126	16.654	Means are not different	
6	92.96977	3	Group 2 to Group 3	5.74821	3.50603126	16.654	Means are not different	
Other Data			Group 2 to Group 4	6.459189	3.50603126	16.654	Means are not different	
			Group 2 to Group 5	8.629005	3.50603126	16.654	Means are not different	
			Group 2 to Group 6	10.68858	3.50603126	16.654	Means are not different	
			Group 3 to Group 4	0.710979	3.50603126	16.654	Means are not different	
			Group 3 to Group 5	2.880795	3.50603126	16.654	Means are not different	
			Group 3 to Group 6	4.940372	3.50603126	16.654	Means are not different	
Level of significance	0.05		Group 4 to Group 5	2.169816	3.50603126	16.654	Means are not different	
Numerator d.f.	6		Group 4 to Group 6	4.229393	3.50603126	16.654	Means are not different	
Denominator d.f.	12		Group 5 to Group 6	2.059577	3.50603126	16.654	Means are not different	
MSW	36.87677							
Q Statistic	4.75							

Anova: Single Factor						
SUMMARY						
Groups	Count	Sum	Average	Variance		
Column 1	3	300	100	0		
Column 2	3	310.9750589	103.658353	69.01907087		
Column 3	3	293.730429	97.91014301	32.16943736		
Column 4	3	291.5974917	97.19916392	100.5644553		
Column 5	3	285.0880434	95.02934779	19.43076555		
Column 6	3	278.9093116	92.96977055	0.076864178		
ANOVA						
Source of Variation	SS	df	MS	F	P-value	F crit
Between Groups	211.6226441	5	42.32452882	1.14772888	0.388241119	3.105875239
Within Groups	442.5211866	12	36.87676555			
Total	654.1438307	17				

MTT N2A/ND-SO3Na Concentrations:

1-0 µg/ml
 2-5 µg/ml
 3-10 µg/ml
 4-25 µg/ml
 5-50 µg/ml
 6-100 µg/ml

ND-SO3Na							
Group	Sample Mean	Sample Size	Comparison	Absolute Difference	Std. Error of Difference	Critical Range	Results
1	100	3	Group 1 to Group 2	3.439372	3.08863531	14.671	Means are not different
2	96.56063	3	Group 1 to Group 3	3.084106	3.08863531	14.671	Means are not different
3	96.91589	3	Group 1 to Group 4	1.574298	3.08863531	14.671	Means are not different
4	98.4257	3	Group 1 to Group 5	2.583769	3.08863531	14.671	Means are not different
5	102.5838	3	Group 1 to Group 6	5.834067	3.08863531	14.671	Means are not different
6	105.8341	3	Group 2 to Group 3	0.355266	3.08863531	14.671	Means are not different
Other Data			Group 2 to Group 4	1.865074	3.08863531	14.671	Means are not different
			Group 2 to Group 5	6.023141	3.08863531	14.671	Means are not different
			Group 2 to Group 6	9.273439	3.08863531	14.671	Means are not different
			Group 3 to Group 4	1.509808	3.08863531	14.671	Means are not different
			Group 3 to Group 5	5.657875	3.08863531	14.671	Means are not different
			Group 3 to Group 6	8.918173	3.08863531	14.671	Means are not different
Level of significance	0.05		Group 4 to Group 5	4.158067	3.08863531	14.671	Means are not different
Numerator d.f.	6		Group 4 to Group 6	7.408365	3.08863531	14.671	Means are not different
Denominator d.f.	12		Group 5 to Group 6	3.250298	3.08863531	14.671	Means are not different
MSW	28.619						
Q Statistic	4.75						

Anova: Single Factor						
SUMMARY						
Groups	Count	Sum	Average	Variance		
Column 1	3	300	100	0		
Column 2	3	289.6818841	96.56062804	16.611913		
Column 3	3	290.7476831	96.91589435	15.74780323		
Column 4	3	295.2771061	98.42570203	58.92411983		
Column 5	3	307.7513079	102.5837693	7.044816266		
Column 6	3	317.5022016	105.8340672	73.38537287		
ANOVA						
Source of Variation	SS	df	MS	F	P-value	F crit
Between Groups	193.5435962	5	38.70871925	1.352552974	0.308156257	3.105875239
Within Groups	343.4280504	12	28.6190042			
Total	536.9716466	17				

MTT N2A/CdO Concentrations:

1-0 µg/ml

2-5 µg/ml

3-10 µg/ml

4-25 µg/ml

5-50 µg/ml

CdO							
Group	Sample Mean	Sample Size	Comparison	Absolute Difference	Std. Error of Difference	Critical Range	Results
1	100	3	Group 1 to Group 2	85.37333	2.97892115	13.882	Means are different
2	14.62667	3	Group 1 to Group 3	86.29	2.97892115	13.882	Means are different
3	13.71	3	Group 1 to Group 4	98.47134	2.97892115	13.882	Means are different
4	1.528661	3	Group 1 to Group 5	98.4355	2.97892115	13.882	Means are different
5	1.564498	3	Group 2 to Group 3	0.916667	2.97892115	13.882	Means are not different
Other Data			Group 2 to Group 4	13.09801	2.97892115	13.882	Means are not different
			Group 2 to Group 5	13.06217	2.97892115	13.882	Means are not different
Level of significance			Group 3 to Group 4	12.18134	2.97892115	13.882	Means are not different
Numerator d.f.			Group 3 to Group 5	12.1455	2.97892115	13.882	Means are not different
Denominator d.f.			Group 4 to Group 5	0.035837	2.97892115	13.882	Means are not different
MSW							
Q Statistic							

Anova: Single Factor						
SUMMARY						
Groups	Count	Sum	Average	Variance		
Column 1	3	300	100	0		
Column 2	3	43.88	14.62666667	27.20343333		
Column 3	3	41.13	13.71	105.8623		
Column 4	3	4.585982767	1.528660922	0.015451056		
Column 5	3	4.693494601	1.5644982	0.028384323		
ANOVA						
Source of Variation	SS	df	MS	F	P-value	F crit
Between Groups	20855.78435	4	5213.946086	195.8516633	1.88837E-09	3.478049691
Within Groups	266.2191374	10	26.62191374			
Total	21122.00348	14				

MTT N2A/T-ND Concentrations:

1-0 µg/ml
 2-5 µg/ml
 3-10 µg/ml
 4-25 µg/ml
 5-50 µg/ml
 6-100 µg/ml

N2A and ND-TAMRA									
Group	Sample Mean	Sample Size	Comparison	Absolute Difference	Std. Error of Difference	Critical Range	Results		
1	100	3	Group 1 to Group 2	0.712052	3.42099842	16.25	Means are not different		
2	99.28795	3	Group 1 to Group 3	3.652088	3.42099842	16.25	Means are not different		
3	96.33791	3	Group 1 to Group 4	2.158197	3.42099842	16.25	Means are not different		
4	102.1582	3	Group 1 to Group 5	0.058368	3.42099842	16.25	Means are not different		
5	100.0584	3	Group 1 to Group 6	1.531037	3.42099842	16.25	Means are not different		
6	101.531	3	Group 2 to Group 3	2.950036	3.42099842	16.25	Means are not different		
			Group 2 to Group 4	2.870249	3.42099842	16.25	Means are not different		
			Group 2 to Group 5	0.77042	3.42099842	16.25	Means are not different		
			Group 2 to Group 6	2.243089	3.42099842	16.25	Means are not different		
			Group 3 to Group 4	5.820284	3.42099842	16.25	Means are not different		
			Group 3 to Group 5	3.720456	3.42099842	16.25	Means are not different		
			Group 3 to Group 6	5.193125	3.42099842	16.25	Means are not different		
			Group 4 to Group 5	2.099829	3.42099842	16.25	Means are not different		
			Group 4 to Group 6	0.62716	3.42099842	16.25	Means are not different		
			Group 5 to Group 6	1.472669	3.42099842	16.25	Means are not different		
Other Data									
Level of significance	0.05								
Numerator d.f.	6								
Denominator d.f.	12								
MSW	35.10969								
Q Statistic	4.75								

Anova: Single Factor						
SUMMARY						
Groups	Count	Sum	Average	Variance		
Column 1	3	300	100	0		
Column 2	3	297.863844	99.28794801	54.11690684		
Column 3	3	289.0137369	96.33791231	7.055351752		
Column 4	3	306.4745902	102.1581967	0.546096413		
Column 5	3	300.1751044	100.0583681	143.7371355		
Column 6	3	304.5931115	101.5310372	5.202652928		
ANOVA						
Source of Variation	SS	df	MS	F	P-value	F crit
Between Groups	62.57332261	5	12.51466452	0.35644474	0.86842632	3.105875239
Within Groups	421.3162868	12	35.10969056			
Total	483.8896094	17				

MTT HaCat/T-ND Concentrations:

1-0 µg/ml
2-5 µg/ml
3-10 µg/ml
4-25 µg/ml
5-50 µg/ml
6-100 µg/ml

HaCat and ND-TAMRA						
Group	Sample Mean	Sample Size	Comparison	Absolute Difference	Std. Error of Difference	Critical Range Results
1	100	3	Group 1 to Group 2	12.22892	4.33493531	20.591 Means are not different
2	87.77108	3	Group 1 to Group 3	2.50502	4.33493531	20.591 Means are not different
3	97.49498	3	Group 1 to Group 4	1.420683	4.33493531	20.591 Means are not different
4	98.57932	3	Group 1 to Group 5	15.02175	4.33493531	20.591 Means are not different
5	84.97825	3	Group 1 to Group 6	4.665328	4.33493531	20.591 Means are not different
6	95.33467	3	Group 2 to Group 3	9.723896	4.33493531	20.591 Means are not different
Other Data			Group 2 to Group 4	10.80823	4.33493531	20.591 Means are not different
			Group 2 to Group 5	2.792838	4.33493531	20.591 Means are not different
			Group 2 to Group 6	7.563588	4.33493531	20.591 Means are not different
			Group 3 to Group 4	1.084337	4.33493531	20.591 Means are not different
			Group 3 to Group 5	12.51673	4.33493531	20.591 Means are not different
Level of significance	0.05		Group 3 to Group 6	2.160308	4.33493531	20.591 Means are not different
Numerator d.f.	6		Group 4 to Group 5	13.60107	4.33493531	20.591 Means are not different
Denominator d.f.	12		Group 4 to Group 6	3.244645	4.33493531	20.591 Means are not different
MSW	56.37499		Group 5 to Group 6	10.35643	4.33493531	20.591 Means are not different
Q Statistic	4.75					

Anova: Single Factor						
SUMMARY						
Groups	Count	Sum	Average	Variance		
Column 1	3	300	100	0		
Column 2	3	263.313253	87.77108434	67.08793003		
Column 3	3	292.4849398	97.49497992	149.3390984		
Column 4	3	295.7379518	98.57931727	7.151069136		
Column 5	3	254.934739	84.97824632	22.4035281		
Column 6	3	286.0040161	95.33467202	92.26832867		
ANOVA						
Source of Variation	SS	df	MS	F	P-value	F crit
Between Groups	573.4609021	5	114.6921804	2.034451369	0.145478015	3.105875239
Within Groups	676.4999086	12	56.37499238			
Total	1249.960811	17				

MTT Mac/T-ND Concentrations:

1-0 µg/ml
 2-5 µg/ml
 3-10 µg/ml
 4-25 µg/ml
 5-50 µg/ml
 6-100 µg/ml

Mac							
Group	Sample Mean	Sample Size	Comparison	Absolute Difference	Std. Error of Difference	Critical Range	Results
1	100	3	Group 1 to Group 2	7.705742	3.30115372	15.68	Means are not different
2	92.29426	3	Group 1 to Group 3	3.891826	3.30115372	15.68	Means are not different
3	96.10817	3	Group 1 to Group 4	2.629252	3.30115372	15.68	Means are not different
4	102.6293	3	Group 1 to Group 5	9.891156	3.30115372	15.68	Means are not different
5	90.10884	3	Group 1 to Group 6	13.92517	3.30115372	15.68	Means are not different
6	86.07483	3	Group 2 to Group 3	3.813916	3.30115372	15.68	Means are not different
Other Data			Group 2 to Group 4	10.33499	3.30115372	15.68	Means are not different
			Group 2 to Group 5	2.185415	3.30115372	15.68	Means are not different
			Group 2 to Group 6	6.219428	3.30115372	15.68	Means are not different
			Group 3 to Group 4	6.521078	3.30115372	15.68	Means are not different
			Group 3 to Group 5	5.999331	3.30115372	15.68	Means are not different
			Group 3 to Group 6	10.03334	3.30115372	15.68	Means are not different
			Group 4 to Group 5	12.52041	3.30115372	15.68	Means are not different
			Group 4 to Group 6	16.55442	3.30115372	15.68	Means are different
Level of significance	0.05		Group 5 to Group 6	4.034014	3.30115372	15.68	Means are not different
Numerator d.f.	6						
Denominator d.f.	12						
MSW	32.69285						
Q Statistic	4.75						

Anova: Single Factor					
SUMMARY					
Groups	Count	Sum	Average	Variance	
Column 1	3	300	100	0	
Column 2	3	276.8827744	92.29425813	0.718126529	
Column 3	3	288.3245223	96.10817411	0.868329237	
Column 4	3	307.8877551	102.6292517	0.013269934	
Column 5	3	270.3265306	90.10884354	5.009625619	
Column 6	3	258.2244898	86.07482993	189.5477347	
ANOVA					
Source of Variation	SS	df	MS	F	P-value
Between Groups	582.132811	5	116.4265622	3.561224258	0.033165177
Within Groups	392.3141721	12	32.69284768		
Total	974.4469831	17			
F crit					
					3.105875239

ROS N2A/CB Concentrations:

1-0 µg/ml
2-5 µg/ml
3-10 µg/ml
4-25 µg/ml
5-50 µg/ml
6-100 µg/ml

CB ROS							
Group	Sample Mean	Sample Size	Comparison	Absolute Difference	Std. Error of Difference	Critical Range	Results
1	1	3	Group 1 to Group 2	0.003455	0.05935024	0.2819	Means are not different
2	0.996545	3	Group 1 to Group 3	0.117189	0.05935024	0.2819	Means are not different
3	1.117189	3	Group 1 to Group 4	0.467826	0.05935024	0.2819	Means are different
4	1.467826	3	Group 1 to Group 5	0.179084	0.05935024	0.2819	Means are not different
5	1.179084	3	Group 1 to Group 6	0.087831	0.05935024	0.2819	Means are not different
6	0.912169	3	Group 2 to Group 3	0.120644	0.05935024	0.2819	Means are not different
Other Data			Group 2 to Group 4	0.471281	0.05935024	0.2819	Means are different
			Group 2 to Group 5	0.182538	0.05935024	0.2819	Means are not different
			Group 2 to Group 6	0.084376	0.05935024	0.2819	Means are not different
			Group 3 to Group 4	0.350637	0.05935024	0.2819	Means are different
			Group 3 to Group 5	0.061895	0.05935024	0.2819	Means are not different
Level of significance	0.05		Group 3 to Group 6	0.20502	0.05935024	0.2819	Means are not different
Numerator d.f.	6		Group 4 to Group 5	0.288742	0.05935024	0.2819	Means are different
Denominator d.f.	12		Group 4 to Group 6	0.555657	0.05935024	0.2819	Means are different
MSW	0.010567		Group 5 to Group 6	0.266915	0.05935024	0.2819	Means are not different
Q Statistic	4.75						

Anova: Single Factor						
SUMMARY						
Groups	Count	Sum	Average	Variance		
Column 1	3	3	1	0		
Column 2	3	2.989635781	0.99654526	0.001112218		
Column 3	3	3.351567303	1.117189101	0.00055505		
Column 4	3	4.403477503	1.467825834	0.033695972		
Column 5	3	3.537251246	1.179083749	0.026417693		
Column 6	3	2.736507446	0.912169149	0.001623184		
ANOVA						
Source of Variation	SS	df	MS	F	P-value	F crit
Between Groups	0.590835709	5	0.118167142	11.18228417	0.000348958	3.105875239
Within Groups	0.126808233	12	0.010567353			
Total	0.717643942	17				

ROS/N2A ND-row concentrations:

1-0 µg/ml
2-10 µg/ml
3-25 µg/ml
4-50 µg/ml
5-100 µg/ml

ND-row							
Group	Sample Mean	Sample Size	Comparison	Absolute Difference	Std. Error of Difference	Critical Range	Results
1		3	Group 1 to Group 2	0.240598	0.14520692	0.6767	Means are not different
2	0.759402	3	Group 1 to Group 3	0.269304	0.14520692	0.6767	Means are not different
3	0.730696	3	Group 1 to Group 4	0.33073	0.14520692	0.6767	Means are not different
4	0.66927	3	Group 1 to Group 5	0.378634	0.14520692	0.6767	Means are not different
5	0.621366	3	Group 2 to Group 3	0.028705	0.14520692	0.6767	Means are not different
Other Data			Group 2 to Group 4	0.090132	0.14520692	0.6767	Means are not different
Level of significance			Group 2 to Group 5	0.138035	0.14520692	0.6767	Means are not different
Numerator d.f.			Group 3 to Group 4	0.061426	0.14520692	0.6767	Means are not different
Denominator d.f.			Group 3 to Group 5	0.10933	0.14520692	0.6767	Means are not different
MSW			Group 4 to Group 5	0.047904	0.14520692	0.6767	Means are not different
Q Statistic							

Anova: Single Factor						
SUMMARY						
Groups	Count	Sum	Average	Variance		
Column 1	3	3	1	0		
Column 2	3	2.278205181	0.759401727	0.033270703		
Column 3	3	2.192088288	0.730696096	0.058983406		
Column 4	3	2.007809898	0.669269966	0.105130678		
Column 5	3	1.86409907	0.621366357	0.118890948		
ANOVA						
Source of Variation	SS	df	MS	F	P-value	F crit
Between Groups	0.257508205	4	0.064377051	1.017736172	0.443550264	3.478049691
Within Groups	0.63255147	10	0.063255147			
Total	0.890059675	14				

ROS/N2A ND-COOH concentrations:

1-0 µg/ml
2-10 µg/ml
3-25 µg/ml
4-50 µg/ml
5-100 µg/ml

ND-COOH									
Group	Sample Mean	Sample Size	Comparison	Absolute Difference	Std. Error of Difference	Critical Range	Results		
1	1	3	Group 1 to Group 2	0.131162	0.0604746	0.2818	Means are not different		
2	0.868838	3	Group 1 to Group 3	0.09562	0.0604746	0.2818	Means are not different		
3	0.90438	3	Group 1 to Group 4	0.084737	0.0604746	0.2818	Means are not different		
4	0.915263	3	Group 1 to Group 5	0.113887	0.0604746	0.2818	Means are not different		
5	0.886113	3	Group 2 to Group 3	0.035542	0.0604746	0.2818	Means are not different		
Other Data			Group 2 to Group 4	0.046425	0.0604746	0.2818	Means are not different		
Level of significance			Group 2 to Group 5	0.017275	0.0604746	0.2818	Means are not different		
Numerator d.f.			Group 3 to Group 4	0.010883	0.0604746	0.2818	Means are not different		
Denominator d.f.			Group 3 to Group 5	0.018267	0.0604746	0.2818	Means are not different		
MSW			Group 4 to Group 5	0.02915	0.0604746	0.2818	Means are not different		
Q Statistic									

Anova: Single Factor							
SUMMARY							
Groups	Count	Sum	Average	Variance			
Column 1	3	3	1	0			
Column 2	3	2.606513937	0.868837979	1.15002E-06			
Column 3	3	2.71313877	0.90437959	0.016371281			
Column 4	3	2.745788695	0.915262898	0.025364825			
Column 5	3	2.658338532	0.886112844	0.013120411			
ANOVA							
Source of Variation	SS	df	MS	F	P-value	F crit	
Between Groups	0.030909687	4	0.007727422	0.704315574	0.606789898	3.478049691	
Within Groups	0.109715334	10	0.010971533				
Total	0.140625021	14					

ROS/N2A ND-COONa concentrations:

1-0 µg/ml
2-10 µg/ml
3-25 µg/ml
4-50 µg/ml
5-100 µg/ml

ND-COONa							
Group	Sample Mean	Sample Size	Comparison	Absolute Difference	Std. Error of Difference	Critical Range	Results
1	1	3	Group 1 to Group 2	0.074965	0.11667811	0.5437	Means are not different
2	1.074965	3	Group 1 to Group 3	0.054451	0.11667811	0.5437	Means are not different
3	1.054451	3	Group 1 to Group 4	0.203795	0.11667811	0.5437	Means are not different
4	0.796205	3	Group 1 to Group 5	0.475011	0.11667811	0.5437	Means are not different
5	0.524989	3	Group 2 to Group 3	0.020514	0.11667811	0.5437	Means are not different
			Group 2 to Group 4	0.27876	0.11667811	0.5437	Means are not different
			Group 2 to Group 5	0.549976	0.11667811	0.5437	Means are different
			Group 3 to Group 4	0.258246	0.11667811	0.5437	Means are not different
			Group 3 to Group 5	0.529462	0.11667811	0.5437	Means are not different
			Group 4 to Group 5	0.271216	0.11667811	0.5437	Means are not different
Other Data							
Level of significance	0.05						
Numerator d.f.	5						
Denominator d.f.	10						
MSW	0.040841						
Q Statistic	4.66						

Anova: Single Factor						
SUMMARY						
Groups	Count	Sum	Average	Variance		
Column 1	3	3	1	0		
Column 2	3	3.224895556	1.074965185	0.037748346		
Column 3	3	3.163352316	1.054450772	0.000267555		
Column 4	3	2.388614984	0.796204995	0.001622899		
Column 5	3	1.574967317	0.524989106	0.164567912		
ANOVA						
Source of Variation	SS	df	MS	F	P-value	F crit
Between Groups	0.646159673	4	0.161539918	3.955303843	0.035402048	3.478049691
Within Groups	0.408413423	10	0.040841342			
Total	1.054573096	14				

ROS/N2A ND-SO₃Na Concentrations:

1-0 µg/ml
2-10 µg/ml
3-25 µg/ml
4-50 µg/ml
5-100 µg/ml

ND-SO ₃ Na									
Group	Sample Mean	Sample Size	Comparison	Absolute Difference	Std. Error of Difference	Critical Range	Results		
1		3	Group 1 to Group 2	0.105273	0.11482663	0.5351	Means are not different		
2	0.894727	3	Group 1 to Group 3	0.002929	0.11482663	0.5351	Means are not different		
3	0.997071	3	Group 1 to Group 4	0.106899	0.11482663	0.5351	Means are not different		
4	1.106899	3	Group 1 to Group 5	0.016433	0.11482663	0.5351	Means are not different		
5	1.016433	3	Group 2 to Group 3	0.102344	0.11482663	0.5351	Means are not different		
			Group 2 to Group 4	0.212173	0.11482663	0.5351	Means are not different		
			Group 2 to Group 5	0.121706	0.11482663	0.5351	Means are not different		
			Group 3 to Group 4	0.109829	0.11482663	0.5351	Means are not different		
			Group 3 to Group 5	0.019362	0.11482663	0.5351	Means are not different		
			Group 4 to Group 5	0.090466	0.11482663	0.5351	Means are not different		
Other Data									
Level of significance 0.05									
Numerator d.f. 5									
Denominator d.f. 10									
MSW 0.039555									
Q Statistic 4.66									

Anova: Single Factor						
SUMMARY						
Groups	Count	Sum	Average	Variance		
Column 1	3	3	1	0		
Column 2	3	2.684180328	0.894726776	0.03523957		
Column 3	3	2.991211903	0.997070634	0.011773882		
Column 4	3	3.320697998	1.106899333	0.121194962		
Column 5	3	3.049299384	1.016433128	0.029568905		
ANOVA						
Source of Variation	SS	df	MS	F	P-value	F crit
Between Groups	0.068228296	4	0.017057074	0.431219163	0.783247331	3.478049691
Within Groups	0.395554639	10	0.039555464			
Total	0.463782935	14				

MTT/N2A Ag13 Concentrations

1-0 µg/ml
 2-5 µg/ml
 3-10 µg/ml
 4-25 µg/ml
 5-50 µg/ml
 6-100 µg/ml

Ag13								
Group	Sample Mean	Sample Size	Comparison	Absolute Difference	Std. Error of Difference	Critical Range	Results	
1	100	3	Group 1 to Group 2	17.01145	4.20970908	19.996	Means are not different	
2	82.98855	3	Group 1 to Group 3	23.1812	4.20970908	19.996	Means are different	
3	76.8188	3	Group 1 to Group 4	46.20055	4.20970908	19.996	Means are different	
4	53.79945	3	Group 1 to Group 5	72.40833	4.20970908	19.996	Means are different	
5	27.59167	3	Group 1 to Group 6	86.2327	4.20970908	19.996	Means are different	
6	13.7673	3	Group 2 to Group 3	6.169752	4.20970908	19.996	Means are not different	
Other Data			Group 2 to Group 4	29.1891	4.20970908	19.996	Means are different	
			Group 2 to Group 5	55.39687	4.20970908	19.996	Means are different	
			Group 2 to Group 6	69.22125	4.20970908	19.996	Means are different	
			Group 3 to Group 4	23.01935	4.20970908	19.996	Means are different	
			Group 3 to Group 5	49.22712	4.20970908	19.996	Means are different	
			Group 3 to Group 6	63.05149	4.20970908	19.996	Means are different	
			Group 4 to Group 5	26.20777	4.20970908	19.996	Means are different	
Level of significance	0.05		Group 4 to Group 6	40.03215	4.20970908	19.996	Means are different	
Numerator d.f.	6		Group 5 to Group 6	13.82437	4.20970908	19.996	Means are not different	
Denominator d.f.	12							
MSW	53.16495							
Q Statistic	4.75							

Anova: Single Factor						
SUMMARY						
Groups	Count	Sum	Average	Variance		
Column 1	3	300	100	0		
Column 2	3	248.9656413	82.9885471	202.4857513		
Column 3	3	230.4563854	76.81879512	95.90051052		
Column 4	3	161.3983425	53.79944751	2.215703448		
Column 5	3	82.77502071	27.59167357	11.30277956		
Column 6	3	41.30190569	13.7673019	7.084964603		
ANOVA						
Source of Variation	SS	df	MS	F	P-value	F crit
Between Groups	16899.99028	5	3379.998056	63.57568203	3.24009E-08	3.105875239
Within Groups	637.9794189	12	53.16495157			
Total	17537.9697	17				

MTT/N2A Ag28 Concentrations

1-0 µg/ml
 2-5 µg/ml
 3-10 µg/ml
 4-25 µg/ml
 5-50 µg/ml
 6-100 µg/ml

Ag28							
Group	Sample Mean	Sample Size	Comparison	Absolute Difference	Std. Error of Difference	Critical Range	Results
1	100	3	Group 1 to Group 2	3.18708	0.21666063	1.0291	Means are different
2	96.81292	3	Group 1 to Group 3	13.48679	0.21666063	1.0291	Means are different
3	86.51321	3	Group 1 to Group 4	29.42282	0.21666063	1.0291	Means are different
4	70.57718	3	Group 1 to Group 5	52.38251	0.21666063	1.0291	Means are different
5	47.61749	3	Group 1 to Group 6	72.50674	0.21666063	1.0291	Means are different
6	27.49326	3	Group 2 to Group 3	10.29971	0.21666063	1.0291	Means are different
Other Data			Group 2 to Group 4	26.23574	0.21666063	1.0291	Means are different
Level of significance			Group 2 to Group 5	49.19543	0.21666063	1.0291	Means are different
Numerator d.f.			Group 2 to Group 6	69.31966	0.21666063	1.0291	Means are different
Denominator d.f.			Group 3 to Group 4	15.93603	0.21666063	1.0291	Means are different
MSW			Group 3 to Group 5	38.89572	0.21666063	1.0291	Means are different
Q Statistic			Group 3 to Group 6	59.01995	0.21666063	1.0291	Means are different
			Group 4 to Group 5	22.95969	0.21666063	1.0291	Means are different
			Group 4 to Group 6	43.08392	0.21666063	1.0291	Means are different
			Group 5 to Group 6	20.12423	0.21666063	1.0291	Means are different

Anova: Single Factor						
SUMMARY						
Groups	Count	Sum	Average	Variance		
Column 1	3	300	100	0		
Column 2	3	290.4387586	96.81291954	0.373320755		
Column 3	3	259.5396288	86.5132096	0.235277613		
Column 4	3	211.7315388	70.5771796	0.189446269		
Column 5	3	142.8524613	47.61748711	0.023972931		
Column 6	3	82.47976581	27.49325527	0.022935342		
ANOVA						
Source of Variation	SS	df	MS	F	P-value	F crit
Between Groups	12558.62978	5	2511.725956	17835.73445	8.69603E-23	3.105875239
Within Groups	1.689905821	12	0.140825485			
Total	12560.31969	17				

MTT/N2A Ag43 Concentrations

1-0 µg/ml
 2-5 µg/ml
 3-10 µg/ml
 4-25 µg/ml
 5-50 µg/ml
 6-100 µg/ml

Ag43							
Group	Sample Mean	Sample Size	Comparison	Absolute Difference	Std. Error of Difference	Critical Range	Results
1	100	3	Group 1 to Group 2	0.130569	0.29375203	1.3953	Means are not different
2	100.1306	3	Group 1 to Group 3	3.380374	0.29375203	1.3953	Means are different
3	103.3804	3	Group 1 to Group 4	8.367418	0.29375203	1.3953	Means are different
4	91.63258	3	Group 1 to Group 5	7.072851	0.29375203	1.3953	Means are different
5	92.92715	3	Group 1 to Group 6	56.8399	0.29375203	1.3953	Means are different
6	43.1601	3	Group 2 to Group 3	3.249805	0.29375203	1.3953	Means are different
Other Data			Group 2 to Group 4	8.497987	0.29375203	1.3953	Means are different
			Group 2 to Group 5	7.20342	0.29375203	1.3953	Means are different
			Group 2 to Group 6	56.97047	0.29375203	1.3953	Means are different
			Group 3 to Group 4	11.74779	0.29375203	1.3953	Means are different
			Group 3 to Group 5	10.45323	0.29375203	1.3953	Means are different
			Group 3 to Group 6	60.22027	0.29375203	1.3953	Means are different
Level of significance	0.05		Group 4 to Group 5	1.294567	0.29375203	1.3953	Means are not different
Numerator d.f.	6		Group 4 to Group 6	48.47248	0.29375203	1.3953	Means are different
Denominator d.f.	12		Group 5 to Group 6	49.76705	0.29375203	1.3953	Means are different
MSW	0.258871						
Q Statistic	4.75						

Anova: Single Factor						
SUMMARY						
Groups	Count	Sum	Average	Variance		
Column 1	3	300	100	0		
Column 2	3	300.3917084	100.1305695	0.407043608		
Column 3	3	310.1411231	103.3803744	0.415804291		
Column 4	3	274.8977475	91.63258249	0.217666078		
Column 5	3	278.7814474	92.92714913	0.285181106		
Column 6	3	129.4803101	43.16010338	0.227529492		
ANOVA						
Source of Variation	SS	df	MS	F	P-value	F crit
Between Groups	7722.167276	5	1544.433455	5966.040505	6.19588E-20	3.105875239
Within Groups	3.106449151	12	0.258870763			
Total	7725.273725	17				

MTT/N2A Ag10Disp Concentrations

1-0 µg/ml
 2-5 µg/ml
 3-10 µg/ml
 4-25 µg/ml
 5-50 µg/ml
 6-100 µg/ml

Ag10Disp								
Group	Sample Mean	Sample Size	Comparison	Absolute Difference	Std. Error of Difference	Critical Range	Results	
1	100	3	Group 1 to Group 2	2.72347	0.5877652	2.7919	Means are not different	
2	102.7235	3	Group 1 to Group 3	7.090582	0.5877652	2.7919	Means are different	
3	107.0906	3	Group 1 to Group 4	35.11253	0.5877652	2.7919	Means are different	
4	64.88747	3	Group 1 to Group 5	83.39609	0.5877652	2.7919	Means are different	
5	16.60391	3	Group 1 to Group 6	99.06569	0.5877652	2.7919	Means are different	
6	0.93431	3	Group 2 to Group 3	4.367112	0.5877652	2.7919	Means are different	
Other Data			Group 2 to Group 4	37.836	0.5877652	2.7919	Means are different	
			Group 2 to Group 5	86.11956	0.5877652	2.7919	Means are different	
Level of significance	0.05		Group 2 to Group 6	101.7892	0.5877652	2.7919	Means are different	
Numerator d.f.	6		Group 3 to Group 4	42.20312	0.5877652	2.7919	Means are different	
Denominator d.f.	12		Group 3 to Group 5	90.48668	0.5877652	2.7919	Means are different	
MSW	1.036404		Group 3 to Group 6	106.1563	0.5877652	2.7919	Means are different	
Q Statistic	4.75		Group 4 to Group 5	48.28356	0.5877652	2.7919	Means are different	
			Group 4 to Group 6	63.95316	0.5877652	2.7919	Means are different	
			Group 5 to Group 6	15.6696	0.5877652	2.7919	Means are different	

Anova: Single Factor						
SUMMARY						
Groups	Count	Sum	Average	Variance		
Column 1	3	300	100	0		
Column 2	3	308.1704102	102.7234701	2.230974007		
Column 3	3	321.2717473	107.0905824	3.635231905		
Column 4	3	194.6624014	64.88746713	0.046193374		
Column 5	3	49.81172009	16.6039067	0.21819768		
Column 6	3	2.80292876	0.934309587	0.087825871		
ANOVA						
Source of Variation	SS	df	MS	F	P-value	F crit
Between Groups	32596.34536	5	6519.269071	6290.278974	4.51093E-20	3.105875239
Within Groups	12.43684567	12	1.036403806			
Total	32608.7822	17				

MTT/N2A Ag26Disp Concentrations

1-0 µg/ml
 2-5 µg/ml
 3-10 µg/ml
 4-25 µg/ml
 5-50 µg/ml
 6-100 µg/ml

Ag26Disp									
Group	Sample Mean	Sample Size	Comparison	Absolute Difference	Std. Error of Difference	Critical Range	Results		
1	100	3	Group 1 to Group 2	3.99951	0.53120661	2.5232	Means are different		
2	96.00049	3	Group 1 to Group 3	0.057387	0.53120661	2.5232	Means are not different		
3	99.94261	3	Group 1 to Group 4	2.912575	0.53120661	2.5232	Means are different		
4	97.08743	3	Group 1 to Group 5	14.13584	0.53120661	2.5232	Means are different		
5	85.86416	3	Group 1 to Group 6	30.28928	0.53120661	2.5232	Means are different		
6	69.71072	3	Group 2 to Group 3	3.942123	0.53120661	2.5232	Means are different		
			Group 2 to Group 4	1.086935	0.53120661	2.5232	Means are not different		
Other Data			Group 2 to Group 5	10.13633	0.53120661	2.5232	Means are different		
Level of significance			Group 2 to Group 6	26.28977	0.53120661	2.5232	Means are different		
Numerator d.f.			Group 3 to Group 4	2.855188	0.53120661	2.5232	Means are different		
Denominator d.f.			Group 3 to Group 5	14.07845	0.53120661	2.5232	Means are different		
MSW			Group 3 to Group 6	30.2319	0.53120661	2.5232	Means are different		
Q Statistic			Group 4 to Group 5	11.22327	0.53120661	2.5232	Means are different		
			Group 4 to Group 6	27.37671	0.53120661	2.5232	Means are different		
			Group 5 to Group 6	16.15344	0.53120661	2.5232	Means are different		

Anova: Single Factor						
SUMMARY						
Groups	Count	Sum	Average	Variance		
Column 1	3	300	100	0		
Column 2	3	288.0014697	96.00048992	1.139838516		
Column 3	3	299.8278398	99.94261326	0.971647786		
Column 4	3	291.2622756	97.08742519	1.14623964		
Column 5	3	257.5924788	85.8641596	1.54195344		
Column 6	3	209.1321503	69.71071676	0.279568994		
ANOVA						
Source of Variation	SS	df	MS	F	P-value	F crit
Between Groups	2104.533176	5	420.9066352	497.2073867	1.79074E-13	3.105875239
Within Groups	10.15849675	12	0.846541396			
Total	2114.691673	17				

MTT/N2A Ag52Disp Concentrations

1-0 µg/ml

2-5 µg/ml

3-10 µg/ml

4-25 µg/ml

5-50 µg/ml

6-100 µg/ml

Ag52Disp							
Group	Sample Mean	Sample Size	Comparison	Absolute Difference	Std. Error of Difference	Critical Range	Results
1	100	3	Group 1 to Group 2	4.111706	2.35463381	11.185	Means are not different
2	95.88829	3	Group 1 to Group 3	3.903181	2.35463381	11.185	Means are not different
3	103.9032	3	Group 1 to Group 4	10.23583	2.35463381	11.185	Means are not different
4	89.76417	3	Group 1 to Group 5	16.05134	2.35463381	11.185	Means are different
5	83.94866	3	Group 1 to Group 6	52.08687	2.35463381	11.185	Means are different
6	47.91313	3	Group 2 to Group 3	8.014887	2.35463381	11.185	Means are not different
Other Data			Group 2 to Group 4	6.124126	2.35463381	11.185	Means are not different
Level of significance			Group 2 to Group 5	11.93964	2.35463381	11.185	Means are different
Numerator d.f.			Group 2 to Group 6	47.97516	2.35463381	11.185	Means are different
Denominator d.f.			Group 3 to Group 4	14.13901	2.35463381	11.185	Means are different
MSW			Group 3 to Group 5	19.95452	2.35463381	11.185	Means are different
Q Statistic			Group 3 to Group 6	55.99005	2.35463381	11.185	Means are different
			Group 4 to Group 5	5.815511	2.35463381	11.185	Means are not different
			Group 4 to Group 6	41.85104	2.35463381	11.185	Means are different
			Group 5 to Group 6	36.03553	2.35463381	11.185	Means are different

Anova: Single Factor						
SUMMARY						
Groups	Count	Sum	Average	Variance		
Column 1	3	300	100	0		
Column 2	3	287.6648825	95.88829417	22.77346843		
Column 3	3	311.7095424	103.9031808	23.83665685		
Column 4	3	269.2925033	89.76416776	22.27121891		
Column 5	3	251.8459695	83.94865651	23.80490716		
Column 6	3	143.739392	47.91313066	7.111155335		
ANOVA						
Source of Variation	SS	df	MS	F	P-value	F crit
Between Groups	6235.192216	5	1247.038443	74.9741993	1.25419E-08	3.105875239
Within Groups	199.5948134	12	16.63290111			
Total	6434.787029	17				

MTT/N2A AgNO₃ Concentrations

1-0 µg/ml
2-0.1 µg/ml
3-0.5 µg/ml
4-1 µg/ml
5-2.5 µg/ml
6-5 µg/ml

AgNO ₃							
Group	Sample Mean	Sample Size	Comparison	Absolute Difference	Std. Error of Difference	Critical Range	Results
1	100	3	Group 1 to Group 2	3.181299	2.58292607	12.269	Means are not different
2	103.1813	3	Group 1 to Group 3	1.564078	2.58292607	12.269	Means are not different
3	101.5641	3	Group 1 to Group 4	97.84864	2.58292607	12.269	Means are different
4	2.15136	3	Group 1 to Group 5	98.55161	2.58292607	12.269	Means are different
5	1.448388	3	Group 1 to Group 6	97.19303	2.58292607	12.269	Means are different
6	2.806967	3	Group 2 to Group 3	1.61722	2.58292607	12.269	Means are not different
Other Data			Group 2 to Group 4	101.0299	2.58292607	12.269	Means are different
			Group 2 to Group 5	101.7329	2.58292607	12.269	Means are different
Level of significance	0.05		Group 2 to Group 6	100.3743	2.58292607	12.269	Means are different
Numerator d.f.	6		Group 3 to Group 4	99.41272	2.58292607	12.269	Means are different
Denominator d.f.	12		Group 3 to Group 5	100.1157	2.58292607	12.269	Means are different
MSW	20.01452		Group 3 to Group 6	98.75711	2.58292607	12.269	Means are different
Q Statistic	4.75		Group 4 to Group 5	0.702971	2.58292607	12.269	Means are not different
			Group 4 to Group 6	0.656607	2.58292607	12.269	Means are not different
			Group 5 to Group 6	1.358579	2.58292607	12.269	Means are not different

Anova: Single Factor						
SUMMARY						
Groups	Count	Sum	Average	Variance		
Column 1	3	300	100	0		
Column 2	3	309.5438957	103.1812986	10.27758711		
Column 3	3	304.692235	101.5640783	106.6652111		
Column 4	3	6.454078654	2.151359551	0.590938782		
Column 5	3	4.345164171	1.448388057	0.687310967		
Column 6	3	8.420899777	2.806966592	1.866079197		
ANOVA						
Source of Variation	SS	df	MS	F	P-value	F crit
Between Groups	44520.93096	5	8904.186192	444.8862955	3.47517E-13	3.105875239
Within Groups	240.1742544	12	20.0145212			
Total	44761.10521	17				

MTT/N2A/Polysaccharide Alone Concentrations

1-0 ng/ml

2-100 ng/ml

3-1000 ng/ml

4-10, 000 ng/ml

Polysaccharide									
Group	Sample Mean	Sample Size	Comparison	Absolute Difference	Std. Error of Difference	Critical Range	Results		
1	100	3	Group 1 to Group 2	1.096091	2.45311922	11.113	Means are not different		
2	101.0961	3	Group 1 to Group 3	8.092088	2.45311922	11.113	Means are not different		
3	108.0921	3	Group 1 to Group 4	2.115768	2.45311922	11.113	Means are not different		
4	102.1158	3	Group 2 to Group 3	6.995998	2.45311922	11.113	Means are not different		
			Group 2 to Group 4	1.019678	2.45311922	11.113	Means are not different		
			Group 3 to Group 4	5.97632	2.45311922	11.113	Means are not different		
Other Data									
Level of significance	0.05								
Numerator d.f.	4								
Denominator d.f.	8								
MSW	18.05338								
Q Statistic	4.53								

Anova: Single Factor						
SUMMARY						
Groups	Count	Sum	Average	Variance		
Column 1	3	300	100	0		
Column 2	3	303.2882723	101.0960908	70.0693577		
Column 3	3	324.2762652	108.0920884	1.994506854		
Column 4	3	306.3473053	102.1157684	0.149662084		
ANOVA						
Source of Variation	SS	df	MS	F	P-value	F crit
Between Groups	117.6449332	3	39.21497774	2.17216799	0.169216401	4.066180557
Within Groups	144.4270533	8	18.05338166			
Total	262.0719865	11				

ROS N2A/Ag26Disp Concentrations:

1-0 µg/ml
2-5 µg/ml
3-10 µg/ml
4-25 µg/ml
5-50 µg/ml
6-100 µg/ml

Ag Disp New							
Group	Sample Mean	Sample Size	Comparison	Absolute Difference	Std. Error of Difference	Critical Range	Results
1	1	3	Group 1 to Group 2	0.060234	0.07224412	0.3432	Means are not different
2	1.060234	3	Group 1 to Group 3	0.022653	0.07224412	0.3432	Means are not different
3	1.022653	3	Group 1 to Group 4	0.195893	0.07224412	0.3432	Means are not different
4	1.195893	3	Group 1 to Group 5	0.271398	0.07224412	0.3432	Means are not different
5	1.271398	3	Group 1 to Group 6	0.751101	0.07224412	0.3432	Means are different
6	1.751101	3	Group 2 to Group 3	0.037581	0.07224412	0.3432	Means are not different
			Group 2 to Group 4	0.135659	0.07224412	0.3432	Means are not different
Other Data			Group 2 to Group 5	0.211164	0.07224412	0.3432	Means are not different
Level of significance	0.05		Group 2 to Group 6	0.690868	0.07224412	0.3432	Means are different
Numerator d.f.	6		Group 3 to Group 4	0.173241	0.07224412	0.3432	Means are not different
Denominator d.f.	12		Group 3 to Group 5	0.248745	0.07224412	0.3432	Means are not different
MSW	0.015658		Group 3 to Group 6	0.728449	0.07224412	0.3432	Means are different
Q Statistic	4.75		Group 4 to Group 5	0.075505	0.07224412	0.3432	Means are not different
			Group 4 to Group 6	0.555208	0.07224412	0.3432	Means are different
			Group 5 to Group 6	0.479704	0.07224412	0.3432	Means are different

Anova: Single Factor						
SUMMARY						
Groups	Count	Sum	Average	Variance		
Column 1	3	3	1	0		
Column 2	3	3.180700881	1.060233627	0.001211574		
Column 3	3	3.067957522	1.022652507	0.00098013		
Column 4	3	3.587679188	1.195893063	0.031435328		
Column 5	3	3.814192824	1.271397608	0.028685893		
Column 6	3	5.253303693	1.751101231	0.031632906		
ANOVA						
Source of Variation	SS	df	MS	F	P-value	F crit
Between Groups	1.194312853	5	0.238862571	15.25533829	7.6841E-05	3.105875239
Within Groups	0.187891661	12	0.015657638			
Total	1.382204514	17				

ROS N2A/Ag25 Concentrations:

1-0 µg/ml
2-5 µg/ml
3-10 µg/ml
4-25 µg/ml
5-50 µg/ml
6-100 µg/ml

Ag-25nm							
Group	Sample Mean	Sample Size	Comparison	Absolute Difference	Std. Error of Difference	Critical Range	Results
1	1	3	Group 1 to Group 2	0.021385	0.09020054	0.4285	Means are not different
2	0.978615	3	Group 1 to Group 3	0.056474	0.09020054	0.4285	Means are not different
3	1.056474	3	Group 1 to Group 4	0.172691	0.09020054	0.4285	Means are not different
4	1.172691	3	Group 1 to Group 5	0.478864	0.09020054	0.4285	Means are different
5	1.478864	3	Group 1 to Group 6	0.447918	0.09020054	0.4285	Means are different
6	1.447918	3	Group 2 to Group 3	0.077858	0.09020054	0.4285	Means are not different
Other Data			Group 2 to Group 4	0.194075	0.09020054	0.4285	Means are not different
Level of significance			Group 2 to Group 5	0.500249	0.09020054	0.4285	Means are different
Numerator d.f.			Group 2 to Group 6	0.469302	0.09020054	0.4285	Means are different
Denominator d.f.			Group 3 to Group 4	0.116217	0.09020054	0.4285	Means are not different
MSW			Group 3 to Group 5	0.422391	0.09020054	0.4285	Means are not different
Q Statistic			Group 3 to Group 6	0.391444	0.09020054	0.4285	Means are not different
			Group 4 to Group 5	0.306174	0.09020054	0.4285	Means are not different
			Group 4 to Group 6	0.275227	0.09020054	0.4285	Means are not different
			Group 5 to Group 6	0.030946	0.09020054	0.4285	Means are not different

Anova: Single Factor						
SUMMARY						
Groups	Count	Sum	Average	Variance		
Column 1	3	3	1	0		
Column 2	3	2.935846176	0.978615392	0.024566985		
Column 3	3	3.169420648	1.056473549	0.014625815		
Column 4	3	3.518072114	1.172690705	0.01107115		
Column 5	3	4.436592852	1.478864284	0.065740582		
Column 6	3	4.343753388	1.447917796	0.030445949		
ANOVA						
Source of Variation	SS	df	MS	F	P-value	F crit
Between Groups	0.746614837	5	0.149322967	6.117684201	0.004850934	3.105875239
Within Groups	0.292900965	12	0.024408414			
Total	1.039515802	17				

APPENDIX C
Statistics for MTT and ROS Assays for Macrophages and CNMs

MTT Mac/ND-row concentrations:

1-0 µg/ml
2-25 µg/ml
3-50 µg/ml
4-100 µg/ml

ND-row							
Group	Sample Mean	Sample Size	Comparison	Absolute Difference	Std. Error of Difference	Critical Range	Results
1	100	3	Group 1 to Group 2	10.38205	3.00610986	13.618	Means are not different
2	89.61795	3	Group 1 to Group 3	18.68605	3.00610986	13.618	Means are different
3	81.31395	3	Group 1 to Group 4	21.73362	3.00610986	13.618	Means are different
4	78.26638	3	Group 2 to Group 3	8.30394	3.00610986	13.618	Means are not different
			Group 2 to Group 4	11.35157	3.00610986	13.618	Means are not different
			Group 3 to Group 4	3.047571	3.00610986	13.618	Means are not different
Other Data							
Level of significance	0.05						
Numerator d.f.	4						
Denominator d.f.	8						
MSW	27.11009						
Q Statistic	4.53						

Anova: Single Factor						
SUMMARY						
Groups	Count	Sum	Average	Variance		
Column 1	3	300	100	0		
Column 2	3	268.8538358	89.61794526	0.219411381		
Column 3	3	243.9418537	81.31395122	108.1289318		
Column 4	3	234.7991405	78.26638018	0.092014467		
ANOVA						
Source of Variation	SS	df	MS	F	P-value	F crit
Between Groups	852.3058094	3	284.1019365	10.47956472	0.003812741	4.066180557
Within Groups	216.8807152	8	27.1100894			
Total	1069.186525	11				

MTT Mac/CB Concentrations:

1-0 µg/ml
2-25 µg/ml
3-50 µg/ml
4-100 µg/ml

CB							
Group	Sample Mean	Sample Size	Comparison	Absolute Difference	Std. Error of Difference	Critical Range	Results
1	100	3	Group 1 to Group 2	20.76986	0.77527123	3.512	Means are different
2	79.23014	3	Group 1 to Group 3	43.1357	0.77527123	3.512	Means are different
3	56.8643	3	Group 1 to Group 4	57.85163	0.77527123	3.512	Means are different
4	42.14837	3	Group 2 to Group 3	22.36585	0.77527123	3.512	Means are different
			Group 2 to Group 4	37.08178	0.77527123	3.512	Means are different
			Group 3 to Group 4	14.71593	0.77527123	3.512	Means are different
Other Data							
Level of significance	0.05						
Numerator d.f.	4						
Denominator d.f.	8						
MSW	1.803136						
Q Statistic	4.53						

Anova: Single Factor						
SUMMARY						
Groups	Count	Sum	Average	Variance		
Column 1	3	300	100	0		
Column 2	3	237.6904258	79.23014192	0.939289234		
Column 3	3	170.5928871	56.8642957	5.074857369		
Column 4	3	126.4451003	42.14836677	1.198399246		
ANOVA						
Source of Variation	SS	df	MS	F	P-value	F crit
Between Groups	5798.051361	3	1932.683787	1071.845547	9.32607E-11	4.066180557
Within Groups	14.4250917	8	1.803136462			
Total	5812.476453	11				

MTT Mac/MWNT Concentrations:

1-0 µg/ml
2-25 µg/ml
3-50 µg/ml
4-100 µg/ml

MWNT							
Group	Sample Mean	Sample Size	Comparison	Absolute Difference	Std. Error of Difference	Critical Range	Results
1	100	3	Group 1 to Group 2	43.57957	0.54208315	2.4556	Means are different
2	56.42043	3	Group 1 to Group 3	59.3077	0.54208315	2.4556	Means are different
3	40.6923	3	Group 1 to Group 4	54.7	0.54208315	2.4556	Means are different
4	45.3	3	Group 2 to Group 3	15.72813	0.54208315	2.4556	Means are different
			Group 2 to Group 4	11.12043	0.54208315	2.4556	Means are different
			Group 3 to Group 4	4.607702	0.54208315	2.4556	Means are different
Other Data							
Level of significance	0.05						
Numerator d.f.	4						
Denominator d.f.	8						
MSW	0.881562						
Q Statistic	4.53						

Anova: Single Factor						
SUMMARY						
Groups	Count	Sum	Average	Variance		
Column 1	3	300	100	0		
Column 2	3	169.2612963	56.4204321	2.019457103		
Column 3	3	122.076897	40.69229898	0.681227655		
Column 4	3	135.9000018	45.30000061	0.825564892		
ANOVA						
Source of Variation	SS	df	MS	F	P-value	F crit
Between Groups	6600.705865	3	2200.235288	2495.836094	3.19206E-12	4.066180557
Within Groups	7.052499299	8	0.881562412			
Total	6607.758364	11				

MTT Mac/SWNT Concentrations:

1-0 µg/ml
2-25 µg/ml
3-50 µg/ml
4-100 µg/ml

SWNT							
Group	Sample Mean	Sample Size	Comparison	Absolute Difference	Std. Error of Difference	Critical Range	Results
1	100	3	Group 1 to Group 2	61.90369	0.36095751	1.6351	Means are different
2	38.09631	3	Group 1 to Group 3	72.74169	0.36095751	1.6351	Means are different
3	27.25831	3	Group 1 to Group 4	75.64818	0.36095751	1.6351	Means are different
4	24.35182	3	Group 2 to Group 3	10.83799	0.36095751	1.6351	Means are different
			Group 2 to Group 4	13.74448	0.36095751	1.6351	Means are different
			Group 3 to Group 4	2.906487	0.36095751	1.6351	Means are different
Other Data							
Level of significance	0.05						
Numerator d.f.	4						
Denominator d.f.	8						
MSW	0.390871						
Q Statistic	4.53						

Anova: Single Factor						
SUMMARY						
Groups	Count	Sum	Average	Variance		
Column 1	3	300	100	0		
Column 2	3	114.2889165	38.0963055	0.527811465		
Column 3	3	81.7749353	27.25831177	0.085484857		
Column 4	3	73.05547309	24.35182436	0.950187561		
ANOVA						
Source of Variation	SS	df	MS	F	P-value	F crit
Between Groups	11370.66571	3	3790.221904	9696.86211	1.40581E-14	4.066180557
Within Groups	3.126967764	8	0.390870971			
Total	11373.79268	11				

MTT Mac/CdO Concentrations:

1-0 µg/ml

2-25 µg/ml

3-50 µg/ml

CdO							
Group	Sample Mean	Sample Size	Comparison	Absolute Difference	Std. Error of Difference	Critical Range	Results
1	100	3	Group 1 to Group 2	79.7281	1.8551059	8.0512	Means are different
2	20.2719	3	Group 1 to Group 3	96.52657	1.8551059	8.0512	Means are different
3	3.473431	3	Group 2 to Group 3	16.79846	1.8551059	8.0512	Means are different
Other Data							
Level of significance	0.05						
Numerator d.f.	3						
Denominator d.f.	6						
MSW	10.32425						
Q Statistic	4.34						

Anova: Single Factor						
SUMMARY						
Groups	Count	Sum	Average	Variance		
Column 1	3	300	100	0		
Column 2	3	60.81568652	20.27189551	30.26853455		
Column 3	3	10.42029371	3.473431235	0.704226646		
ANOVA						
Source of Variation	SS	df	MS	F	P-value	F crit
Between Groups	15956.13753	2	7978.068763	772.7501639	5.7836E-08	5.14325285
Within Groups	61.94552239	6	10.32425373			
Total	16018.08305	8				

ROS Mac/ND-row Concentrations:

1-0 µg/ml

2-25 µg/ml

3-50 µg/ml

4-100 µg/ml

ND-row							
Group	Sample Mean	Sample Size	Comparison	Absolute Difference	Std. Error of Difference	Critical Range	Results
1	1	3	Group 1 to Group 2	0.115187	0.0320149	0.145	Means are not different
2	1.115187	3	Group 1 to Group 3	0.014517	0.0320149	0.145	Means are not different
3	1.014517	3	Group 1 to Group 4	0.007012	0.0320149	0.145	Means are not different
4	0.992988	3	Group 2 to Group 3	0.10067	0.0320149	0.145	Means are not different
			Group 2 to Group 4	0.122198	0.0320149	0.145	Means are not different
			Group 3 to Group 4	0.021529	0.0320149	0.145	Means are not different
Other Data							
Level of significance	0.05						
Numerator d.f.	4						
Denominator d.f.	8						
MSW	0.003075						
Q Statistic	4.53						

Anova: Single Factor						
SUMMARY						
Groups	Count	Sum	Average	Variance		
Column 1	3	3	1	0		
Column 2	3	3.345560394	1.115186798	2.7E-05		
Column 3	3	3.043551361	1.01451712	0.002078		
Column 4	3	2.978965131	0.992988377	0.010195		
ANOVA						
Source of Variation	SS	df	MS	F	P-value	F crit
Between Groups	0.029293675	3	0.009764558	3.17561	0.084970523	4.066180557
Within Groups	0.024598888	8	0.003074861			
Total	0.053892563	11				

ROS Mac/CB Concentrations:

- 1-0 µg/ml
- 2-25 µg/ml
- 3-50 µg/ml
- 4-100 µg/ml

CB							
Group	Sample Mean	Sample Size	Comparison	Absolute Difference	Std. Error of Difference	Critical Range	Results
1		3	Group 1 to Group 2	5.589893	0.25416265	1.1514	Means are different
2	6.589893	3	Group 1 to Group 3	7.040259	0.25416265	1.1514	Means are different
3	8.040259	3	Group 1 to Group 4	11.26868	0.25416265	1.1514	Means are different
4	12.26868	3	Group 2 to Group 3	1.450366	0.25416265	1.1514	Means are different
			Group 2 to Group 4	5.67879	0.25416265	1.1514	Means are different
			Group 3 to Group 4	4.228423	0.25416265	1.1514	Means are different
Other Data							
Level of significance	0.05						
Numerator d.f.	4						
Denominator d.f.	8						
MSW	0.193796						
Q Statistic	4.53						

Anova: Single Factor						
SUMMARY						
Groups	Count	Sum	Average	Variance		
Column 1	3	3	1	0		
Column 2	3	19.76967941	6.589893136	0.391534342		
Column 3	3	24.12077819	8.040259395	0.343749947		
Column 4	3	36.80604868	12.26868289	0.039899553		
ANOVA						
Source of Variation	SS	df	MS	F	P-value	F crit
Between Groups	195.0203643	3	65.00678811	335.4393353	9.49269E-09	4.066180557
Within Groups	1.550367682	8	0.19379596			
Total	196.570732	11				

ROS Mac/SWNT Concentrations:

1-0 µg/ml
2-25 µg/ml
3-50 µg/ml
4-100 µg/ml

SWNT							
Group	Sample Mean	Sample Size	Comparison	Absolute Difference	Std. Error of Difference	Critical Range	Results
1		3	Group 1 to Group 2	18.35105	0.29324786	1.3284	Means are different
2	19.35105	3	Group 1 to Group 3	14.71262	0.29324786	1.3284	Means are different
3	15.71262	3	Group 1 to Group 4	12.10334	0.29324786	1.3284	Means are different
4	13.10334	3	Group 2 to Group 3	3.638428	0.29324786	1.3284	Means are different
			Group 2 to Group 4	6.247707	0.29324786	1.3284	Means are different
			Group 3 to Group 4	2.609278	0.29324786	1.3284	Means are different
Other Data							
Level of significance	0.05						
Numerator d.f.	4						
Denominator d.f.	8						
MSW	0.257983						
Q Statistic	4.53						

Anova: Single Factor						
SUMMARY						
Groups	Count	Sum	Average	Variance		
Column 1	3	3	1	0		
Column 2	3	58.05313975	19.35104658	0.205097056		
Column 3	3	47.1378547	15.71261823	0.073614752		
Column 4	3	39.31001961	13.10333987	0.753219914		
ANOVA						
Source of Variation	SS	df	MS	F	P-value	F crit
Between Groups	569.0949117	3	189.6983039	735.3133922	4.18956E-10	4.066180557
Within Groups	2.063863446	8	0.257982931			
Total	571.1587752	11				

ROS Mac/MWNT Concentrations:

1-0 µg/ml
2-25 µg/ml
3-50 µg/ml
4-100 µg/ml

MWNT							
Group	Sample Mean	Sample Size	Comparison	Absolute Difference	Std. Error of Difference	Critical Range	Results
1	1	3	Group 1 to Group 2	18.9716	1.06307914	4.8157	Means are different
2	19.9716	3	Group 1 to Group 3	22.011	1.06307914	4.8157	Means are different
3	23.011	3	Group 1 to Group 4	18.67487	1.06307914	4.8157	Means are different
4	19.67487	3	Group 2 to Group 3	3.039398	1.06307914	4.8157	Means are not different
			Group 2 to Group 4	0.29673	1.06307914	4.8157	Means are not different
			Group 3 to Group 4	3.336128	1.06307914	4.8157	Means are not different
Other Data							
Level of significance	0.05						
Numerator d.f.	4						
Denominator d.f.	8						
MSW	3.390412						
Q Statistic	4.53						

Anova: Single Factor						
SUMMARY						
Groups	Count	Sum	Average	Variance		
Column 1	3	3	1	0		
Column 2	3	59.9147995	19.97159983	3.935384852		
Column 3	3	69.03299384	23.01099795	4.823068593		
Column 4	3	59.02460858	19.67486953	4.80319361		
ANOVA						
Source of Variation	SS	df	MS	F	P-value	F crit
Between Groups	910.209094	3	303.4030313	89.48854961	1.70533E-06	4.066180557
Within Groups	27.12329411	8	3.390411764			
Total	937.3323881	11				

MTT Mac/CB/Growth Media Concentrations:

1-0 µg/ml
2-25 µg/ml
3-50 µg/ml
4-100 µg/ml

CBgrowthmedia									
Group	Sample Mean	Sample Size	Comparison	Absolute Difference	Std. Error of Difference	Critical Range	Results		
1	100	3	Group 1 to Group 2	8.81875	3.9825145	18.041	Means are not different		
2	91.18125	3	Group 1 to Group 3	17.06394	3.9825145	18.041	Means are not different		
3	82.93606	3	Group 1 to Group 4	1.034298	3.9825145	18.041	Means are not different		
4	101.0343	3	Group 2 to Group 3	8.24519	3.9825145	18.041	Means are not different		
			Group 2 to Group 4	9.853048	3.9825145	18.041	Means are not different		
			Group 3 to Group 4	18.09824	3.9825145	18.041	Means are different		
Other Data									
Level of significance	0.05								
Numerator d.f.	4								
Denominator d.f.	8								
MSW	47.58127								
Q Statistic	4.53								

Anova: Single Factor						
SUMMARY						
Groups	Count	Sum	Average	Variance		
Column 1	3	300	100	0		
Column 2	3	273.5437509	91.18125029	0.332203999		
Column 3	3	248.8081808	82.93606028	10.71665791		
Column 4	3	303.1028941	101.034298	179.2761987		
ANOVA						
Source of Variation	SS	df	MS	F	P-value	F crit
Between Groups	646.9725564	3	215.6575188	4.532404048	0.038829932	4.066180557
Within Groups	380.6501212	8	47.58126515			
Total	1027.622678	11				

MTT Mac/CB/Dose Media Concentrations:

1-0 µg/ml
2-25 µg/ml
3-50 µg/ml
4-100 µg/ml

CB dosing media							
Group	Sample Mean	Sample Size	Comparison	Absolute Difference	Std. Error of Difference	Critical Range	Results
1	100	3	Group 1 to Group 2	20.76986	0.77527123	3.512	Means are different
2	79.23014	3	Group 1 to Group 3	43.1357	0.77527123	3.512	Means are different
3	56.8643	3	Group 1 to Group 4	57.85163	0.77527123	3.512	Means are different
4	42.14837	3	Group 2 to Group 3	22.36585	0.77527123	3.512	Means are different
			Group 2 to Group 4	37.08178	0.77527123	3.512	Means are different
			Group 3 to Group 4	14.71593	0.77527123	3.512	Means are different
Other Data							
Level of significance	0.05						
Numerator d.f.	4						
Denominator d.f.	8						
MSW	1.803136						
Q Statistic	4.53						

Anova: Single Factor						
SUMMARY						
Groups	Count	Sum	Average	Variance		
Column 1	3	300	100	0		
Column 2	3	237.6904258	79.23014192	0.939289234		
Column 3	3	170.5928871	56.8642957	5.074857369		
Column 4	3	126.4451003	42.14836677	1.198399246		
ANOVA						
Source of Variation	SS	df	MS	F	P-value	F crit
Between Groups	5798.051361	3	1932.683787	1071.845547	9.32607E-11	4.066180557
Within Groups	14.4250917	8	1.803136462			
Total	5812.476453	11				

R702034083

VITA

Amanda M. Schrand

Born January 24, 1977 in Pordenone, Italy

Currently residing at 2649 Corlington Drive Kettering, OH 45440

(937) 297-9990

EDUCATION & WORK EXPERIENCE

- 1999** Bachelor of Science with Honors, Biological Sciences, Wright State University, Dayton, OH, Hewitt Memorial Academic Scholarship
- 2000-2005** Research Technician, UES, Inc., Wright Patterson Air Force Base, Dayton, OH
- 2001** Master of Science, Biological Sciences, Wright State University, Dayton, OH, Graduate Teaching Assistantship
- 2005-Present** Associate Research Scientist, UDRI, Dayton, OH
- 2007** PhD, Materials Engineering, University of Dayton, Dayton, OH, DAGSI Tuition Assistantship and ORAU Fellowship

PUBLICATIONS

Hussain S, Javorina A, Schrand A, Duhart H, Ali S, Schlager J (2006) The Interaction of Manganese Nanotubes with PC-12 Cells Induces Dopamine Depletion. *J. Tox. Sci.* 92 (2): 456-463.

Schrand AM, Huang H, Carlson C, Schlager JJ, Ōsawa E, Hussain SM, Dai L (2007) Are Diamond Nanoparticles Cytotoxic? *J. Phys. Chem. B* 111 (1): 2-7.

Skebo, JE, Grabinski CM, Schrand AM, Schlager JJ, Hussain SM (2007) Assessment of Metal Nanoparticle Agglomeration, Uptake, and Interaction Using a High Illuminating System. *Int. J. Tox.* 26: 135-141.

Wagner AJ, Bleckmann CA, Murdock RC, Schrand AM, Schlager JJ, Hussain SM. (2007) Cellular Interaction of Different Forms of Aluminum Nanoparticles in Rat Alveolar Macrophages. *J. Phys. Chem. B* 111 (25): 7353-7359.

Schrand AM, Dai L, Schlager JJ, Hussain SM, Ōsawa E (2007) Differential Biocompatibility of Carbon Nanotubes and Nanodiamonds. *Diamond Rel. Mat.* 16 (12): 2118-2123.

Schrand AM, Szczublewski K, Schlager JJ, Dai L, Hussain SM (2007) Interaction and Biocompatibility of Multi-walled Carbon Nanotubes in PC-12 Cells. *Int. J. Neuroprot. Neuroregen.* 3 (2): 115-121.

Murdock RC, Braydich-Stolle L, Schrand AM, Schlager JJ, Hussain SM (2007) Characterization of Nanomaterial Dispersion in Solution Prior to *In Vitro* Exposure Using Dynamic Light Scattering Technique. *Tox. Sci.* Online September 13.

FIELDS OF STUDY

Nanomaterials, Engineering, Characterization, Toxicity, Cell Culture